Ring/Chain *versus* Network: Architecture Induced by Self- *versus* Pairwise- Association of Telechelic Polymers

Thesis by

Boyu Li

In Partial Fulfillment of the Requirements for

the degree of

Doctor of Philosophy

Caltech

CALIFORNIA INSTITUTE OF TECHNOLOGY

Pasadena, California

2016

(Defended May 10th, 2016)

Boyu Li
ORCID: orcid.org/0000-0002-7648-3745

ACKNOWLEDGEMENTS

Coming to Caltech five years ago was like entering a new world for me: new country, new language and a fantastic new environment for science. I am grateful to all of the people who have helped me complete this thesis, academically or personally.

First, I would like to thank my advisor, Prof. Julie Kornfield, for being such a caring, encouraging, and inspiring mentor. I felt a strong match with Julie the first time I talked with her during my first quarter at Caltech. Over the years, she has enlightened me with her passion for beautiful science, her pursuit for accuracy, and her insights in polymer sciences. "Be quantitative!" She always says. And indeed, I will carry it with me for my whole life. I treasure the great advice from the members of my committee (Professors David Tirrell, Dan Weitekamp and Bob Grubbs), for example, the gestures in giving presentations and tips in writing a NSF-level proposal, etc. There are not that many places on earth where a student can learn from world-renowned scientists. And I appreciate their time and energy spent in reviewing my proposals and thesis. I would also like to thank Prof. Zhen-Gang Wang for his wonderful course of Polymer Physics, which was illuminating, intuitive, and fun. It is one of the direct reasons that I fell in love with polymer physics coming from an organic chemistry background.

I enjoyed the time working and living at Caltech, thanks to the people around me. It was also a great pleasure to have the awesome former and current lab-mates in the Kornfield lab. For the first half of my PhD thesis, I worked with other great scientists on a polymeric fuel additive for mist-control and drag-reduction. Dr. Ming-Hsin (Jeremy Wei) taught me ring-opening metathesis polymerization (ROMP) and how to use chain-transfer agents (CTA) to install associative end groups. Dr. Simon Jones gave me great advices on polymer synthesis and writing. I was inspired by Dr. Virendra Sarohia, who was involved in the major US-UK collaboration in the late-1970s and early-1980s, for inspiring me to work on associative polymers for mist control to improve aviation safety. I cherish the conversations with Zuli on topics from women in science to daily life. I enjoyed discussing polymer physics with Joey and Paul, and the trips we had together for beam-time. The MRS conference trips with

Karthik and Tiziana will always be among my happy memories. It has been fun chatting with Dan, Amy, and Artemis about almost everything in life. Nothing is more enjoyable than delicious Asian food. I love our exploration of Asian restaurants with Dennis, Bo, and Zach. I am happy to have been able to talk with Rachel, Ben, and Red during recruitment and then work with them now. I am really grateful for the help and support from these wonderful people.

I have always been amazed at how people all over the campus, or even off campus, can be so helpful. Bilin Zhuang, a PhD at Prof. Zhen-Gang Wang's group, has been a great friend and shared her positive attitude to life with me. Dr. Xuelian He, a visiting scholar from East China University of Science and Technology (ECUST), helped synthesize the polymer backbone control used in my thesis. Kuang Shen, a former PhD at Prof. Shu-ou Shan's lab, taught me experimental techniques involving proteins and helped me settle down when I first started. Alex Tucker-Schwartz, a former postdoc from Prof. Rustem Ismagilov's group, has been a nice big-brother and provided enormous help for job searching. Jeff Groseth offered his insights when our ancient instruments were down. Jayesh Patel is such an amazing expert and teacher, and kept all of our rheometers functioning beautifully. Andy Meyer came to rescue, helping us switch the Wyatt light scattering device to batch mode, when we had only two weeks left for manuscript submission. Marcy Fowler, Andrea Arias, Yvette Grant, Sarah Mojarad, and Kate Davies have kept the Kornfield group in pace and organized.

Last but not least, I would love to thank my family for supporting and loving me under any circumstances. The life wisdoms shared with me by my parents are so valuable, keeping me positive during all of the years. I especially want to thank my husband, who is everything I ever wanted. He is a great listener, even when I complained about similar issues over and over again. I am grateful that we have had a chance to share our PhD experience, and understand each other so well.

ABSTRACT

Non-covalent associations, including hydrophobic interaction or ionic interaction for self-association, and metal coordination or hydrogen-bonding for complementary-association, have been widely used as key interactions in supramolecules formation with telechelic associative polymers. And a specific application of long associative telechelic polymers has been developed by our group for the mist-control and drag-reduction of liquid fuels. During the research on this project, self- and pairwise-associative telechelic polymers are able to be compared for the first time, and are shown to display distinct associative patterns. In order to design materials with the desired properties, it is imperative to understand the relationships between polymer chemical structure and their topology and dynamics.

In this thesis, self-associative telechelic polymer refers to α,ω-di(isophthalic acid) polycyclooctadiene (DA-PCOD), which can associate with itself through its acid ends. When tertiary amine-ended polymer is added into the mixture, isophthalic acid preferably associates pairwisely with tertiary amine due to the higher binding strength of charge-assisted hydrogen bond. And the 1:1 molar ratio mixture of α,ω-di(isophthalic acid) and α,ω-di(di(tertiary amine)) PCOD (DA/DB-PCOD) is named as pairwise-associative telechelic polymers. DA-PCOD is capable of multimeric association via directional hydrogen bonding due to the specific chemical structure of the isophthalic acid end, while DA/DB-PCOD exhibits dynamics that strikingly resembles that for linear covalent polymers. Temperature determines the binding strength of self- and pairwise- end association, and furthermore, the fraction of unbound ends and the distribution and topology of formed supramolecules/aggregates. Polymer length affects the dynamics of DA-PCOD mainly through determining the concentration of the end groups. And the net effect of chain length on the dynamics of DA/DB-PCOD is non-monotonic and varies with the specific temperature and concentration. The knowledge of structure-property relationships obtained from this work will enable future design of end group entities and other properties of these associative telechelic polymers for their specific applications.

PUBLISHED CONTENT AND CONTRIBUTIONS

M.-H. Wei*, B. Li*, R. L. A. David, S. C. Jones, V. Sarohia, J. A. Schmitigal & J. A. Kornfield (*: authors contributed equally), "Mega-supramolecules for safer, cleaner fuel by end-association of long telechelic polymers", *Science*, **2015**, *350*, 72-75. DOI: 10.1126/science.aab0642
> B. Li focused on the viscometry, multi-angle laser light scattering (MALLS) and small angle neutron scattering (SANS) characterization of the supramolecules, participated in the polymer synthesis, preliminary diesel generator test and high speed impact experiment, and prepared the manuscript and supplementary information.

B. Li, J. Kim, J. A. Kornfield, "A Molecular Picture for the Thermo-Reversibility of Gels Formed by Isophthalic Acid-Ended Telechelic Polymers", ***MRS Proceedings***, **2015**, *1794*, 9-14. DOI: 10.1557/opl.2015.638
> B. Li performed the experiments (rheology and SANS) in this work, and prepared the manuscript.

Materials Research Society Fall Meeting, Boston, Massachusetts (Dec 2015)
Temperature and Chain Length Effects on the Topology and Thermodynamics of Soft Gels Formed by Telechelic Polymers with Hydrogen-Bonding Ends (talk)
> B. Li performed the experiments in this work, and gave the oral presentation.

Materials Research Society Spring Meeting, San Francisco, California (April 2015)
End-Associative Polymers in Organic Liquids: From Mist Control to Ultra-Soft Gels (talk)
> B. Li performed the experiments (rheology and SANS) in this work, and gave the oral presentation.

TABLE OF CONTENTS

LIST OF FIGURES

LIST OF TABLES

LIST OF SCHEMES

Chapter I

Introduction to Association of Telechelic Polymers

Non-covalent associations, including hydrophobic or ionic interactions for self-association, and metal coordination or hydrogen-bonding for complementary-association, have been widely used as key interactions in supramolecules formation with telechelic associative polymers. The study of self-associative telechelic polymers, especially the hydrophobically modified ethylene oxide-urethanes (HEURs), has attracted great attention due to their ability to control rheological properties such as viscosity, gelation, shear-thinning, and thickening behavior in water-based coatings and paints. Numerous studies on their structure-rheology relationship have been reported [1-11].

After 1990s, the complementary association adopting metal coordination and hydrogen-bonding became well recognized as an approach to mimic nature in material development, improving material characteristics of conventional polymers, conferring better capacity for processing and sensitivity to various environmental stimuli (including temperature, ion content and redox reaction, etc.) [12-23]. A number of complementary-associative end-motifs have then been synthesized and applied to supramolecular chemistry [12-23]. However, the dynamics of the formed supramolecules has rarely been covered, and systematic investigations are missing on how dynamics of supramolecules can be affected by relevant factors, including polymer concentration, temperature and polymer chain length, etc [22-23]. These studies are needed since they can both identify the structure-function relationship for supramolecular formation, and serve as a guide for rational design of supramolecules and the related functional materials.

In this introduction, prior literature on self-associative and complementary-associative telechelic polymers is reviewed (Section 1.1 and 1.2). Specific applications of long associative telechelic polymers in mist-control and drag-reduction developed by our group are then introduced (Section 1.3). During the research on this project, self- and pairwise-associative telechelic polymers are able to be compared for the first time in literature (to our knowledge), and have been shown to display distinct associative patterns. This inspired further investigations into the morphology, dynamics, and structure-function relationship of these two systems: the main topic addressed in this thesis (Section 1.4).

It will be shown in this thesis that our self-associative telechelic polymers are capable of multimeric association *via* pairwise hydrogen bonding due to the specific chemical structure of the ends, while the pairwise-associative telechelic polymers exhibit dynamics that strikingly resembles that of linear covalent polymers. The morphology and dynamics of self- and pairwise- association system differ from each other qualitatively, simply resulting from a difference in chemical functionality of half of the end groups, which make up <0.5% of the total polymer composition. Polymer concentration, temperature, and chain length significantly affect the morphology and dynamics of both systems significantly.

To provide a foundation for the discussion of our self- and pairwise-associative telechelic polymers, some basic concepts relevant to these polymer systems are reviewed in this chapter, including the conformation and dynamics of linear covalent polymer solutions (Section 1.5), and properties of hydrogen bonds (Section 1.6). Although by no means exhaustive, it is hoped that this brief review of polymer physics will make the work accessible to a more general audience.

1.1 Literature on self-associative telechelic polymers

Early research on self-associative telechelic polymers focused on ionomer telechelic polymers, which refers to a telechelic polymer with ionized ends. Their capacity in dramatically modifying the rheological behavior of non-polar solutions has attracted great attention since the 1980s [8-11]. Some reports on ionomers will be introduced in Chapter 5. After the development of water-based coatings and paints, more efforts were devoted to water-soluble self-associative polymers, among which hydrophobically modified poly(ethylene oxides) have been the most widely studied and applied to control rheological properties such as viscosity, gelation, shear-thinning, and thickening behavior [1]. These polymers used to be synthesized by attaching the hydrophobic ends to PEOs using urethane (isocyanate) coupling groups, and therefore they are also called hydrophobically modified ethylene oxide-urethanes (HEURs). Their morphology and rheological properties have been systematically studied, and can be found in numerous reports [1-7]. Therefore, HEURs have been chosen as the model system for self-associative telechelic polymers in this chapter.

1.1.1 Micelle formation and linear viscoelasticity of HEURs
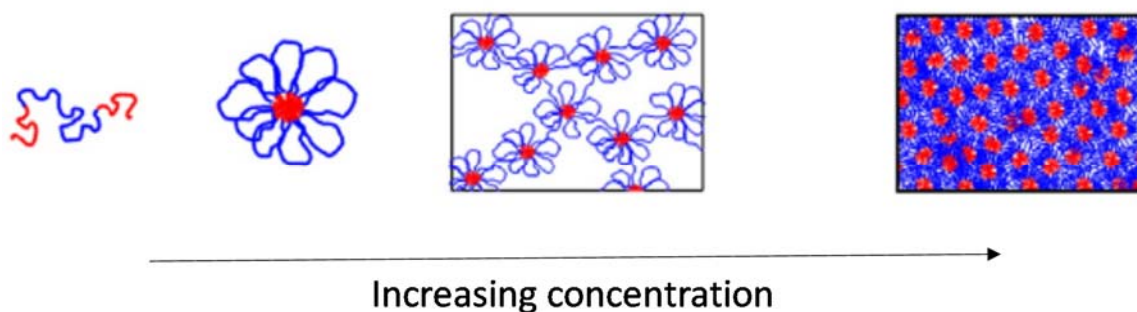
Figure 1.1 (Figure reproduced from reference [1]) Schematics on the formation of flower-like micelles and interconnected networks.

HEURs form flower-like micelles at low concentrations, and the "petals" (loops) turn into bridges between micelles as the polymer concentration is increased, and eventually, interconnected network forms [1] (Figure 1.1). The formation of micelle structures has been well confirmed by various methods, including fluorescence measurements, dynamic light scattering, and static light scattering [7].

The linear viscoelasticity of the resulting "gels" (or thick solutions) shows rather simple dynamic features: their dynamic moduli curves could be fitted by the Maxwell model with a single relaxation time [2] (Figure 1.2A). It has been demonstrated that the relaxation time is dominated by the exchange or dissociation process of the hydrophobic end from micelle cores, and not related to entanglement effect as postulated in some earlier theories [2]. The telechelic polymers relax *via* Rouse-like dynamics following by end-group exchange/disengagement. The relaxation time thus follows an Arrhenius-type temperature dependence with an activation energy (E_a) that reflects the end association strength (Figure 1.2B). When oscillatory shear tests are performed at various temperatures, the dynamic moduli curves of HEUR solutions at various temperatures can be superimposed into a master curve, and the high-frequency modulus does not change with temperature either. Since the solution viscosity is the product of the plateau modulus and the longest relaxation time, both the solution viscosity and relaxation time follow the Arrhenius behavior with an activation energy that is controlled by the end groups: $\eta \sim \tau \sim \exp\left(\frac{Ea}{kT}\right)$ (Figure 1.2B). The

invariable high-frequency modulus with temperature also indicates that the topology of the

network does not change with temperature – only the exchange time of the end group does.
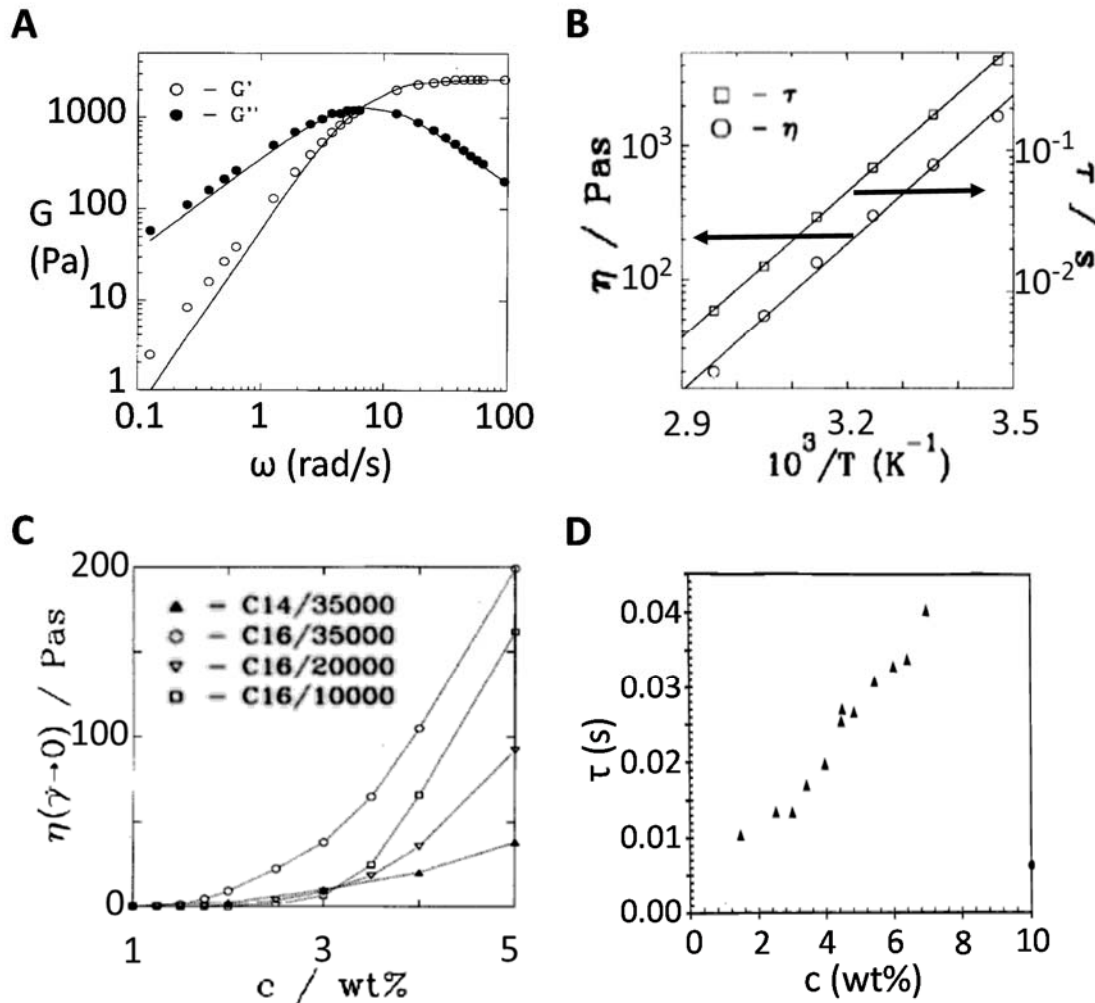
Figure 1.2 (Figures reproduced from reference [2]) **A.** Storage modulus G' and loss modulus G'' of 7 wt% C16/35 (M_w = 35 kg/mol, PEO with C16 hydrophobe). Here, wt%=%w/v. Lines represent fits of single-relaxation Maxwell model. **B.** Arrhenius plots of Newtonian viscosity and relaxation time for C16/35 (M_w = 35 kg/mol, PEO with C16 hydrophobe) at 10%w/v. **C.** Effect of polymer concentration (%w/v) on the low shear viscosity of four HEURs at 298 K. (Example of the nomenclature: C14/35000, a HERU with a C14 hydrophobe end and M_w = 35 kg/mol.) **D.** Relaxation time as function of polymer concentration for C16/35 (M_w = 35 kg/mol, PEO with C16 hydrophobe) at 298K. The line represents a scaling function of $\tau = \tau_0 f(c\sqrt{M})$.

The concentration dependence of the relaxation time, high-frequency modulus, and solution viscosity is more complicated. The viscosity of these polymer solutions depends strongly on the polymer concentration: it increases roughly as the concentration squared or cubed at low concentrations and linearly with the concentration at high concentrations (Figure 1.2C). Since the relaxation time only increases slightly with concentration (Figure 1.2D, within the same order of magnitude), while the high-frequency modulus shoots up orders of magnitude, it is clear that the concentration dependence of the viscosity is determined by that of the high-frequency modulus [2].

1.1.2 Theories on HEURs

1.1.2.1 Reversible network theory

Many theories have been developed to depict a molecular picture for the association of HEURs, with the controversy concentrating on explaining the high-frequency modulus. The reversible network theory by Tanaka and Edwards (1992) assumes the micellar network to be homogeneous and attributes the stress relaxation modulus to elastic stretching and compression of the bridging chains between hydrophobic domains to form the network [3], as described for permanent cross links by the theory of rubber elasticity [24]. All telechelic chains are assumed to be elastically effective or say, to be "bridges" (Figure 1.3A). As such, the high-frequency modulus G_∞ equals $\frac{n}{V}kT$, where $\frac{n}{V}$ is the total number of elastically effective chains (bridges) per volume. The low shear viscosity follows directly as $G_\infty \tau$, with τ, the relaxation time, for activated exchange of an end
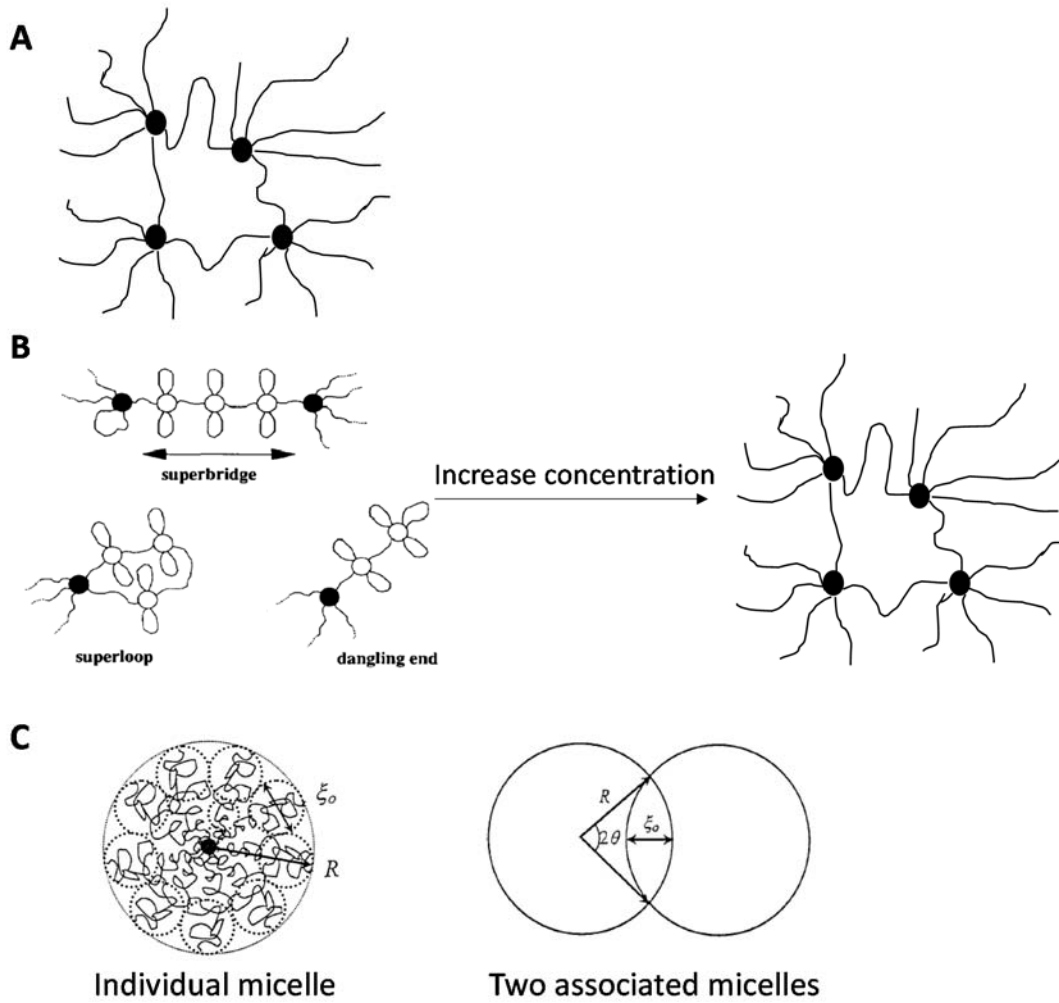
Figure 1.3 Schematic representation of the molecular hypothesis of various theories. A. Tanaka and Edwards [3] assumed the micellar network to be homogeneous and all telechelic chains to be elastically effective. **B.** Annable et al. [2] introduced a change in network topology with increasing concentration to explain the nonlinear concentration dependence of high frequency modulus and relaxation time. **C.** Semenov *et al* and Pham *et al* [4-6] postulated that the dynamic of the system is determined by the interaction between micelles, and furthermore, by the micelle structure.

between micellar cores. However, the theory predicts a linear dependence of high-frequency modulus and solution viscosity on concentration, whereas in practice they are found to be more like quadratic or cubic at low concentrations.

Annable *et al.* developed a model in 1993 modifying Tanaka and Edwards' theory, to relate the nonlinear concentration dependence of τ and G_∞ to the network topology [2]. An

elementary statistical-mechanical model, supported by Monte Carlo simulations, is used to argue that micelles are built predominantly from loops at low concentrations, while at high concentrations, a fully developed network is composed of micelles linked by bridging chains. More specifically, the distribution of individual telechelic chains into different states (loops or bridges) as a function of concentration is analyzed. When the concentration is low, most telechelic chains form loops, leading to various complex local topologies, including superbridges, superloops, and dangling ends (Figure 1.3B, left). The micelles with "functionality" (number of bridges coming from that micelle) equal or less than 2 are not exactly elastically effective, since the dissociation of one bridge in the middle of the superbridges will cause the whole chain to relax (Figure 1.3B, left, white circles). In this case, the number of elastically effective chains, which is the refined $\frac{n}{V}$, should be equal to the number of micelles with functionality bigger than 2, and it is found to increase quadratically with concentration at low concentrations. At high concentration, the fraction of loops decreases to a point at which almost all telechelic chains behave as bridges (Figure 1.3B, right), which recovers the scenario in Tanaka and Edwards' theory and has the high-frequency modulus (G_∞) increasing linearly with polymer concentration.

The same argument can be applied to the concentration dependence of relaxation time τ: the micelle structures relax faster at low concentration because of the existence of superbridges (Figure 1.2D; Figure 1.3B, left). Annable's statistical analysis modifies the classical reversible network theory to allow for loops and micelle functionalities of variable size, and correlates semi-quantitatively with the experimental observations [2]. Although the model deduced the aggregation number to be less than 10, which conflicts with much

of the aggregation number data in literature, reversible network theory is one of the most widely applied theories for the rheology of self-associative telechelic polymers.

1.1.2.2 "Interacting micelle theory"

Another theory, which we will refer to as 'interacting micelle theory', postulates that the dynamics of the system is determined by the interaction between micelles, and furthermore, by the micelle structure [4-6]. Each individual micelle is considered to consist of a compact hydrophobic core surrounded by a corona of the long soluble parts of the telechelic polymers that form loops. This structure resembles that of a star polymer with its arm exhibiting swollen conformation due to the excluded volume effect in good solvent (Figure 1.3C, left). And the size of the micelle can then be calculated as a power law of the aggregation number (p, number of ends in one micelle core): $R \sim p^{1/5}s$, in which R is the radius of the spherical micelle, and s is the end-to-end distance of one arm, which is half of the length of one telechelic polymer [5]. Since all arms are expected to end within a close range of R, the outermost blob size (ξ_0) can be derived also as a function of p and s: $\xi_0 \sim p^{-3/10}s$.

To predict the size of the micelle formed with a given HEUR moleucule, the free energy of micellization is taken into consideration, which balances the interfacial energy against the energy of stretching the end blocks to form the core, the configurational entropy, and excluded-volume interactions of the soluble chains that form the corona. Minimizing the free energy sets the most probable size of the micelle, in terms of the average aggregation number and micellar radius. In fact, the aggregation number is predicted to depend on both the hydrophobe size and the chain length of telechelic polymers, and also weakly on polymer concentrations probably due to the screening of excluded volume effect at high

concentrations [7]. The statement is supported by experimental observation [7] and in contrast to Annable's model, which assumes constant and small aggregation number.

Normally two star polymers in good solvent repel each other due to excluded volume effect. However, flower-like micelles *attract* each other because of the entropy gain from the exchange of end blocks between cores of flower-like micelles [4-6]. This exchange of end blocks doubles the configurations available to the hydrophobes, and thereby reduces the free energy for micelles by roughly 1 kT per chain in the area of contact (Figure 1.3C, right). Assuming that two spherical micelles overlap by $\xi_0/2$, the density of bridging chain in the contact area should be the overlap area of $\pi\xi_0 R$ divided by the area per blob ξ_0^2. And the attraction energy can be estimated as: $\frac{Ea}{kT} = \pi\frac{R}{\xi_0} \sim p^{1/2}$, correlating the interaction between micelles with the aggregation number p [5]. When p is large, which is often observed with HEURs [7], the attraction energy between micelles becomes large as well. A phase separation of HEUR solution into a macrophase of densely packed "flowers" where the micelles are connected by bridges and a dilute macrophase with little isolated micelle is predicted by the theory and later proved experimentally [4,5].

From the point of view of micellar structures, the solution viscoelasticity should depend on the interaction between micelles, which is determined by both the entropy and excluded volume of the polymer chain. By combining the intermicellar potential mentioned above with the formalism developed for relating the modulus to pair potentials for colloidal dispersions, an expression is obtained depicting a high-frequency modulus (G_∞) that varies with micellar size, volume fraction, and aggregation number:

$G_\infty \sim kTp^{3/2}f(\varphi)N_0/R_H^3$,

where R_H is the hydrodynamic radius of an isolated micelle and N_0 refers to the number of nearest neighbors and can be calculated from volume fraction and intermicellar energy [6]. In other words, the theory argues that the origin of the high-frequency modulus is the pairwise interacting potential between micelles, which is ultimately determined by the micelle structure (size, aggregation number, *etc.*).

Compared to reversible network theory, the interacting micelle theory covers the micellization phenomenon in dilute condition and connects the interaction between micelles with the dynamic of micelle solutions at intermediate concentrations: the dissociation/association kinetics of the hydrophobe controls the relaxation time and viscosity, while the modulus depends on the interaction potential between micelles, which includes excluded volume effects. Presumably, the structure and behavior reach the reversible network limit when all chains form bridges and excluded volume interactions are fully screened.

1.1.2.3 Comparison between reversible network theory and interacting micelle theory

In summary, reversible network theory treats the micelle solutions as a simple network, with its relaxation and viscosity controlled by the dissociation/exchange process of the hydrophobic ends. To account for the non-linear concentration dependence of the high-frequency modulus, Annable *et al* introduced the concept that more loops are transformed to bridges as the concentration increases, leading to a higher number of elastically effective chains. The same argument also explains the concentration dependence of the relaxation time. On the other hand, interacting micelle theory focuses on the molecular structure of the micelle solutions and relates the viscoelasticity with the basic structural parameters, including the aggregation number and the size of the micelles. It points out that the excluded volume effect should be taken into consideration in the interaction between micelles and in the contribution to the high-frequency modulus. The specific issues covered in these two types of theories are summarized in Table 1.1.

Table 1.1 A comparison between the reversible network theory and interacting micelle theory in terms of the issues covered.

	Reversible Network Theory	Interacting Micelle Theory
Large aggregation number	No	Yes
Concentration dependence of high-frequency modulus	Yes	Yes
Concentration dependence of relaxation time	Yes	No
Dependence of aggregation number on chain length	No	Yes
Dependence of aggregation number on concentration	No	Indirect

Despite the discrepancy in some other assumptions of these theories, one thing that should be noted is that both the reversible network theory and the interacting micelle theory assume that the aggregation number of end groups within a micelle core does not change with temperature, which is in agreement with the experimental data showing no temperature-dependent topological change.

1.2 Literature on complementary-associative telechelic polymers

Since the 1990s, the combination of supramolecular chemistry and polymer science has emerged in the form of supramolecular polymer chemistry to improve material characteristics of conventional polymers, conferring better capacity for processing and sensitivity to various environmental stimuli (including temperature, ion content, and redox reaction, etc.)[12-14]. The interactions exploited the most in supramolecular polymer chemistry are metal coordination and hydrogen bonding [12,15].

Numerous end motifs capable of complementary association have been synthesized and utilized for supramolecular chemistry (Figure 1.4). Hydrogen bonding is an ideal interaction as it provides excellent directionality, sensitivity to heat, and tunable binding strength and reversibility [12,14]. The telechelic polymers utilizing hydrogen bond association may behave as thermoplastic elastomers. The association constants of metal coordination interactions are higher, and thus the metal-linked polymers are more stable. When metal coordination and hydrogen bonding are combined in telechelic polymer systems, orthogonal self-assembly is readily achievable, providing materials with more functions and complexity [15,21,23]. Here, the discussion will focus on the hydrogen bonding interaction, since it is more related to the telechelic systems presented in this thesis.

The most widely applied hydrogen bonding end group is 2-ureido-4[1H]-pyrimidinone (UPy), which is developed by P. Sijbesma *et al.* in 1997, and in fact kick-started the field of supramolecular polymer chemistry (Figure 1.4A) [16]. UPy binds complementarily with itself *via* four hydrogen bonds (thus "self-complementary"), and has an association constant $> 10^7$ M^{-1} in $CDCl_3$ at room temperature. It can be utilized in the small molecule form, assembling into structures resembling linear polymers in bulk [16], or be attached to the end of telechelic polymers, facilitating the construction of block copolymer architectures [17-19].

Other hydrogen bonding units contain two counterparts that associate complementarily, for example 2,7-diamido-1,8-naphthyridine (DAN) with ureidoguanosine (UG), and Hamilton

A. Hydrogen bonding
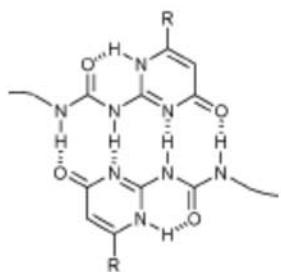
Ureidopyrimidinone (UPy)
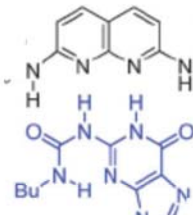
2,7-diamido-1,8-naphthyridine (DAN) + Ureidoguanosine (UG)
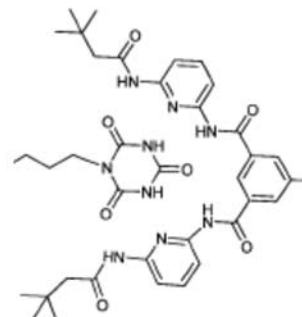
Hamilton receptor (HR) + Cyanuric acid (CA)

B. Metal coordination
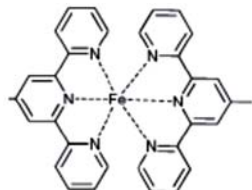
Terpyridine/Fe
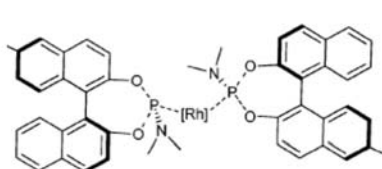
MonoPhos/Rh
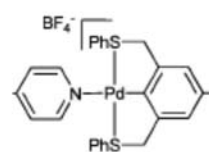
Pyridine/Pd-Pincer

Figure 1.4 Representative reversible complementary associations ([12, 15]).

receptor (HR) with cyanuric acid (CA) (Figure 1.4A) [12,20-22]. They are thus named pairwise-associative ends in this thesis. The stoichiometry of the two types of ends plays an important role in supramolecule formation. When the molar ratio of the two types is 1:1, the pairwise association is complete.

Many synthetic methods have been developed to give access to various monotelechelic, symmetric telechelic and heterotelechelic polymers [12-13, 15-23]. These telechelics then self-assemble into diblock, triblock, and multiblock copolymer architectures, the formation of which have been well documented in literature using techniques including ^{1}H-NMR, viscometry, and DLS [12-13, 15-23]. However, the dynamics of the formed supramolecules has rarely been covered. And systematic investigations are missing on how dynamics of supramolecules can be affected by relevant factors, including polymer concentration, temperature, and polymer chain length, etc [22-23]. These studies are needed since they can both identify the structure-function relationship for supramolecular formation, and serve as a guide for rational design of supramolecules and the related functional materials. The goal of this thesis is to fill in some gaps in this field.

1.3 Mega-supramolecules developed for mist-control and drag-reduction

[Dr. R. L. Ameri David, Dr. Ming-Hsin Wei, Dr. Simon Jones, and Dr. Virendra Sarohia were the pioneers on this project in our group. Their contributions are greatly appreciated. The project will not exist or last without their efforts. Dr. Ming-Hsin Wei is currently working on the commercialization of these polymers as drag-reduction agents.]

Inspired by the development in self-assembly of polymers, our group has designed and studied a series of associative telechelic polymers to develop a fuel additive capable of

mist-control and drag-reduction, but without all the adverse effects that the previously developed polymers have.

Before our telechelic polymers, the polymers used for mist-control and drag-reduction were exclusively ultra-long polymers ($M_w \geq 5,000$ kg/mol). They exhibit dramatic effects on fluid dynamics even at low concentration (e.g., ≤ 100 ppm confers mist control [25-26] and drag reduction [27]). The key to both functions is the ability of polymers to store energy as they stretch, such that the fluid as a whole resists elongation. The high potency of ultra-long linear polymers is due to the onset of chain stretching at low elongation rates and their high ultimate conformational elongation [28]. Unfortunately, ultra-long backbones undergo chain scission during routine handling because hydrodynamic tension builds up along the backbone to a level that breaks covalent bonds; this "shear degradation" continues until the chains shorten to a point that their valuable effects are lost ($M_w < 1,000$ kg/mol) [27]. Assembly of end-associative polymers creates supramolecules that can potentially break and re-associate reversibly, but formation of such mega-supramolecules ($M_w \geq 5,000$ kg/mol) at low concentration has never been realized for two reasons: end-to-end association, at low concentration, predominantly leads to rings of a small number of chains [29-30] and the size of the building blocks is limited because literature suggests that end association is disfavored when they are longer than 100 kg/mol [12,31].

To develop a fuel additive capable of mist-control and drag-reduction, our group focused on supramolecules soluble in low-polarity fluids. Transportation relies on such liquid fuels, presenting the risk of explosive combustion in the event of impact, such as in the 1977 Tenerife airport disaster—an otherwise-survivable runway collision that claimed 583 lives in the post-crash fireball. Subsequent tests of ultra-long, associative polymers (e.g., ICI's

"FM-9," >3,000 kg/mol copolymer, 5 mol% carboxyl units) in fuel increased the drop diameter in post-impact mist [25,32], resulting in a relatively cool, short-lived fire. However, these polymers interfered with engine operation [33], and their ultra-long backbone—essential for mist control—degraded upon pumping [27]. Motivated to solve the above dilemma, our group proposed mega-supramolecules at low concentration that behave like ultra-long polymers, exhibiting expanded ("self-avoiding") conformation at rest and capable of high elongation under flow, and avoid the shear degradation drawback, utilizing the reversible dissociation of the ends to protect the covalent backbone.

Our group realized that to mimic ultra-long polymers, it is most efficient to have association occurring at chain ends and be predominantly pairwise. Recent studies have shown that pairwise association is readily achieved for short chains with $M_w \leq 50$ kg/mol using hydrogen bonding [12,15-16, 34-38]. However, short chain lengths ($M_w \leq 50$ kg/mol) favor rings formation, which provide little rheological contribution (Figure 1.5A, left). And long chain lengths disfavor rings due to high entropy cost in ring closure. Despite prior reports indicating that end association becomes difficult with increasing chain length [11-12,31], our group explored the possibility of forming supramolecules with long telechelic polymers ($M_w \geq 400$ kg/mol) at low concentration (< 1 wt%) (Figure 1.5A, right).

Dr. Ameri David developed a statistical mechanics model based on ring-chain equilibrium theory to guide the selection of molecular structures for supramolecules formation while he was a graduate student in the Kornfield group. The model computed the distribution of cyclic and linear supramolecules as a function of concentration, backbone length, and end-association strength. It predicts that an adequate concentration of mega-supramolecules
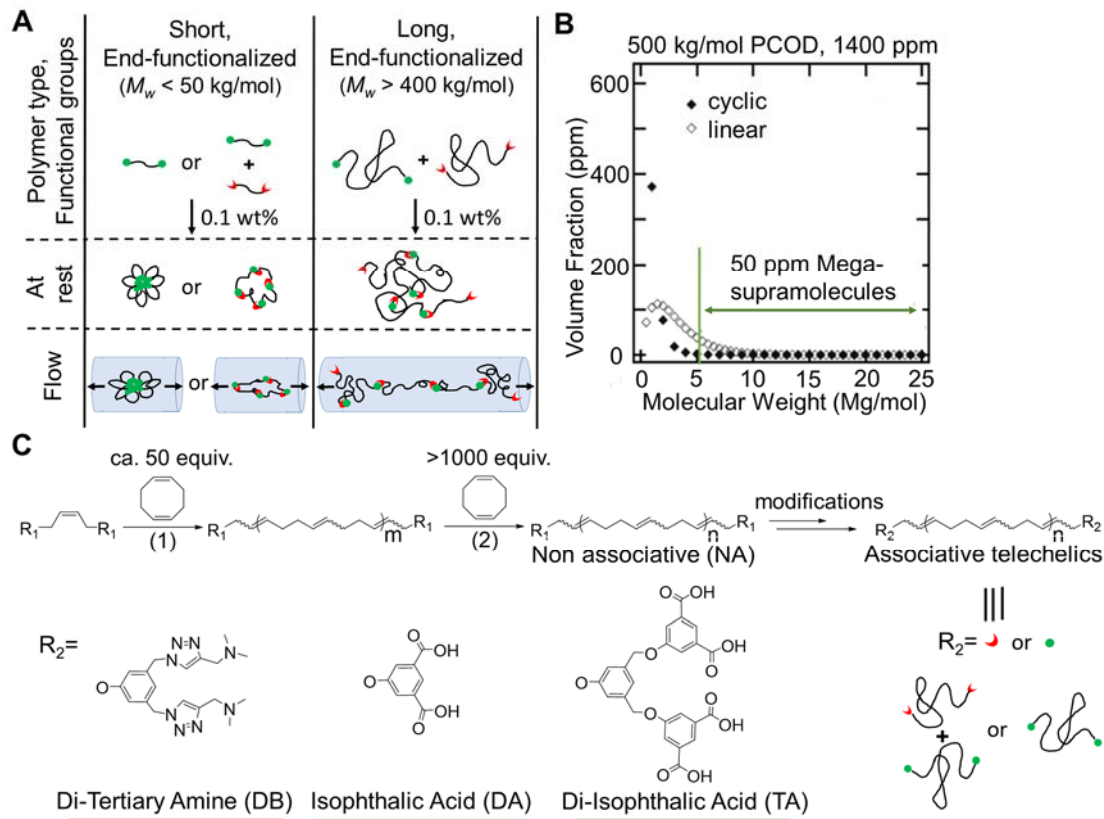
Figure 1.5 A. Proposed assembly of long telechelic polymers into mega-supramolecules (right; linear and cyclic (not shown)) compared to that of prior end-associative telechelics (left) in terms of degree of polymerization (DP) and conformations at rest and in elongational flow. **B.** Ring-chain equilibrium distribution of cyclic (filled) and linear (open) supramolecules. **C.** Synthesis of telechelics (non-associative with R_1 end-groups, chloro- or ester- ended) and post-polymerization conversion to associative telechelics (R_2 end-groups, bottom). (1): Grubbs II, dichloromethane (DCM), 40°C, 1h; (2): Grubbs II, DCM, 40°C, until stir bar stops (>5 min), equivalents of COD for desired molecular weight. DA: di-acid. DB: di-base. TA: tetra-acid.

(e.g., >50ppm of supramolecules with $M_w \geq 5{,}000$ kg/mol [26]) can be formed by long telechelic polymers, with a concentration of 1,400ppm, a backbone length of approximately 6,000 Kuhn segments (M_w=500 kg/mol for polycyclooctadiene, PCOD), and a pairwise type end-association with an energy of 16-18 kT (Figure 1.5B).

To achieve the association energy recommended by the theory, charge-assisted hydrogen bond (CAHB) was chosen [39], which will be described in detail in Section 1.6. Simply

placing two tertiary amines at each end of the "di-base" chains (DB) and two carboxylic acids at each end of the "di-acid" chains (DA) (Figure 1.5C) provides an association strength of 16-18 kT. To obtain the desired telechelic polymers with parameters guided by the model, Dr. Ming-Hsin Wei, when he was a graduate student in the Kornfield group, adopted a two-step ring-opening metathesis polymerization (ROMP) protocol in the presence of a chain transfer agent (CTA) (Figure 1.5C) [40-41], and introduced dendron structure to the end groups, so that discreet numbers of acid/base units (di-functional ends, denoted DA/DB and tetra-functional ends, denoted TA) can be attached to the ends of CTAs and eventually the polymers (Figure 1.5C). Cyclooctadiene (COD) is selected as the monomer because it has an adequate ring strain to drive ROMP and provides a backbone that has both strength [42] and solubility in hydrocarbons. Telechelics of the required length (M_w ≥400 kg/mol, up to 1000 kg/mol if desired) and end functionality (>95%) are thus synthesized. End groups have been installed after polymerization by conversion of ester- or chloride-ended polymers (which serve as non-associative controls, NA), with degrees of conversion >95% (Figure 1.5C).

The formation of mega-supramolecules is evident from solution viscosity and multi-angle laser light scattering (MALLS) measurements. Shear viscosities show that our longer telechelics do associate into supramolecules (e.g., at 2 mg/ml in cyclohexane, 300k DA/DB gives a shear viscosity comparable to 670k NA, Figure 1.6A; this holds for the solvents tetralin and Jet-A, as well, Figure 1.6B). Multi-million molecular weight supramolecules are confirmed by MALLS (Figure 1.6C). At concentrations as low as 0.22mg/ml (0.028%wt), 670 kg/mol pairwise-associative telechelic polymers form supramolecules with an apparent M_w of 2,200 kg/mol (Figure 1.6C). Small angle neutron scattering (SANS)

confirms that the supramolecules formed by pairwise end-associative polymers exhibit expanded conformation. The conformation on length scales up to the radius of gyration (R_g) of the individual chains is just as open for end-associative chains as it is for the corresponding non-associative chains: at $q>2\pi/R_g\approx0.03$ 1/Å their scattering patterns coincide (Figure 1.6D). Together, MALLS and SANS reveal the molecular basis of the
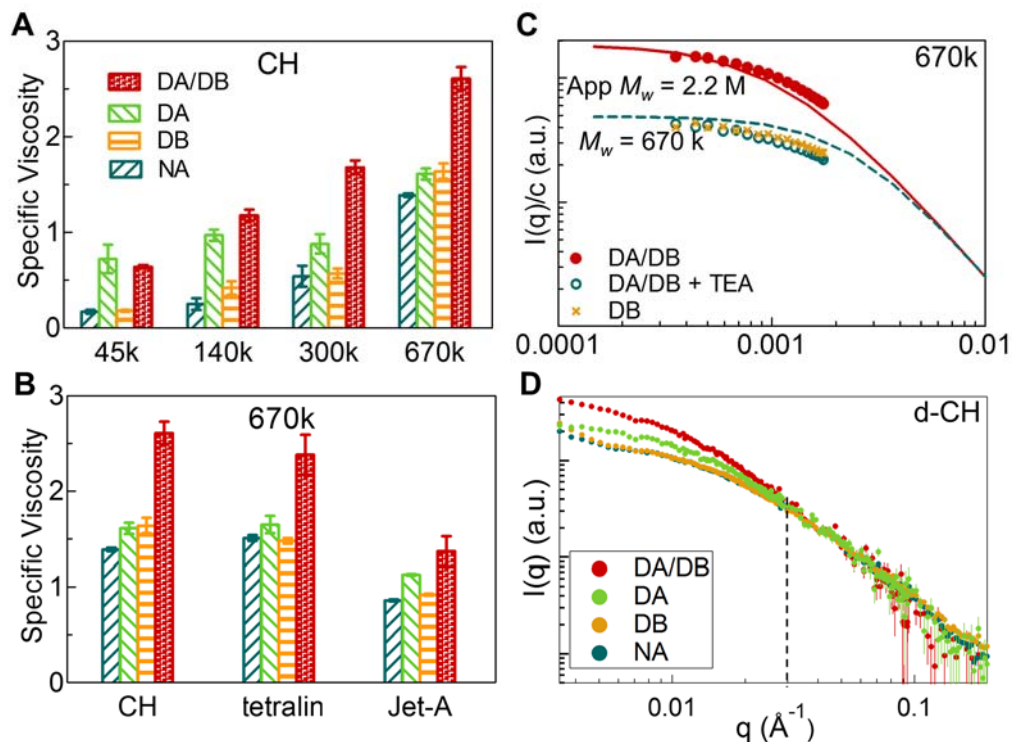
Figure 1.6 Evidence of supramolecules in solutions of eqimolar mixture of α,ω-di(isophthalic acid) and α,ω-di(di(tertiary amine)) polycyclooctadienes (DA/DB). A. Effect of telechelics size (k ≡ kg/mol) on specific viscosity of supramolecular solutions and controls in cyclohexane (CH) at 2 mg/ml (0.25%wt, 25°C). **B.** Effect of solvent on specific viscosity for 2 mg/ml (0.25%wt) solutions (25°C) of telechelics having M_w=670k due to both polarity and solvent quality for the backbone. **C.** Static light scattering (35°C) shows that association of ~670k DA with DB chains in CH at 0.22mg/ml (0.028%wt) produces supramolecules (filled) with an apparent M_w greater than 2,000 kg/mol, which separate into individual building blocks (x) when an excess of a small-molecule tertiary amine is added (open symbols, 10 ul/ml of triethylamine, TEA). Curves show predictions of the model for complementary telechelics 1,000 kg/mol in solution at 1400 ppm (solid, supramolecules; dashed, non-associated telechelics). **D.** Concentration-normalized SANS intensities (25°C) for 50k telechelics in d12-cyclohexane at concentrations well below the overlap concentration of NA (2 mg/ml for NA and DB; 0.05 mg/ml for DA and DA/DB).
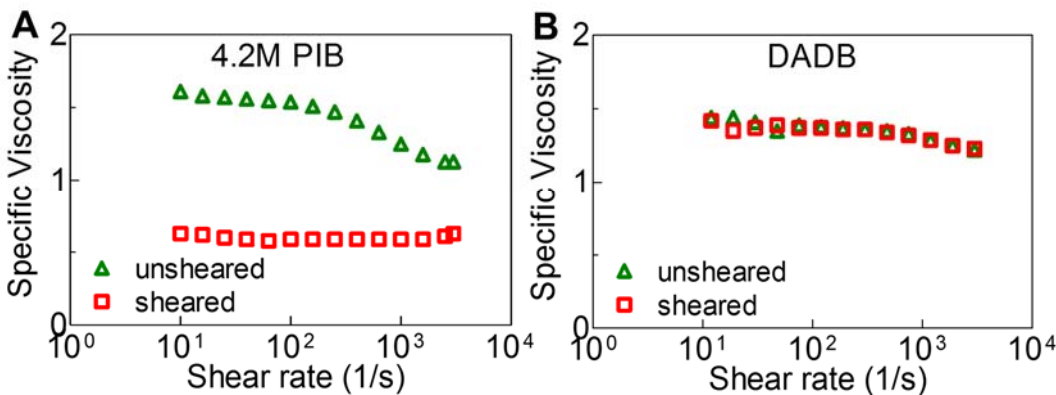
Figure 1.7 A. The decrease of specific viscosity for 4.2M PIB 1.6 mg/ml (0.2%wt) in Jet-A at 25°C after approximately 60 passes through a Bosch fuel pump (sheared) relative to as-prepared (unsheared) indicates shear degradation. **B.** Specific viscosities of 2.4 mg/ml (0.3%wt) of a 1:1 molar ratio of α,ω-di(isophthalic acid) and α,ω-di(di(tertiary amine)) polycyclooctadienes (~670kg/mol DA/DB) in Jet-A at 25°C, sheared *vs.* unsheared.

rheological behavior (Figure 1.6A-B)—complementary end association into mega-supramolecules with expanded conformations.

These mega-supramolecules were then tested for drag-reduction and mist-control effects, and proved to be effective. Unlike ultra-long polyisobutylene (4.2M PIB, 4,200 kg/mol) (Figure 1.7A), LTPs survive repeated passage through a fuel pump (Figure 1.7B) and allowed fuel to be filtered easily. Experiments under turbulent pipe flow compare the drag-reduction effect of an ultra-long polymer with that of mega-supramolecules: for a given pressure drop, the increase of volumetric flow rate with telechelic polymers (670k DA/DB at 0.1%wt) is comparable to that with ultra-long linear polyisobutylene (4,200 kg/mol PIB at 0.02%wt)—with the distinction that telechelic polymers retain their efficacy after multiple passes. Similarly, high-speed impact experiments designed by Dr. Virendra Sarohia show that, unlike ultralong PIB, mega-supramolecules retain their efficacy in mist-control after repeated passage through a fuel pump. For untreated Jet-A fuel, the impact conditions generate a fine mist through which flames rapidly propagate into a hot fireball

within 60 ms. Polymer-treated fuel samples are tested in two forms: as prepared ("unsheared") and after approximately 60 passes through a fuel pump ("sheared"). Ultra-long PIB (4,200 kg/mol, 0.35%wt) is known to confer mist control that prevents flame propagation (Figure 1.8A, top left); however, "sheared" PIB loses efficacy (Figure 1.8A, top right). Telechelic polymers (TA) provide mist control both before and after severe shearing (Figure 1.8A, bottom), confirming their resistance to shear degradation. Moreover,
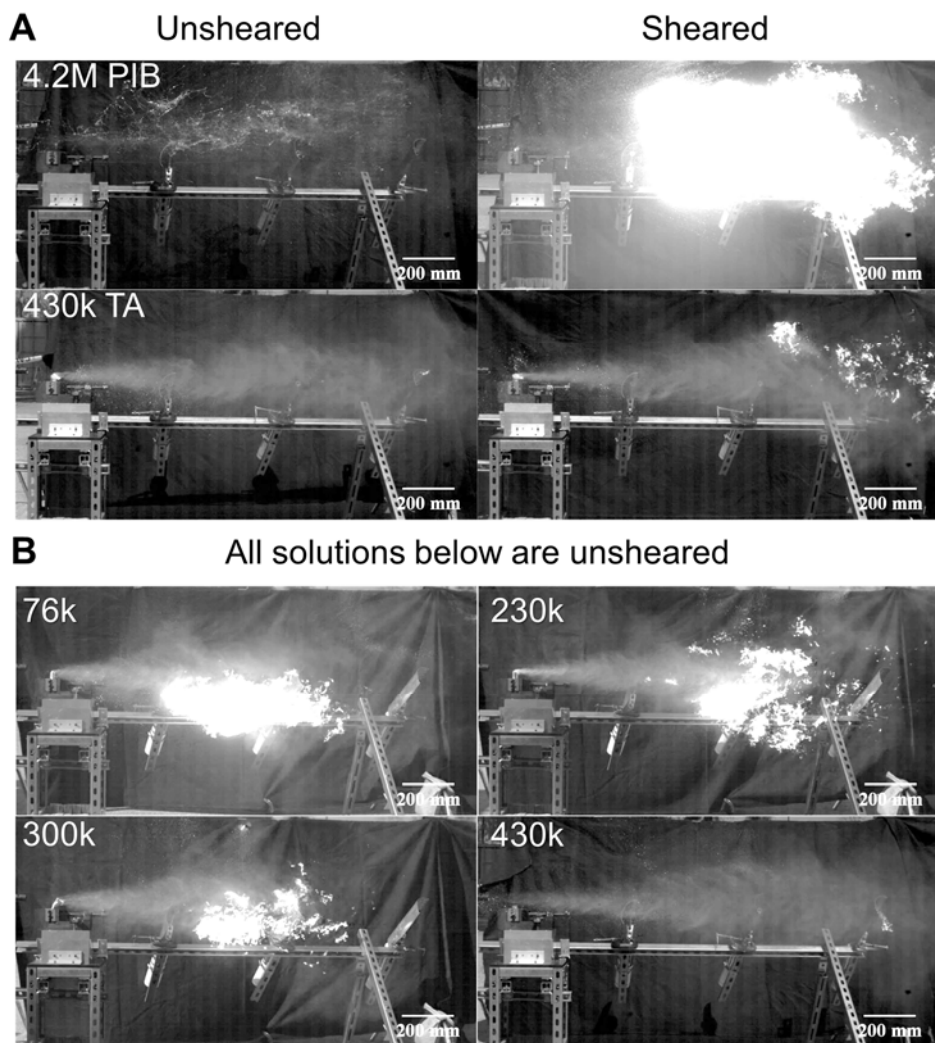
Figure 1.8 Impact test in the presence of ignition sources (60 ms after impact, maximal flame propagation) for Jet-A solutions treated with 4.2M PIB or α,ω-di(di-isophthalic acid) polycyclooctadienes (TA). **A.** Jet-A with 4.2M PIB (0.35% wt) and Jet-A with 430k TA (0.3% wt), "unsheared" and "sheared" as in Figure 1.7. **B.** Effect of TA molecular weight (76 kg/mol to 430 kg/mol) in Jet-A at 0.5% wt (unsheared).

the test also proves that chain length of the telechelics plays a crucial role in mist control (Figure 1.8B), consistent with the hypothesis that mega-supramolecules are the active species conferring the observed effect.

In summary, long telechelic associative polymers with the end-association strength (16-18 kT) and chain lengths ($M_w \geq 400$ kg/mol) predicted by theory have been developed and found to indeed form mega-supramolecules even at low concentration. They cohere well enough to confer benefits typically associated with ultra-long polymers—including mist control and drag reduction. These mega-supramolecules reversibly dissociate under flow conditions that would break covalent bonds, allowing the individual long telechelic associative polymers to survive pumping and filtering.

1.4 From mist control to polymer physics

As mentioned above, our group developed associative telechelic polycyclooctadiene (PCOD) ended with acid and tertiary amine for mist control application. The isophthalic acid-ended polycylcooctadiene (DA-PCOD) can associate with itself through its acid ends. When amine-ended polymer is added into the mixture, isophthalic acid preferably associates pairwisely with tertiary amine due to the higher binding strength of charge-assisted hydrogen bond (see details in Section 1.6). And the 1:1 molar ratio mixture of isophthalic acid-ended and tertiary amine-ended PCOD (DA/DB-PCOD) is referred to as pairwise-associative telechelic polymers.

Despite the extensive studies on both self-associative system and pairwise-associative system in literature, the comparison between the dynamics of these two systems has never been performed in literature because of the fundamentally distinct association mechanism

(hydrophobic interaction, or ionic interaction for self-association *versus* metal coordination or hydrogen-bonding for pairwise-association). The telechelic PCOD systems described here have exactly matching backbone and only half of the end groups are different ($< 0.5\%$ of total weight), providing the opportunity for systematic comparison between these two systems (DA-PCOD *versus* DA/DB-PCOD).

Although the work described above has focused on the mist-control effect of these telechelic polymers, the viscometry and SANS results indeed indicate that the fundamental association pattern of DA-PCOD and DA/DB-PCOD differs, even though only < 0.5 wt% of the chemical composition is changed by adding equiv. molar of DB-PCOD. Some more questions are thus generated, as listed below. It was fascinating to me to dig deeper into the physics of their association in solutions and interpret the underlying structure-function relationship, which I hope will facilitate the rational design of supramolecules in the future.

1) Are the association mechanisms of DA-PCOD and DA/DB-PCOD solutions qualitatively different?

2) The association of DA-PCOD is called self-association because it literally binds with itself. However, is the association self-complementary in nature, like the case with UPy? Or does it make contact to other traditional self-associative telechelic polymers, including hydrophobically modified urethane-ethoxylates (HEURs), which are based on multimeric association? If it is multimeric, is the association of DA-PCOD due to hydrogen bonds, or the micro-phase separation brought by low solubility of acid in non-polar solvents?

3) Pairwise-associative polymers (DA/DB-PCOD) are supposed to form linear and cyclic supramolecular species. How are these supramolecules similar and different from linear covalent polymers, in terms of topology and dynamics?

4) Temperature, concentration and polymer chain length have known to be important factors that affect the conformation and dynamics of polymer systems. The previous work focuses on the behavior of these telechelic polymers at room temperature in dilute conditions. How do the DA-PCOD and DA/DB-PCOD systems respond to various temperatures, concentrations and chain lengths?

I performed a series of dynamics and conformational studies to answer these questions, which will be illustrated in following chapters. To provide a foundation for the discussion of our self- and pairwise-associative telechelic polymers, some basic concepts are reviewed relevant to these polymer systems, for example the conformation and dynamics of linear covalent polymer solutions (Section 1.5), and properties of hydrogen bonds (Section 1.6).

1.5 Conformation and dynamics of linear covalent polymer solutions

1.5.1 Concentration regimes and length scales

Polymer concentration is an important parameter describing the property of polymer solutions, which can be expressed in various units, including volume fraction φ and weight percent concentration C (in w/w%, or say wt%). Volume fraction φ is more frequently used for polymer physics theories. When the polymer concentration is low, the weight of polymer in the solution is negligible compared to the solvent weight; thus C is proportional to volume fraction φ, with the ratio of polymer density (ρ_{pol}) divided by solvent density (ρ_{sol}) as a coefficient: $C = \varphi (\rho_{pol}/ \rho_{sol})$. The weight percent concentration C will be utilized

in the thesis because the polymer concentrations used here are all low enough that C has almost the same scaling dependence as the volume fraction φ in the theory, and C is easier to manage for solution preparation.

Polymer solutions can be divided to several regimes according to their polymer concentration [43]. These concentration-based regimes give rise to different length scales in polymer chains, within which the polymer conformation and dynamics show distinct features. Polymer solutions in different concentration regimes thus exhibit distinct rheological behavior.

In dilute solutions of a good solvent, each individual polymer chain is far from each other and exhibits self-avoiding walk conformation with radius of gyration $Rg \sim bN^{0.588}$, where b is the Kuhn segment length and N is the number of Kuhn segments that one polymer
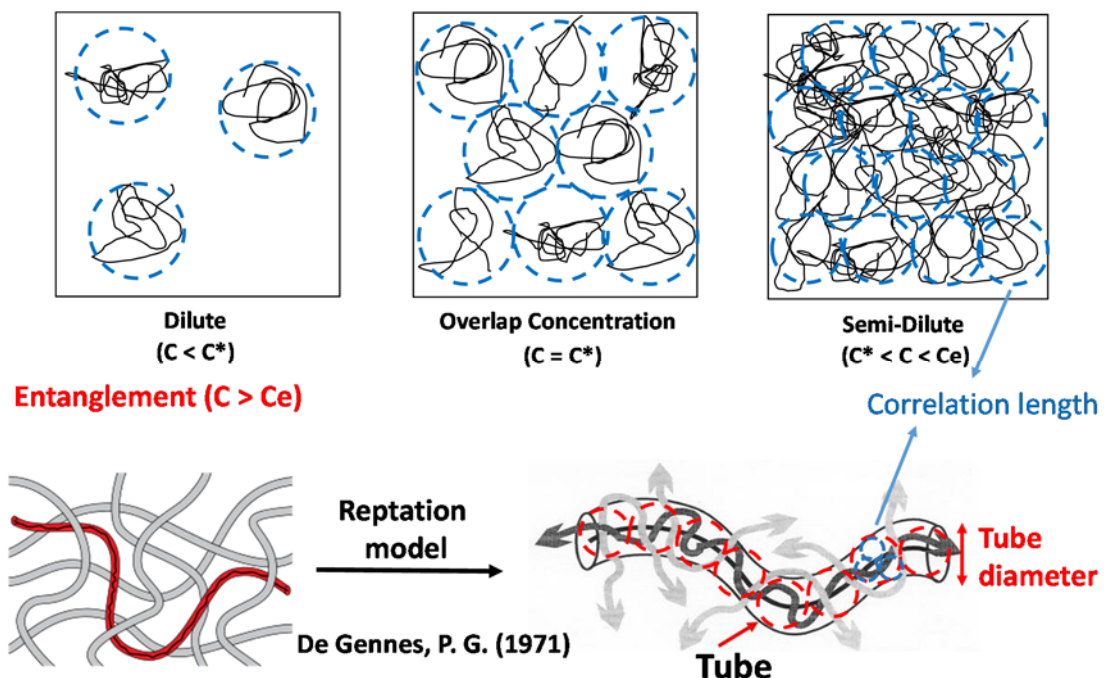
Figure 1.9 Schematics of the concentration regimes of dilute, semidilute unentangled, and semidilute entangled regimes. Purple line represents one polymer coil that spans several correlation blobs in semidilute solutions.

contains (Figure 1.9, top left). Overlap concentration (C^*, C refers to w/w%, or say wt%, in the following text) is the critical concentration at which the total pervaded volume of all polymer chains equals the volume of the solution (Figure 1.9, top middle). Since at the overlap concentration the pervaded volume of polymers is space-filling, the volume fraction of polymer within its pervaded volume is the same as the total volume fraction in the solution. Therefore, overlap concentration is connected to the chain length through a power law relationship: $C^* \approx \varphi^* \approx Nb^3/R^3 \approx Nb^3/(N^\nu b)^3 \approx N^{1-3\nu} \sim N^{-0.76}$ for $\nu = 0.588$ in good solvent. The solvent quality and the excluded volume effect is enhanced by high temperature, and therefore the overlap concentration decreases with increasing temperature. For athermal solvent, the overlap concentration does not depend on temperature.

As polymer concentration increases beyond C^*, chains start to interpenetrate and the solution is called semidilute (Figure 1.9, top right). A critical length scale comes up for semidilute solutions: the correlation length, ξ. Monomers within the correlation length are from the same polymer chain, while monomers beyond the scale are indistinguishable in terms of their origin, in which case both the excluded volume effect and the hydrodynamic force are screened. Therefore, the polymer chain conserves self-avoiding walk conformation within ξ, but behaves as an ideal chain at length scale larger than ξ. Assuming the correlation blob of size ξ contains g Kuhn monomers, and because swollen conformation persists within the length scale of ξ, ξ should obey the following relationship: $\xi = bg^\nu$. On the other hand, the correlation volumes are space-filling. Therefore, the volume fraction of polymer within the correlation volumes should be the same as the volume fraction of polymer in the whole solution: $\varphi = gb^3/\xi^3$. Generalizing the above two equations

on ξ and φ, the concentration dependence of ξ is thus: $\xi \approx b\varphi^{-v/(3v-1)} \approx bC^{-v/(3v-1)}$. The correlation length thus decreases with increasing polymer concentration.

As the concentration increases even further, beyond another critical concentration (entanglement concentration, C_e), each polymer chain is topologically constrained by the others because they cannot cross each other (Figure 1.9, bottom). The phenomenon is called entanglement. Solutions with $C > C_e$ are called semidilute entangled solutions, and the ones with $C^* < C < C_e$ are called semidilute unentangled solutions. The quantitative expression for C_e will be discussed more in details in Section 1.5.3.2.

The most widely accepted and utilized theory on entangled polymers is Edwards' tube model [44], which treats the collective confinement as a tube-like constraining potential, restricting the polymer chain inside. The minima of the constraining potentials lie in the middle of the tube structure, and is called the primitive path. A polymer chain can only diffuse along the tube (called "reptation") while the transverse motion is constrained. The tube is described by tube diameter, a, within which the free energy of polymer chain's transverse fluctuation is on the order of kT. Tube diameter (a) depends on both the polymer concentration and an intrinsic property of polymer backbone, entanglement molar mass ($M_e = N_e M_0$, M_0 is the molar mass for a Kuhn segment): $a(C) \approx a(1)C^{-v/(3v-1)} \approx bN_e(1)^{1/2}C^{-v/(3v-1)} \approx bN_e(1)^{1/2}C^{-0.76}$ for good solvent. Within different length scales separated by the correlation length (ξ) and the tube diameter (a), the polymer chain relaxes differently, the details of which will be covered in Section 1.5.3.2.

1.5.2 Molecular models for the dynamics of polymers

Dynamics describes the motion of bodies under the action of forces. In solutions, a small colloidal particle experiences fluctuations of the number of solvent molecules hitting it randomly from different directions, resulting in its Brownian diffusion. The Stokes-Einstein-Sutherland law of diffusion gives an expression for the diffusion coefficient of a spherical particle in a liquid: $D = \frac{kT}{6\pi\eta R}$, in which η is the viscosity of the liquid and R is the radius of the particle. A polymer is a large molecule connected with many repeating units, which is more complicated compared to a simple colloidal particle. Many molecular models have been developed for the dynamics of polymers, including Zimm model, Rouse model, and reptation model (see below).

1.5.2.1 Zimm model

When a particle is moving through the solvent, it drags some of the surrounding solvent molecules with it, and these molecules, in turn, impart force on other particles within a certain range. This long-range force acting on solvent molecule and other particles that arises from the diffusion of one particle is called hydrodynamic interaction. In dilute solutions of polymers, the hydrodynamic interaction between monomers plays a significant role and cannot be neglected. Therefore, Zimm model [45] treats the pervaded volume of the whole polymer chain as a solid object, with the size $R \approx bN^v$ (Figure 1.10A). The friction coefficient for this solid object in a solvent with viscosity η_s is then $\zeta_Z \approx \eta_s R$. According to Einstein relation, its diffusion coefficient is inversely proportional to the friction coefficient: $D_z = \frac{kT}{\zeta_Z} \approx kT/(\eta_s R) \approx kT/(\eta_s bN^v)$. The characteristic time is then named the Zimm time τ_Z, during which a polymer chain diffuses a length scale of the order of its own size. It can be calculated as the following: $\tau_Z \approx R^2 / D_z \approx \frac{\eta_s}{kT} R^3 \approx \frac{\eta_s}{kT} b^3 N^{3v} \approx \tau_0 N^{3v}$, in which $\tau_0 = \frac{\eta_s}{kT} b^3$.
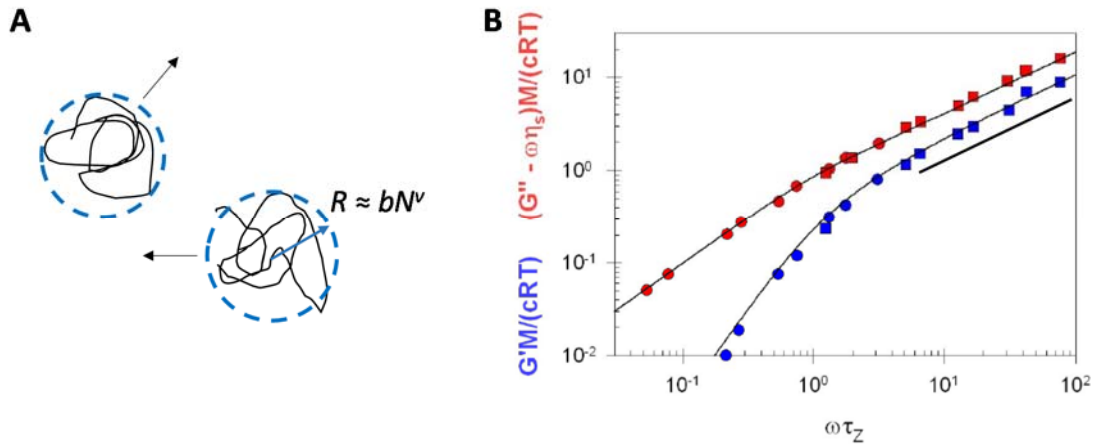
Figure 1.10 A. Schematic representation showing that Zimm model treats the pervaded volume of the whole polymer chain as a solid object with the size $R \approx bN^v$. **B.** (Figure reproduced from reference [47]) Linear viscoelastic response expressed in terms of reduced moduli, for dilute polystyrene (MW = 860 kg/mol) solutions in two θ-solvents [46]. Red are reduced loss moduli, blue are reduced storage moduli, circles are in decalin at 16 ℃, squares are in di-2-ethylhexylphthalate at 22 ℃. Curves are predictions of the Zimm model with $v = ½$ (Fig. 8.7 in [43]). The black line reflects a slope of 2/3.

Since polymers are fractal objects, a section consisting of g monomer relaxes the same way as the whole chain. The relaxation of a polymer chain is composed of N different relaxation modes, each with a mode index p (p=1,2,3,…,N); and mode p contains N/p beads. Each mode has its own relaxation time $\tau_p \approx \tau_0 (N/p)^{3v}$, by which time p modes have not yet relaxed. Each unrelaxed mode contributes energy of order kT to the stress relaxation modulus, giving the following scaling law: $G(t) \approx (kT/b^3) \, C \, (t/\tau_0)^{-1/(3v)}$, for $\tau_0 < t < \tau_Z$. At time scales longer than the Zimm time, τ_Z, the stress relaxation modulus decays exponentially. An excellent approximation of the stress relaxation modulus covering the full time scale is therefore the product of the power law equation shown above and an exponential cutoff: $G(t) \approx (kT/b^3) \, C \, (t/\tau_0)^{-1/(3v)} \exp(-t/\tau_Z)$, for $t > \tau_0$ [43]. In oscillatory shear experiments, the Zimm model predicts that G'(ω) and G''(ω) both exhibit a power law dependence on the

frequency in the intermediate frequency regime: $G'(\omega) \sim G''(\omega) \sim \omega^{1/3\nu}$, for $1/\tau_Z \ll \omega \ll$

$1/\tau_0$, while $G' \sim \omega^2$ and $G'' \sim \omega$ in the terminal region depict pure liquid behavior.

According to the above calculation, in a θ-solvent ($\nu = \frac{1}{2}$), the Zimm time is proportional

to the chain length (N) to the order of 3/2, and the storage and loss modulus (G' and G'')

should present in the form of two parallel lines with a slope of 2/3 in a log-log plot against

frequency. This prediction has been well proved experimentally by the dynamics of dilute

polystyrene solutions in two θ-solvents [46] (Figure 1.10B). For good solvent ($\nu = 3/5$), the

Zimm time is predicted to be proportional with the chain length (N) to the order of 9/5, and

the storage and loss modulus (G' and G'') curves should have a slope of 5/9. Unfortunately,

the Zimm model's prediction in the case of good solvent is less straightforward, possibly

due to the fact that the excluded volume effect diminishes the hydrodynamic force [47]. In

summary, the Zimm model takes the long-range hydrodynamic interaction into account,

and applies to the dynamics of polymer dilute solutions.

1.5.2.2 Rouse model

In the Rouse model, the polymer is seen as being a chain composed of N beads connected

with springs [48] (Figure 1.11A). Each bead feels the friction from the solvent

independently with friction coefficient ζ. The solvent is assumed to be freely draining
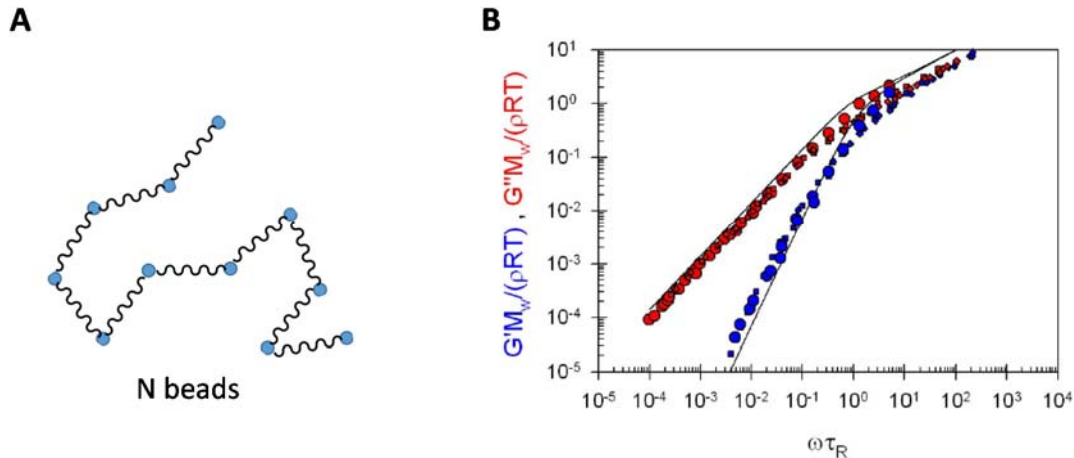
Figure 1.11 A. Schematic representation showing that Rouse model treats the polymer chain as N beads connected by springs, each with its own friction coefficient. **B.** (Figure reproduced from reference [47]) Plot of reduced moduli against $\omega\tau_R$, for unentangled polystyrene melts at 160 ℃ [49]. Red are reduced loss moduli, blue are reduced storage moduli, large circles are M_w =8900 g/mol, small squares are M_w = 14800 g/mol, small diamonds are M_w = 28900 g/mol. Curves are predictions of the Rouse model.

through the chain as the chain diffuses, which means that hydrodynamic effect is neglected.

The total friction coefficient of the whole chain is $\zeta_R = N\zeta$. The Rouse time (τ_R), during which the polymer diffuses a distance of its own size, is thus related to N with the following power law: $\tau_R \approx \frac{\zeta}{kT} NR^2 \approx \frac{\zeta}{kT} b^2 N^{1+2\nu} \approx \tau_0 N^{1+2\nu}$, in which $\tau_0 = \frac{\zeta}{kT} b^2$, describing the motion of an individual bead, and ν is the reciprocal of the fractal dimension of polymer. For ideal chains, $\nu = \frac{1}{2}$, τ_R is proportional to the square of N: $\tau_R \approx \tau_0 N^2$.

The scaling argument described above for the relaxation models in the Zimm model can be applied to the Rouse model as well. Each mode has its own relaxation time $\tau_p \approx \tau_0 (N/p)^2$, by which time p modes have not relaxed yet. Each unrelaxed mode contributes energy of order kT to the stress relaxation modulus, giving the following scaling law: $G(t) \approx (kT/b^3)$ $C (t/\tau_0)^{-1/2}$, for $\tau_0 < t < \tau_R$. At time scales longer than the Rouse time τ_R, the stress relaxation modulus decays exponentially. An excellent approximation of the stress relaxation

modulus covering the full time scale is therefore a product of the power law equation shown above and an exponential cutoff: $G(t) \approx (kT/b^3) \, C \, (t/\tau_0)^{-1/2} \exp(-t/\tau_R)$, for $t > \tau_0$. In oscillatory shear experiments, the Rouse model predicts an equal value for $G'(\omega)$ and $G''(\omega)$ with a power law dependence on the frequency in the intermediate frequency regime: $G'(\omega) = G''(\omega) \sim \omega^{1/2}$, for $1/\tau_R \ll \omega \ll 1/\tau_0$.

The success of Rouse model in the melts of polymers that are too short to entangle is evident experimentally (Figure 2.11B). The storage and loss moduli are divided by a factor of $\rho RT/M$ (ρ is the mass density), which is the time-independent term in equation for stress relaxation modulus. The reduced moduli are plotted against $\omega \tau_R$ for the melt of polystyrene chains with three chain lenths (M_w=8.9, 14.8 and 28.9 kg/mol) at a reference temperature of 160 ℃ [49]. All three molecular weights are close to the entanglement molecular weight (M_e = 17 kg/mol), and are generally considered too small to develop significant entanglement. As shown in Figure 2B, these data sets do show the slope of ½ at high frequencies, as expected by Rouse model. It has been proved that Rouse model applies for the situations when hydrodynamic force is screened, including certain length scale in semidilute solutions unentangled polymer melt [43].

1.5.2.3 Reptation model

De Gennes proposed the reptation model in 1971 [50] to describe the dynamics of entangled polymers, utilizing the Edward's tube model [44]. Recall Edward's tube model as a tube-like constraining potential, restricting the polymer chain inside (Figure 1.12A), and the primitive path as the minima of the constraining potentials lie in the middle of the tube structure. A polymer chain can only diffuse freely along the tube, and its transverse fluctuation is confined around the primitive path with a free energy on the order of kT. The

thermal energy thus defines the width of the tube, called the tube diameter a. The tube diameter for polymer melt is labeled $a(1)$, while the one for semidilute entangled solutions at concentration C is named $a(C)$, which will be covered later.

Since polymer chains behave ideally in a polymer melt, the number of Kuhn segments within the length scale of one tube diameter should follow the relationship: $a(1) \approx bN_e(1)^{1/2}$. And the strand containing $N_e(1)$ Kuhn segments, named an entanglement strand, is generally considered a basic unit for entanglement development and for network elasticity. A polymer chain can be considered a random walk constituted by $N/N_e(1)$ entanglement strands of size a: $R \approx a\sqrt{N/Ne(1)}$. The average contour length <L> for the primitive path can also be calculated as a product of the entanglement strand size and the number of strands: $<L> \approx a\ (N/N_e) \approx bN/\sqrt{Ne(1)}$.

With all the length scales in hand, the diffusion pattern of an entangled polymer chain can be discussed. De Gennes' reptation model [50] suggests that within the length scale of a tube diameter a, or say an entanglement strand, the chain does not feel the topological constraint and follows the Rouse dynamics with a relaxation time $\tau_e \approx \tau_0\ N_e^2$. At length scale larger than the tube diameter, the chain can only diffuse curvilinearly along the primitive path within the tube following Rouse diffusion coefficient: $D_c \approx \frac{kT}{N\zeta}$. Similar as in the other molecular model, the longest relaxation time corresponds to the time scale that a chain moves a distance on the order of its own size. Since the diffusion in entangled situation is limited to reptation-like motion, it refers to the time that a chain needs to diffuse out of the contour length of the tube, which is called reptation time: $\tau_{rep} \approx <L>^2/D_c \approx$

$(b^2N^2/N_e(1)) \frac{N\zeta}{kT} \approx \frac{\zeta}{kT} b^2\ N_e(1)^2\ (\frac{N}{Ne(1)})^3$.
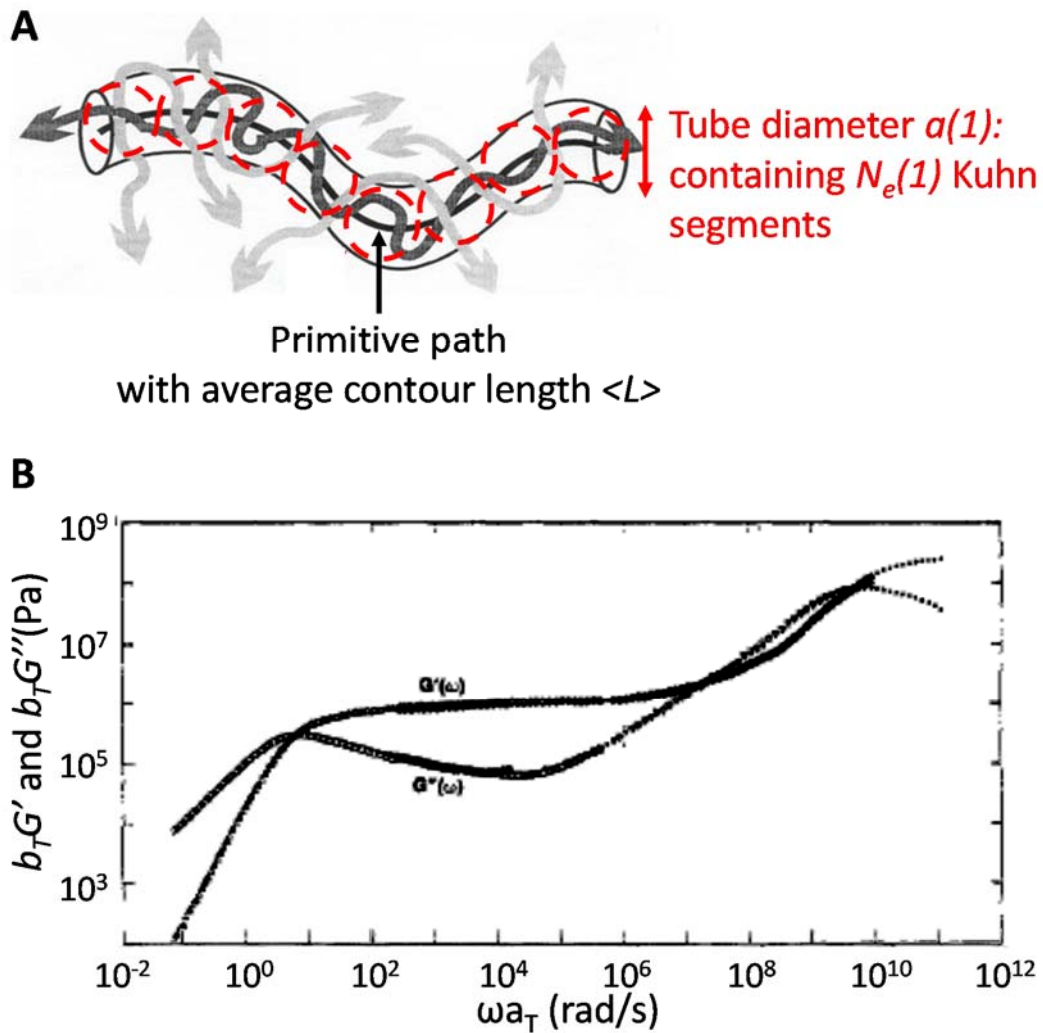
Figure 1.12 A. Schematic representation of Edwards' tube model. **B.** (Figure reproduced from reference [52]) Dynamic modulus master curves for 1,4-polybutadiene *(M_w = 130 kg/mol)* at the reference temperature $T = 25\,℃$.

Thus reptation model predicts that the reptation time τ_{rep} is proportional to cube of polymer length, which is in close approximation to the scaling exponent experimental measurement $\tau \approx M^{3.4}$. To capture the discrepancy between 3 and 3.4, some modifications of the reptation model were later proposed, named tube length fluctuation [51]. In analogy to chemically crosslinked network [24], each entanglement strand, with its molecular weight of M_e, contributes $1kT$ to the plateau modulus of high molecular weight polymer melt (G_e): $G_e =$

$\rho RT/M_e$. The stress relaxation prediction, including the reptation time and plateau modulus, by reptation model agrees fairly well with experimental results with entangled polymer melt (Figure 1.12B) [52]. In fact, the entanglement molecular weight (M_e) is considered as an intrinsic characteristic specific to one polymer backbone, and is usually calculated through the plateau modulus (G_e) of the melt of that type of polymer with high molecular weight: $M_e = \rho RT/G_e$, since G_e is easier to measure. Besides the melt of high molecular weight polymers, reptation model is also applied to the entangled polymer solutions in the semidilute regime, which will be discussed next.

1.5.3 Dynamics for polymer solutions in the semidilute regime

As mentioned in Section 1.5.1, various concentration regimes give rise to different length scales in the polymer chain, within which the polymer conformation and dynamics show distinct features. Polymer solutions in different concentration regimes thus exhibit distinct rheological behavior. This thesis will focus on the semidilute regime, which is further divided into the semidilute unentangled and semidilute entangled regimes by two critical concentrations: overlap concentration C* and entanglement concentration C_e.

1.5.3.1 Dynamics for semidilute unentangled solutions

In the concentration range of $C^* < C < C_e$, chains start to interpenetrate each other but entanglement is not yet formed. As polymers chains overlap with each other, a new length scale comes up: correlation length (ξ). In good solvents, the correlation length (ξ) is the critical length scale that separates two modes of stress relaxation. Within ξ, a polymer chain is supposed to keep the self-avoiding walk conformation and to behave like it is in dilute solution, following the Zimm model. Assuming a correlation blob with size ξ contains g Kuhn monomers, then g can be calculated as $g = C\,(\xi/b)^3 \approx C^{-1/(3v-1)}$, since $\xi \approx bC^{-v/(3v-1)}$, as derived in Section 1.5.1. The relaxation time within size ξ is then $\tau_\xi \approx \xi^2/D_z \approx \dfrac{\eta s}{kT}\,\xi^3 \approx \dfrac{\eta s}{kT}\,b^3\,C^{-3v/(3v-1)}$. And the storage and loss modulus is proposed to follow a power law dependence on the frequency with a slope of 5/9 at time scale shorter than τ_ξ (Figure 1.13A). The stress relaxation modulus also follows the Zimm model: $G(t) \approx (kT/b^3)\,C\,(t/\tau_0)^{-1/(3v)}$,
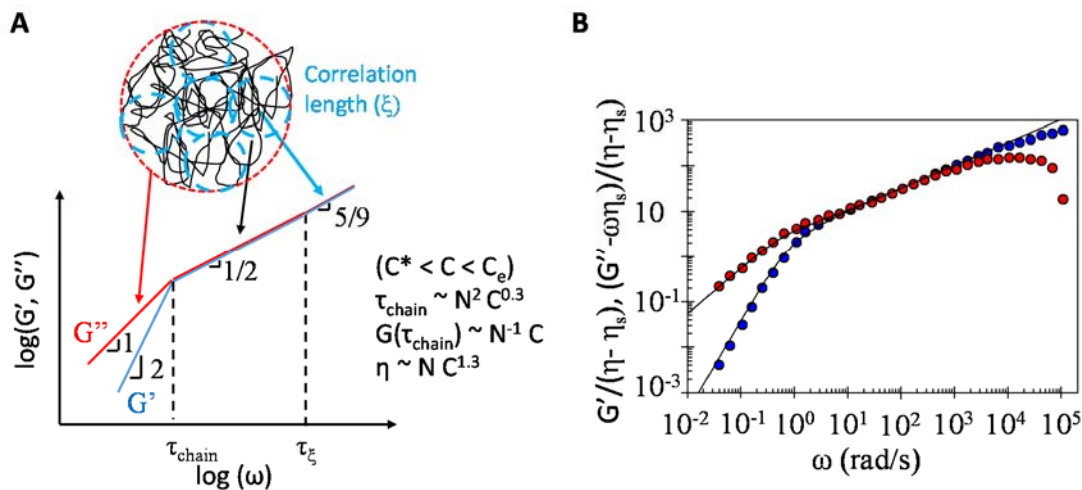
Figure 1.13 A. Theoretical predictions on how the dynamic moduli (G', G'') change with frequency for semidilute unentangled solutions. **B.** (Figure reproduced from reference [53]) Reduced storage modulus (G', blue) and reduced loss modulus (G'', red) from oscillatory flow birefringence studies of a semidilute unentangled $M_w = 400$ kg/mol poly(α-methyl styrene) solution (c = 0.105 g/cm^3) in a high-viscosity solvent, Arochlor at 25 °C. Lines are predictions of the Rouse model.

for $\tau_0 < t < \tau_\xi$. At the crossover time $t = \tau_\xi$, the stress relaxation modulus can be expressed as $G(\tau_\xi) \approx (kT/b^3) \, C \, (\tau_\xi / \tau_0)^{-1/(3v)} \approx (kT/b^3) \, C^{3v/(3v-1)}$.

At length scales larger than ξ, both the excluded volume effect and hydrodynamic forces are screened. The polymer chain behaves ideally and the presumption for Rouse dynamics is fulfilled. Thus, a polymer can be seen as a random walk of N/g correlation blobs with size ξ and relaxation time τ_ξ. And the relaxation of the whole chain is $\tau_{chain} \approx \tau_\xi \, (N/g)^2 \approx \frac{\eta s}{kT}$ $\xi^3 (N/g)^2 \approx \frac{\eta s}{kT} b^3 \, N^2 C^{(2-3v)/(3v-1)} \approx \frac{\eta s}{kT} b^3 \, N^2 C^{0.3}$, with $v = 3/5$ (Figure 1.13A). The storage and loss modulus follow a power law dependence on the frequency with a slope of ½ as expected for Rouse dynamics at the intermediate time scale (Figure 1.13A, $\tau_{chain} < t < \tau_\xi$). The stress relaxation modulus in this time range follows the Rouse model: $G(t) \approx G(\tau_\xi)$ $(t/\tau_\xi)^{-1/2} \approx (kT/b^3) \, C^{3v/(3v-1)} (t/\tau_\xi)^{-1/2}$, for $\tau_\xi < t < \tau_{chain}$. At the longest relaxation time $t = \tau_{chain}$, the stress relaxation modulus can be determined as $G(\tau_{chain}) \approx (kT/b^3) \, C^{3v/(3v-1)} (\tau_{chain}/\tau_\xi)^{-1/2}$ $\approx (kT/b^3) \, N^{-1}C$. The solution viscosity is controlled by the longest relaxation time (τ_{chain}): $\eta \approx G(\tau_{chain}) \, \tau_{chain} \approx NC^{1.3}$.

Experimental data agrees with the theory prediction that the longest relaxation process for semidilute unentangled solutions of covalent linear polymers at length scale larger than a correlation length is Rouse-like. Figure 1.13B shows dynamic moduli curves obtained from oscillatory flow birefringence studies of a semidilute unentangled $M_w = 400$ kg/mol poly(α-methyl styrene) solution at 0.105 g/cm^3 [53]. A distinct Rouse slope of ½ is observed in the plot, confirming the predicted Rouse dynamics.

1.5.3.2 Dynamics for semidilute entangled solutions

For semidilute entangled solutions ($C > C_e$) in good solvents, two length scales play an important role in the dynamics: the correlation length (ξ), and the tube diameter (a). The size of the correlation length has the same dependence on concentration as described above: $\xi \approx bC^{-v/(3v-1)} \approx bC^{-0.76}$ for $v = 0.588$. The number of Kuhn segments contained in a correlation blob (g) follows the equation $g = C (\xi/b)^3 \approx C^{-1/(3v-1)} \approx C^{-1.3}$. The chain is then a random walk of correlation blobs, with its size $R \approx \xi (N/g)^{1/2} \approx b N^{1/2} C^{-(2v-1)/(3v-1)}$.

The tube diameter in semidilute entangled solutions in good solvent is much larger compared to the tube diameter in the melt ($a(1)$), and is proportional to the correlation length ξ: $a(C) \approx a(1) C^{-v/(3v-1)} \approx a(1)C^{-0.76}$ for $v = 0.588$, because the correlation length describes the distance between binary intermolecular contacts, which control the entanglements between chains [43].

With the concentration dependence of the tube diameter, the critical concentration identifying the semidilute entangled regime, the entanglement concentration C_e, can finally be defined. The concentration at which the tube diameter $a(C)$ equals the coil size R is the entanglement concentration C_e: $C_e \approx [N_e(1)/N]^{(3v-1)} \approx [N_e(1)/N]^{0.76}$ for $v = 0.588$.

Another parameter that can be derived from the tube diameter is the number of Kuhn segments contained in the entanglement strand, $N_e(C)$. The chain segment within the length of a tube diameter $a(C)$, which is an entanglement strand, is a random walk containing $N_e(C)/g$ correlation blobs with length ξ. Thus the two length scales have the following relationship: $a(C) \approx \xi\sqrt{N_e(C)/g}$. The concentration dependence of $N_e(C)$ is then solved using the expression of $a(C)$, ξ and g: $N_e(C) \approx N_e(1) C^{-1/(3v-1)}$.

The two length scales, the correlation length (ξ), and the tube diameter (a), separate three modes of stress relaxation presented in semidilute entangled solutions. Within the correlation length ξ, the chain remains self-avoiding walk conformation, and the relaxation follows the Zimm model: $\tau_\xi \approx \xi^2 / D_z \approx \frac{\eta s}{kT} \xi^3 \approx \frac{\eta s}{kT} b^3 C^{-3v/(3v-1)}$. The storage and loss modulus is proposed to exhibit a power law dependence on the frequency with a slope of 5/9 at time scale shorter than τ_ξ (Figure 1.14A).

At length scales between the correlation length ξ and the tube diameter $a(C)$, the entanglement strand can be seen as a random walk of $N_e(C)/g$ correlation blobs with size ξ and relaxation time τ_ξ, and follows Rouse-like dynamics. The relaxation time of an entanglement strand (τ_e) is then expressed as $\tau_e \approx \tau_\xi (N_e(C)/g)^2 \approx \frac{\eta s}{kT} b^3 N_e(1)^2 C^{-3v/(3v-1)}$. The dynamic moduli should present a power law dependence on the frequency with a slope of 1/2 at time scale $\tau_\xi < t < \tau_e$ (Figure 1.14A).

At length scales larger than the tube diameter $a(C)$, the polymer chain can only diffuse curvilinearly along the tube, the motion of which is described by the reptation model (Figure 1.14A, $\tau_e < t < \tau_{rep}$). The longest relaxation time of the polymer chain can thus be represented by the reptation time: $\tau_{rep} \approx \tau_e \, (N/\, N_e(C))^3 \approx \frac{\eta s}{kT} b^3 \, (\xi/b)^3 \, (N_e(C)/g)^2 \, (N/\, N_e(C))^3$

$\approx \frac{\eta s}{kT} b^3 \, (N^3/\, N_e(1)) \, C^{3(1-v)/(3v-1)} \approx \frac{\eta s}{kT} b^3 \, (N^3/\, N_e(1)) \, C^{1.6}$ for $v = 0.588$. As explained earlier in reptation model, the rubbery plateau modulus is determined by the number density of entanglement strands, which is the reciprocal of the occupied volume of one entanglement strand consisting of $N_e(C)/g$ correlation blobs with size $\xi^3 : \xi^3 \, N_e(C)/g \approx a(C)^2 \, \xi$. The plateau modulus is thus $G_e(C) \approx kT/(a(C)^2\xi) \approx kTC/(N_e(C)b^3) \approx G_e(1) \, C^{3v/(3v-1)} \approx G_e(1) \, C^{2.3}$ for $v = 0.588$. Note that the plateau modulus does not depend on the length of the polymer but only on polymer concentration. The solution viscosity is controlled by the longest relaxation mode which is the reptation mode (τ_{rep}): $\eta \approx G_e(C)\tau_{rep} \approx N^3 C^{3.9}$.
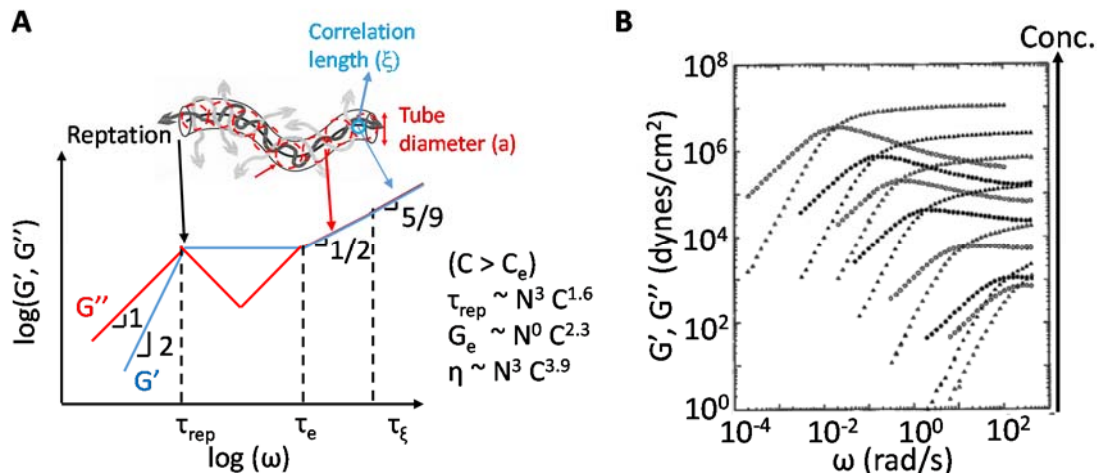
Figure 1.14 A. Theoretical predictions on how the dynamic moduli (G', G'') change with frequency for semidilute entangled solutions. **B.** (Figure reproduced from reference [54]) Oscillatory shear data on neutral polybutadiene $M_w = 925$ kg/mol entangled solutions. Polymer melt and six solutions in the good solvent phenyloctane at 25 ℃ with volume fraction of polymer from top to bottom $\varphi = 1$, $\varphi = 0.488$, $\varphi = 0.280$, $\varphi = 0.140$, $\varphi = 0.0621$, $\varphi = 0.0274$, and $\varphi = 0.0214$. All solutions are entangled since $\varphi_e = 0.01$.

Table 1.2 Scaling predictions of length scales and parameters for terminal polymer dynamics in dilute, simidilute unentangled and semidilute entangled solutions in good solvents. Note that the predictions for dilute solutions in good solvents do not correlate with experimental data as well as the case in θ-solvents, because the excluded volume effect diminishes the hydrodynamic forces, which works against the presumption of the Zimm model.

	Dilute	Semidilute unentangled	Semidilute entangled
Critical concentration	-	$C^* \sim N^{-0.76}$	$C_e \sim [N_e(1)/N]^{0.76}$
Concentration range	$C < C^*$	$C^* < C < C_e$	$C > C_e$
Correlation Blob Size (ξ)	-	$\xi \sim N^0 C^{-0.76}$	$\xi \sim N^0 C^{-0.76}$
Tube diameter ($a(C)$)	-	-	$a(C) \sim N^0 C^{-0.76}$
Longest relaxation time	$\tau_Z \sim N^{1.76} C^0$	$\tau_{chain} \sim N^2 C^{0.3}$	$\tau_{rep} \sim N^3 C^{1.6}$
Terminal modulus	$G(\tau_Z) \sim N^{-1} C^1$	$G(\tau_{chain}) \sim N^{-1} C^1$	$G_e \sim N^0 C^{2.3}$
Specific Viscosity	$\eta_{sp} \sim N^{0.76} C^1$	$\eta_{sp} \sim N^1 C^{1.3}$	$\eta_{sp} \sim N^3 C^{3.9}$

These predicted concentration dependences of the reptation time and plateau modulus are indeed observed in experimental data of solutions of linear covalent polymers in good solvent, as shown with the oscillatory shear data on polybutadiene (M_w = 925 kg/mol) solutions with concentrations from slightly above the entanglement concentration all the way to the melt (Figure 1.14B)[54].

In summary, many molecular models have been developed for the dynamics of polymers over the past 70 years, including the Zimm model, Rouse model, and reptation model. Specifically for polymer solutions, the Zimm model applies to the dynamics of dilute solutions, the Rouse model applies to the longest relaxation process for semidilute unentangled solutions, and the reptation model applies to the longest relaxation process for semidilute entangled solutions. Table 1.2 summarizes the power law dependence of relaxation time, characteristic modulus and solution viscosity on the polymer length, and concentration for these three concentration regimes.

1.6 Nature of the end associations of DA-PCOD and DA/DB-PCOD

As mentioned above, our group has developed self-associative polymers (di-acid-ended PCOD, DA) and pairwise associative polymers (di-acid-ended paired with di-amine-ended
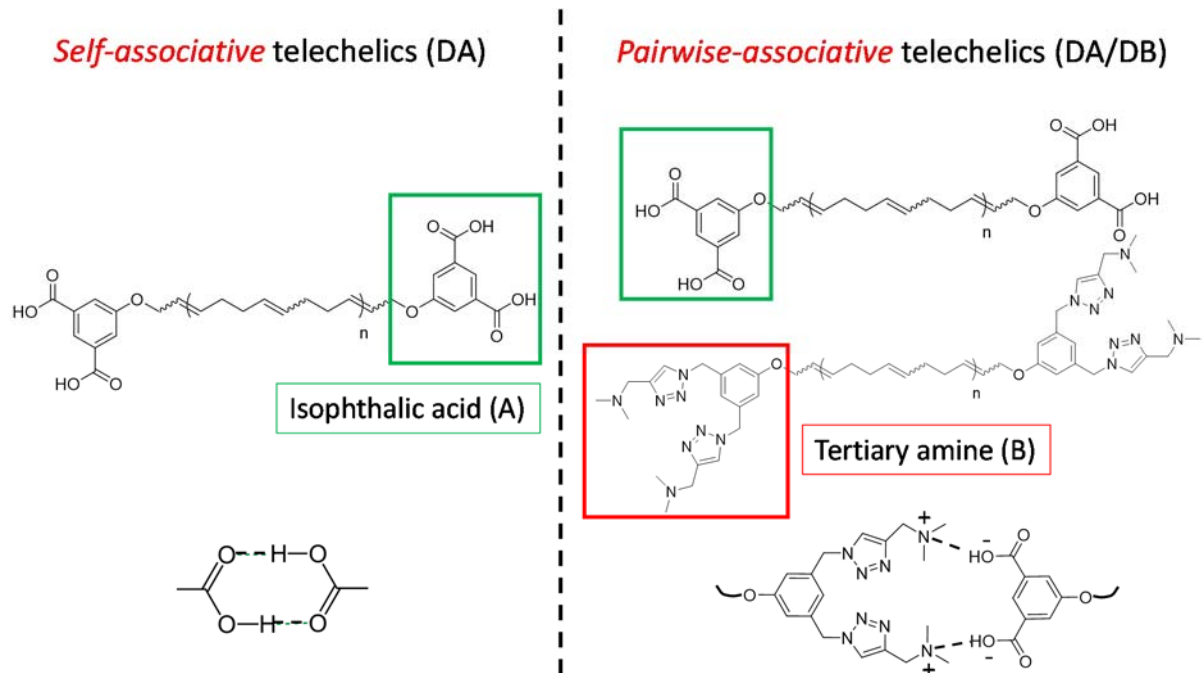
Figure 1.15 Structures of self-associative telechelics (DA) and pairwise-associative telechelics (DA/DB) and the nature of their end association.

PCOD, DA/DB) for mist control applications. Self-associative telechelic refers to isophthalic acid-ended polycylcooctadiene (Di-acid PCOD, DA-PCOD), which has a hydrophobic backbone and isophthalic acid as the end group (Figure 1.15, left). DA-PCOD may associate with itself through the hydrogen bonding between carboxylic acid dimers (Figure 1.15, left). The rationale for hydrogen bonding being the association mechanism, not the low solubility of isophthalic acid, will be demonstrated in more details in Chapter 3. When DA-PCOD is paired with di-tertiary amine ended polycylcooctadiene (Di-Base PCOD, DB-PCOD) at 1:1 molar ratio, the acid and amine can bind with each other pairwisely. The polymer pair is thus named pairwise-associative polymer (Figure 1.15, right). The end associations of DA and DA/DB are later demonstrated to both originate from hydrogen bonding (Chapter 2 and 3), although still differ in their specific chemical properties, and furthermore, in their binding strength.

1.6.1 Classification of conventional hydrogen bonds

To better apprehend the large number and variety of H-bonds observed in nature, G.Gilli and P.Gilli have classified H-bonds into many groups, with the group containing the most electronegative main group elements (N, O, F, Cl, and Br) named "Conventional H-bonds" [55]. Due to the high electronegativity, conventional H-bonds are among the strongest H-bonds discovered. They are further subdivide into 6 subgroups, 5 of which are relevant to the discussion in this thesis (Figure 1.16) [55].

Ordinary H-bonds are the most widely occurring in nature. They are not assisted by any cooperative effects or other factors (e.g. charge), and thus have only weak strength. The H-bond between water molecules is a representative OHB (Figure 1.16, top).

A resonance-assisted H-bond (RAHB) has a donor or acceptor atoms at the end of a short π-conjugated structure. The resonance of π-conjugation provides synergetic effect to the H-bond, enhancing its strength. The association between carboxylic acid dimers, which guides the self-association of DA, is a good example for RAHB (Figure 1.16, middle). The strength of the H-bond of carboxylic acid dimers is thus stronger than an OHB.

When the H-bond is assisted by charge, it is called charge-assisted H-bond (CAHB) and is much stronger than an OHB (Figure 1.16, bottom). Depending on the charge in the system, CAHB is divided into three types: negative charge- (-), positive charge- (+), and double charge- (±) assisted H-bond. (-)CAHB has a net negative charge in the association pair, and is exemplified by the R-OH acids with their own conjugated salt. (+)CAHB has a net positive charge in the association pair, and applies to the situation with two identical

Classification of "Conventional H-bonds"
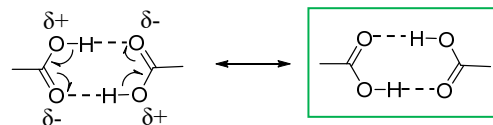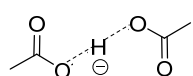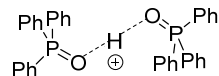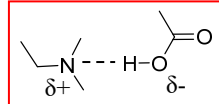
Figure 1.16 Five subgroups of conventional hydrogen bonds containing most electronegative main group elements (N, O, F, Cl and Br).

molecules bridged by a proton donated by a strong acid. (±)CAHB consists of a pair of acid and base, with the pK_a of the acid and the pK_a of the conjugate acid of the base being very close. The association between isophthalic acid (DA) and tertiary amine (DB) belongs to the (±)CAHB category.

1.6.2 H-bond strength

The strength of a H-bond is directly related to its bond length D, which is the distance between the donor and acceptor atom (D = d(D–H--A)). To quantify and compare H-bond strength, the binding enthalpy (ΔH) is usually utilized. In experimental studies, the activation energy directly measured and calculated through the slope of the Van't Hoff plot or Arrhenius plot is also the enthalpy (ΔH). However, it should be noted that the thermodynamic value that is directly related to the dissociation constant K_d is the Gibbs free energy (ΔG): $K_d = \exp(\Delta G/kT)$, while $\Delta G = \Delta H - T\Delta S$. In other words, H-bond formation is a process of balancing the enthalpy gain due to association and the entropy cost due to loss of degrees of freedom, otherwise referred to as enthalpy-entropy compensation. The standard enthalpy (ΔH) and standard entropy (ΔS) in the H-bond formation are generally constant and independent of temperature in hydrogen bonding systems [56-58]. However, the H-bond strength (ΔG) decreases linearly with increasing absolute temperature since $\Delta G = \Delta H - T\Delta S$. For the enthalpy-entropy compensation, a relationship correlating ΔS and ΔH, $\Delta H = \beta\Delta S$, has been developed by Pimentel and McClellan in 1971 [59], and confirmed by Joesten and Schaad in 1974 [60]. β has been referred as the compensation temperature, and found to be related to the type of H-bond donor/acceptor pairs [59-60]. Specifically, β equals 453 ± 54 K for the interactions between benzoic/acetic acid (unsubstituted and substituted) and tertiary amine (triethyl-, tripropyl-

Table 1.3 The bond length (D= d(D–H- -A)), binding enthalpy (Δ*H*) and binding strength (Δ*G*) for some typical H-bonds

	OHB (H$_2$O)	RAHB (one H-bond in the carboxylic acid dimer)	(±)CAHB (carboxylic acid/amine)
D (Å)	2.70-2.84 [55]	2.62-2.67 [55]	~ 2.52[a]
Binding Enthalpy (Δ*H*)	~4.5 kcal/mol (~19 kJ/mol) [55,62]	~ 7 ± 1 kcal/mol (~29 ± 4 kJ/mol) [56-57,63]	12 ~ 16 kcal/mol (50 ~ 67 kJ/mol) [61]
Binding Strength (Δ*G*)	-	~ 8 ± 1 kJ/mol [56,66]	~ 20 ± 3 kJ/mol [61,64-65]

[a]. The value is for the association between a carboxylic acid and a modified pyridine [55]

and tributyl- amine) [61]. At 298K, the binding free energy Δ*G* of the H-bond is thus estimated to be nearly 30% of its corresponding Δ*H* in most environments of practical interest (non-polar solvents and molecular crystals) [55].

To predict the H-bond strength of charge assisted hydrogen bonds, a theoretical principle is proposed by G.Gilli and P.Gilli: the *pK*$_a$ equalization principle [39,55], which is the hypothesis that the driving force of H-bond strengthening is to a result of the progressive reduction of the difference between the acidic constants of the donor and acceptor groups: Δ*pK*$_a$ = *pK*$_{AH}$(D-H) - *pK*$_{BH+}$(A-H+). Homomolecular (-)CAHBs and (+)CAHBs, having ΔpKa = 0 by definition, as well as the acid-base pairs ((±)CAHBs) endowed with very small Δ*pK*$_a$ values (within 0-2 units), are all known to give rise to remarkably shorter and more energetic H-bonds [39]. In the association pair of isophthalic acid and tertiary amine, the *pK*$_a$ for isophthalic acid is 3.46, and the *pK*$_a$ for the conjugate acid of trimethylamine

is 3 since the pK_b for trimethylamine is 11, leading to a $\Delta pK_a = 0.46$. This low ΔpK_a suggests a very strong association between DA/DB.

Also relevant to the discussion in this thesis, some properties for the H-bond of water, of carboxylic acid dimers and of the carboxylic acid/amine pair are listed in Table 1.3. The properties of the H-bonds between water [55,62] and various carboxylic acid dimers [55-57,63,66] has been extensively studied in literature. Most studies of carboxylic acid dimers are performed in vapor phase. Since one isophthalic acid contains two carboxylic acid dimers and four H-bonds in total, the binding strength (ΔG) can be obtained as 8*4 = 32 kJ/mol, which corresponds to around 13 kT at 298K.

Binding enthalpy and free energy have been experimentally measured for the association between carboxylic acid and tertiary amine in various organic solvent, which is 12~16 kcal/mol or $50 \sim 67$ kJ/mol [61] for ΔH and 4.7 ± 0.6 kcal/mol or 20 ± 3 kJ/mol for ΔG [61,64-65]. Therefore the free energy (ΔG) for the two CAHBs between isophthalic acid and tertiary amine is estimated to be ~ 40 kJ/mol, which is 16 kT at 298K.

1.6.3 Temperature dependence of H-bond strength

It has been well documented in literature that systems based on hydrogen bonds depend highly on temperature. The standard enthalpy ΔH and standard entropy ΔS in the H-bond formation can be calculated through the Van't Hoff plot of hydrogen bonding systems, and are found to be a constant and independent of temperature in the temperature range encountered in this thesis (0 to 60℃) [56-58]. However, the H-bond strength (ΔG), which is directly related to the dissociation constant K_d, decreases linearly with increasing

Table 1.4 The estimated bonding free energy (ΔG) and dissociation constant (K_d) using Van't Hoff equation, $\ln (K_1/K_2) = -\frac{\Delta H}{R} (\frac{1}{T2} - \frac{1}{T1})$, with 25 ℃ as the reference temperature.

		60℃ (333 K)	25℃ (298 K)	0℃ (273 K)
DA/DB	ΔH (kJ/mol)	100 ~ 134 (non-polar solvent)		
	ΔG (kJ/mol)	30 ± 3	40	46 ± 3
	K_d (μM) = exp(ΔG/RT)	8 ~ 33	0.11	0.0008 ~0.003
DA	ΔH (kJ/mol)	100 ~ 134 (vapor)		
	ΔG (kJ/mol)	22 ± 2	32	39 ± 2
	K_d (μM) = exp(ΔG/RT)	160 ~ 670	2.26	0.016 ~ 0.056

absolute temperature since $\Delta G = \Delta H - T\Delta S$. Therefore, the dissociation constant (K_d) decreases with decreasing temperature.

The Van't Hoff equation is generally utilized to describe the temperature dependence of the dissociation constant (K_d): $\ln (K_1/K_2) = -\frac{\Delta H}{R} (\frac{1}{T2} - \frac{1}{T1})$. In this thesis, experiments will be performed in the range of 0 to 60 ℃. The binding free energy (ΔG) for DA and DA/DB has been estimated above to be $13kT$ and $16kT$ at 298K respectively, from which the corresponding K_d can be calculated using the equation $K_d = \exp(\Delta G/kT)$. The binding enthalpy ΔH for DA and DA/DB is also shown above. Using 298K as the reference temperature, the K_d for DA and DA/DB at other temperatures (e.g. 0℃ and 60℃) are deduced using Van't Hoff equation (Table 1.4).

Another method is available to estimate K_d from the bond strength (ΔG) value at each temperature. Take DA/DB association as an example. It is mentioned earlier that a relationship between ΔH and ΔS for H-bond systems has been generalized: $\Delta H = \beta \Delta S$, with

Table 1.5 The estimated bonding free energy (ΔG) and dissociation constant (K_d) using enthalpy-entropy compensation, $\Delta G_1/\Delta G_2 = (\beta - T_1)/(\beta - T_2)$, with 25 ℃ as the reference temperature.

		60 ℃ (333 K)	25 ℃ (298 K)	0 ℃ (273 K)
DA/DB	ΔG (kJ/mol)	30 ± 3	40	46 ± 3
	K_d (µM) = exp(ΔG/RT)	6 ~ 49	0.11	0.0004 ~0.003

β referring as the compensation temperature [55,59-60]. Specifically, β equals 453 ± 54 K for the interactions between benzoic/acetic acid (unsubstituted and substituted) and tertiary amine (triethyl-, tripropyl-, and tributyl- amine) [61]. The temperature dependence of ΔG can then be derived: $\Delta G = (\beta - T) \Delta S$. For DA and DA/DB, the H-bond free energy (ΔG) of the DA/DB association is roughly estimated for 60 ℃ (333K) and 0 ℃ (273K) from the value at 25 ℃ (298K), using β values of 410, 450 and 510 (Table 1.5). The change in the above estimated ΔG with temperature for the DA/DB pair is in good agreement with literature: around 20% change in ΔG is induced by varying 30K [56-58]. The corresponding H-bond dissociation constant (K_d) at various temperatures is thus calculated using the equation: $K_d = \exp(\Delta G/kT)$ (Table 1.5). The K_d values obtained using the two methods (Van't Hoff and enthalpy-entropy compensation) are on the same order of magnitude (Table 1.4 *versus* Table 1.5).

Because of the exponential relationship between dissociation constant (K_d) and free energy (ΔG), a 10% variation in ΔG causes a ~ 4-fold variation in K_d (Table 1.4 and Table 1.5). However, this variation is very small compared to the change induced by temperature. Increasing the temperature by 30K leads to roughly two orders of magnitude of increase in dissociation constant for both systems, indicating that DA and DA/DB association are strongly temperature-dependent.

1.7 Scope of each chapter

The goal of this work is to investigate the morphology and dynamics of the self- and pairwise-association systems, answer the questions stated in Section 1.4, and seek to interpret the underlying structure-function relationship. I hope this work will facilitate the rational design of supramolecules in the future.

The problem will be approached one factor at a time in the following chapters. Chapter 2 compares DA- with DA/DB-PCOD systems using polymers at one chain length (50 kg/mol) at one temperature (0 ℃) with a series of concentrations (Figure 1.17). Self-associative telechelic polymers (DA-PCOD) are demonstrated to be capable of multimeric association via pairwise hydrogen bonding due to the specific chemical structure of the ends, while the pairwise-associative telechelic polymers (DA/DB-PCOD) exhibit dynamics that strikingly resembles that for linear covalent polymers. The morphology and dynamics of self- and pairwise- association system differ from each other qualitatively, simply because of the difference in the chemical entities of half of the ends, which take <0.5% of total polymer composition. And concentration is shown to affect the topology and distribution of supramolecule formation.
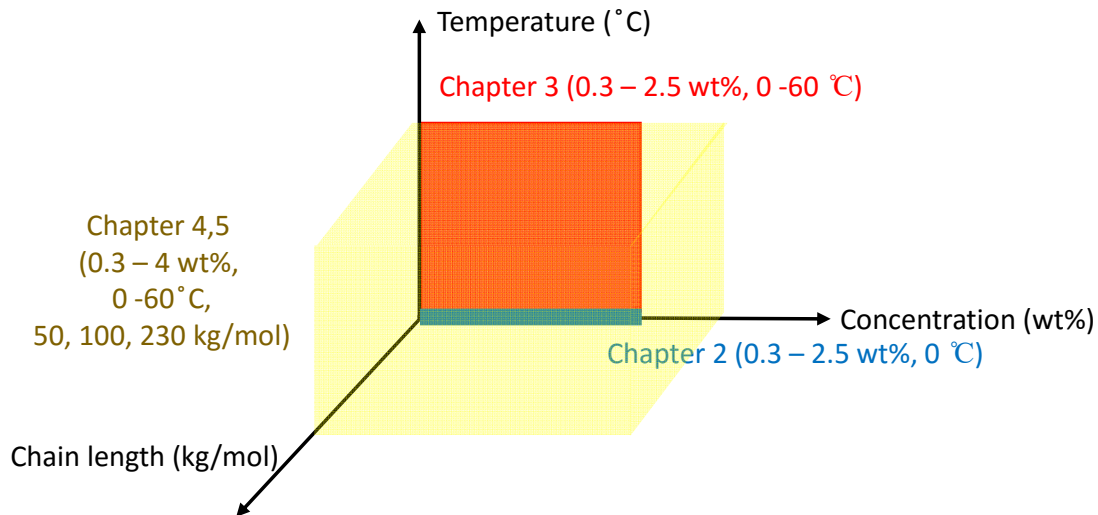
Figure 1.17 Summary of the range of parameters discussed in each chapter

Chapter 3 discusses the temperature effect on the morphology and dynamics of both systems (Figure 1.17). Temperature determines the binding strength of self- and pairwise-end association, and furthermore, the fraction of unbound ends and the distribution and topology of formed supramolecules/aggregates. Both rheology and small angle neutron scattering (SANS) data confirm a change in topology with temperature for both systems.

Chapter 4 and 5 focus on DA/DB-PCOD and DA-PCOD solutions, respectively, with one more parameter, chain length, taken into account (Figure 1.17). For DA/DB-PCOD, an interesting non-monotonic chain length effect is discovered. In fact, the chain length effect is found dependent on the specific temperature and concentration. For DA-PCOD, chain length plays its role through determining the concentration of end groups. An apparent "pairwise-association" pattern is observed with DA-PCOD when the end group concentration is low. In summary, polymer concentration, temperature, and chain length affect the morphology and dynamics of both systems significantly.

Appendix A describes the synthesis and characterization of the small molecule chain transfer agents (CTA) and telechelic polymers.

References

[1] C. Chassenieux, T. Nicolai, L. Benyahia, *Current Opinion in Colloid & Interface Science,* **2011***, 16*, 18-26.

[2] T. Annable, R. Buscall, R. Ettelaie, D. Whittlestone, *Journal of Rheology* **1993**, *37*, 695-726.

[3] F. Tanaka & S. F. Edwards, *Macromolecules,* **1992**, *25*, 1516-1523.

[4] A.N. Semenov, J.-F. Joanny & A. R. Khokhlov, *Macromolecules,* **1995,** *28*, 1066-1075.

[5] Q. T. Pham, W. B. Russel, J. C. Thibeault, W. Lau, *Macromolecules,* **1999**, *32*, 2996-3005.

[6] Q. T. Pham, W. B. Russel, J. C. Thibeault, W. Lau, *Macromolecules,* **1999**, *32*, 5139-5146.

[7] X.-X. Meng, W. B. Russel, *Macromolecules* **2005,** *38,* 593-600

[8] G. Broze, R. Jérôme, P. Teyssié, *Macromolecules* **1982**, *15*, 1300-1305.

[9] G. Broze, R. Jérôme, P. Teyssié, *Macromolecules* **1982**, *15*, 920-927.

[10] M. R. Tant, G. L. Wilkes, J. P. Kennedy, *J. Appl. Polym. Sci.*, **1991**, *42*, 523-532.

[11] M. R. Tant, K. A. Mauritz, & G. L. Wilkes, *Ionomers: Synthesis, Structure, Properties and Applications*, Blackie Academic and Professional, London, 1997, chap. 4.

[12] S. K. Yang, A. V. Ambadec, M. Weck, *Chem. Soc. Rev.*, **2011**, *40*, 129–137.

[13] G. R. Whittell, M. D. Hager, U. S. Schubert, I. Manners, *Nature Mater.*, **2011**, *10*, 176–188.

[14] T. F. A. de Greef, E. W. Meijer, *Nature*, **2008**, *453*, 171-173.

[15] S.-L. Li, T. Xiao, C. Lin, L. Wang, *Chem. Soc. Rev.*, **2012**, *41*, 5950–5968.

[16] P. Sijbesma *et al*, *Science*, **1997**, *278*, 1601-1604.

[17] K. E. Feldman, M. J. Kade, T. F. A. de Greef, E. W. Meijer, E. J. Kramer, C. J. Hawker, *Macromolecules*, **2008**, *41*, 4694-4700.

[18] K. Yamauchi, J. R. Lizotte, D. M. Hercules, M. J. Vergne, T. E. Long, *J. Am. Chem. Soc.*, **2002**, *124*, 8599-8604.

[19] A. D. Celiz and O. A. Scherman, *Macromolecules*, **2008**, *41*, 4115-4119.

[20] S. K. Yang, A. V. Ambade, M. Weck, *J. Am. Chem. Soc.,* **2010**, *132*, 1637–1645.

[21] A. V. Ambade, C. Burd, M. N. Higley, K. P. Nair and M. Weck, *Chem.-Eur. J.*, **2009**, *15*, 11904-11911.

[22] T. Park, S. C. Zimmerman, *J. Am. Chem. Soc.,* **2006**, *128*, 13986-13987.

[23] H. Hofmeier, R. Hoogenboom, M. E. L. Wouters, U. S. Schubert, *J. Am. Chem. Soc.,* **2005**, *127*, 2913-2921.

[24] P. J. Flory, *Proc. R. Soc. London, Ser. A*, **1976**, *351*, 351.

[25] G. H. McKinley, T. Sridhar, *Annu. Rev. Fluid Mech.* **2002**, *34*, 375-415.

[26] K. K. Chao, C. A. Child, E. A. Grens II, M. C. Williams, *AIChE J.* **1984**, *30*, 111-120.

[27] R. W. Paterson & F. H. Abernathy, *J. Fluid Mech.* **1970**, *43*, 689-710.

[28] R. G. Larson, *The structure and Rheology of Complex Fluids*, Oxford Univ. Press, New York, 1999, pp. 132-142.

[29] H. Jacobson, W. H. Stockmayer, *J. Chem. Phys.* **1950**, *18*, 1600-1606.

[30] K. F. Freed, *J. Chem. Phys.* **2012**, *136*, 244904.

[31] M. A. Winnik & A. Yekta, *Curr. Opin. Colloid Interface Sci.* **1997**, *2*, 424-436.

[32] S. T. J. Peng & R. F. Landel, *J. Non-Newton Fluid* **1983**, *12*, 95-111.

[33] National Research Council (U.S.). Committee on Aviation Fuels with Improved Fire Safety. *Aviation fuels with improved fire safety:a proceedings.* National Academy Press, Washington, D.C., 1997.

[34] J.-M. Lehn, *Science* **2002**, *295*, 2400-2403.

[35] T. Aida, E. W. Meijer & S. I. Stupp, *Science* **2012**, *335*, 813-817.

[36] A. K. Boal *et al., Nature* **2000**, *404*, 746-748.

[37] A. S. Tayi *et al., Nature* **2012**, *488*, 485-489.

[38] O. Ikkala & G. ten Brinke, *Science* **2002**, *295*, 2407-2409.

[39] P. Gilli, et al, *Acc. Chem. Res.*, **2009**, *42*, 33–44.

[40] M. A. Hillmyer, S. T. Nguyen & R. H. Grubbs, *Macromolecules* **1997**, *30*, 718-721.

[41] S. Ji, T. R. Hoye & C. W. Macosko, *Macromolecules* **2004**, *37*, 5485-5489.

[42] M. R. Nyden, , S. I. Stoliarov, P. R. Westmoreland, Z. X. Guo, C. Jee, *Mat. Sci. Eng. A-struct.* **2004**, *365*, 114–121.

[43] M. Rubinstein, R. H. Colby, *Polymer Physics*, Oxford Univ. Press, Oxford, 2003.

[44] S. F. Edwards, *Proc. Phys. Soc.*, **1967**, *91*, 513.

[45] B. Zimm, *J. Chem. Phys.,* **1956**, *24*, 269-278.

[46] R. M. Johnson, J. L. Schrag, J. D. Ferry, *Polym. J.* **1970**, *1*, 742-749.

[47] R. H. Colby, *Rheol. Acta*, **2010**, *49*, 425-442.

[48] P. Rouse, *J. Chem. Phys.,* **1953**, *21*, 1272-1280.

[49] S. Onogi, T. Masuda, K. Kitagawa, *Macromolecules*, **1970**, *3*, 109-116.

[50] P. G. De Gennes, *J. Chem. Phys.*, **1971**, *55*, 572–571.

[51] M. Doi, *J. Polym. Sci. Polym. Lett. Ed.* **1981**, *19*, 265-273.

[52] R. H. Colby, L. J. Fetters, W. W. Graessley, *Macromolecules*, **1987**, *20*, 2226–2237.

[53] T. P. Lodge, J. W. Miller, J. L. Schrag, *J. Polym. Sci. Polym. Phys. Ed.*, **1982**, *20*, 1409–1425.

[54] R. H. Colby, L. J. Fetters, W. G. Funk, W. W. Graessley, *Macromolecules*, **1991**, *24*, 3873 – 3882.

[55] G.Gilli, P.Gilli, *The Nature of the Hydrogen Bond: outline of a comprehensive hydrogen bond theory.* Oxford Univ. Press, 2009.

[56] A. D. H. Clague, H. J. Bernstein, *Spectrochim. Acta*, **1969**, *25*, 593-596.

[57] G. Allen, J. G. Watkinson, K. H. Webb, *Spectrochim. Acta*, **1966**, *22*, 807-814.

[58] L.Sun, C. D. Wick, J. I. Siepmann, M. R. Schure, *J. Phys. Chem. B,* **2005,** *109,* 15118-15125.

[59] G. C. Pimentel, A. L. McClellan, *Annu. Rev. Phys. Chem.*, **1971**, *22*, 347-385.

[60] M.D. Joesten, L. J. Schaad, *Hydrogen bonding*, Marcel Dekker: New York, 1974.

[61] E. N. Gur'yanova, I. P. GoI'dshtein, T. I. Perepelkova, *Russian Chemical Reviews*, **1976**, *45*, 792–806.

[62] W. Klopper, et al, *Phys. Chem. Chem. Phys.*, **2000**, *2*, 2227-2234.

[63] E. W. Johnson, L. K. Nash, *J. Am. Chem. Soc.*, **1950**, *72*, 547–556

[64] M. M. Davis, M. Paabo, *J. Am. Chem. Soc.*, **1960**, *82*, 5081–5084.

[65] H. Nakanishi, H. Morita, S. Nagakura, *J. Mol. Spectrosc.*, **1977**, *65*, 295-305.

[66] J. Chocholoušová, J. Vacek, P. Hobza, *J. Phys. Chem. A* **2003,** *107,* 3086-3092.

Chapter II

Dynamics of Associative Telechelic Polymers

2.1 Introduction

For mist control application, our group developed self-associative polymers and pairwise associative polymers. Self-associative telechelic refers to isophthalic acid-ended polycylcooctadiene (Di-acid PCOD, DA-PCOD), which has a hydrophobic backbone (PCOD) and isophthalic acid ends capable of associating with themselves (Figure 2.1A). When DA-PCOD is paired with di-tertiary amine ended polycylcooctadiene (Di-Base PCOD, DB-PCOD) at 1:1 molar ratio, the acid and amine can preferentially bind with each other pairwisely through charge-assisted hydrogen bond. The polymer pair is thus named pairwise associative polymer (Figure 2.1B). The viscometry and small angel neutron scattering results in the previous study suggest that self-associative and pairwise-associative polymers exhibit distinct association pattern, even though the polymer backbones are exactly the same, and only half of the end groups (< 0.5% of total weight) are different [1].

Extensive research has been performed on self-associative polymers, including hydrophobically modified urethane-ethoxylates (HEURs). They form flower-like micelles, which start to bridge with each other as the concentration increases and form interconnected network [2]. The association of DA-PCOD is called self-association because it literally binds with itself. However, it is unknown before this work whether the
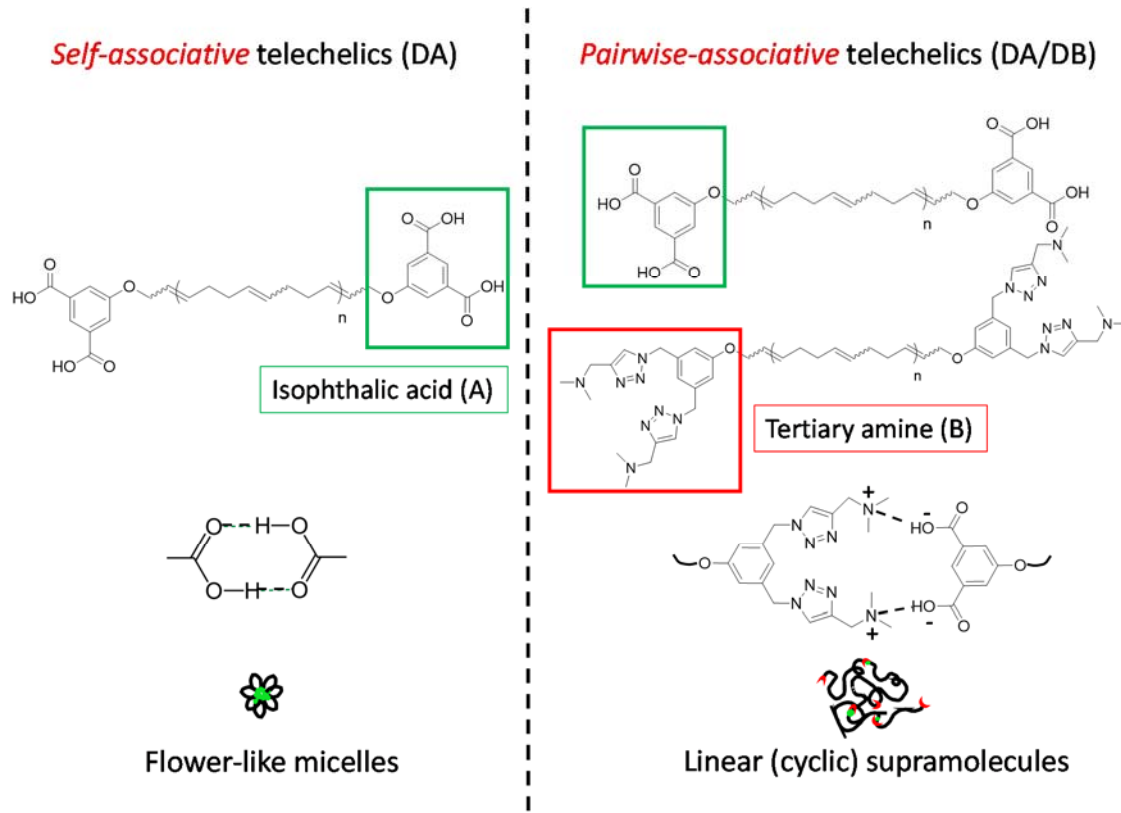
Figure 2.1 Schematic representations of self-associative telechelics (DA-PCOD) and pairwise-associative telechelics (DA/DB-PCOD).

association is self-complementary in nature like the case with ureido-pyrimidinone (UPy), or DA-PCOD makes contact to the HEURs, which are based on multimeric association (Figure 2.1A). If it is multimeric, the association of DA-PCOD may be due to hydrogen bonds, or the micro-phase separation brought by low solubility of acid in non-polar solvents. It is intriguing to answer these questions by examining the dynamics of DA-PCOD.

DA/DB PCODs are expected to form linear and cyclic supramolecules due to their pairwise end association (Figure 2.1B). Over the past 40 years, numerous telechelic polymers capable of non-covalent pairwise-association, including metal coordination and hydrogen-bonding, have been synthesized and developed [3-8]. Although the formation of complex

copolymer architectures (diblock, triblock, and multiblock copolymers) by pairwise-associative telechelic polymers has been well demonstrated in prior reports, little systematic study has been performed on the dynamics of the supramolecules and how the dynamics responds to changes in concentration, temperature, and polymer chain length, etc [3-5]. These studies can identify the structure-function relationship for supramolecular formation, and serve as a guidance for rational design of supramolecules and the related functional materials.

The goal of this chapter is to compare the dynamics of DA-PCOD with HEURs, and DA/DB-PCOD with linear covalent polymers. The concentration effect of their dynamics is also covered. To provide the necessary background for discussing the dynamics of DA/PCOD and DA/DB-PCOD, the rheology of hydrophobically modified urethane-ethoxylates (HEURs) and linear covalent polymer solutions is reviewed in this section, with an emphasis on their concentration dependence. In addition, the theory that describes the distribution of individual telechelic polymers into linear and cyclic supramolecules, ring-chain equilibrium, is introduced here.

2.1.1 Rheology of hydrophobically modified urethane-ethoxylates (HEURs)

The most extensively studied self-associative polymer in literature is hydrophobically modified urethane-ethoxylates (HEURs), which have been applied as thickening agents in water-borne coatings, paints, and inks to control rheological properties such as viscosity, gelation, shear-thinning, and thickening behavior [2]. The descriptions of their rheological and other properties can be found in numerous reports [2, 9-13].

These polymers form flower-like micelles at low concentrations, and the "petals" (loops) turn into bridges between micelles as concentration is increased, and eventually, interconnected network forms [2]. The resulting gels (or thick solutions) give dynamic moduli curves which can be fitted by the Maxwell model with a single relaxation time (Figure 2.2A). The relaxation time is governed by the diffusion of hydrophobic end escaping the micelle core, as demonstrated by Annable *et al* [9]. The telechelic polymers relax *via* Rouse-like dynamics following by end-group exchange/disengagement.

The concentration dependence of the relaxation time, high-frequency modulus, and solution viscosity is more complicated. The viscosity of these polymer solutions has strong dependence on the polymer concentrations: it increases roughly as the concentration squared or cubed at low concentrations and linearly with the concentration at high
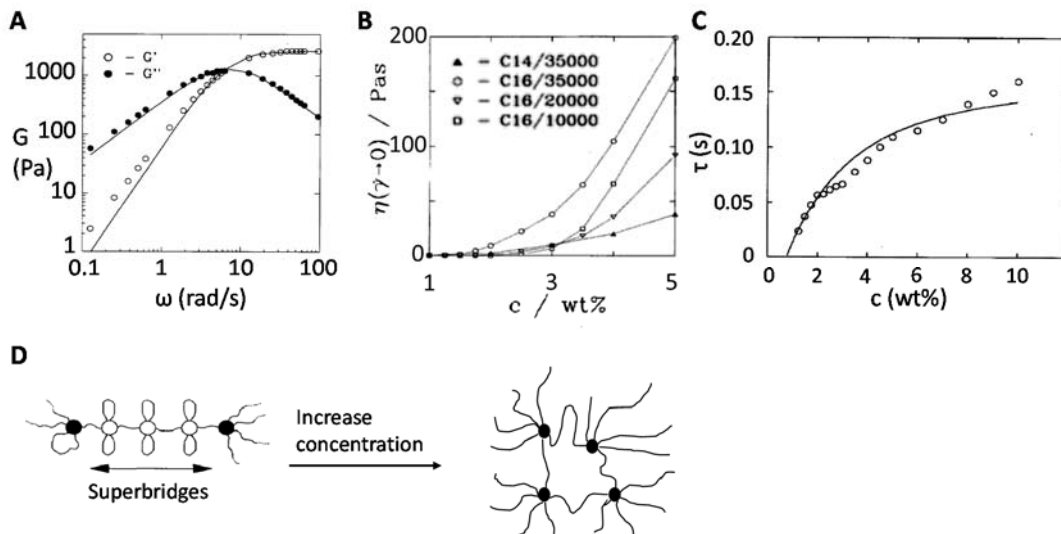
Figure 2.2 reproduced from reference [9]. A. Storage modulus G' and loss modulus G'' of 7 wt% C16/35 (M_w = 35 kg/mol, PEO with C16 hydrophobe, overlap concentration C* = 23.3 mg/ml). Here, wt%=%w/v. Lines represent fits of single-relaxation Maxwell model. **B.** Effect of polymer concentration (%w/v) on the low shear viscosity of four HEURs at 298 K. (Example of the nomenclature: C14/35000, a HEUR with a C14 hydrophobe end and M_w = 35 kg/mol.) **C.** Relaxation time as function of polymer concentration for C16/35 (M_w = 35 kg/mol, PEO with C16 hydrophobe) at 298K. The line represents a scaling function of $\tau = \tau_0 f(c\sqrt{M})$. **D.** Schematic representation of the topological change with concentration for HEURs.

concentrations (Figure 2.2B). The relaxation time increases slightly with increasing concentration (Figure 2.2C, within the same order of magnitude). Since the solution viscosity is the product of high frequency modulus and relaxation time, and the high frequency modulus shoots up orders of magnitude with concentration, it is clear that the concentration dependence of the viscosity is determined by that of the high frequency modulus [9].

Annable *et al* explained the above concentration dependence by introducing a topological change of the micelle structure as a function of polymer concentration [9]. Loops are favored at low concentration and a large fraction of telechelic polymers are distributed into local topologies like superbridges (Figure 2.2D, left), with many micelles having functionality equaling to or less than 2. Since the dissociation of one of the bridging chain in the middle relaxes the whole superbridge structure, the relaxation time is shortened and the modulus is low. Increasing concentration turns more loops into bridges (Figure 2.2D, right), leading to higher fraction of elastically effective chains, and thus higher modulus and longer relaxation time.

2.1.2 Dynamics of linear covalent polymer solutions

For a better comparison with the rheology of the supramolecules formed by our pairwise-associative polymers, the dynamics of solutions of linear covalent polymers, which has been elucidated 30 years ago, is briefly summarized here, with a more detailed description in Chapter 1. Linear covalent polymer solutions transit from dilute to semidilute unentangled, and to semidilute entangled regime as the concentration increases. The two critical concentrations that separate the three regimes are the overlap concentration (C*,

$C* \sim N^{-0.76}$ for an athermal solvent, N refers to the number of Kuhn segments in each chain)

and the entanglement concentration (C_e, $C_e \sim [\frac{Ne(1)}{N}]^{0.76}$ for an athermal solvent).

In each concentration regime, the solution dynamics shows particular pattern. In a dilute

solution (C<C*), the relaxation of a polymer chain obeys Zimm model [14], and the

solution viscosity scales linearly with polymer concentration: $\eta \sim C^1$. In a semidilute

unentangled solution (C*<C<C_e) of a good solvent, the longest relaxation process is the

Rouse-like relaxation [15] of the polymer chain at a length scale larger than the correlation

length. The storage/loss moduli curve displays a distinct power law region with a slope of

½ followed by the terminal region (Figure 2.3A, [16]). The viscosity in this regime scales

linearly with chain length and to the order of 1.3 with concentration: $\eta \approx N^1 C^{1.3}$. In a

semidilute entangled solution (C>C_e) of a good solvent, De Gennes' reptation model [17]

describes well the dominant relaxation mode, with a plateau modulus (reptation modulus)
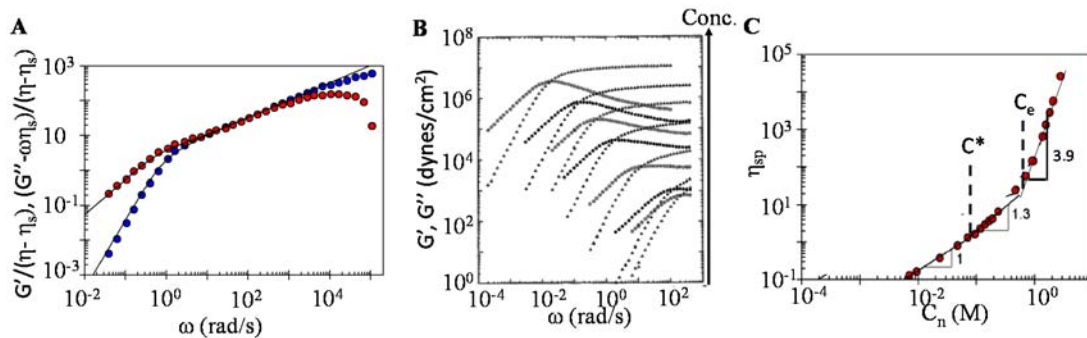
Figure 2.3 A. (Figure reproduced from reference [16].) Reduced storage modulus (G', blue) and reduced loss modulus (G", red) from oscillatory flow birefringence studies of a semidilute unentangled M_w = 400 kg/mol poly(α-methyl styrene) solution (c = 0.105 g/cm³) in a high-viscosity solvent, Arochlor at 25℃. Lines are predictions of the Rouse model. **B.** (Figure reproduced from reference [18].) Oscillatory shear data on neutral polybutadiene M_w = 925000 entangled solutions. Polymer melt and six solutions in the good solvent phenyloctane at 25℃ with volume fraction of polymer from top to bottom φ =1, φ = 0.488, φ = 0.280, φ = 0.140, φ = 0.0621, φ = 0.0274, and φ = 0.0214. All solutions are entangled since φ_e = 0.01. **C.** (Figure reproduced from reference [19].) The specific viscosity in the good solvent ethylene glycol of poly(2-vinyl pyridine) plotted as functions of the number density of monomers.

$G_e \sim N^0 C^{2.3}$ depending only on the polymer concentration but not on the polymer length, and a reptation time as the longest relaxation time $\tau_{rep} \sim N^3 C^{1.6}$ (Figure 2.3B [18]). The viscosity is controlled by the reptation relaxation with a stronger dependence on both N and C: $\eta \approx G_e \tau_{rep} \approx N^3 C^{3.9}$.

The above theoretical predictions for both semidilute unentangled and semidilute entangled solutions have been well supported by experimental data (Figure 2.3A,B). The dependence of solution viscosity η on polymer concentration C varies from $\eta \sim C^1$ to $\eta \sim C^{1.3}$, and to $\eta \sim C^{3.9}$ as the solution shifts from dilute to semidilute unentangled, and to semidilute entangled regime (Figure 2.3C, [19]).

2.1.3 Ring-chain equilibrium

The supramolecules formed by DA/DB-PCOD is expected to consist of linear and cylic species with various sizes, the distribution of which is determined by many factors, including temperature, the polymer concentration, etc. The theory that describes how the individual building blocks assemble into linear or cyclic products is ring-chain equilibrium, first developed by Jacobson and Stockmayer in 1950 for polycondensation reaction [20]. After 2000s, the ring-chain equilibrium theory starts to be applied to the physical assembly of bi-functional associative small molecules (such as ureido-pyrimidone (UPy) functionalized ones) and pairwise-associative telechelic polymers [7, 21-22].

One of the key predictions of the theory is that the partitioning of monomers into linear products increases as the total monomer concentration increases [7, 20-22]. Due to the high association enthalpy of the ends, telechelic polymers need to be brought together to ensure the enthalpy gain from end association, leading to conformational entropy lost for the backbone of the telechelic polymers. In dilute solutions, individual polymer coils are isolated from each other (Figure 2.4, left top). The formation of small rings (e.g. dimer, Figure 2.4, left bottom) is favored, because the entropy cost for restricting multiple chains in close proximity to form large supramolecules is expected to be enormous. As concentration increases, the average distance between polymer coils decreases, reducing the entropy cost; thus larger cyclic and linear species are likely to form. In semidilute
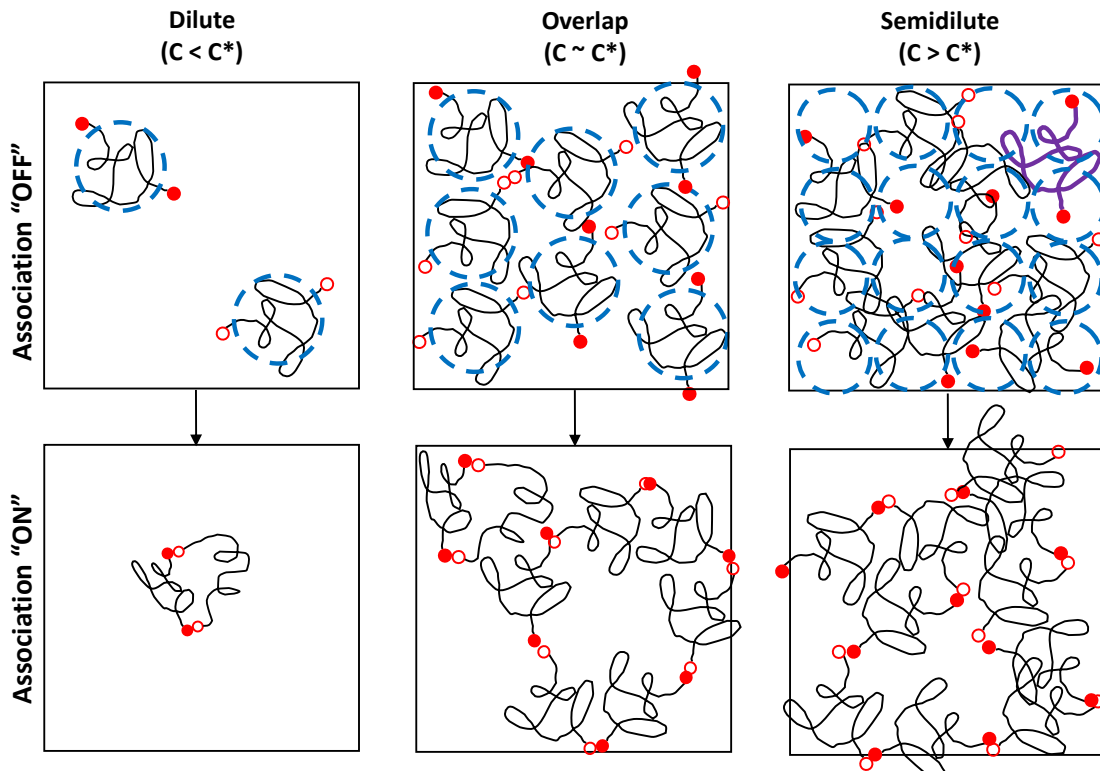
Figure 2.4 Schematic illustration on the concentration dependence of ring-chain equilibrium. The purple chain shows that polymer coils are well percolated, and each coil spans several correlation blobs.

solutions, the telechelic polymers are well percolated (Figure 2.4, right top), resulting in much less entropy cost to link multiple chains together, enabling the formation of long linear supramolecules (Figure 2.4, right bottom).

A statistical mechanical model has been developed by Dr. Ameri David based on ring-chain equilibrium concept, specifically on the supramolecule formation with pairwise-
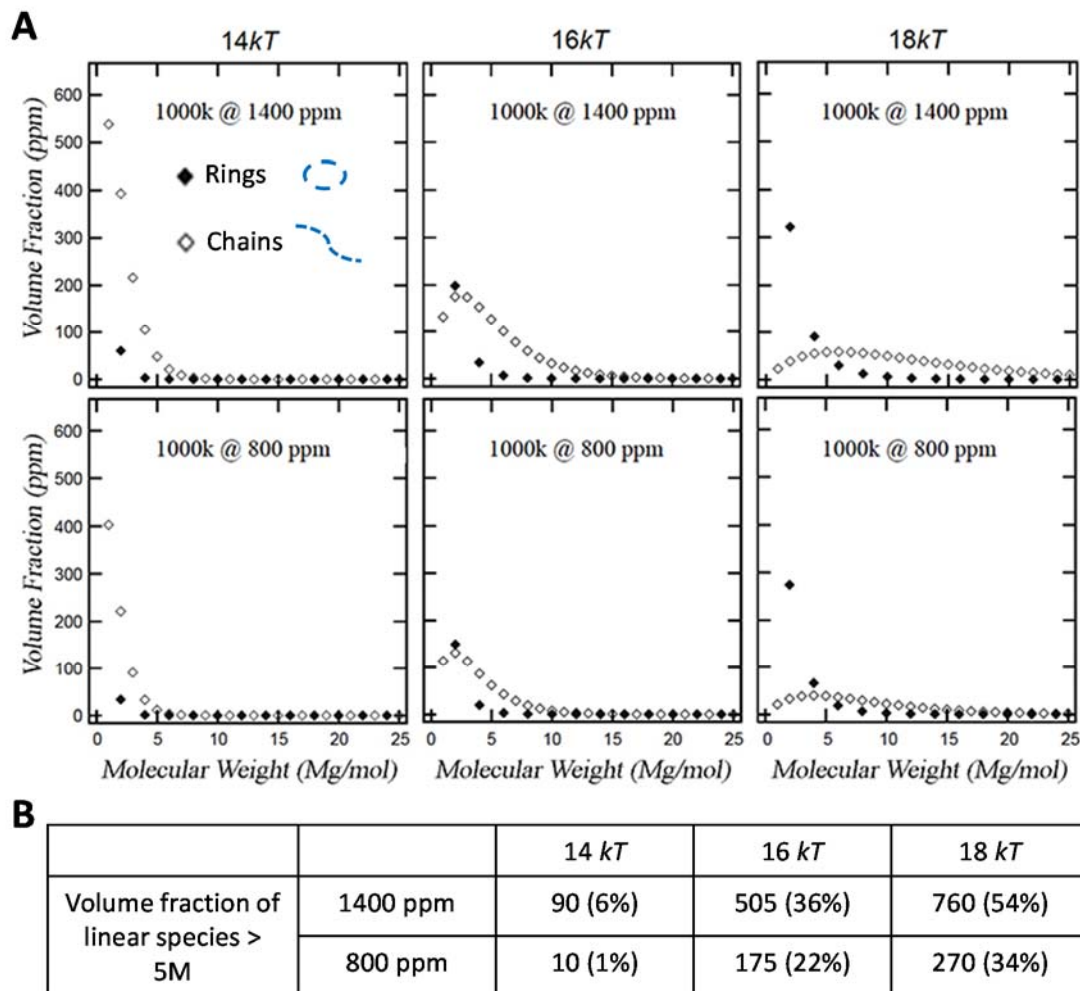
Figure 2.5 A. Model predictions on the equilibrium concentrations of supramolecular species with various sizes as functions of polymer concentration for three different values of the strength of interaction 14kT (left), 16kT (middle) and 18kT (right) (open diamond: linear supramolecules; solid diamond: cyclic supramolecules) [1]. **B.** The accumulated volume fraction of linear species with molecular weight > 5000 kg/mol (5-mer supramolecules) calculated from the figure in Part A. The value in parentheses is the fraction of these long species in the total polymer concentration.

associative telechelic polymers in dilute solutions (Figure 2.5A) [1]. The molecular weight, end-association strength, and total concentration of individual telechelics are adopted as variables. Model results show that the fraction of the linear species with molecular weight larger than 5000 kg/mol (5-mer by individual 1000 kg/mol telechelics) increases significantly as the total polymer concentration increases from 800 ppm to 1400 ppm (Figure 2.5B). It is clear that distribution of the telechelics into longer supramolecules is favored at higher polymer concentration for all computed end-association strengths, as expected in the ring-chain equilibrium theory. Although this model focused on the dilute regime, it is reasonable to postulate that in the semidilute solutions of DA/DB-PCOD, long supramolecules should be favored as the polymer concentration increases as well.

2.1.4 Scope of Chapter 2

Literature showed that self-associative system and pairwise-associative system differ significantly, because of the different association topology and the fundamentally distinct association mechanism (hydrophobic interaction, or ionic interaction for self-association *versus* hydrogen-bonding for pairwise-association). The telechelic polymers described here (DA-PCOD *versus* DA/DB-PCOD) have exactly matching backbone and only half of the end groups to be different (< 0.5% of total weight), providing the opportunity for comparison between the dynamics of these two systems. And it is discovered that such a minute change in chemical composition indeed alters the association strength, topology and solution dynamics completely.

In addition, the dynamics of self-associative telechelic polymer (DA-PCOD) at one molecular weight (M_w = 50 kg/mol) is examined and compared to that of HEURs. The data shows that DA-PCOD exhibits similar dynamic properties and concentration dependence

as HEURs. The dynamics of pairwise-associative telechelic polymer (DA/DB-PCOD) is also investigated. The relaxation of their formed supramolecules displays striking similarity with that of linear covalent polymer solution.

2.2 Experimental

2.2.1 Materials

The decahydronaphthalene (decalin, mixture of cis/trans) used as the solvent for rheology experiments and 2,6-Di-tert-butyl-4-methylphenol (BHT) used as an anti-oxidant in the polymer solution were purchased from Sigma Aldrich and used as received. The polyisobutylene (PIB, M_w = 4,200 kg/mol, M_n = 3,100 kg/mol referred as 4.2M PIB) used as a linear covalent polymer control was also purchased from Sigma Aldrich. The non-associative polycyclooctadiene control (1.1M PCOD, M_w = 1.08 Mg/mol) was synthesized by Dr. Xuelian He *via* ring opening metathesis polymerization (ROMP) with alkane-ended chain transfer agent (CTA). The isophthalic acid-ended polycyclooctadiene (DA-PCOD) was synthesized *via* ring opening metathesis polymerization (ROMP) with custom-made isophthalic acid-ended chain transfer agent (CTA). The di-tertiary amine ended polycyclooctadiene (DB-PCOD) was synthesized *via* ring opening metathesis polymerization (ROMP) with custom-made chloride-ended chain transfer agent (CTA), followed by two steps of post-polymerization modification. The synthetic schemes of CTAs, ROMP procedure, post-polymerization modification, and the characterization (GPC and NMR) of the CTAs and telechelic polymers were described in Appendix A.

2.2.2 Solution preparation

Solutions of polymers (PIB: 4.2M polyisobutylene, DA: isophthalic acid-ended polycyclooctadiene, and DA/DB: equiv. molar ratio of isophthalic acid-ended polycyclooctadiene and di-tertiary amine-ended polycyclooctadiene) were prepared by weighing out polymer on a Mettler precision balance (±0.01mg) into new glass scintillation vials with PTFE lined caps and subsequently adding the appropriate amount of decalin using a precision syringe (±1%). The decalin was pretreated with 0.1 wt% of BHT. The solutions of telechelic polymers were placed on a wrist-action shaker at room temperature overnight. The solutions of PIB were charged with a magnetic stir bar and stirred at 250 min^{-1} overnight to avoid shear degradation that may be induced by wrist-action shaking.

2.2.3 Rheological measurement

Steady shear viscosity and oscillatory shear dynamic moduli were measured from 0℃ to 60℃ with a strain-controlled rheometer TA ARES-RFS, equipped with a cone-plate geometry (angle 2°, diameter 50mm) and a solvent vapor trap. The steady shear rate range typically was chosen from 100 s^{-1} to 1 s^{-1} (or 10 s^{-1} to 0.1 s^{-1}) based on the temperature and polymer composition for each run to avoid overloading the force transducer. The viscosities are averages of values obtained at low shear rates that give viscosity independent of shear rate.

An oscillatory shear strain sweep was performed from 0.5% to 50% at 10 rad/s frequency at 0℃ and 25℃ for each polymer solution to measure the strain range for linear viscoelasticity. A strain within the linear range was chosen for the subsequent frequency sweep, which was usually 1%, 5%, 10%, or 20% strain, depending on the concentration and temperature. Dynamic moduli were measured for each polymer solution from 0℃ to 60℃ with frequency ranging from 100 rad/s to a lower frequency of 1 rad/s, or 0.1 rad/s,

or 0.01 rad/s, depending on the relaxation time for the specific composition and temperature.

2.3 Results

2.3.1 Rheology of DA-PCOD

Here, shear rheology and oscillatory rheology experiments were performed with isophthalic acid-ended polymers (DA-PCOD, M_w = 50 kg/mol) in decahydronaphthalene (decalin) with concentrations of 0.15 wt% ~ 2.5 wt% and 0.6 wt% ~ 2.5 wt%, respectively. Decalin is an athermal solvent for the PCOD backbone, which means that PCOD exhibits swollen ("self-avoiding") conformation in decalin.
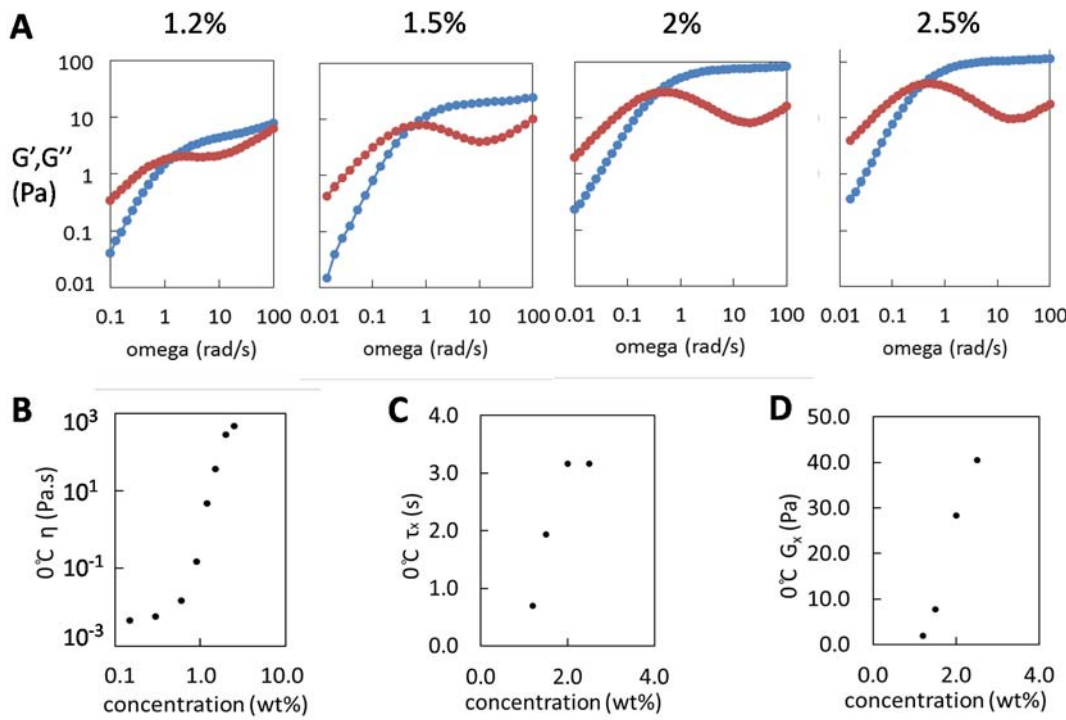
Figure 2.6 Rheology data for DA-PCOD (M_w = 50 kg/mol) at 0 ℃. **A.** Storage (G', blue circles) and loss modulus (G", red circles) at concentrations from 1.2 wt% to 2.5 wt%. **B.** Low shear viscosity as a function of polymer concentration. **C.** Relaxation time as a function of polymer concentration. The relaxation times are calculated using the crossover frequencies measured in part **A**. **D.** Crossover modulus (G_x) as a function of polymer concentration.

The dynamic moduli of DA-PCOD at concentrations of 1.2% (1.5C*) or more exhibit a crossover frequency $(G'(\omega_x)=G''(\omega_x))$ that separates the terminal regime at lower frequency from an elastic plateau at higher frequency (Figure 2.6A). The curves resemble the Maxwell model with single relaxation time (Figure 2.6A, Cole-Cole plots and more data shown in Chapter 3). At 0℃, the high frequency plateau modulus increases and the crossover frequency (ω_x) decreases of DA-PCOD decreases slightly with increasing polymer concentration (Figure 2.6C and D). The steady shear viscosity at 0℃ increases strongly with concentration at concentrations higher than around 1 wt% (Figure 2.6B), which is close to the overlap concentration of 50 kg/mol PCOD without associative ends (~0.8 wt%, the specific viscosity of non-associative PCOD at 0.8 wt% is 1, data not shown). At lower concentration, the effect of concentration is much weaker (approximately linearly). The dynamic moduli pattern for DA-PCOD at lower concentrations will be discussed in more detail in Chapter 5.

2.3.2 Rheology of linear covalent polymer

Polyisobutylene (PIB, Figure 2.7A) was chosen as a linear covalent polymer control for this thesis for two reasons: 1) high molecular weight PIB is readily commercially available with a reasonable price (4,200 kg/mol PIB: \$80.4 for 100 grams from Sigma Aldrich), and 2) PIB backbone has similar polarity and solubility as the PCOD backbone used in our telechelic system.

Oscillatory rheology experiments were performed with 4.2M PIB ($M_w = 4,200$ kg/mol) in decalin at 0℃ at concentrations of 0.6 wt%, 1.2 wt% and 2 wt% (Figure 2.7B). All three concentrations are in the semidilute regime, since the calculated overlap concentration of 4.2M PIB ($C^*\sim N^{-0.76}$) should be around 0.06 wt%, much lower than the above

concentrations. The curve obtained at 1.2% has shape matching that for semidilute unentangled solutions of covalent linear polymers (Figure 2.3A), exhibiting a power law regime with a slop of ½ at high frequency (10 to 100 rad/s). The curve obtained with 2% solution clearly features a crossover of G' and G'', suggesting that the polymers are entangled. The change in the shape of dynamic moduli curves as the concentration increases from 0.6% to 2% indicates that the solution transits from semidilute unentangled to entangled regime.

These experimental data are in good agreement with theoretical predictions and literature result. The entanglement concentration (φ_e, volume fraction) for 4.2M PIB in a good
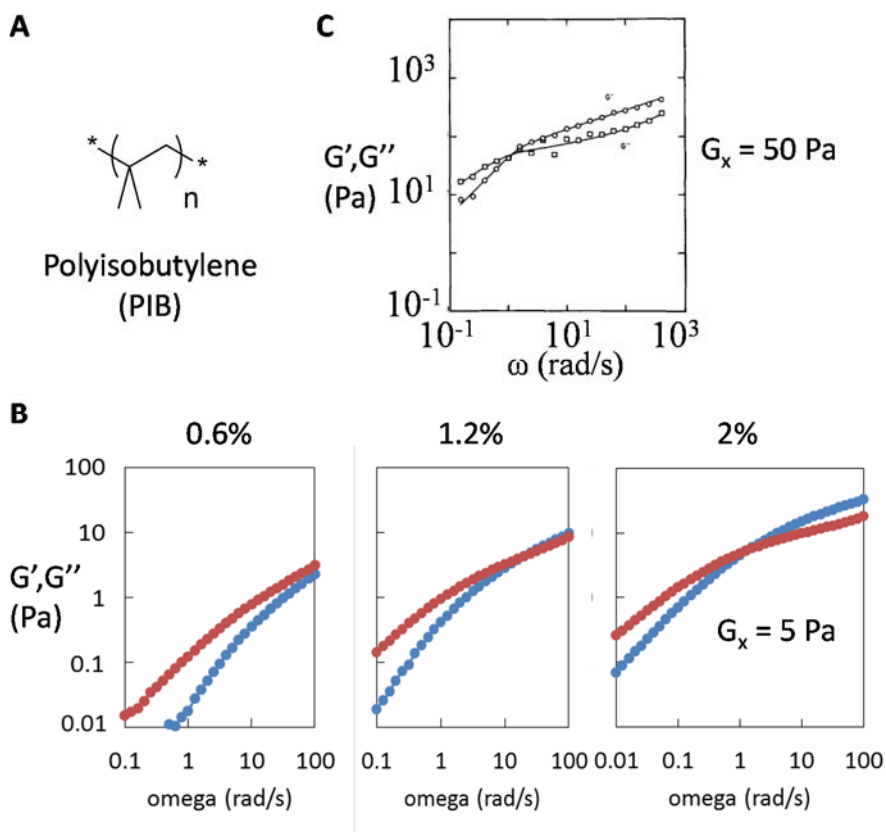
Figure 2.7 A. Structure of polyisobutylene (PIB). **B.** Storage modulus G' (blue circles) and loss modulus G'' (red circles) of PIB (M_w = 4,200 kg/mol) at 0 ℃ at concentrations of 0.6 wt%, 1.2 wt% and 2 wt%. **C.** (Figure reproduced from reference [23]) Dynamic moduli G' and G'' versus frequency for a 50 mg/ml (5.6 wt%) solution of linear PIB (MW = 1,300 kg/mol) in decalin at 27 ℃.

solvent like decalin can be theoretically estimated using the equation $\varphi_e \sim [\frac{Ne(1)}{N}]^{0.76}$, in

which $N_e(1)$ is the number of Kuhn segments in an entangled strand of PIB melt. φ_e can be

converted to weight percent concentration (C_e, in wt%) by multiplying the ratio of

d(PIB)/d(decalin) (d refers to density), when the overall polymer concentration is low. The

calculated C_e is around 0.7%, which is on the same order of magnitude with the

experimental value (between 1.2% and 2%). The shape of measured dynamic moduli curve

clearly resembles the curve in literature for a semidilute entangled solution of PIB (Figure

2.7C, [23]). For semidilute entangled solutions, the plateau modulus follows the scaling

equation of $G_e \approx N^0 C^{2.3}$, and the crossover modulus (G_x) should obey the same relationship.

Then an estimated G_x for 2 wt% PIB solution can be calculated from the literature G_x for

5.6 wt% solution, with the value of 4.7 Pa, which exactly matches the measured G_x here (5

Pa). The analysis confirms that the current data agrees well with both theoretical prediction

and literature.
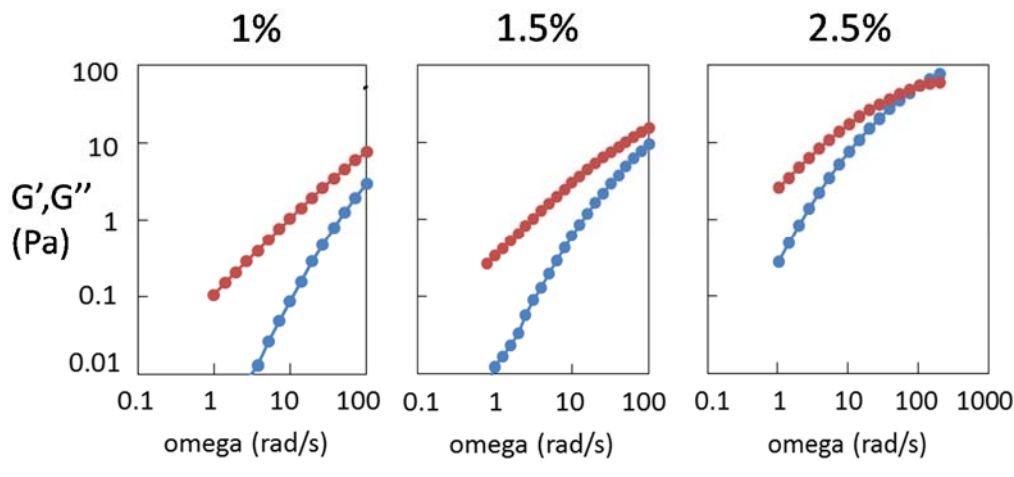
Figure 2.8 Storage (G', blue circles) and loss modulus (G", red circles) of PCOD ($M_w = 1,100$ kg/mol) at 0 ℃ at concentrations of 1 wt%, 1.5 wt% and 2.5 wt%.

A polycyclooctadiene backbone with molecular weight of 1100 kg/mol (PCOD, $M_w = 1100$ kg/mol) is also adopted as a control. The oscillatory test was performed at 0 ℃ at 1, 1.5 and 2.5 wt% in decalin (Figure 2.8). The dynamic moduli curves at 1 wt% and 1.5 wt% depict mostly terminal region within the frequency limit. A clear crossover is displayed with 2.5 wt% solution, indicating the presence of entanglement.

2.3.3 Rheology of pairwise-associative polymer

Little systematic study has been performed on the dynamics of the formed supramolecules [3-5], and how the dynamics can be affected by relevant factors, including polymer concentration, temperature, polymer chain length, *etc.* This chapter focuses on the effect of polymer concentration on the dynamics of pairwise-associative polymers and the comparison with the dynamics of linear covalent polymers.
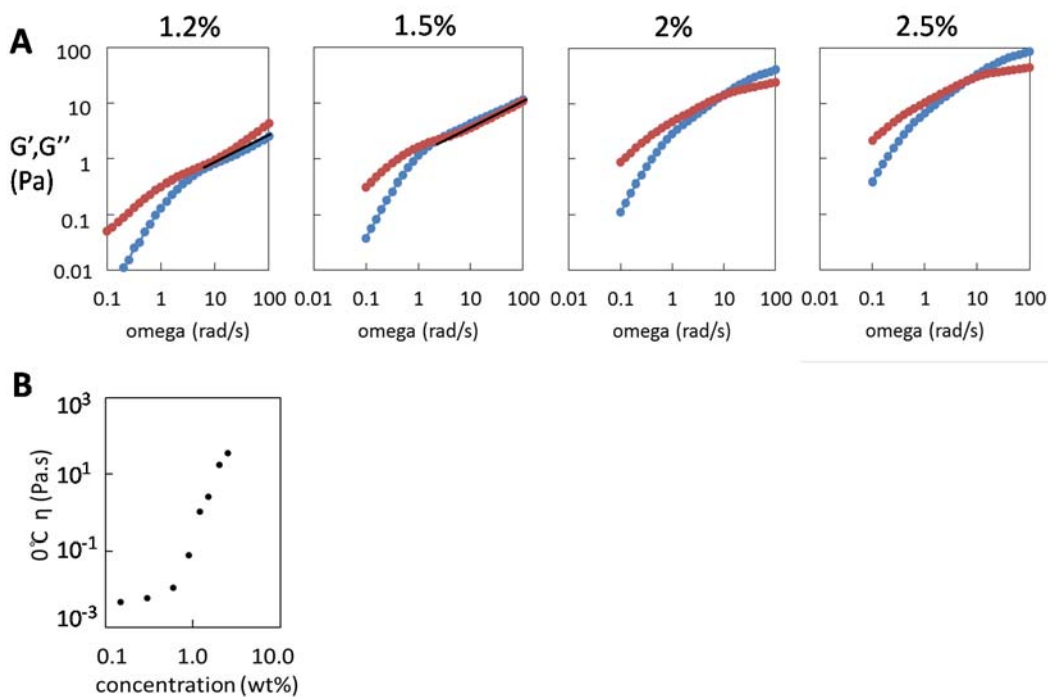
Figure 2.9 Rheology data for DA/DB-PCOD (M_w = 50 kg/mol) at 0 ℃. A. Storage modulus G' (blue circles) and loss modulus G'' (red circles) of DA/DB at concentrations from 1.2 wt% to 2.5 wt%. **B.** Low shear viscosity as function of polymer concentration.

In contrast to DA-PCOD, the dynamic moduli of a 1:1 mixture of isophthalic acid-ended polymers and di-tertiary amine ended polymers (denoted DA/DB-PCOD, M_w = 50 kg/mol) reviewed much stronger effects of concentration over the same range of total polymer concentration (1.2 wt% ~ 2.5 wt%). At concentrations of 1.2 wt% and 1.5 wt%, the dynamic moduli above the terminal region are roughly parallel to one another, with G' and G" approximately equal, near a power-law behavior with G'~G"~ $\omega^{1/2}$ (Figure 2.9A, 10-100 rad/s for 1.2 wt% and 1-100 rad/s for 1.5 wt%, the black line in the figure depicts slope of ½). The relaxation qualitatively changes with further increase in concentration to 2 wt% or more. A crossover frequency is clearly visible, but it occurs more than a decade above the terminal regime (Figure 2.9A, 2 wt% and 2.5 wt%). The broadening of the relaxation spectrum and the increase in the modulus at high frequency produce an increase of viscosity (Figure 2.9B), but it is considerably weaker than that of DA-PCOD (Figure 2.6B).

2.4 Discussion

2.4.1 Self-associative polymers *versus* pairwise-associative polymers

2.4.1.1 Mechanism for the multimeric association of self-associative polymers

The oscillatory rheology data suggests that isophthalic acid ended polymers do bear similarity with the conventional self-associative polymers (HEURs) in the sense that the solution dynamics resembles the Maxwell relaxation model with single relaxation time (Figure 2.6A) and the shear viscosity of their solutions have similar dependence on polymer concentrations (Figure 2.6B). It can be postulated that DA-PCOD does form flower-like micelles. As the concentration increases, the micelles significantly percolate and bridge with each other, enhancing the solution viscosity dramatically.
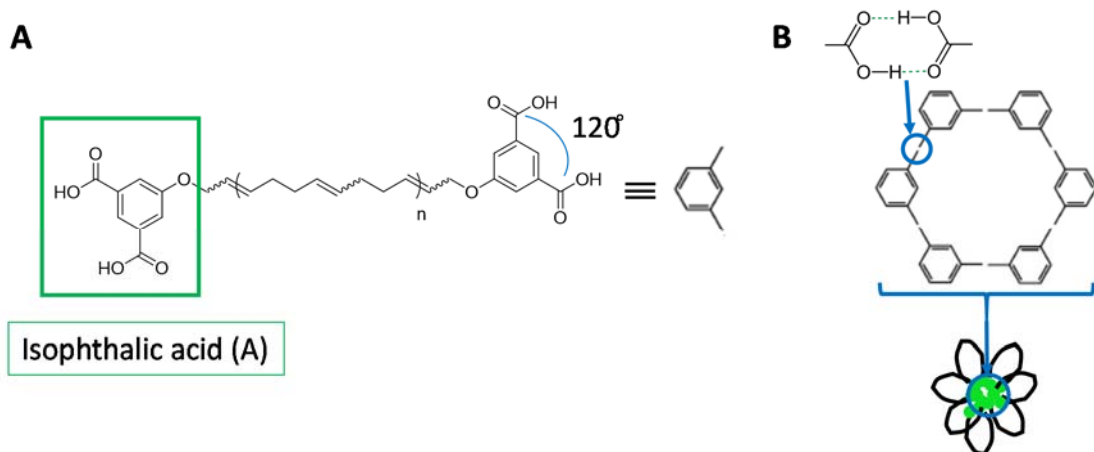
Figure 2.10 A. The isophthalic acid end has two carboxylic acid groups with a 120° angle in-between. **B.** (Figure inspired by reference [26]) Multiple isophthalic acid ends associate with each other forming the micelle core. The six membered ring (middle) is the most stable state for self-assembly of isophthalic acid on a surface (2D) as a small molecule, and does not necessarily represent the aggregation number for DA telechelics.

How does the isophthalic acid end manage to form multimeric association, while the hydrogen bond is pairwise? One postulation is that the isophthalic acid self-associates through micro phase separation due to its low solubility in hydrocarbon solvents, like in the case of hydrophobic ends of HEURs. However, this is proven not true by the temperature dependence of the solutions of these telechelics, which will be illustrated in Chapter 3.

A more reasonable postulation is that the isophthalic acid associates through hydrogen bonding between carboxylic acids, and, forms multimeric association due to its particular chemical structure. There is a 120° angel between the two carboxylic acid groups in the isophthalic acid (Figure 2.10A) due to their meta-positioning on the benzene ring, which leads to a 120° angel between the two hydrogen bonding dimers generated from the acid groups (Figure 2.10B), since the bond angle for hydrogen bonds is 180°. Therefore multiple isophthalic acid ends are able to associate with each other. It should be noted that the six-membered ring structure shown in Figure 2.10B is the most stable state for the self-

assembly of isophthalic acid on a surface (2D) as a small molecule [24-25], and does not necessarily represent the optimal aggregation number for isophthalic acid ended telechelics (DA-PCOD). The 3D assembly nature and the entropic effect of polymer chains may complicate the thermodynamically stable aggregation number. In conclusion, the chemical structure of isophthalic acid determines that the mechanism of the multimeric association of DA-PCOD is interestingly the pairwise hydrogen bonds between carboxylic acids.

2.4.1.2 Relaxation modes of pairwise-associative polymers

For the solutions of pairwise-associative polymers, two relaxation modes are expected to exist: 1) the conformation relaxation of the supramolecules formed by pairwise-associative polymers, and 2) the dissociation of the charge-assisted hydrogen bonding between
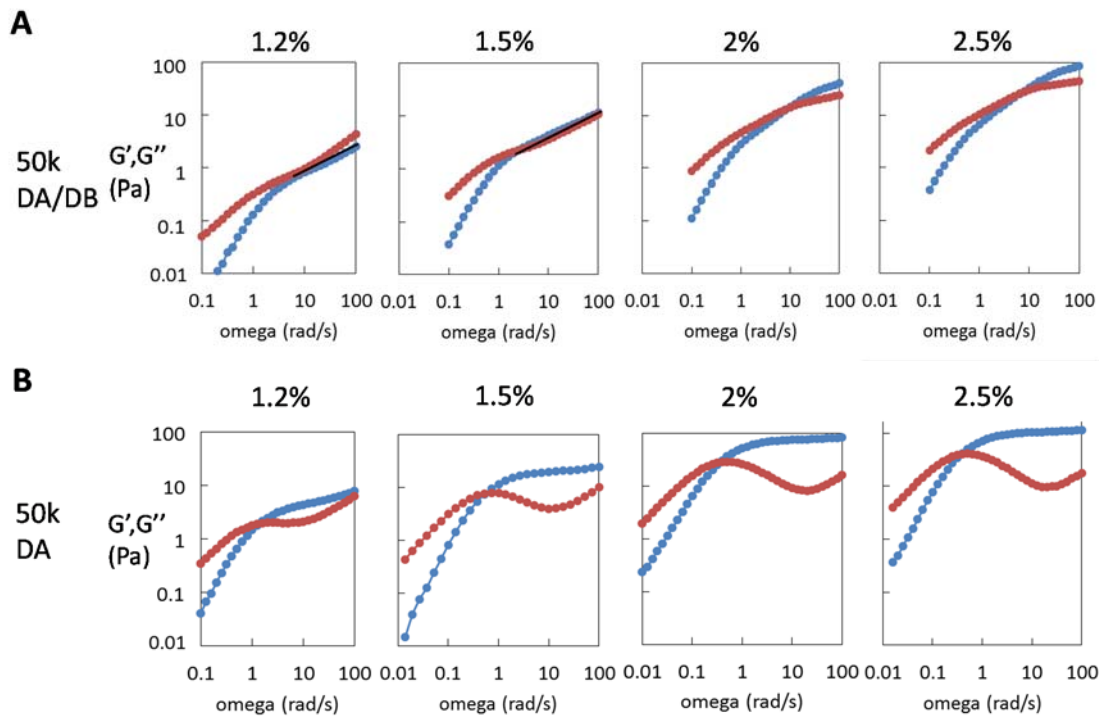
Figure 2.11 Comparison between the oscillatory rheology data for DA/DB-PCOD (M_w = 50 kg/mol) and that for DA-PCOD (M_w = 50 kg/mol) at 0 ℃. A. Storage modulus G' (blue circles) and loss modulus G" (red circles) of DA/DB-PCOD at concentrations from 1.2 wt% to 2.5 wt%. **B.** Storage modulus G' (blue circles) and loss modulus G" (red circles) of DA-PCOD at concentrations from 1.2 wt% to 2.5 wt%.

isophthalic acid (DA) and di-tertiary amine (DB). The measured relaxation patterns of these solutions (Figure 2.11A) show significant resemblance to the dynamics of semidilute unentangled solutions and semidilute entangled solutions of linear covalent polymers (Figure 2.3 AB), suggesting the dominant relaxation process is the conformation relaxation of the supramolecules. Surprisingly, it appears that the dissociation of DA/DB does not occur in the measured relaxation process.

To illustrate this phenomenon, the difference between the binding strength of DA's self-association and that of DA/DB pairwise-association need to be considered. The association between isophthalic acid and di-tertiary amine (DA/DB) has a binding free energy (ΔG) of 40 kJ/mol (16 kT) at 298K, while the free energy (ΔG) for the self-association of isophthalic acid (DA) is 32 kJ/mol (13 kT), as stated in Chapter 1. This statement has been well supported experimentally in our previous work: ^{1}H-NMR data showed that all isophthalic acid groups on DA-PCOD chains were consumed by association with tertiary amine when equiv. molar of DB-PCOD was added to the solution [1]. DA/DB pair indeed binds much tighter than DA's self-association.

The end-exchange time (τ_{ex}), which is inverse dissociation rate constant ($1/k_d$), is related to an activation energy (E_a) through Arrhenius equation, $\tau_{ex} \sim A \exp(E_a/RT)$. Although the kinetic activation energy (E_a) cannot be replaced by the thermodynamic energy (ΔG) in calculating the end-exchange time (τ_{ex}), literature has observed correlation between thermodynamic energy and end-exchange time: high hydrogen bonding strength slows down its dissociation [27-28], and hence the lifetime of DA/DB binding should be longer than that of DA.

The end-exchange time (τ_{ex}) of DA is measured directly as the relaxation time of DA-PCOD solutions (Figure 2.11B). The dissociation of DA/DB, if it ever occurs within the measured time scale, should occur at much lower frequency than the crossover frequency for DA-PCOD solutions. Obviously, the crossover frequency for DA-PCOD is already in the terminal region in the dynamic curves for DA/DB-PCOD solutions at corresponding concentration (Figure 2.11, part A compared with part B for each concentration). Therefore, even if DA/DB does exchange at a specific frequency in the terminal region, the resulting fragments of supramolecules should have their Rouse relaxation faster than the original supramolecules due to their shorter length, and then appear to relax "instantaneously" at that specific frequency, causing no change to the dynamic curve. Consequently, the measured relaxation patterns of these semidilute solutions of pairwise-associative polymers only depict the conformation relaxation of their formed supramolecules and do not give information on the DA/DB association itself, as the association never breaks before the supramolecules relax completely.

In summary, due to the qualitatively different association mechanism (multimeric end-association *versus* one-to-one end-association), the semidilute solutions of self-associative and pairwise-associative polymers exhibit distinct dynamics, even though their polymer backbones are exactly the same, and only half of the end groups (< 0.5% of total weight) are different. DA-PCOD forms flower-like micelles which are bridged into a network in semidilute solutions, and its relaxation is determined by the dissociation/exchange rate of the isophthalic acid end between the micelle cores. Pairwise-associative polymers form linear and cyclic supramolecules. The measured relaxation pattern demonstrates the conformation relaxation of the supramolecules formed by pairwise-associative telechelics

Table 2.1 Molecular characteristics of polyisobutylene (PIB) and 1,,4-polybutadiene (1,4-PB) at 25°C [29].

	PIB	1,4-PB
b (Å)	12.5	9.9
M_0 (g/mol)	274	113
$G_e(1)$ (MPa)	0.34	1.15
$N_e(1)$	24	18

b (Å): Kuhn length; M_0: the molar mass of a Kuhn segment; $G_e(1)$: the entanglement plateau in melts; $N_e(1)$: number of Kuhn segments in one entanglement strand.

as if the supramolecules are stable linear polymers, while the isophthalic acid and tertiary amine ends are held tightly together before the supramolecules relax completely.

2.4.2 Pairwise-associative polymers *versus* linear covalent polymers

2.4.2.1 Backbone property: PIB *versus* PCOD (1,4-PB)

PIB is chosen as the linear covalent polymer control due to its similar polarity and solubility as the PCOD backbone, which has the same structure as perfect 1,4-PB. However, the detailed molecular properties of PIB still differ from 1,4-PB: 1) PIB is slightly stiffer than 1,4-PB (shown with b (Å) in Table 2.1), and 2) only 2 carbons out of 4 within one monomer constitute the backbone for PIB, while all carbons are on the backbone for 1,4-PB, partially explaining their difference in M_0 (Kuhn segment molar mass, Table 2.1).

Their dynamic properties, which are more relevant to our discussion here, differ as well. The size of their entanglement strand is different (Table 2.1, $G_e(1)$ and $N_e(1)$). Besides, the relaxation time for a Kuhn monomer (τ_0) is related to the Kuhn length: $\tau_0 \approx \frac{\eta s}{kT} b^3$. Then a ratio of the monomer relaxation time of these two backbone can be estimated: τ_0 (PIB)/ τ_0 (PB) = $[b(\text{PIB})/b(\text{PB})]^3$ = 2.

Table 2.2 Overlap and entanglement concentrations for non-associative 50 kg/mol PCOD

	C* ($\eta_{sp} = 1$, decalin)	$C_e \sim [N_e(1)/N]^{0.76}$
50k	0.8 wt% [a]	8.3 wt% [b]

[a.] C* for 50k non-associative chains: measured using viscometry

[b.] C_e : calculated using the equation $C_e \approx [Ne(1)/N]0.76 \approx [Me/M]0.76$. The entanglement molar mass (*Me)* for 1,4-polybutadiene in the melt at 25°C is 1900 g/mol, and $Ne(1) = 18$ [29].

2.4.2.2 The dynamics of pairwise-associative polymers compared to linear covalent polymers

For ease of comparison between pairwise-associative polymers and linear covalent polymers, critical concentrations are estimated for the polymer backbone (polycyclooctadiene, same structure as perfect 1,4-polybutadiene, with no end association) of 50kg/mol (Table 4.2). The C* is measured by viscometry of a 50 kg/mol non-associative telechelic PCOD. The concentration at which the specific viscosity of the polymer solution equals 1 is chosen as the overlap concentration C*, since $\eta_{sp} = (\eta- \eta_s)/ \eta_s \approx \varphi^* N^{3v-1} \approx N^{1-3v}$ $N^{3v-1} \approx 1$ at φ^* according to Zimm model [14]. The entanglement concentration is calculated using the equation $C_e \approx [N_e(1)/N]^{0.76} \approx [M_e/M]^{0.76}$. Theoretically, the ratio between C_e and C* should be on the order of $[N_e(1)/N]^{0.76}/ N^{-0.76} \approx N_e(1)^{0.76} \approx 9$, since the $N_e(1)$ for 1,4-polybutadiene at 25°C is 18. The measured C* for 50 kg/mol is around 1/10 that of the calculated C_e (Table 4.2, 0.8 wt% *versus* 8.3 wt%), in consistence with the theoretical value fairly well. The concentration range chosen for studying the dynamics of 50 kg/mol DA/DB-PCOD (1.2 wt% to 2.5 wt%) then corresponds to 1.5C* ~ 3C* for the 50k backbone, which makes these DA/DB-PCOD solutions slightly semidilute, and definitely not concentrated enough to be entangled.

A

1.2% 1.5% 2% 2.5%

50k DA/DB G',G" (Pa)

omega (rad/s)

B

1.2% 2%

4.2M PIB G',G" (Pa)

Unentangled:
$$\tau_{chain} \approx \tau_0 N^2 C^{0.31}$$
$$G_{chain} \approx (kT/b^3)N^{-1}C^1$$
$$\eta \sim NC^{1.3}$$

Entangled:
$$\tau_{rep} \approx \tau_0 N^3 C^{1.6}/N_e(1)$$
$$G_e \approx G_e(1)N^0 C^{2.3}$$
$$\eta \sim N^3 C^{3.9}$$

omega (rad/s)

C

1.5% 2.5%

1.1M PCOD G',G" (Pa)

omega (rad/s)
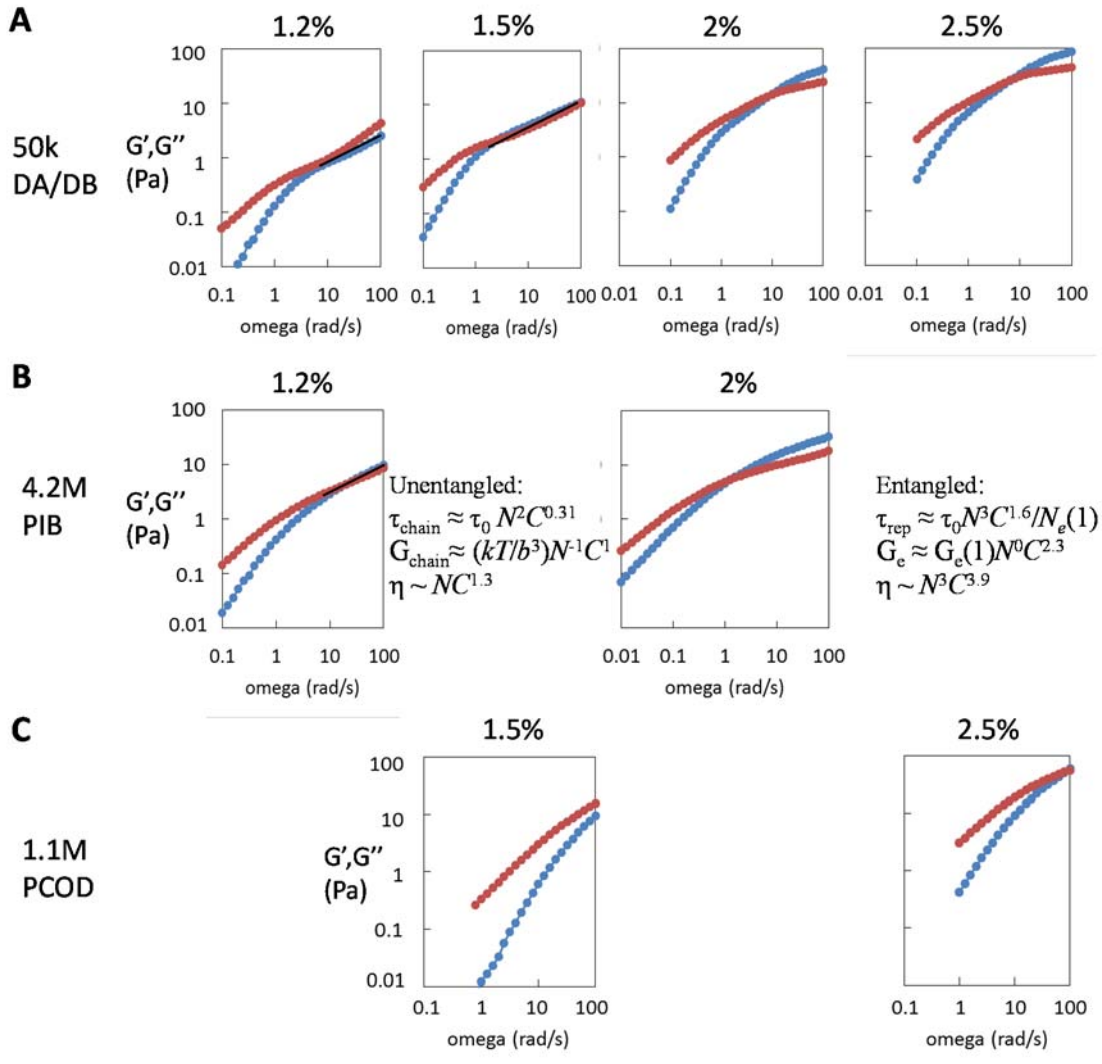
Figure 2.12 Comparison between the oscillatory rheology data for solutions of DA/DB-PCOD (M_w = 50 kg/mol) and that of linear covalent polymers at 0 ℃. Storage (G', blue circles) and loss modulus (G", red circles) of **A.** DA/DB at concentrations from 1.2 wt% to 2.5 wt%. **B.** 4.2M PIB (M_w = 4,200 kg/mol) at concentrations of 1.2 wt% and 2 wt%. **C.** 1.1M PCOD (M_w = 1,100 kg/mol) at concentrations of 1.5 wt% and 2.5 wt%. The black lines depict the slope of ½.

However, the solutions of DA/DB-PCOD show marked dynamic features of semidilute unentangled solutions at 1.2 and 1.5 wt%, and then mimic semidilute entangled solutions as the concentration is increased to 2 wt% (Figure 2.12A). It is even more surprising that supramolecules formed by short telechelic polymer (50 kg/mol PCOD, N = 442) can exhibit dynamics comparable to that of a linear covalent polymer (4,200 kg/mol PIB, N =

15,328) with a 35-fold longer chain length (Figure 2.12A compared to B), motivating us to dig deeper into the supramolecules.

DA/DB-PCOD forms a distribution of linear and cyclic supramolecular species with various sizes, among which the longer species in the solutions relax slower and dominate the rheological behavior of the solutions over the shorter species. Since the dynamics of these species resembles that of linear covalent polymers, a naively simplified treatment is made: the supramolecular species that are effective for the strikingly long relaxation are treated as an ultralong linear covalent polymer. And the size and concentration of these rheologically effective species can be estimated by a semi-quantitative analysis comparing the dynamic moduli of DA/DB-PCOD with that of linear covalent polymer controls (4.2M PIB and 1.1M PCOD). Despite the overly simplified treatment, the result seems to agree qualitatively well with the prediction of ring-chain equilibrium.

2.4.2.2.1 Estimation of the rheologically effective species in the semidilute unentangled solutions of DA/DB-PCOD (1.2 wt%)

The 1.2 wt% solutions for DA/DB-PCOD and 4.2M PIB display intriguingly similar features in their dynamic moduli curves, with a distinct power law region with a slope of ½, suggesting that both solutions are in the semidilute unentangled regime (Figure 2.12A and B, 1.2%). Thus, 4.2M PIB 1.2% solutions is utilized as the control for unentangled solutions. If the rheologically effective species are treated as one linear covalent polymer, its length (N_{eff}) and concentration should contribute to the modulus (G_{chain}) and relaxation time (τ_{chain}) according to the scaling relationship proposed for linear polymer (like 4.2M PIB) (Figure 2.12). Therefore their size (N_{eff}) and concentration can be estimated by

comparing the modulus (G_{chain}) and relaxation time (τ_{chain}) of DA/DB-PCOD with that of PIB.

The terminal relaxation time for the two solutions, when the power law region stops and the terminal region begins, is very close (τ_{chain} (DADB) $\approx$ 0.08 to 0.1 s; τ_{chain} (PIB) $\approx$ 0.06 to 0.1 s). Considering the difference in the monomer relaxation time for two backbones, τ_0 (PB)/τ_0 (PIB) = 1/2 as stated above, the effective supramolecules in 50k DA/DB solution then has a length around 1.2 ~ 2 fold of the length for 4.2M PIB (N(PIB)=15,328; N_{eff} = 24524 $\pm$ 6131), and a molecular weight of ~ 2,771 $\pm$ 693 kg/mol (M_0 = 113 g/mol for 1,4-PB) (Figure 2.13, left).

On the other hand, the terminal modulus (G_{chain}) is expected to proportional to concentration and inverse proportional to N and b^3: $G_{chain} \approx (kT/b^3)N^{-1}C^1$. Considering the relationship of N_{eff}/N(PIB)= 1.2 ~ 2 and $[b(\text{PIB})/b(\text{PB})]^3$ = 2 obtained above, the G_{chain} for PIB is supposed to be 60% ~ 100% of that of DA/DB-PCOD solution if all individual telechelic polymers distribute into the effective species. On the contrary, the G_{chain} of 1.2 wt% 50k DA/DB-PCOD solution is about 25% of that of 4.2M PIB solution, suggesting that only a small fraction of DA/DB-PCOD (15% ~ 25%) form species that are rheologically effective. And the rest of telechelic polymers (75% ~ 85%) distribute into cyclic and linear species with smaller sizes (Figure 2.13, left).

2.4.2.2.2 Estimation of the rheologically effective species in the semidilute entangled solutions of DA/DB-PCOD (2 and 2.5 wt%)

At concentrations >2 wt%, curves for 50k DA/DB-PCOD, 1.1M PCOD and 4.2M PIB all exhibit a crossover of G' and G'', indicating that the DA/DB-PCOD may be entangled just

like 1.1M PCOD and 4.2M PIB (Figure 2.12). The effective supramolecular species in DA/DB-PCOD solutions are again simplified as one linear polymer. The scaling relationships that guide the dynamic parameters in the semidilute entangled solutions are $\tau_{rep} \approx \tau_0 N^3 C^{1.6}/N_e(1)$ and $G_e \approx G_e(1)N^0 C^{2.3}$. The reptation time τ_{rep} depends strongly on chain length N ($\sim N^3$), while the modulus depends only on concentration and is independent of N. Therefore, the ratio of relaxation time (τ_{rep}) gives information on the chain length, and the fraction of the effective supramolecular species can be evaluated through the crossover modulus (G_x), which is generally considered proportional to the plateau modulus (G_e) (Table 2.3).

First, the two 50k DA/DB-PCOD solutions at 2 wt% and 2.5 wt% are compared with each other to examine 1) whether the crossover is truly due to entanglement, and 2) whether the length and the fraction of effective species changes as concentration increases from 2 to 2.5 wt%. Theoretically, if entanglement is the dominant relaxation mode, the ratio of G_x

1.2%	2%	2.5%
< 25%	> 70%	> 70%
~ 2,771 ± 693 kg/mol	~ 2,400 ± 300 kg/mol	~ 2,400 ± 300 kg/mol
>75%	< 30%	< 30%
Collection of smaller rings and chains	Collection of smaller rings and chains	Collection of smaller rings and chains
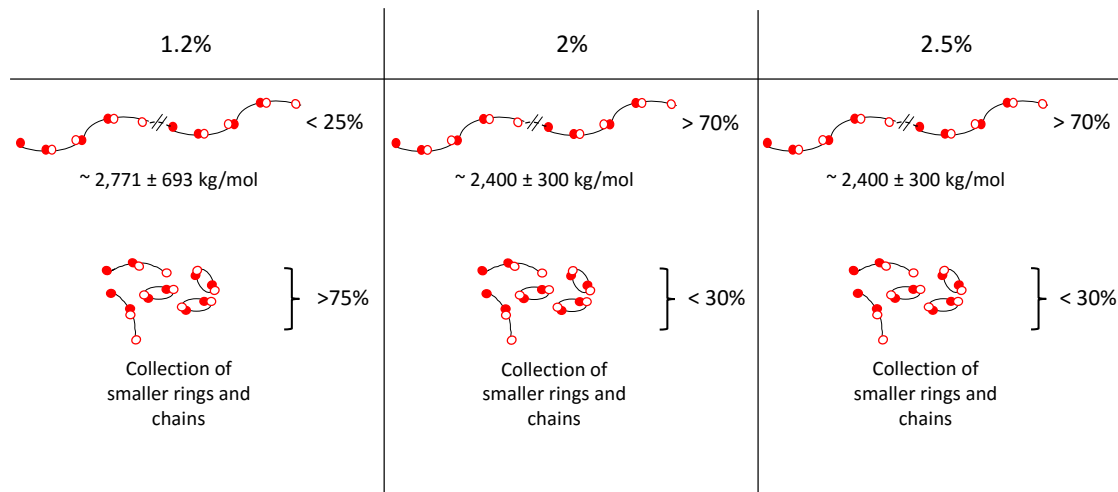
Figure 2.13 Simplified representations of the roughly estimated fractions of the rheologically effective species in the solutions of 50k DA/DB-PCOD at three concentrations: 1.2 wt%, 2 wt% and 2.5 wt%. Red and white circles represent acid and amine ends.

Table 2.3 The crossover modulus (G_x) and relaxation time (τ_x) for the solutions of 50k DA/DB-PCOD, 4.2M PIB and 1.1M PCOD in decalin at 0°C.

	4.2M PIB 2%	50k DA/DB 2%	1.1M PCOD 2.5%	50k DA/DB 2.5%
G_x (Pa)	5±0.4	15±2	50±5	28±3
τ_x (s)	0.6±0.1	0.11±0.02	0.013±0.003	0.14±0.02

(2.5 wt%): G_x (2 wt%) should be $(\frac{2.5}{2})^{2.3}$, which is 1.7. The measured crossover modulus for the two concentrations gives a ratio of 28/15 = 1.86 (Table 2.3), which is close to the theoretical prediction. This result demonstrates that the crossover is indeed the result of entanglement, and indicates that the fraction of the dominant supramolecules does not change much for as concentration increases from 2 wt% to 2.5 wt% (Figure 2.13, right column).

The reptation time varies significantly with both polymer length and concentration: $\tau_{rep} \sim N^3 C^{1.6}$. An increase in polymer concentration from 2 wt% to 2.5 wt% will extend the relaxation time by $(\frac{2.5}{2})^{1.6} = 1.4$ fold. This calculated value matches the experimental data (Table 2.2B, τ_{rep} (2%) = 0.11±0.02s, τ_{rep} (2.5%) = 0.14±0.02s), indicating that the average length of the dominant supramolecular species is the same for the two concentrations. Therefore, both the fraction and the length of the effective supramolecular species of 50 DA/DB-PCOD solutions vary only slightly with polymer concentration in the semidilute entangled regime (Figure 2.13, middle and right column).

Next, the 2 wt% DA/DB-PCOD solution is compared to 2 wt% PIB solution. The crossover modulus (G_x) for 50k DA/DB solution at 2 wt% triples that for the 4.2M PIB solution at the same concentration (Table 2.3, 15±2 Pa compared to 5±0.4 Pa), giving a ratio around

3 ± 0.6. Considering the equation of $G_e \approx G_e(1)N^0C^{2.3}$ and the fact that the $G_e(1)$ for 1,4-PB backbone is 3.4 times that of PIB backbone (Table 2.1), the difference in the crossover modulus of the two solutions (DA/DB-PCOD *versus* PIB) can be mostly accounted for just by the discrepancy in $G_e(1)$ for 1,4-PB and PIB backbones, and the dominant supramolecular species takes 70%~100% of total compositions in the 50k DA/DB solution at 2 wt% (Figure 2.11, middle column). Comparing to the value of 15 ~25% in the 1.2 wt% DA/DB-PCOD solution, the fraction of rheologically effective species increases dramatically as the solution transits from unentangled to entangled regime.

Then the 2.5 wt% DA/DB-PCOD solution is compared with that of 2.5 wt% PCOD. Although their crossover modulus should theoretically be very close (<30% difference) considering the large fraction of effective supramolecules, a bigger discrepancy exists in our measured data (50 ± 5 Pa versus 28 ± 3 Pa, $\sim 50\%$). It may because that the 1.1M PCOD is synthesized using another method, which may cause slight change in backbone properties. However, the ratio in their relaxation times can still provide a rough assessment on the length of effective species based on the relationship $\tau_{rep} \approx \tau_0 N^3 C^{1.6}$, which is $\sim 2,400 \pm 300$ kg/mol (N(DA/DB) $= 21239 \pm 2655$).

Data shows that 50 kg/mol DA/DB-PCOD forms long supramolecules at 0℃ that relax as if they are ultralong polymers (> 1,000 kg/mol, Figure 2.13), although the estimation of the average length of effective species has large variation because of the scatter in the measurement of relaxation time and the difference in the chemical structures of the linear polymer control and the DA/DB-PCOD backbone.

A simplification is made by treating the supramolecular species that contributes to the long relaxation as a linear covalent polymer with one average length. However, a linear

supramolecule with $M_w \sim 2,400$ kg/mol contains > 40 chains of 50 kg/mol DA/DB-PCOD linked together, which hardly exists in real world, especially in solutions at concentrations as low as 1.2 to 2.5 wt%. In fact, data obtained using DA/DB-PCOD with higher molecular weights confirms that the strikingly long relaxation time here may be a result of some more complicated interactions, which will be explained more in Chapter 4. Nevertheless, this simplified treatment explains the observed Rouse-like (at 1.2 and 1.5%) and reptation-like (at 2 and 2.5%) dynamics, allows comparison with the dynamics of linear covalent polymers, and provides a means to analyze the fraction of these effective species and its concentration dependence.

2.4.2.3 Concentration dependence of the viscosity of DA/DB-PCOD solutions

To explain the change in dynamic moduli, we hypothesized that the distribution of supramolecular species varies when the solution shifts from semidilute unentangled regime (1.2 wt%) to semidilute entangled regime (2 wt%). More individual pairwise-associative chains assemble into long supramolecules that contribute to rheological properties as the concentration increases from 1.2 wt% to 2 wt% (Figure 2.13).

This hypothesis is consistent with the shear viscometry data obtained with 50k DA/DB at a series of concentrations. For linear covalent polymers, the dependence of specific viscosity η_{sp} on polymer concentration C varies from $\eta_{sp} \sim C^1$ to $\sim C^{1.3}$, and to $\sim C^{3.9}$ as the concentration increases from C<C*, to C*<C<C$_e$, and to >C$_e$ (Figure 2.14A). From the above oscillatory experiments, the solutions of pairwise-associative telechelic polymers show a transition from unentangled to entangled regime as the concentration rises from 1.5 wt% to 2 wt%, indicating that the "apparent C$_e$" should be between 1.5 wt% and 2 wt%. Interestingly, the shear viscometry data of the same polymer solutions demonstrates that
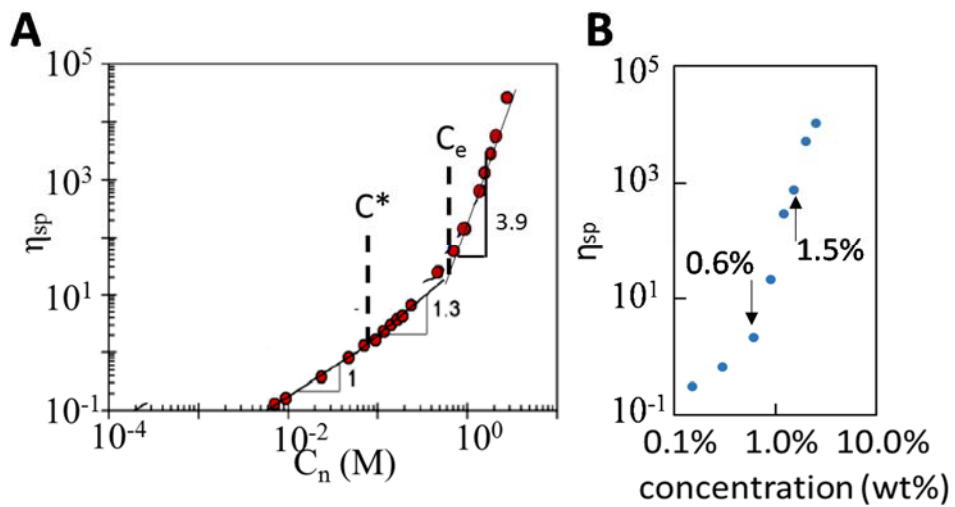
Figure 2.14 A. (Figure reproduced from reference [19]) The specific viscosity in the good solvent ethylene glycol of poly(2-vinyl pyridine) plotted as functions of the number density of monomers. **B.** The specific viscosity of 50 kg/mol DA/DB-PCOD in the solution of decalin at 0°C plotted against the polymer concentration in wt%.

the dramatic change in slope occurs at concentration around 0.6 wt% (Figure 2.14B), much lower than 1.5 wt%. The apparent discrepancy between oscillatory data and shear viscometry data can be explained by the change in supramolecular distribution with concentrations.

The fraction of longer linear species increases considerably in the concentration range of 0.6 wt% - 1.5 wt%, offering extra contribution to the solution viscosity additional to the scaling relationship on polymer concentration, leading to an early escalating slope in the log-log plot of specific viscosity against concentration (Figure 2.14B). The combination of the oscillatory rheology data and the shear viscometry data provides strong support to the hypothesis on the concentration-dependent distribution of supramolecular species.

2.5 Conclusions

50k DA-PCOD shows dynamic features similar to those of HEURs at 0°C in the sense that the solution dynamics resembles the Maxwell relaxation model with one dominant

relaxation time and the shear viscosity of their solutions have similar dependence on polymer concentrations. It is postulated that DA-PCOD is capable of multimeric association *via* directional hydrogen bonding due to the specific chemical structure of the isophthalic acid end.

50k DA/DB-PCOD solutions at 0℃ exhibit dynamics that strikingly resembles that for linear covalent polymers. Its solution in decalin at 0℃ transits from being semidilute unentangled at 1.2 wt% to being semidilute entangled at 2.5 wt%, similar to the transition normally seen with solutions of linear covalent polymer (such as 4.2M PIB). It is likely that DA/DB-PCOD indeed assembles into linear/cyclic supramolecules that relax like linear covalent polymers.

The conformational relaxation of the supramolecules formed by DA/DB-PCOD dominates the solution dynamics, while the DA/DB ends appear not to dissociate/exchange in the process. The distribution of supramolecular species varies with concentration. And more specifically, the fraction of the rheologically effective species are much higher at higher concentrations (e.g. > 70% at 2 wt% and 2.5 wt%) compared to lower concentrations (e.g. < 25% at 1.2 wt%), which is consistent with the prediction of ring-chain equilibrium and the statistical mechanical model on pairwise-associative polymers (Section 2.1.3).

References

[1] M.-H. Wei*, B. Li*, R. L. A. David, S. C. Jones, V. Sarohia, J. A. Schmitigal & J. A. Kornfield (*: authors contributed equally), *Science*, **2015**, *350*, 72-75.

[2] C. Chassenieux, T. Nicolai, L. Benyahia, *Current Opinion in Colloid & Interface Science,* **2011***, 16*, 18-26.

[3] T. Park, S. C. Zimmerman, *J. Am. Chem. Soc.,* **2006**, *128*, 13986-13987.

[4] H. Hofmeier, R. Hoogenboom, M. E. L. Wouters, U. S. Schubert, *J. Am. Chem. Soc.,* **2005**, *127*, 2913-2921

[5] T. F. A. de Greef, G. Ercolani, G. B. W. L. Ligthart, E. W. Meijer, R. P. Sijbesma, *J. Am. Chem. Soc.,* **2008**, *130*, 13755-13764.

[6] S. K. Yang, A. V. Ambade, M. Weck, *Chem. Soc. Rev.* **2011**, *40*, 129–137.

[7] R. P. Sijbesma *et al.*, *Science* **1997**, *28*, 1601-1604.

[8] S. K. Yang, A. V. Ambade, M. Weck, *J. Am. Chem. Soc.,* **2010**, *132*, 1637–1645

[9] T. Annable, R. Buscall, R. Ettelaie, & D. Whittlestone, *Journal of Rheology,* **1993**, *37*, 695-726.

[10] F. Tanaka & S. F. Edwards, *Macromolecules,* **1992**, *25*, 1516-1523.

[11] A.N. Semenov, J.-F. Joanny & A. R. Khokhlov, *Macromolecules,* **1995,** *28*, 1066-1075.

[12] Q. T. Pham, W. B. Russel, J. C. Thibeault, W. Lau, *Macromolecules,* **1999**, *32*, 2996-3005.

[13] Q. T. Pham, W. B. Russel, J. C. Thibeault, W. Lau, *Macromolecules,* **1999**, *32*, 5139-5146.

[14] B. Zimm, *J. Chem. Phys.,* **1956**, *24*, 269-278.

[15] P. Rouse, *J. Chem. Phys.,* **1953**, *21*, 1272-1280.

[16] Lodge, T. P., Miller, J. W. and Schrag, J. L. *J. Polym. Sci. Polym. Phys. Ed.*, **1982**, *20*, 1409–1425.

[17] P. G. De Gennes, *J. Chem. Phys.*, **1971**, *55*, 572–571.

[18] R. H. Colby, L. J. Fetters, W. G. Funk, W. W. Graessley, *Macromolecules*, **1991**, *24*, 3873 – 3882.

[19] S. Dou, R. H. Colby, *J. Polym. Sci. Polym. Phys.* **2006**, *44*, 2001-2013.

[20] H. Jacobson, W. H. Stockmayer, *J. Chem. Phys.* **1950**, *18*, 1600-1606.

[21] A. T. ten Cate, et al, *J. Am. Chem. Soc.* **2004**, *126*, 3801–3808

[22] S. K. Yang, A. V. Ambade, and M. Weck *Chem. Eur. J.* **2009**, *15*, 6605–6611.

[23] M. R. Tant, G. L. Wilkes, J. P. Kennedy, *J. Appl. Polym. Sci.*, **1991**, *42*, 523-532.

[24] N. Martsinovich, A. Troisi, *J. Phys. Chem. C* **2010,** *114,* 4376–4388.

[25] M. Lackinger, W. M. Heckl, *Langmuir*, **2009**, *25*, 11307–11321.

[26] S. De Feyte *et al*, *Nano Letters*, **2003**, 3, 1485–1488.

[27] L. E. Cramer, K. G. Spears, *J. Am. Chem. Soc.*, **1978**, *100*, 221–227.

[28] J. Zheng, M. D. Fayer, *J. Phys. Chem. B* **2008,** *112,* 10221–10227.

[29] J. E. Mark, *Physical Properties of Polymers Handbook,* 2nd ed, Springer-Verlag, New York, 2007, Chap 25.

Chapter III

Effect of Temperature on Associative Telechelic Polymers

3.1 Introduction

In Chapter 2, the distinct dynamics of self-associative polymers (di-acid-ended PCOD, DA) and pairwise associative polymers (di-acid-ended paired with di-amine-ended PCOD, DA/DB) have been discussed, as well as their concentration dependence. Self-associative and pairwise-associative polymers are demonstrated to exhibit dramatically different features, even though their polymer backbones are exactly the same, and only half of the end groups (< 0.5% of total weight) are different.

The dynamics of DA-PCODs makes contact with prior literature on self-associative polymers. It is demonstrated that DA-PCODs form flower-like micelles as expected, which start to form bridges with each other and assemble into interconnected network as their concentration increases. The resulting viscous solutions give dynamic modulus curves which can be fitted by the Maxwell model with a single relaxation time. This relaxation time is governed by the diffusion of hydrophobic end escaping the micelle core [1]. The viscosity and high-frequency modulus of these polymer solutions strongly depends on the polymer concentrations. In addition, the relaxation time also increases slightly with increasing concentration. Both features resemble the behavior of HEUR systems and can be explained by the concentration-dependent topological change of the micelle structures [1].

DA/DB PCODs are proved to form a distribution of cyclic and linear supramolecules due to their pairwise end association, with the long linear species dominating the solution dynamics. The dynamics of the supramolecules formed by 50k DA/DB PCOD at 0℃ resembles that of linear covalent polymers. As the concentration increases from 1.2 wt% to 2.5 wt%, the solution of 50k DA/DB PCOD exhibits a transition from the semidilute unentangled to the semidilute entangled regime just like linear covalent polymers. A semi-quantitative analysis on the oscillatory data of DA/DB-PCOD solution compared to that of linear covalent polymers leads to the postulation that the supramolecular species that dominate the solution dynamics have an apparent length over 1000 kg/mol at all four concentrations. And the fraction of the rheologically effective species increases significantly as the concentration rises from 1.2 wt% to 2 wt%. The supramolecules formed by DA/DB-PCOD consist of an ensemble of linear and cyclic species having a range of molecular weights. This makes the DA/DB-PCOD system similar but distinct from linear covalent polymers.

In this chapter, the effect of temperature is brought into consideration. Temperature can affect a process during which an activation energy is involved, including chemical reactions, diffusion of particles and the dynamics of polymers. The simplest model to depict the temperature dependence is Arrhenius model, correlating one parameter, e.g. solution viscosity (η), with an activation energy E_a: $\eta \sim \exp\left(\dfrac{Ea}{kT}\right)$. When the activation energy is large, the parameter has high dependence on temperature.

DA/DB-PCOD binds with charge assisted hydrogen bond (CAHB), which is expected to have high activation energy. It will be demonstrated in this chapter that DA-PCOD's self-

association is also based on directional hydrogen bond, instead of micro phase separation due to low solubility. Therefore, strong temperature effect should be anticipated on the dynamics of both telechelic polymer solutions [2]. Temperature dependence of the binding strength may affect the end association equilibrium, and the structures and compositions of the supramolecules as well.

The goal of this section is to build on the fundamental concepts and review the prior literature related to the temperature's effect on the dynamics of our self- and pairwise-associative system. The following aspects will be covered: 1) the effect of temperature on the dynamics of linear covalent polymers, 2) the effect of temperature on the dynamics of HEURs, and 3) the effect of temperature on the end association equilibrium of DA and DA/DB.

3.1.1 Temperature effect on the dynamics of linear covalent polymers

3.1.1.1 Time-temperature superposition

In all the models developed for the dynamics of linear covalent polymer, including the Zimm model, the Rouse model, and the reptation model, the temperature effect is covered. It is assumed that the relaxation time (τ) associated with each mode can all be written as a product of the monomer relaxation time (τ_0) and a power law of N (number of Kuhn segments) with an exponent containing ν (reciprocal of the fractal dimension) and some other temperature-independent terms (including concentration factors). Normally, ν depends weakly on temperature. In this chapter, the solvent chosen is an athermal solvent for the backbone, meaning $\nu = 0.588$ regardless the temperature. Therefore the weak temperature dependence of ν and the polymer coil size can be readily omitted. The

temperature dependence of the relaxation time can be attributed solely to the monomer relaxation time ($\tau_0 \sim \frac{\zeta}{kT} b^2$), which means that the T-dependence of polymer solution mainly resides in that of the friction coefficient of the polymer backbone in the solvent.

The models also assume that the relaxation time of each mode has the same temperature dependence ($\tau \sim \frac{\zeta}{T}$). This has an important implication on polymer dynamics: the linear viscoelastic data obtained at different temperatures can be superimposed, which is known as the Time-Temperature Superposition (TTS) principle [3].

In general, the stress relaxation modulus $G\ (t,\ T)$ at two temperatures (T and T_0) can be superimposed by a horizontal shift on the time axis (shift factor a_T) and a much weaker vertical shift on the modulus axis (shift factor b_T): $G\ (t,\ T) = b_T\ G\ (\frac{t}{a_T},\ T_0)$, with T_0 identified as the reference temperature.

Thus, in oscillatory shear experiments, the storage and loss modulus both follow the time-temperature superposition principle: $G'\ (\omega, T) = b_T\ G(\omega a_T,\ T_0)$, $G''\ (\omega, T) = b_T\ G(\omega a_T,\ T_0)$. The time shift factor (a_T) depends on the friction coefficient and the temperature: $a_T = (\zeta T_0)/(\zeta_0 T)$. The modulus shift factor (a_T) depends on the polymer density and the temperature: $b_T = (\rho T)/(\rho_0 T_0)$, since the stress relaxation modulus is proportional to the product of polymer density and temperature ($G(t) \sim \rho T$) and the polymer density varies weakly with temperature.

Since the viscosity equals the product of the relaxation time and the modulus at that time, the temperature dependence of viscosity is: $\eta = \eta_0\ a_T\ b_T$. As shown above, the strongest temperature-dependent parameter is the friction coefficient. The simplest model to depict

the temperature dependence of the friction coefficient is the Arrhenius model with an activation energy Ea: $\eta \sim \tau \sim \exp\left(\frac{Ea}{kT}\right)$. When the natural log of the viscosity (ln η) is plotted against inverse absolute temperature (1/T), the data points should form a linear line, the slope of which can be used to calculate an activation energy (Ea).

3.1.1.2 Temperature dependence of the solution viscosity of linear covalent polymer at low concentrations

The temperature dependence of the viscosity of polymer melt and polymer solutions has been examined in detail since the 1940s. The activation energy Ea has been observed to be influenced by various factors, including the molecular structure of polymers, chain rigidity, solvent quality, possible polymer-solvent interaction, polymer concentration, *etc* [4,5]. Tager *et al.* reported a detailed study of polyisobutylene (PIB, 1,200 kg/mol) solutions, from the dilute state to the melt [5]. It was demonstrated that from very low concentrations up to the PIB melt state, E_a increases monotonically (but not linearly) with concentration from the value of Ea of pure solvents (12.1 kJ/mol for cyclohexane) to E_a for the polymer melt at 67 kJ/mol. When the volume fraction of the polymer is low (<0.05, roughly corresponding to < 5 wt% concentration), E_a of the PIB solution is close to (a little higher than) that of the pure solvent.

3.1.2 Temperature effect on the dynamics of HEUR solutions

The most extensively studied self-associative polymer in literature is hydrophobically modified urethane-ethoxylate (HEUR), which has been applied as thickening agents in water-borne coatings, paints, and inks to control rheological properties such as viscosity, gelation, shear-thinning, and thickening behavior [6]. The descriptions of their rheological
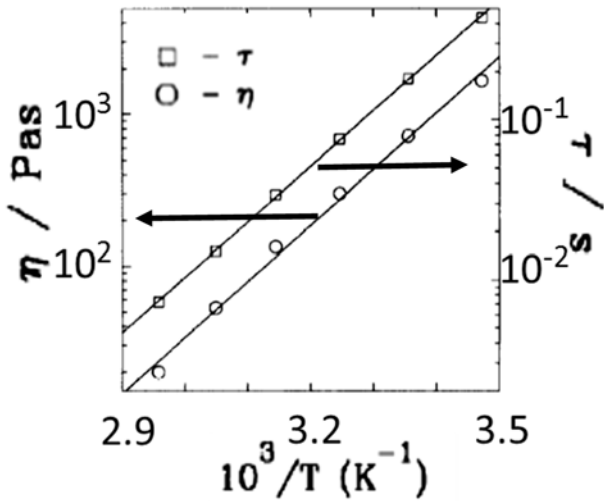
Figure 3.1 (Figure reproduced from reference [1]). Arrhenius plots of low shear viscosity and relaxation time for C16/35K at 10%w/v. (C16/35K, a HERU with a C16 hydrophobe end and M_w = 35 kg/mol.)

and other properties can be found in numerous reports [1,6-11]. Due to the hydrophobic effect of their hydrocarbon ends, these polymers form flower-like micelles at low concentrations. The "petals" (loops) turn into bridges between micelles as concentration is increased, and eventually interconnected networks form [6]. The resulting gels (or thick solutions) present dynamic modulus curves which can be fitted by the Maxwell model with a single relaxation time (Figure 2.2A), which is governed by the diffusion of hydrophobic end escaping the micelle core, proposed by Annable *et al* [1]. The concentration dependence of the viscosity, relaxation time, and high frequency modulus of these solutions has been reviewed in Chapter 2. Here we focus on the temperature effect on the morphology and rheology of HEUR solutions.

Both the relaxation time and the viscosity of the HEUR solutions exhibit strong temperature dependence. The relaxation of the system is determined by the diffusion of hydrophobic end escaping the micelle core, which is associated with an activation energy (*Ea*), which is related to the association energy of the hydrophobic ends. Therefore the

relaxation time strongly depends on temperature. This dependence is expected to be Arrhenius-like: $\tau \sim \exp\left(\frac{Ea}{kT}\right)$ (Figure 3.1). On the other hand, it has been observed in literature that the dynamic modulus curves of HEUR solutions at various temperatures can be superimposed into a master curve, indicating that the micelle structure in the solutions remains constant at all temperatures, and the high frequency modulus does not change with temperature either. Since the solution viscosity is the product of the plateau modulus and the longest relaxation time, the solution viscosity is also temperature dependent and displays Arrhenius-like behavior, just like the relaxation time: $\eta \sim \exp\left(\frac{Ea}{kT}\right)$ (Figure 3.1).

3.1.3 Temperature effect on the end association equilibrium of DA and DA/DB

The association of isophthalic acid (DA) with itself as well as between isophthalic acid and tertiary amine (DA/DB) has been discussed in Chapter 1. DA forms resonance assisted hydrogen bond (RAHB) based on carboxylic acid dimers. DA/DB binds with each other through charge-assisted hydrogen bond (CAHB) [2]. The free energy (ΔG) of the DA and DA/DB association is around 13 kT (32 kJ/mol) [12-13] and 16 kT (40 kJ/mol) [14-16] at room temperature respectively (298K, Figure 4.3A).

It has been well documented in literature that systems based on hydrogen bonds depend highly on temperature. The standard enthalpy (ΔH) and standard entropy (ΔS) in the H-bond formation can be calculated through the Van't Hoff plot of hydrogen bonding systems, and are found to be a constant and independent of temperature in the temperature range encountered in this thesis [17-19]. The H-bond strength (ΔG) decreases linearly with increasing absolute temperature since $\Delta G = \Delta H - T\Delta S$. The corresponding H-bond dissociation constant (K_d) at various temperatures is directly related to ΔG: $K_d = \exp(\Delta G/kT)$ (Figure 4.3A). It is mentioned in Chapter 1 that the temperature dependence of ΔG and K_d can be estimated using Van't Hoff equation: $\ln (K_{d1}/K_{d2}) = - \frac{\Delta H}{R} (\frac{1}{T2} - \frac{1}{T1})$. The H-bond free energy (ΔG) and dissociation constant (K_d) is roughly calculated for 60 ℃ (333K) and 0 ℃ (273K) from the value 16 kT at 25 ℃ (298K) for the DA and DA/DB-PCOD system (Table 3.1). This shift in ΔG with temperature is in good agreement with literature: around 20%

Table 3.1 The estimated bonding free energy (ΔG) and dissociation constant (K_d) using Van't Hoff equation, $\ln (K_1/K_2) = - \frac{\Delta H}{R} (\frac{1}{T2} - \frac{1}{T1})$, with 25 ℃ as the reference temperature.

		60 ℃ (333 K)	25 ℃ (298 K)	0 ℃ (273 K)
DA/DB	ΔH (kJ/mol)	100 ~ 134 (non-polar solvent) [14]		
	ΔG (kJ/mol)	30 ± 3	40[14-16]	46 ± 3
	K_d (µM) = exp(ΔG/RT)	8 ~ 33	0.11	0.0008 ~0.003
DA	ΔH (kJ/mol)	100 ~ 134 (vapor) [12, 19-20]		
	ΔG (kJ/mol)	22 ± 2	32[12-13]	39 ± 2
	K_d (µM) = exp(ΔG/RT)	160 ~ 670	2.26	0.016 ~ 0.056

Table 3.2 The estimated concentration and fraction (in brackets) of unbound end groups for 50k DA and 50k DA/DB at 60, 25, and 0 ℃ at two concentrations (0.6% and 2.5%).

			50k DA	**50k DA/DB**
0.6%	**C total ends= 0.2 mM**	**60 ℃**	140±20 µM (70±10 %)	33±10 µM (33±10 %)
		25 ℃	20 µM (10%)	3.5 µM (4%)
		0 ℃	2.5±0.8 µM (1.3±0.4%)	0.38±0.1 µM (0.4±0.1%)
2.5%	**C total ends= 0.88 mM**	**60 ℃**	400±100 µM (45±12 %)	83±20 µM (20±5%)
		25 ℃	45 µM (5%)	7 µM (2%)
		0 ℃	5.5±1.5 µM (0.6±0.2%)	0.9±0.3 µM (0.2±0.06%)

change in ΔG is induced by varying 30K [19-20] (Table 3.1). As was expected, the dissociation constant decreases with decreasing temperature.

The dissociation constant is directly related to the concentration of unbound ends. The total end group concentration for DA-PCOD solution is the same as the molar concentration of polymer coils multiplied by 2. Since DA/DB-PCOD solution contains equivalent moles of DA and DB ends, the concentration for each type of end equals the molar concentration of polymer coils. Knowing the total concentration for A and B end, the fraction of unbound ends can be estimated using the relationship $K_d = [A][A]/[AA]$ or $K_d = [A][B]/[AB]$ for DA and DA/DB respectively, in which [A] and [B] refer to the unbound end concentration, [AA] (or [AB]) reflects the bound end concentration, and $[A] = C_A - [AA]$ for DA, $[A] = [B] = C_A - [AB]$ for DA/DB (Table 3.2). Temperature has a dramatic effect on the

equilibrium: the fraction of dangling ends is huge for telechelics at high temperature (~ 50% at 60 ℃) and becomes negligible at low temperature (≤ 1% at 0 ℃) (Table 3.2).

3.1.4 Scope of this chapter

In this chapter, the effect of temperature is brought into consideration. The temperature dependence of the solution behavior of HEURs has been investigated extensively (reviewed above). However, little systematic research has been performed on the dynamics of the solutions of pairwise-associative telechelics [21-22] and how the dynamics can be affected by temperature. Mechanical characterization of a bulk sample of ureidopyrimidone (UPy) ended poly(dimethylsiloxanes) (PDMS) demonstrated dynamic features resembling those for entangled polymers but with high temperature dependence. However, no detailed molecular picture has been discussed [23]. A systematic study of the relationship between supramolecular structure and solution dynamics and their temperature dependence can serve as a guide for rational design of supramolecules and the related functional materials.

Thus, I study the temperature effect on the dynamics and morphology of DA-PCOD solutions and compare them to the case with HEURs. The topology of micelle structures formed by DA-PCOD is observed to be temperature-dependent after the solution is heated above 30 ℃, in contrast to HEURs, which has constant topology. I also examine the temperature effect on DA/DB-PCOD solutions. The distribution of supramolecules formed by DA/DB-PCOD is found to shift monotonically with temperature, which makes DA/DB-PCOD dramatically different compared to linear covalent polymers.

3.2 Experimental

3.2.1 Materials

The decahydronaphthalene (decalin, mixture of cis/trans) used for rheology experiments and 2,6-Di-tert-butyl-4-methylphenol (BHT) used as an anti-oxidant in the polymer solution were purchased from Sigma Aldrich. The polyisobutylene (PIB, M_w = 4,200,000 g/mol, M_n = 3,100,000 g/mol referred as 4.2M PIB) used as a linear covalent polymer control was also purchased from Sigma Aldrich. The isophthalic acid-ended polycyclooctadiene (DA-PCOD) was synthesized via ring opening metathesis polymerization (ROMP) with custom-made isophthalic acid-ended chain transfer agent (CTA). The di-tertiary amine ended polycyclooctadiene (DB-PCOD) was synthesized via ring opening metathesis polymerization (ROMP) with custom-made chloride-ended chain transfer agent (CTA), followed by two steps of post-polymerization modification. The synthetic schemes of CTAs, ROMP procedure, post-polymerization modification, and the characterization (GPC and NMR) of the CTAs and telechelic polymers were described in Appendix A.

Deuterated solvent used for SANS experiments (decalin-d18) was purchased from Cambridge Isotope Laboratories. Cylindrical quartz "banjo" cells used in scattering experiments were purchased from Hellma Analytics.

3.2.2 Solution preparation

Decalin was chosen as the solvent for rheology, small angle neutron scattering (SANS) and ^{1}H-NMR experiments, because it is an athermal solvent for the polycyclooctadiene backbones. The conformation of the backbone in decalin does not change with temperature,

and causes little effect on the rheology of the solution. Therefore, any temperature dependence observed in the data can be attributed to the end association only.

Solutions of polymers (PIB: 4.2M polyisobutylene, DA: isophthalic acid-ended polycyclooctadiene, and DA/DB: equiv. molar ratio of isophthalic acid-ended polycyclooctadiene and di-tertiary amine-ended polycyclooctadiene) were prepared by weighing out polymer on a Mettler precision balance ($\pm$0.01mg) into new glass scintillation vials with PTFE lined caps and subsequently adding the appropriate amount of decalin (or d-decalin for SANS) using a precision syringe ($\pm$1%). The decalin was pretreated with 0.1 wt% of BHT. The solutions of telechelic polymers were placed on a wrist-action shaker at room temperature overnight. The solutions of PIB were charged with a magnetic stir bar and stirred at 250 min^{-1} overnight to avoid shear degradation that may be induced by wrist-action shaking.

3.2.3 Rheological measurement

Steady shear viscosity and oscillatory shear dynamic moduli were measured from 0℃ to 60℃ with a strain-controlled rheometer TA ARES-RFS, equipped with a cone-plate geometry (angle 2°, diameter 50mm) and a solvent vapor trap. The steady shear rate range typically was chosen from 100 s^{-1} to 1 s^{-1} (or 10 s^{-1} to 0.1 s^{-1}) based on the temperature and polymer composition for each run to avoid overloading the force transducer. The viscosities are averages of values obtained at low shear rates that give viscosity independent of shear rate.

An oscillatory shear strain sweep was performed from 0.5% to 50% at 10 rad/s frequency at 0℃ and 25℃ for each polymer solution to measure the strain range for linear

viscoelasticity. A strain within the linear range was chosen for the subsequent frequency sweep, which was usually 1%, 5%, 10%, or 20% strain, depending on the concentration and temperature. Dynamic moduli were measured for each polymer solution from 0℃ to 60℃ with frequency ranging from 100 rad/s to a lower frequency of 1 rad/s, or 0.1 rad/s, or 0.01 rad/s, depending on the relaxation time for the specific composition and temperature.

3.2.4 Small angle neutron scattering

Small Angle Neutron Scattering experiments were conducted at the National Institute of Standards and Technology (NIST) on beamline NG-7 and at Oak Ridge National Laboratory (ORNL) on beamline CG-2 at the High Flux Isotope Reactor (HFIR). Samples were placed in Hellma quartz cylindrical cells with 5mm path length used. Temperature was controlled by a recirculating water bath at NIST and by Peltier at ORNL. Scattering experiments were conducted in a temperature range from 0℃ to 60℃. Two-dimensional scattering patterns were taken for each sample using three configurations including detector distances and neutron wavelengths (1m 6Å, 4m 6Å and 13m 6Å at NIST and 1m 4.75Å, 10m 4.75Å and 18.5m 12Å at ORNL). The overall scattering vector ranges were $0.0035 < q(\text{Å}^{-1}) < 0.4$ at NIST and $0.0014 < q(\text{Å}^{-1}) < 0.8$ at ORNL. Priliminary SANS data were acquired at ORNL, and the SANS data presented in this chapter were obtained at NIST.

The 2D scattering patterns were corrected for electronic noise, neutron background, detector sensitivity, and empty cell scattering. They were then normalized by the incident neutron flux and radially averaged resulting in absolute intensity I(q). Patterns for the three detector distances were combined using Igor PRO macros developed by Steve Kline [24] that were also used for subsequent processing and analysis. The solvent background

scattering was collected using pure d18-decalin and subtracted from the data of other telechelic polymer solutions.

3.3 Results

3.3.1 Temperature effect on the rheology of solutions of linear covalent polymers

Oscillatory rheology and shear rheology experiments were performed with 4.2M polyisobutylene (PIB, M_w = 4,200 kg/mol) in decalin at temperatures 60℃ ~ 0℃ at concentrations of 0.6 wt%, 1.2 wt%, and 2 wt%. For each concentration, the shape of storage/loss modulus curves for PIB solutions does not change with the temperature (15℃ to 0℃) and the time-temperature superposition can be performed with the curves, which is expected for solutions of linear covalent polymers (Figure 3.2). The temperature
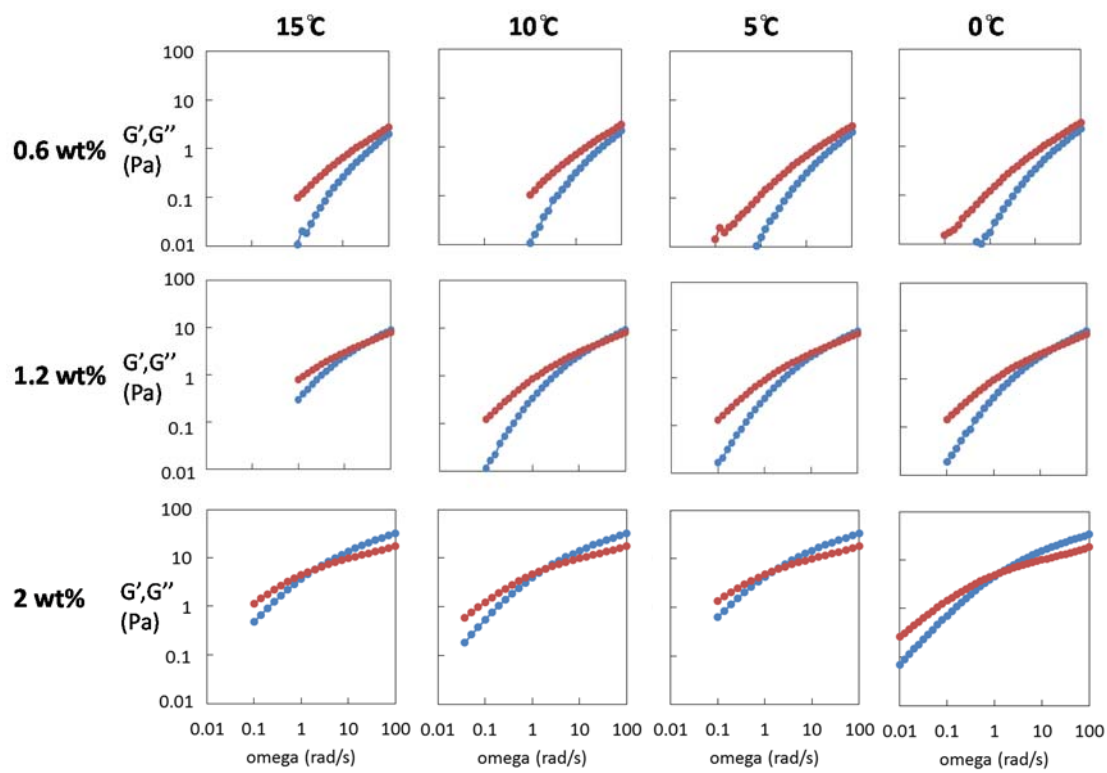
Figure 3.2 Storage (G', blue circles) and loss modulus (G", red circles) for polyisobutylene (PIB, M_w = 4,200 kg/mol) at 15-0℃ at concentrations from 1.2 wt% to 2.5 wt%.
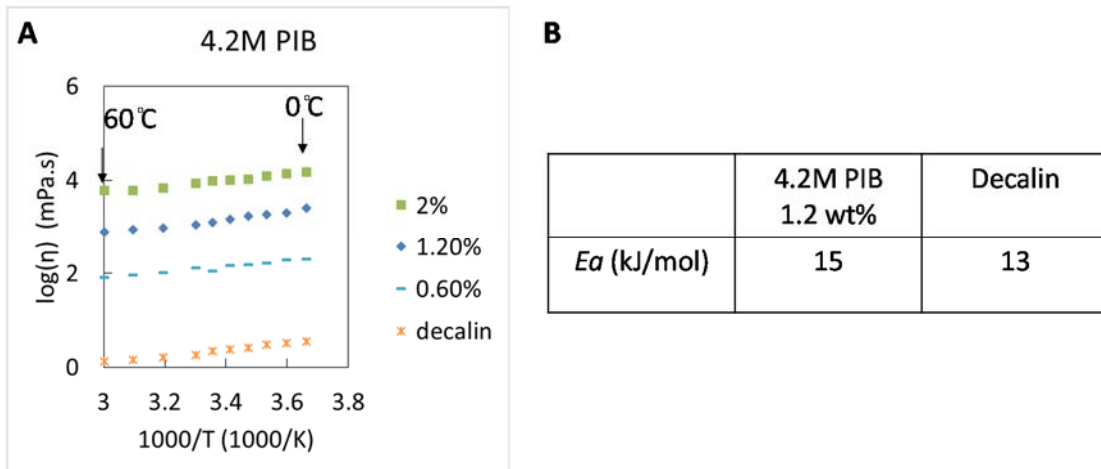
Figure 3.3 A. Arrhenius plots for polyisobutylene (PIB, M_w = 4,200 kg/mol) at concentrations from 1.2 wt% to 2.5 wt%. **B.** The activation energy (E_a) obtained from the slope of the Arrhenius plots for 1.2 wt% 4.2M PIB solution and the pure solvent, decelin.

dependence of the PIB solution viscosity for three concentrations is shown in the Arrhenius plot with the pure solvent, decalin, as a control (Figure 3.3A). It is clear that the Arrhenius slope corresponding to all three concentrations is approximately equal and also close to that of the pure solvent, decalin. The activation energies (Ea) calculated from the plot for 1.2 wt% PIB solution and decalin are listed in Figure 3.3B. These results agree with the literature values [5].

3.3.2 Temperature effect on the rheology of pairwise associative telechelic polymers (DA/DB-PCOD)

Oscillatory rheology and shear rheology experiments were performed with 1:1 molar ratio of isophthalic acid-ended polymers and di-tertiary amine ended polymers (DA/DB-PCOD, M_w = 50 kg/mol) in decalin at temperature range from 0 ℃ to 60 ℃ with concentrations of 1.2 wt% ~ 2.5 wt% and 0.15 wt% ~ 2.5 wt% respectively. The storage/loss modulus are plotted against frequency for solutions of concentrations 1.2 wt% ~ 2.5 wt% at
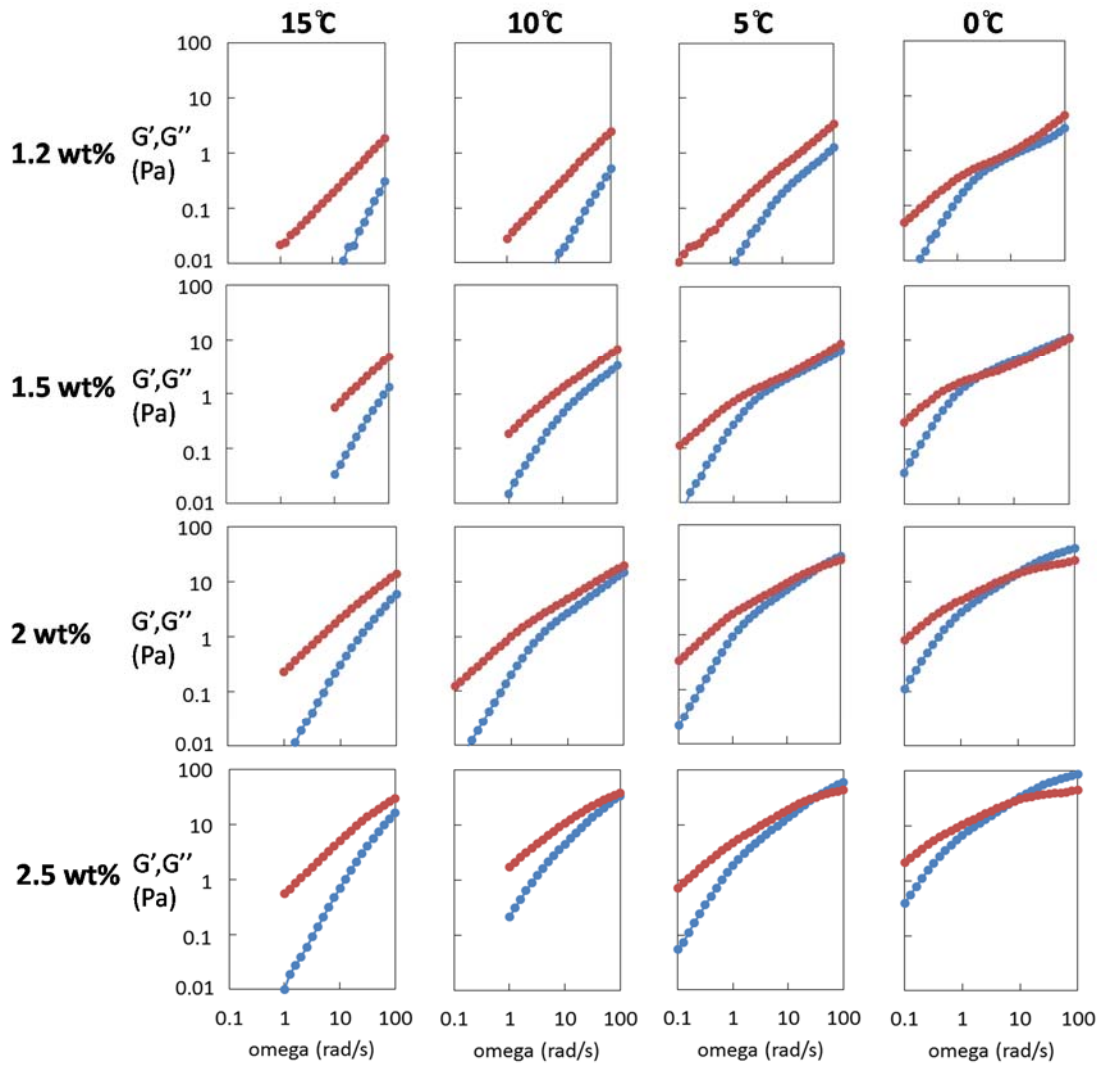
Figure 3.4 Storage (G', blue circles) and loss modulus (G", red circles) for DA/DB-PCOD (M_w = 50 kg/mol) at 15-0℃ at concentrations from 1.2 wt% to 2.5 wt%.

temperatures 15℃ ~ 0℃, where the change in rheology features is most prominent (Figure 3.4).

The effect of concentration on the dynamics of DA/DB-PCOD solutions at 0℃ has been illustrated in Chapter 2. At a fix temperature of 0℃, the dynamics of the solutions resembles that of the semidilute solutions of linear covalent polymers (Figure 3.4, 0℃ column). More specifically, the 1.2 and 1.5 wt% solutions exhibit features of semidilute

unentangled solution (power law regime with slope of ½), and the 2 and 2.5 wt% solutions are in the semidilute entangled regime (a crossover with a entanglement plateau). It indicates that the pairwise-associative polymers do form linear/cyclic supramolecules that relax like linear covalent polymers. By a semi-quantitative analysis of the oscillatory data of DA/DB-PCOD compared to that of linear covalent controls (4.2 M PIB and 1.1 M PCOD), it is postulated that the supramolecular species that dominate the solution dynamics have an effective molar mass on the order of a million (> 1,000 kg/mol). The fraction of the rheologically effective species becomes larger as the concentration rises from 1.2 wt% to 2 wt%. The same trend seems to occur for other temperatures as well (Figure 3.4, 15℃, 10℃, and 5℃), with the modulus and relaxation time both increasing with concentration.

Temperature has even more drastic effect on the dynamics of DA/DB-PCOD solutions. At one fixed concentration, for example 1.2 wt% (Figure 3.3, 1.2 wt% row), the shape of the dynamic curves varies significantly as temperatures decreases from 15℃ to 0℃. Time-temperature superposition cannot be applied to these curves, indicating that the composition of the supramolecules formed by DA/DB-PCOD at each temperature is different. As the solution is cooled, the relaxation time of DA/DB-PCOD is peculiarly prolonged and the curve shape indicates that longer species are dominating the solution dynamics (Figure 3.3, from 15℃ to 0℃). The data suggests that the average size of supramolecules increases as the temperature decreases, which is a qualitatively distinct feature compared to the dynamics of linear covalent polymers.

This hypothesis can be further supported by the Arrhenius plot. The natural log of the solution viscosity (ln η) is plotted against inverse absolute temperature (1/T) for solutions
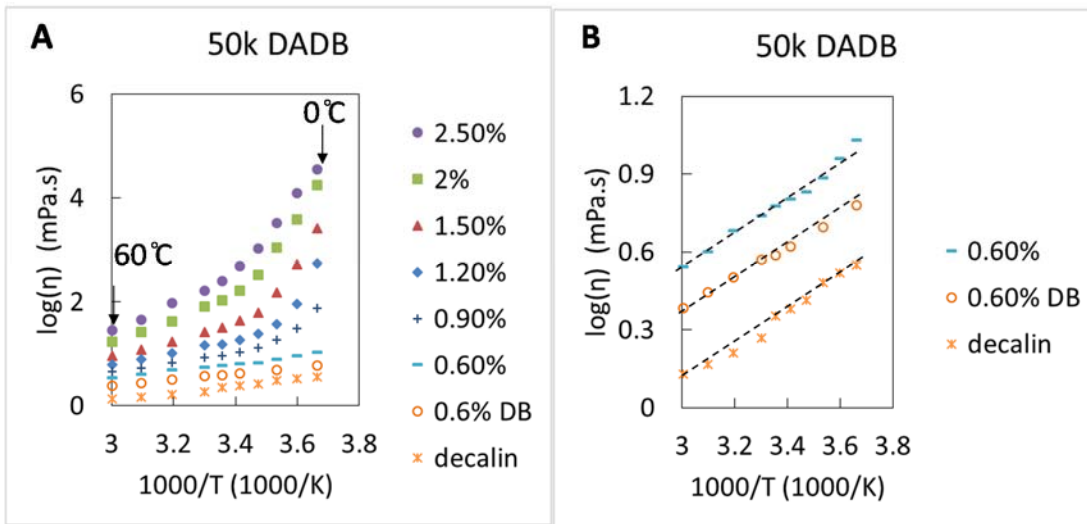
Figure 3.5: A. Arrhenius Arrhenius plots for DA/DB-PCOD (M_w = 50 kg/mol) at concentrations from 0.6 wt% to 2.5 wt%, with pure decalin and 0.6 wt% DB-PCOD (M_w = 50 kg/mol) as controls. **B.** Zoom-in view of the arrhenius Arrhenius plots for DA/DB-PCOD (M_w = 50 kg/mol) at concentrations 0.6 wt%, with pure decalin and 0.6 wt% DB-PCOD (M_w = 50 kg/mol) as controls.

of 50k DA/DB-PCOD at concentrations from 0.6 wt% to 2.5 wt% in the temperature range of 60 ℃ to 0 ℃, pure decalin and 0.6 wt% DB-PCOD (M_w = 50 kg/mol) as controls (Figure 3.5A). In contrast to a straight line in the Arrehnius plot usually in linear covalent polymer solutions (including PIB and DB-PCOD), the plots for DA/DB-PCOD solutions at all concentrations are curved, rising sharply at low temperatures. Even the one obtained with the 0.6 wt% solution, which seems to be straight and parallel to the plot for decalin and DB-PCOD, shows a slight upturn at temperatures below 10 ℃ (Figure 3.5B). The curved Arrhenius plot is consistent with the hypothesis mentioned above: the average size of supramolecules increases with decreasing temperature. This provides extra contribution to the solution viscosity, which causes the nonlinear relationship between the logarithm of viscosity (log(η)) and inverse absolute temperature (1/T).

In summary, the phenomena observed from the above rheology data of 50k DA/DB PCOD solutions at various temperatures, including the oscillatory shear data and the non-linear Arrhenius plot, are all consistent with the hypothesis that the average size of the supramolecular species increases with decreasing temperature.

3.3.3 Temperature effect on the rheology of self-associative telechelic polymers (DA-PCOD)

For solutions of isophthalic acid-ended polymers (DA-PCOD, M_w = 50 kg/mol), oscillatory rheology and shear rheology experiments were performed in decalin at temperatures ranging from 0 ℃ to 60 ℃ with concentrations of 1.2 wt% ~ 2.5 wt% and 0.15 wt% ~ 2.5 wt% respectively. Interestingly, data shows that the temperature dependence of DA-PCOD solutions differ in two temperature ranges: 0 ℃ to 30 ℃ and 30 ℃ to 60 ℃.

3.3.3.1 Constant topology at temperatures of 0 ℃ to 30 ℃

The storage/loss modulus are plotted against frequency for solutions of concentrations 1.2 wt% ~ 2.5 wt% at temperatures 15 ℃ ~ 0 ℃ (Figure 3.6A). All figures follow Maxwell-like dynamics with single relaxation time, confirming the formation of micelle structures. For each concentration, the shape of the curves and the plateau modulus does not change in the temperature range shown here (< 30 ℃). The loss modulus (G'') at high frequency (100 rad/s to 50 rad/s) shifts very slightly with temperature compared to the crossover point (especially obvious at 1.2 wt% and 1.5 wt%), and is likely due to the Rouse-mode relaxation of the polymer chains between two junctions, as suggested by Uneyama *et al* [25]. Other than this fast relaxation mode, the curves obtained at various temperatures for the same concentration can be superimposed with each other. The Maxwell-like dynamics
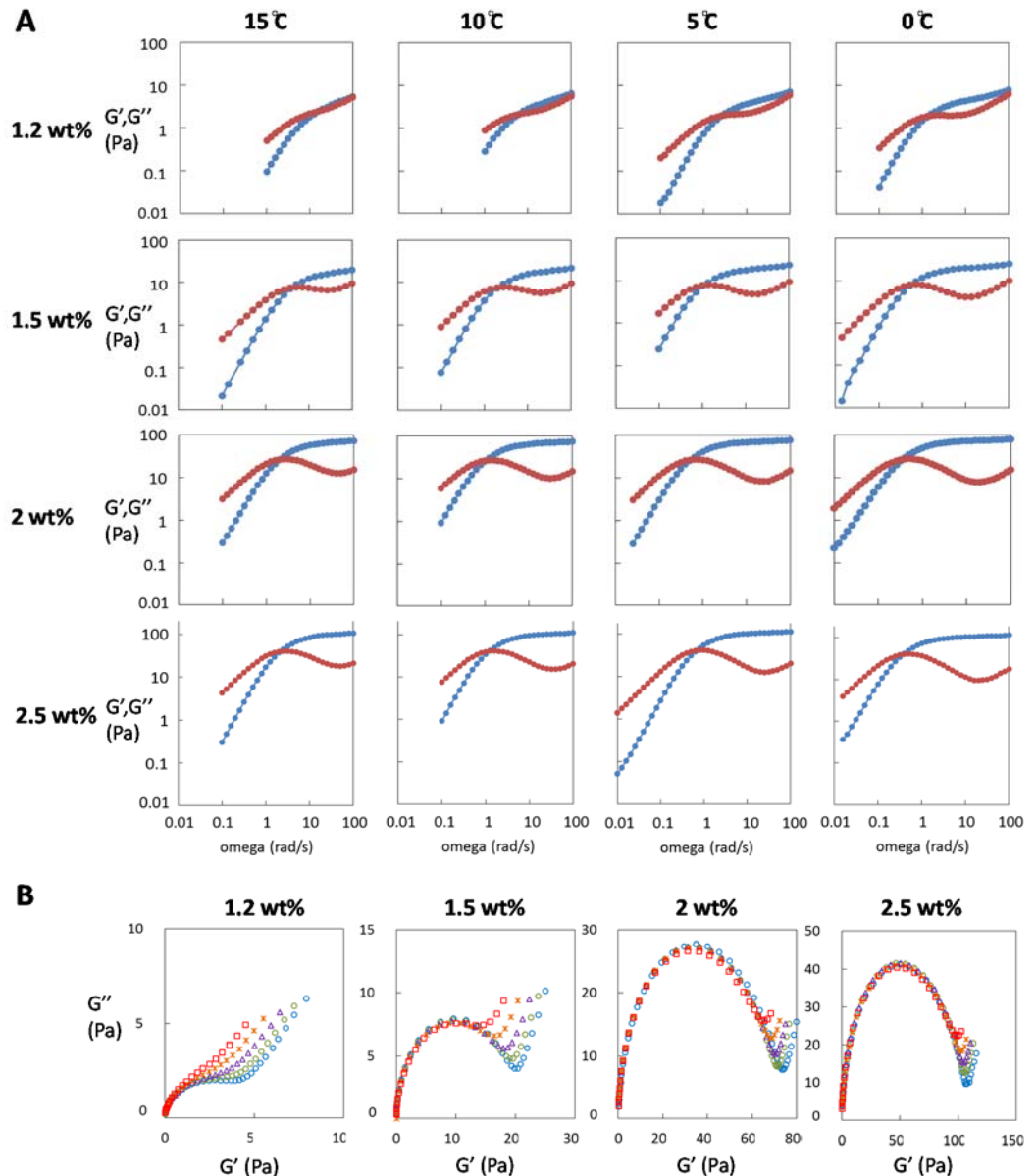
Figure 3.6 A. Storage (G', blue circles) and loss modulus (G", red circles) for DA-PCOD (M_w = 50 kg/mol) at 15-0℃ at concentrations from 1.2 wt% to 2.5 wt%. **B.** Cole-Cole plots for the same solutions at 20-0℃.

and time-temperature superposition (TTS) can be demonstrated more straightforwardly with the Cole-Cole plot (Figure 3.6B), which is a plot of G" versus G' with both of them on a linear scale. If a material is Maxwellian, its Cole-Cole plot shows the form of a semi-circle. It is clear that the Cole-Cole plots for 50k DA-PCOD solutions at all four
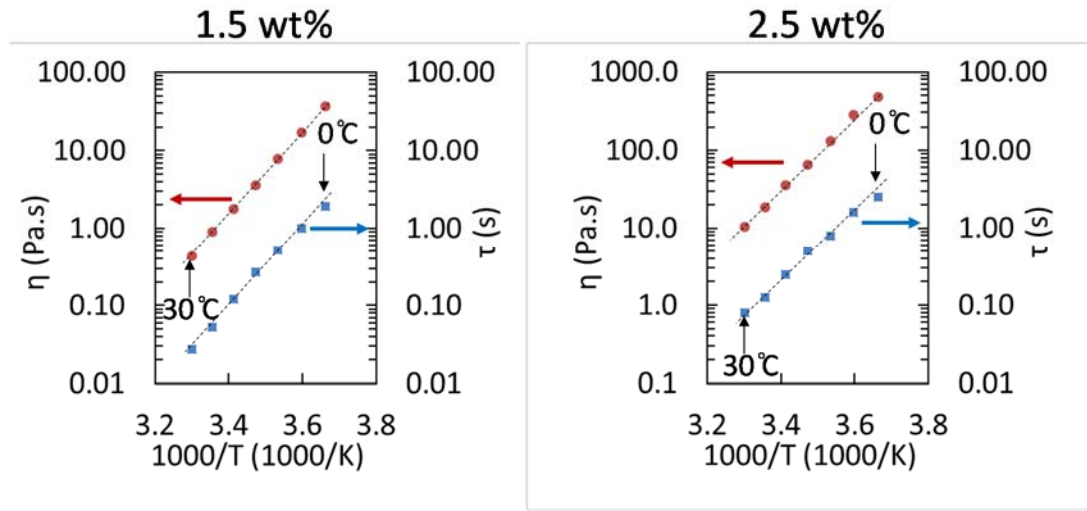
Figure 3.7 Arrhenius plots of low shear viscosity and relaxation time for solutions of DA-PCOD ((M_w = 50 kg/mol)) at 1.5 and 2.5 wt%.

concentrations display a semi-circle shape, supporting the Maxwell-like dynamics. And the storage/loss modulus obtained at various temperatures as fixed concentration overlap each other in the Cole-Cole plot as well, demonstrating the success of TTS (Figure 3.6B). The deviation from TTS at high G' and G'' values corresponds to the fast relaxation mode mentioned earlier at high frequency, which is especially prominent for low concentrations (1.2 wt% and 1.5 wt%). The above oscillatory shear data suggest that 50k DA-PCOD does form micelle-like supramolecules and follows Maxwell-like dynamics. And the morphology of the micelle structures do not change in the temperature range of 0℃ to 30℃ (the data between 20℃ to 30℃ is not shown in Figure 3.6, however, still follows the same trend as described above).

Both the relaxation time and the viscosity of the 50k DA-PCOD solutions demonstrate strong temperature dependence, like the HEUR solutions (Figure 3.1). The Arrhenius plot of the solution viscosity and the relaxation time of the 50k DA-PCOD solutions at 1.5 wt% and 2.5 wt% in the temperature range of 0℃ to 30℃ are shown as an example (Figure 3.7).

For both 1.5 wt% and 2.5 wt% solutions, the Arrhenius plot of the solution viscosity and the relaxation time share the same slope (Figure 3.7), suggesting the activation energy that controls the temperature dependence for both parameters is the same. The activation energy is calculated from the slopes of viscosity of four concentrations is 93 ± 7 kJ/mol. This result is consistent with the observation that the plateau modulus of 50k DA-PCOD solutions (1.2 wt% to 2.5 wt%) remains constant (Fgiure 3.6). The data suggests that the micelle structures do not change with temperature in the temperature range from 0℃ to 30℃. 50k DA-PCOD solutions at temperatures below 30℃ exhibit the same dynamic and morphological features as those of HEUR solutions.

3.3.3.2 Topological change at temperatures of 30℃ to 60℃

However, further rheology data obtained at temperatures higher than 30℃ reveals a different temperature dependence of 50k DA-PCOD solutions. The Arrhenius plot of solution viscosity is extended to 60℃ (total range of 60℃ to 0℃) for solutions of 50k DA-PCOD at various concentrations, with the pure solvent, decalin, as a control (Figure 3.8).
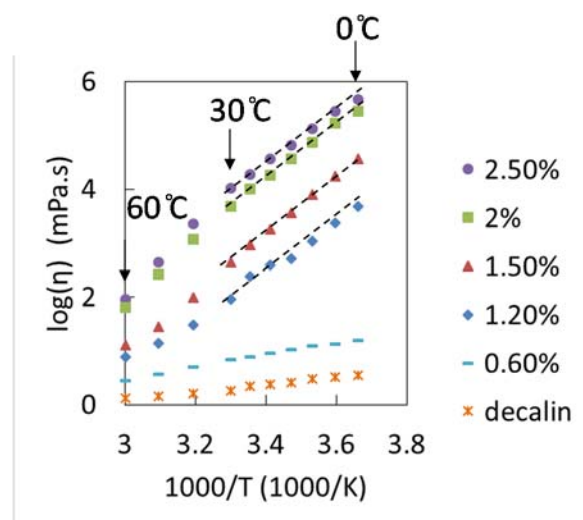
Figure 3.8 Arrhenius plots of low shear viscosity for solutions of DA-PCOD (($M_w = 50$ kg/mol)) at concentrations from 0.6 and 2.5 wt%, in the temperature range of 60-0℃.

The curve for 0.6 wt% solution is much flatter than the others because the concentration is lower than the overlap concentration of 50k non-associative polymer (~ 0.8 wt%), and the micelles have not percolated and formed bridges with each other at this concentration. For the data obtained with solutions at concentrations of 1.2 wt% to 2.5 wt% (Figure 3.8), a clear change in slope is observed at temperature around 30 ℃, suggesting the topology of the micelles changes as the solutions are heated above 30 ℃.

The same trend is also observed with the modified Cole-Cole plot of the 50k DA-PCOD solutions. The Cole-Cole plot, which is normally shown on a linear scale, is more sensitive to data points in the high frequency range (high G' and G''). The measured moduli at temperatures above 30 ℃ are quite small (G' < 1 Pa, G'' < 10 Pa) and their deviation from the TTS is hardly noticeable when shown on a normal linear scale plot. Thus a log-log scale Cole-Cole plot is provided instead for 50k DA-PCOD solutions at 60 ℃ to 0 ℃ to highlight the low value range of G' and G'' (Figure 3.9). For 4.2M PIB, curves of all temperatures overlap with each other well, since the solution composition does not change
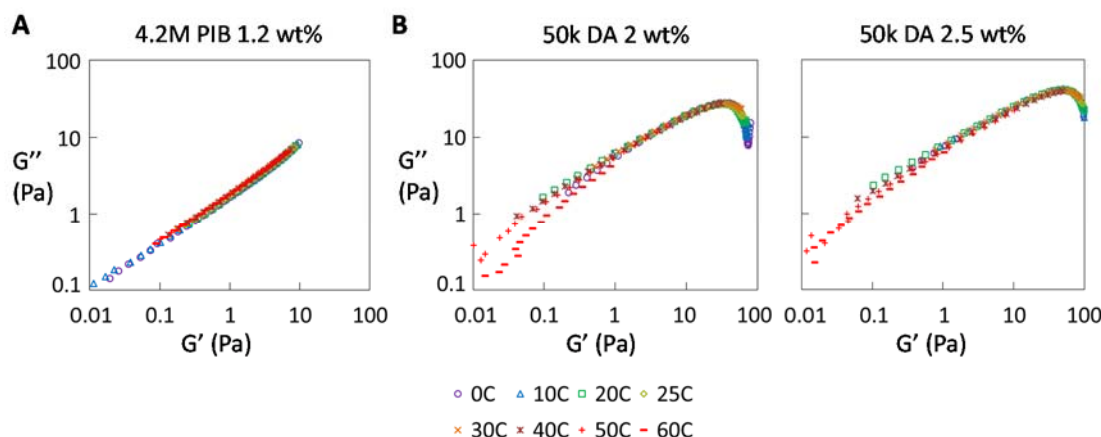
Figure 3.9 Modified Cole-Cole plots for the solutions of for 4.2M PIB at 1.2 wt% and DA-PCOD (M_w = 50 kg/mol) at 2 and 2.5 wt% in the range of 60-0 ℃, to emphasize low G' and G'' values obtained at high temperatures.

with temperature. On the contrary, the curves obtained with 50k DA-PCOD solutions (2 wt% and 2.5 wt%) at temperatures higher than 30℃ show clear deviation from TTS. This observation also supports the hypothesis that the micelle structure in 50k DA-PCOD solutions varies at temperatures above 30℃.

In summary, the DA-PCOD forms flower-like micelles which bridge into connected network as the concentration increases. The solutions in decalin exhibit Maxwell-like dynamics with a single relaxation time, which is determined by the exchange time of the ends from the micelle core. Rheology data shows that the micelle structure does not change at temperatures below 30℃, which leads to a constant plateau modulus. Therefore in this temperature range, the viscosity and the relaxation time of DA-PCOD solutions follow the same Arrhenius-type temperature dependence with one same activation energy, which is calculated to be 93 ± 7 kJ/mol. At temperatures above 30℃, both Arrhenius plot and modified Cole-Cole plot demonstrate a change in the microscopic micelle structure in the solutions, which has not been observed in literature with HEURs. In other words, 50k DA-PCOD solutions exhibit the same dynamic and morphological features as those of HEUR solutions in the temperature range of 0℃ to 30℃, and undergo temperature-dependent change in micelle structures at temperatures higher than 30℃, which makes them different from the traditional self-associative telechelic polymers.

3.3.4 Small angle neutron scattering of associative telechelic polymers

Small angle neutron scattering (SANS) technique is useful in obtaining detailed information about polymer conformation. Neutrons have very short wavelengths (1< λ(Å) <20) probe length scales usually on the order of 1 to 100 nm [26]. Contrast in neutron scattering is derived from nuclear properties which vary randomly from isotope to isotope
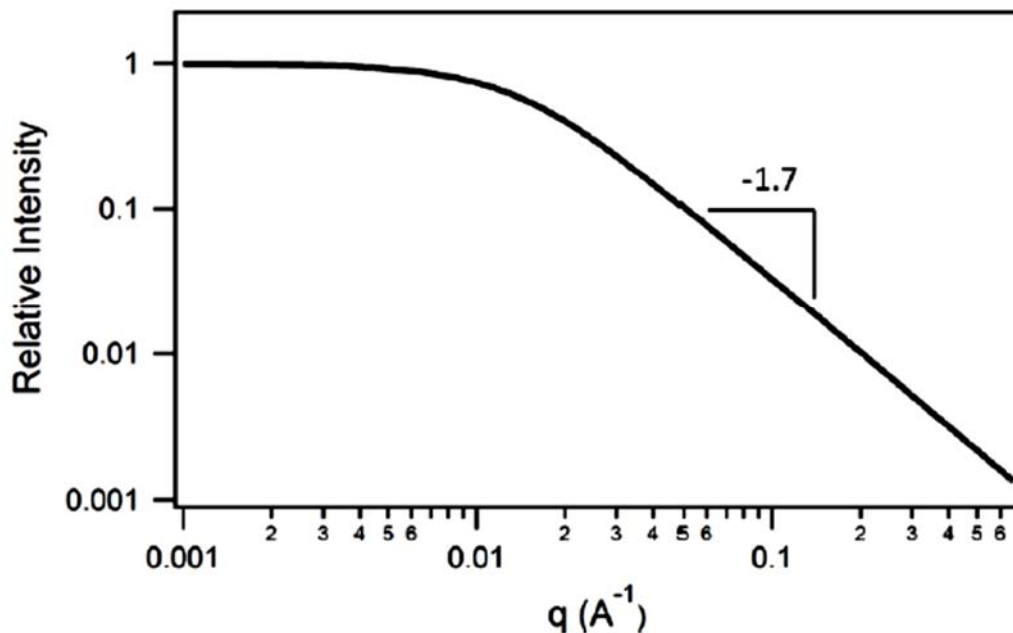
Figure 3.10 (Figure reproduced from Paul Pirogovsky's thesis [27]) Scattering pattern of a polymer coil. This was calculated using the polymer excluded volume scattering function [4] in the IGOR Pro macros written by Steven Kline [24]. The particular coil used has R_g=10nm and v=0.6.

in a fashion that is not related to the atomic number. This is in direct contrast to X-ray scattering. Hydrogen (H) and deuterium (D) have a very large difference in scattering length density (SLD - a parameter used to evaluate the contrast) [26], making the use of deuterated solvents with hydrogenous polymers a powerful tool to study the size and conformation of polymers.

A standard scattering pattern for a linear covalent polymer coil is shown in Figure 3.10. The scattering curve for a fractal object, including polymer coil, can be generally divided into two regions: a Porod region, a plateau region, and the region in-between, the Guinier region. The porod region refers to the higher q section (corresponding to length scales smaller than R_g), where the scattering has power law behavior $I \sim q^{-d}$ with $d = 1/v$ being the mass fractal dimension. In good solvent, $d = 1/0.6 = 1.7$. The scaling for a polymer coil can

be measured directly in this way. At lower q with length scales larger than R_g, the intensity approaches a nearly q-independent plateau, the height of which is proportional to the molecular weight of the object. The section between the power-law and the plateau is the Guinier region, the intensity of which depends on the R_g: $I(q) = I_0 \exp(-q^2 R_g^2/3)$.

SANS patterns were acquired at NIST for 0.6 wt% and 0.3 wt% solutions of 50k telechelic polymers in d18-decalin at various temperatures (Figure 3.11). The three polymer compositions were non-associative PCOD (NA-PCOD, referring to di-chloride ended PCOD which is the precursor for DB-PCOD), isophthalic acid-ended PCOD (DA-PCOD), and isophthalic acid-ended PCOD paired with tertiary amine ended PCOD (DA/DB-PCOD), all with a molecular weight of 50 kg/mol.

All scattering intensities follow a power law dependence $I(q) \sim q^{-m}$ for q>0.04 Å^{-1} and overlap with each other for NA-, DA- and DA/DB-PCOD solutions (Figure 3.11A, at 30℃). This q range corresponds to length scales on the order of 10nm or less and probes the internal structure of the polymer coils. For all three compositions, the Porod slope is measured to be around 1.7, which agrees with the theoretical value for a polymer coil in good solvent. And the fact that the curves for all three compositions (NA, DA, DA/DB) overlap at q>0.04 Å^{-1} confirms that the conformation of the telechelic polymer at length scales within the R_g of individual building block is unperturbed by association.

At lower q values the scattering curves diverge. The scattering for NA-PCOD approaches a plateau depicting the size of an individual telechelic polymer chain, which is fitted to be around 8.3 nm using the polymer excluded volume scattering function [28] in the IGOR Pro macros. The theoretical value for R_g of a 1,4-polybutadiene with M_w = 50 kg/mol can be obtained from literature [29] to be 9.3 nm. This is in good agreement with the measured

value. Both DA and DA/DB solutions exhibit elevated scattering intensities at low q, indicating the formation of supramolecules at 30℃ (Figure 3.11A). The curve for DA-PCOD rises sharply at q<0.005 Å^{-1}, probably because the micelles connect with each other, forming larger aggregates that are out of the measured size limit of SANS.
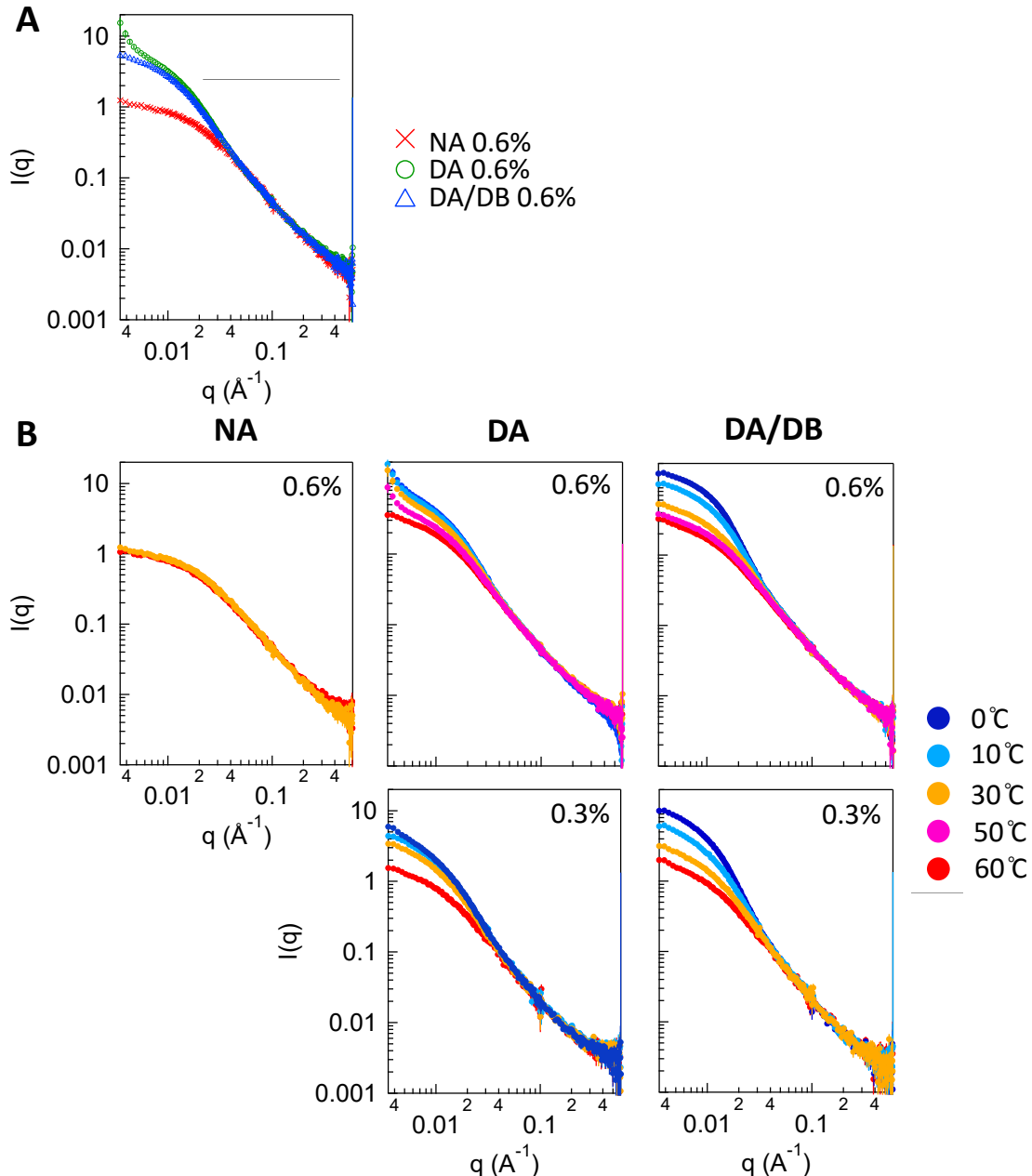
Figure 3.11 The SANS patterns acquired with 50 kg/mol NA-PCOD, DA-PCOD, and DA/DB-PCOD solutions at **A.** 30℃ at 0.6 wt% in d18-decalin, and **B.** 0 to 60℃ at 0.3 and 0.6 wt% in d18-decalin.

SANS patterns for solutions of 50k telechelic polymers (NA, DA and DA/DB) measured at 0℃ to 60℃ are plotted in Figure 3.11B. Decalin is an athermal solvent for the PCOD backbone, which means that the conformation and the size of the backbone coil in decalin solution should not change with temperature. This is indeed observed with NA-PCOD solution, with the curves acquired at 30℃ and 60℃ overlapping each other completely (Figure 3.11B, NA). Therefore, any change in the scattering of DA and DA/DB solutions is due to end association.

For DA-PCOD solutions (0.6 and 0.3 wt%), the curves obtained at temperatures below 30℃ have very similar intensities (difference < 10%, Figure 3.11B, DA). In fact, the curves for 0℃ and 10℃ are almost identical. Above 30℃, the scattering intensities for DA-PCOD decreases with temperature. It indicates that the size and structure of the aggregates formed by DA-PCOD keeps mostly constant at temperatures below 30℃ and starts to change when it's heated above 30℃.

On the other hand, the scattering intensities for DA/DB-PCOD solutions (0.6 and 0.3 wt%) decrease monotonically with increasing temperature, suggesting that the supramolecules formed by DA/DB-PCOD keep growing longer as the solution is cooled. The SANS patterns for both associative systems match the observations from their rheology experiments, confirming the hypothesis regarding the temperature dependence of their supramolecular structures.

Scattering intensities normalized by concentration are plotted for DA-PCOD and DA/DB-PCOD solutions at three temperatures (Figure 3.12). The scatterings for DA-PCOD at two concentrations overlay exactly, except for the lowest q region, where there is an upturn shown by the 0.6% solution. There is no such upturn displayed by the 0.3% solution. This
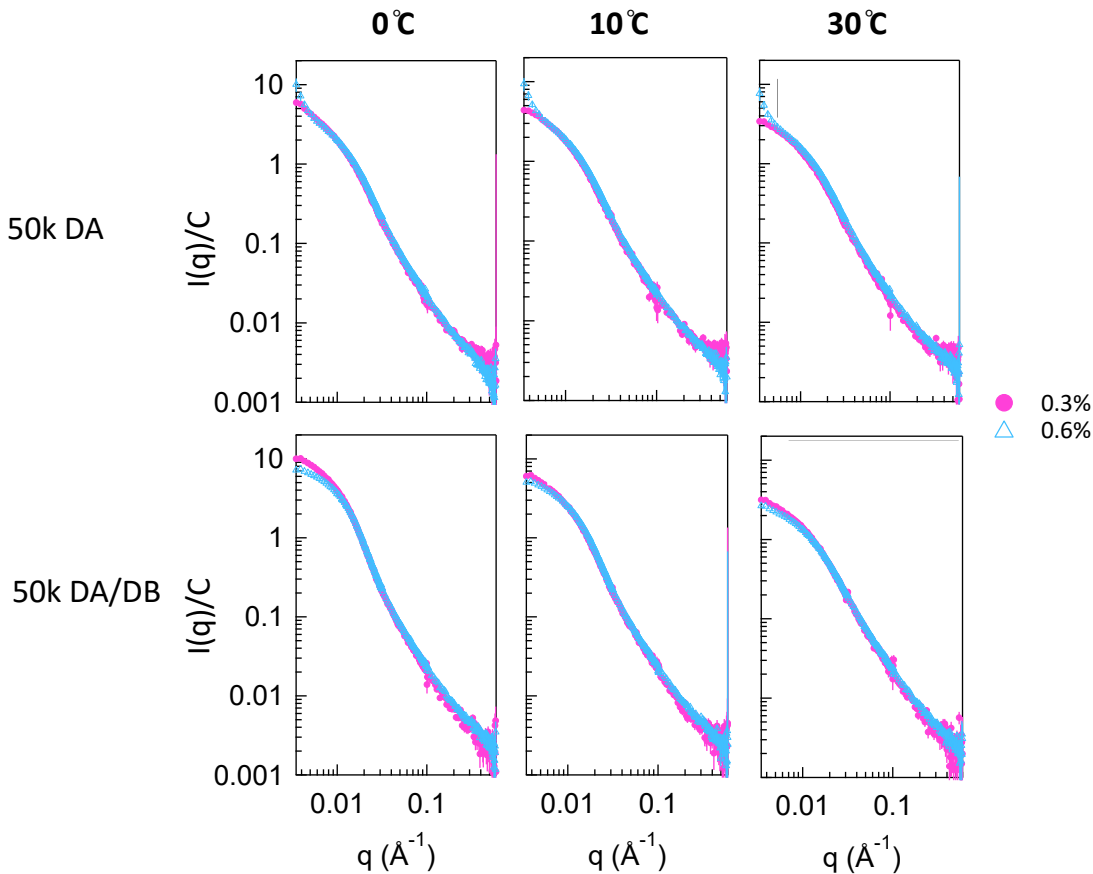
Figure 3.12 Normalized scattering intensities by polymer concentration acquired with 50 kg/mol DA-PCOD and DA/DB-PCOD solutions at 0.3 and 0.6 wt% in d18-decalin at 0 to 30℃.

result indicates that the micelle structure is the same for both concentrations at length scales corresponding to $q < 0.005$ Å^{-1}. Larger clusters of micelles with length scale corresponding to $q > 0.005$ Å^{-1}are formed in the 0.6% DA-PCOD solution, but not in the 0.3% solution.

A different trend is seen with DA/DB-PCOD. The normalized intensities for 0.6% DA/DB-PCOD solution are suppressed compared to the intensities of 0.3% solution at all three temperatures, with suppression obtained at 0℃ being most prominent. This is likely the result of overlap. Although both 0.6% and 0.3% are below the overlap concentration of a 50 kg/mol non-associative PCOD backbone (0.8%), DA/DB-PCOD forms supramolecules with molecular weight much higher than 50 kg/mol, the overlap concentration of which

can be close to or below 0.6% and 0.3%. Therefore the scattering at 0.6% depicts the size of a correlation blob, which is smaller than the actual average size of the supramolecules.

3.4 Discussion

3.4.1 Temperature dependence of the morphology of the self-associative telechelic polymer (DA-PCOD)

3.4.1.1 Two temperature regimes

In this chapter, data obtained using various methods, including oscillatory shear, viscometry, and SANS, all pointed out that there are two temperature regimes in which the morphology of DA-PCOD behave differently: 1) 0℃ to 30℃ and 2) above 30℃.

In the range of 0℃ to 30℃, oscillatory experiments show that the solution dynamics resembles the Maxwell relaxation model with a single relaxation time, suggesting that DA-PCODs do form flower-like micelles. The dynamic modulus curves obtained in this temperature range can be superimposed with each other. The Arrhenius plot of the exchange time and the solution viscosity of DA-PCOD solutions show two parallel linear lines. SANS data indicates that the average supramolecular conformation in the DA-PCOD solutions (0.6% and 0.3%) varies very slightly (< 10%) at temperatures below 30℃. All the above experimental data indicate that the micelle structures formed by DA-PCOD in decalin solutions remains constant in the temperature range of 0℃ to 30℃. The dynamics of the solutions is controlled by the exchange time of the end from the micelle core. The activation energy associated with this process is calculated to be around 93 kJ/mol. These features are similar to those of the traditional self-associative polymers, including HEURs.

When the solution temperature is above 30℃, the temperature dependence of both the morphology and dynamics deviates from the features observed at temperatures below 30℃, and also from the characteristics of HEURs. The storage/loss modulus obtained at temperatures above 30℃ show clear failure of TTS. The Arrhenius curves of the solution viscosity of DA-PCOD solutions at all concentrations display a change in slope around 30℃. The intensity of the SANS pattern at low q (q < 0.02 Å^{-1}) decreases significantly as the solution is heated above 30℃, suggesting an decreasing size of clusters in the DA-PCOD solutions. It is evident that the aggregates formed by DA-PCOD in decalin solutions become smaller as the solution is heated above 30℃, which has not been seen in the HEUR system.

3.4.1.2 Mechanism of the multimeric association of DA-PCOD

The dynamics of DA-PCOD solutions suggest the formation of micelles and multimeric association at the telechelic ends. As stated in Chapter 2, the mechanism of multimeric association used to be postulated that the isophthalic acid self-associates through micro phase separation due to its low solubility in hydrocarbon solvent, like the case with the hydrophobic ends in HEURs.

However, the observation of the two temperature regimes described above suggests that micro phase separation cannot be the mechanism: isophthalic acid remains insoluble in decalin throughout the temperature range tested in our experiments (data not shown here). Since the solvent quality of decalin for PCOD backbone does not change with temperature either, the solubility argument expects the topology of the DA-PCOD micelles to be constant with temperature just like in HEURs. It certainly cannot explain the existence of a critical temperature above which the micellar aggregates become smaller. The

experimental data makes sense only when hydrogen bonding is the mechanism for the multimeric association. Isophthalic acid associates through hydrogen bonding between carboxylic acid groups, but forms multiple association due to its characteristic chemical structure, as described in Chapter 2, Section 2.4.1.1.

3.4.1.3 Postulated molecular picture on the decreasing size of DA-PCOD aggregates

Two molecular pictures can be postulated on the decreasing size of DA-PCOD aggregates above 30℃.

1) The aggregates measured by SANS are already clusters of several micelles, and the clusters dissociate at temperatures above 30℃ into smaller clusters containing fewer micelles. The individual micelle structure does not change with temperature, or say, the aggregation number of ends within one micelle keeps constant (Figure 3.13A). A constant
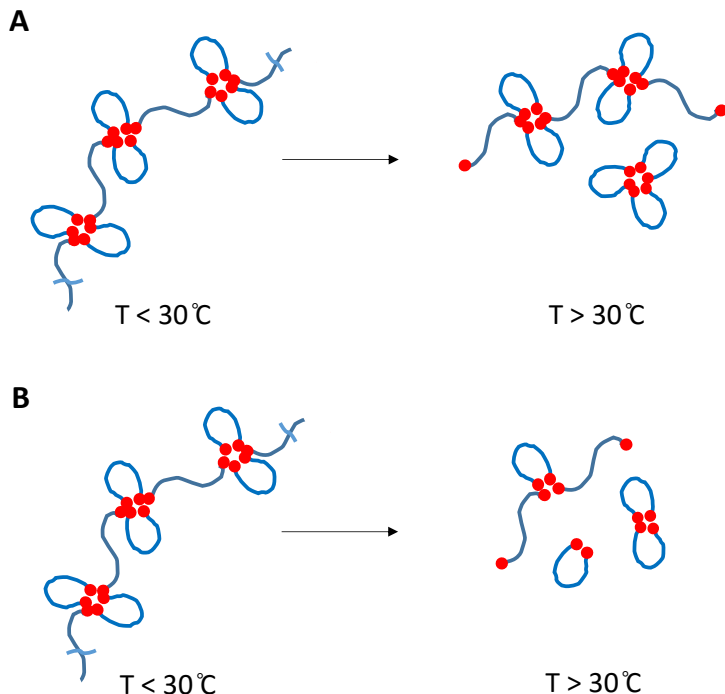
Figure 3.13 Schematics on the postulated topological change above 30℃. **A.** Aggregation number does not change with temperature, similar to the case with HEURs. **B.** Aggregation number decreases with increasing temperature.
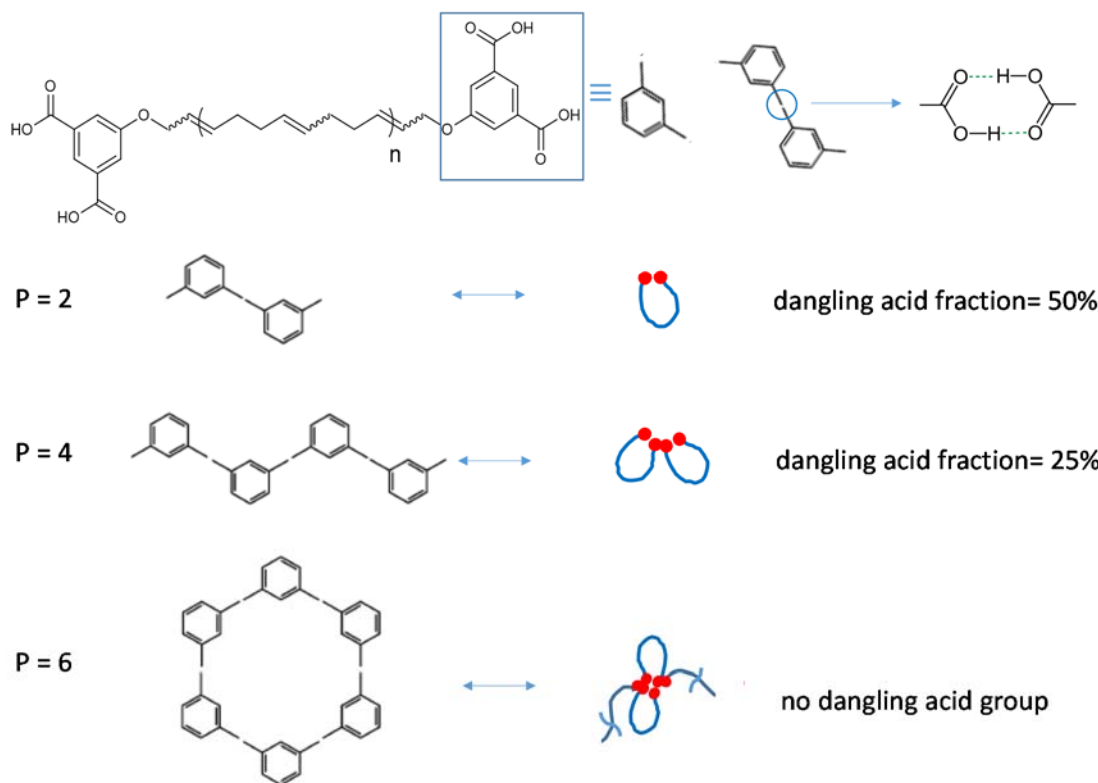
Figure 3.14 (Figure inspired by reference [30]) Hypothesis for the temperature dependence of aggregation number (p).

aggregation number with temperature is generally assumed with HEUR systems, which is confirmed with experimental data.

2) The aggregation number of ends within one micelle decreases at temperatures above 30 °C, causing smaller micelles at higher temperatures (Figure 3.13B).

Since the hydrogen bonding between DA ends guides the end association, scenario 2 with varying aggregation number (p) is more likely to be the real case. As calculated in Section 3.1.3, more than 50% of the carboxylic acid ends are unbound at 60 °C, while the dangling end fraction is less than 10% below 25 °C (Table 3.2). It indicates that almost all ends are bound at low temperature, probably with a higher aggregation number (e.g. 6); however, the structures with p equals 2 or 4 may very likely exist at high temperatures when dangling

Table 3.3 The relaxation time measured and estimated for 50 kg/mol DA-PCOD at 0, 25 and 60℃.

τ (s) measured by rheology	2.0%	2.5%
Est 60℃ [a]	0.003	0.003
25℃	0.13	0.13
0℃	3.16	3.16

[a] Estimated using $\tau = \tau_0 \exp(E_a/RT)$, with $E_a = 87$ kJ/mol obtained using the τ at 0 and 25℃ here, which agrees well with the E_a value obtained via the slopes in the Arrhenius plots of viscosity of DA-PCOD solutions (93±7 kJ/mol).

end fraction is large, resulting in a decreasing aggregation number with increasing temperature (Figure 3.14).

3.4.2 Temperature dependence of the pairwise-associative telechelic polymer (DA/DB-PCOD)

3.4.2.1 Conformational relaxation of the supramolecules dominates the dynamics of DA/DB-PCOD solution

In Chapter 2, it is demonstrated that the conformational relaxation of the supramolecules dominates the dynamics of 50k DA/DB-PCOD at 0℃, in contrast to DA-PCOD. In this chapter, more temperatures are taken into consideration, and large fractions of unbound ends are expected for both DA-PCOD and DA/DB-PCOD at 60℃. Therefore, a natural question rises as to whether the exchange time of DA/DB association is still long enough that the supramolecules relax completely before the end exchanges at 60℃.

To answer this question, the exchange time of DA-PCOD is again examined. As illustrated in Chapter 2, the lifetime of DA/DB binding should be longer than that of DA, since

DA/DB pair binds much tighter than DA's self-association. Literature also shows that high hydrogen bonding strength (ΔG) leads to slow end exchange/dissociation [31-32]. Although the exchange time of DA/DB cannot be measured directly through rheology, the exchange time of DA can (Table 3.3). The data obtained at 2 and 2.5 wt% were chosen to avoid the effect of superbridges that cause underestimation of the exchange time for DA. Using the Arrhenius relationship $\tau = \tau_0 \exp(E_a/RT)$, a τ value at 60℃ can be calculated, which is around 0.003 s. Thus the exchange time of DA/DB can be assumed to be longer than 0.003 s at 60℃. The next step is to compare the Rouse relaxation time of the formed supramolecules with the value 0.003 s.

At 60℃, the fraction of unbound ends for 50 kg/mol DA/DB-PCOD is around 30% (0.6 wt%, Table 3.2), indicating the formation of a 3-mer linear supramolecules with a molecular weight of 150 kg/mol, assuming the cyclic components can be ignored. In this simplified scenario, the relaxation time of a 150 kg/mol linear supramolecule with PCOD backbone is calculated to be ~ $4*10^{-5}$ s using the equation $\tau_{chain} \approx \frac{\eta s}{kT} b^3 N^2 C^{0.3}$ for semidilute unentangled solution in an athermal solvent. It is 1/100 of minimum exchange time of DA/DB ends (0.003 s). The smaller rings and linear species relax even faster. Therefore, it is demonstrated that DA/DB ends exchange/dissociate slow enough that the conformation relaxation of supramolecules dominate the solution dynamics, even at temperature as high as 60℃.

This statement is further confirmed by the viscometry data. In the extreme case that only 3-mer linear supramolecule is formed in 0.6 wt% DA/DB-PCOD solution at 60 ℃, its viscosity should be 3-fold that of the DB-PCOD solution at the same concentration, according to the relationship $\eta \approx NC^{1.3}$ for semidilute unentangled solutions. As the temperature goes down, the distribution shifts to larger supramolecules, leading to bigger contribution to the viscosity, and more significant enhancement over the viscosity of DB-PCOD non-associative control. This is indeed what is observed. The viscosity of 0.6 wt% DA/DB-PCOD solution at 60 ℃ is roughly 2-fold of that for DB-PCOD (Figure 3.15). The discrepancy from 3-fold can be attributed to the presence of cyclic species. And the difference between the viscosities of the two composition does increases with decreasing temperature, as is expected (Figure 3.15). Both theoretical calculation and viscometry data confirm that the conformation relaxation of supramolecules dominate the solution dynamics throughout the temperature range tested (0 to 60 ℃).
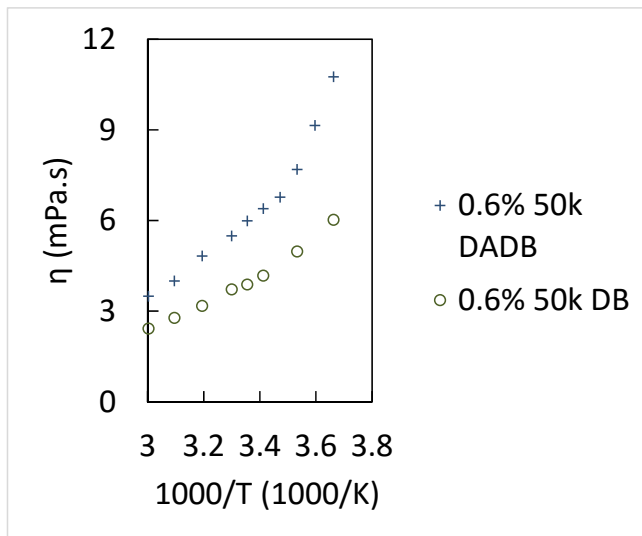
Figure 3.15 Solution viscosity plotted against inverse absolute temperature for 0.6 wt% solutions for 50 kg/mol DA/DB-PCOD and DB-PCOD. Linear scale of viscosity is used to emphasize the difference between the two compositions.

3.4.2.2 Temperature effect on the distribution of supramolecules formed by DA/DB-PCOD

The change in the distribution of linear supramolecules formed by DA/DB-PCOD with temperature has been supported by both SANS and rheology. SANS provides a direct route to observe the average size of the supramolecular species in the solution. The intensity of the SANS spectrum at low q (q < 0.02 Å^{-1}) decreases monotonically as the solution is heated from 0℃ to 60℃, indicating that the average size of supramolecules formed by
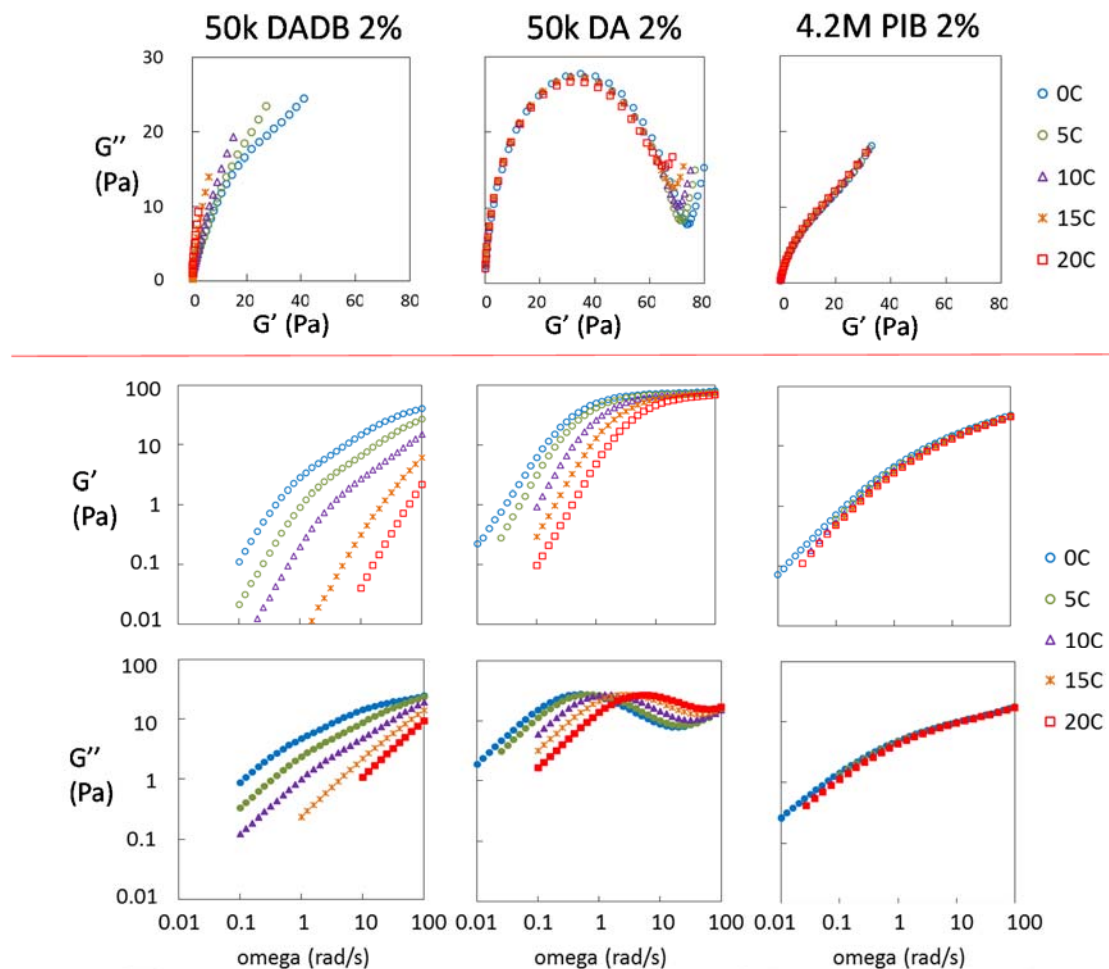
Figure 3.16 Oscillatory shear data of 2 wt% decalin solutions of 50k DA/DB-PCOD, DA-PCOD, and 4.2M PIB at temperatures 0-20℃, in the forms of Cole-Cole plot (top), and with G' and G'' plotted against frequency individually (bottom).

DA/DB-PCOD is directly related to the temperature, and lower temperature favors larger supramolecules.

Rheology methods study the morphology indirectly through the dynamic properties of the supramolecules. Time temperature superposition (TTS) presents a straightforward method to detect changes in solution composition, since the application of TTS principle requires the systems to have constant composition. The oscillatory shear data of 2 wt% decalin solutions of 50k DA/DB-PCOD, 50k DA-PCOD, and 4.2M PIB are plotted in the temperature range of 0℃ to 20℃ as an example (Figure 3.16). The data are laid out in the form of Cole-Cole plot in top line. It is clear that TTS fails for 50k DA/DB-PCOD solution and works for the other two polymer solutions in which the polymer composition stays constant. It confirms a compositional change of supramolecular species in the DA/DB-PCOD solution with temperature.

To give more quantitative information on the temperature dependence, the frequency shift factor a_T is examined. 50k DA/DB-PCOD has a unique temperature dependence, distinct from 50k DA-PCOD and 4.2M PIB (Figure 3.16, middle and bottom line). In the solution of 4.2M PIB and other linear covalent polymers, the shift factor reflects the temperature dependence of the friction coefficient of the polymer backbone in the solvent, which is very weak when the volume fraction of the polymer is low (Figure 3.16, right column). The dynamics of 50k DA-PCOD solutions is dominated by the exchange of the end between micelle cores. The shift factor is determined by the activation energy of the binding between the ends (Figure 3.16 middle column). The shift of 50k DA-PCOD solutions is thus much stronger than that of PIB solution. The shift factor for 50k DA/DB-PCOD solution is larger than either 50k DA-PCOD or PIB solution because it is
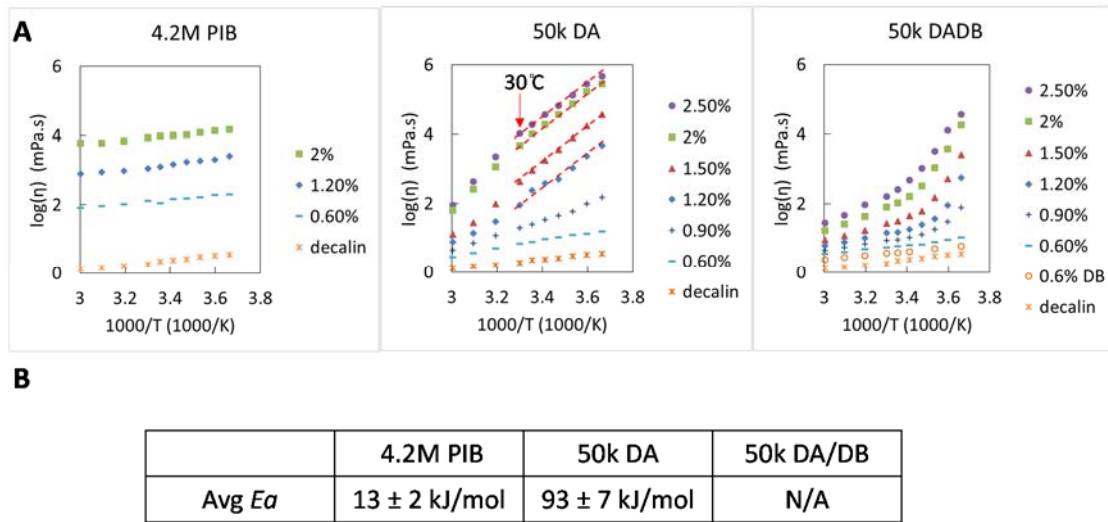
Figure 3.17 A. Arrhenius plot of solutions of 4.2M PIB at 0.6, 1.2, and 2 wt% and 50 kg/mol DA-PCOD and DA/DB-PCOD at concentrations from 0.6 to 2.5 wt% in the temperature range of 0-60℃. **B.** The average activation energy (E_a) calculated through the Arrhenius plot of solution viscosity against inverse temperature for 4.2M PIB (0.6-2 wt%) and 50k DA-PCOD (1.2-2.5 wt%) solutions.

contributed by two factors: 1) the temperature dependence of the friction coefficient of the backbone, and 2) the change in distribution of supramolecular species with temperature; with the latter one being more important.

The Arrhenius plots of 4.2M PIB, 50k DA-PCOD, and 50k DA/DB-PCOD solutions are also compared. The Arrhenius plot takes the form of a linear line when the parameter (here, viscosity η) has a constant activation energy (E_a), which is the case for 4.2M PIB solution in the full temperature range 0℃ to 60℃, and for 50k DA-PCOD in the range of 0℃ to 30℃ (Figure 3.17A, left and middle). The activation energy that governs the dynamic process can be calculated from the slope of the line, which is around 13 kJ/mol for PIB solution and around 97 kJ/mol for DA-PCOD solution (Figure 3.17B). However, the same method does not apply to the 50k DA/DB-PCOD solutions. The average size of the supramolecules formed by DA/DB-PCOD monotonically increases with decreasing temperature, leading to additional contribution to the solution viscosity. The sharp upturn

at low temperatures (around 0 ℃) for 50k DA/DB-PCOD solutions may be the result of some more complicated interactions between cyclic and linear supramolecules, which will be illustrated in Chapter 4. Thus, an activation energy related to the end-association energy between isophthalic acid and tertiary amine cannot be deduced from the Arrhenius plot for DA/DB-PCOD solutions for two reasons: 1) the association between isophthalic acid and tertiary amine does not break/exchange before the supramolecules relax fully; and 2) the temperature dependence of the solution viscosity no longer follows Arrhenius equation.

This temperature-controlled distribution of supramolecules agrees with theoretical prediction. A statistical mechanical model specifically about the supramolecule formation with pairwise-associative telechelic polymers in dilute solutions has been developed by Dr. Ameri David based on ring-chain equilibrium concept, using the molecular weight, end-association strength and total concentration of individual telechelics as variables. The model results show that the distribution of the telechelics into linear supramolecules is affected greatly by the end-association energy (Figure 3.18).

The simulation is carried out at room temperature (298K) with the molecular weight of each telechelic polymer being 1000 kg/mol and the total volume fraction of polymer in the solution being 1,400 ppm, roughly half the overlap concentration of a non-associative backbone with the same length. The binding strength of DA/DB at 298K is around 16 kT (40 kg/mol), which fits the scenario in the middle column (Figure 3.18, middle). The disparity between 16 kT and 18 kT (or between 14 kT and 16 kT) is about 10% of the total binding energy, which is much smaller compared to the energy change brought by varying the temperature from 25 ℃ (298K) to 0 ℃ (273K) (or from 25 ℃ (298K) to 60 ℃ (333K)) as in the experiments here (Table 3.1, Section 3.1.3). The ring-chain equilibrium situation at
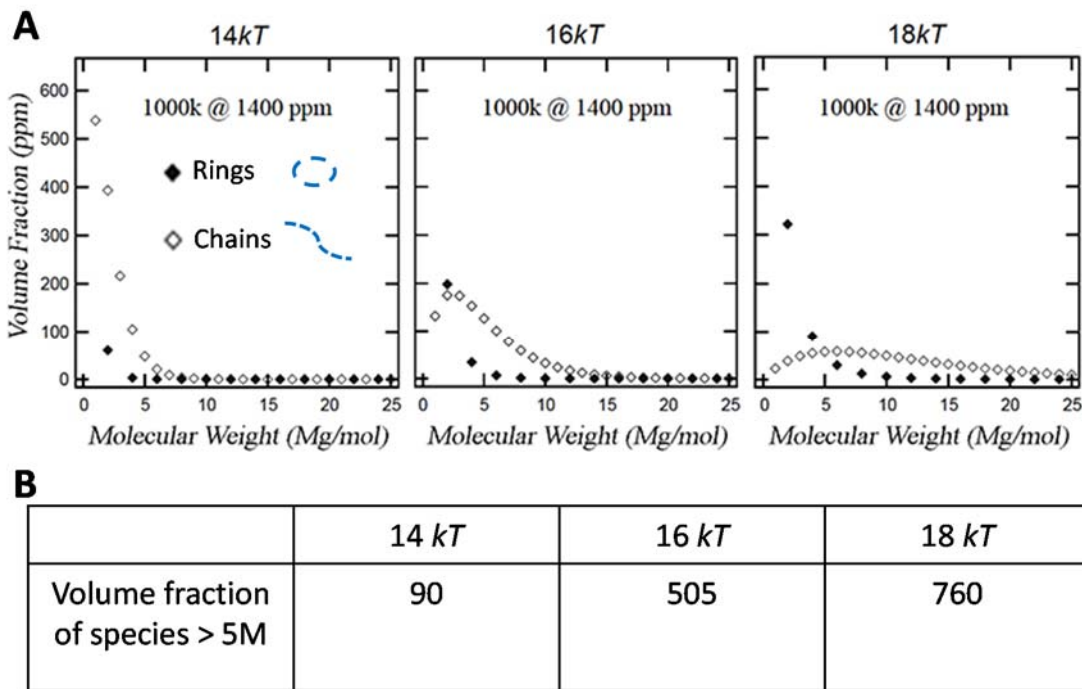
Figure 3.18 A. Model predictions on the equilibrium concentrations of supramolecular species with various sizes as functions of polymer concentration for three different values of the strength of interaction 14*kT* (left), 16*kT* (middle) and 18*kT* (right) (open diamond: linear supramolecules; solid diamond: cyclic supramolecules) [33]. **B.** The accumulated volume fraction of linear species with molecular weight > 5000 kg/mol (5-mer supramolecules) calculated from the figure in Part A.

333K should be way left to the 14 *kT* figure, while the situation at 273K should be way right to the 18 *kT* figure. Nevertheless, the simulation result shines lights on the temperature effect on the distribution of supramolecules.

As the end-association strength increases from 14 *kT* (35 kJ/mol) to 18 *kT* (45 kJ/mol), more telechelic polymers distribute into supramolecules with larger sizes (Figure 3.18A). The volume fraction of linear species with molecular weight higher than 5,000 kg/mol (5-fold of the length of single telechelic building block) is used as an example to quantify the significance of the change in distribution. The value jumps from 90 ppm for 14 *kT* to 505 ppm for 16 *kT* and to 760 ppm for 18 *kT* (Figure 3.18B). The observation from the data in

this chapter that the average size of the supramolecular species increases significantly with decreasing temperature agrees qualitatively with the above theoretical prediction.

3.5 Conclusions

Temperature determines the binding strength of self- and pairwise- end association, and furthermore, the fraction of unbound ends and the distribution and topology of formed supramolecules/aggregates.

Experimental data points out that there are two temperature regimes in which the morphology of DA-PCOD behave differently: 1) 0℃ to 30℃ and 2) above 30℃. The micelle structures formed by DA-PCOD in decalin solutions are shown to remain constant in the temperature range of 0℃ to 30℃. The dynamics of the solutions is controlled by the exchange time of the end from the micelle core, the activation energy associated with which is calculated to be around 93 kJ/mol. These features are similar to those of HEURs. As the solution is heated above 30℃, SANS data suggests that the aggregates formed by DA-PCOD in decalin solutions become smaller, which has not been seen in the HEUR system. It is postulated that the aggregation number of each micelle decreases with temperature at temperatures above 30℃. The hypothesis agrees with the calculation on the end association equilibrium, which indicates that more than 50% of the acid groups are unbound at around 60℃.

For DA/DB-PCOD system, both rheology and small angle neutron scattering (SANS) data confirm that the average size of supramolecules formed by DA/DB-PCOD increases monotonically with decreasing temperature throughout the range tested (0 to 60℃). It is also demonstrated that although the end exchange time of DA/DB should become shorter

at high temperature, DA/DB still exchanges/dissociates slow enough that the conformation relaxation of supramolecules dominate the solution dynamics.

References

[1]7. T. Annable, R. Buscall, R. Ettelaie, & D. Whittlestone, *Journal of Rheology,* **1993**, *37*, 695-726.

[2] G.Gilli, P.Gilli, *The Nature of the Hydrogen Bond: outline of a comprehensive hydrogen bond theory*, Oxford Univ. press, 2009.

[3] M. Rubinstein, R. H. Colby, *Polymer Physics*, Oxford Univ. press, Oxford, 2003. Reprinted 2012.

[4] T. Budtova, P. Navard, *Nord. Pulp Pap. Res. J.*, **2015**, *30*, 99-104.

[5] A.A. Tager, V.Ye. Dreval, F.A. Khasina, *Polym. Sci. USSR*, **1963**, *4*, 1097-1106.

[6] C. Chassenieux, T. Nicolai, L. Benyahia, *Current Opinion in Colloid & Interface Science*, **2011**, *16*, 18-26.

[7] F. Tanaka, S. F. Edwards, *Macromolecules,* **1992**, *25*, 1516-1523.

[8] A.N. Semenov, J.-F. Joanny, A. R. Khokhlov, *Macromolecules,* **1995,** *28*, 1066-1075.

[9] Q. T. Pham, W. B. Russel, J. C. Thibeault, W. Lau, *Macromolecules,* **1999**, *32*, 2996-3005.

[10] Q. T. Pham, W. B. Russel, J. C. Thibeault, W. Lau, *Macromolecules,* **1999**, *32*, 5139-5146.

[11] X.-X. Meng, W. B. Russel, *Macromolecules* **2005,** *38,* 593-600.

[12] A. D. H. Clague, H. J. Bernstein, *Spectrochim. Acta*, **1969**, *25*, 593-596.

[13] J. Chocholoušová, J. Vacek, P. Hobza, *J. Phys. Chem. A* **2003,** *107,* 3086-3092.

[14] E. N. Gur'yanova, I. P. GoI'dshtein, T. I. Perepelkova, *Russian Chemical Reviews*, **1976**, *45*, 792–806.

[15] M. M. Davis, M. Paabo, *J. Am. Chem. Soc.*, **1960**, *82*, 5081–5084.

[16] H. Nakanishi, H. Morita, S. Nagakura, *J. Mol. Spectrosc.*, **1977**, *65*, 295-305.

[17] L.Sun, C. D. Wick, J. I. Siepmann, M. R. Schure, *J. Phys. Chem. B,* **2005,** *109,* 15118-15125.

[18] A. D. H. Clague, H. J. Bernstein, *Spectrochim. Acta*, **1969**, *25*, 593-596.

[19] G. Allen, J. G. Watkinson, K. H. Webb, *Spectrochim. Acta*, **1966**, *22*, 807-814.

[20] E. W. Johnson, L. K. Nash, *J. Am. Chem. Soc.*, **1950**, *72*, 547–556.

[21] T. Park, S. C. Zimmerman, *J. Am. Chem. Soc.,* **2006**, *128*, 13986-13987.

[22] H. Hofmeier, R. Hoogenboom, M. E. L. Wouters, U. S. Schubert, *J. Am. Chem. Soc.,* **2005**, *127*, 2913-2921.

[23]11. J. H. K. Ky Hirschberg, F. H. Beijer, H. A. van Aert, P. C. M. M. Magusin, R. P. Sijbesma, E. W. Meijer, *Macromolecules,* **1999,** *32,* 2696-2705.

[24]1. S. R. Kline, *J. Appl. Crystallogr.*, **2006**, *39*, 895-900.

[25] T. Uneyama, S. Suzuki, H. Watanabe, *Phys. Rev. E*, **2012**, *86*, 031802.

[26] J. S. Higgins, H. Benoît, *Polymers and neutron scattering*. Clarendon Press. Oxford. 1994.

[27] P. Pirogovsky, PhD. Dissertation, California Institute of Technology, 2013.

[28] B. Hammouda, *SANS from homogeneous polymer mixtures: a unified overview*, in *Polymer Characteristics*. Springer. 1993, p. 87-133.

[29] L. J. Fetters, N. Hadjichristidis, J S. Lindner, J. W. Mays, *J. Phys. Chem. Ref. Data.,* **1994**, *23*, 619- 640.

[30] S. De Feyte *et al*, *Nano Letters*, **2003**, 3, 1485–1488.

[31] L. E. Cramer, K. G. Spears, *J. Am. Chem. Soc.*, **1978**, *100*, 221–227.

[32] J. Zheng, M. D. Fayer, *J. Phys. Chem. B* **2008,** *112,* 10221–10227.

[33] M.-H. Wei*, B. Li*, R. L. A. David, S. C. Jones, V. Sarohia, J. A. Schmitigal & J. A. Kornfield (*: authors contributed equally), *Science*, **2015**, *350*, 72-75.

Chapter IV

Effect of Chain Length on Pairwise-Associative Telechelic Polymers

4.1 Introduction

DA/DB PCODs are expected to form linear and cyclic supramolecules due to their pairwise end association. The distinct morphology and dynamics of pairwise associative polymers (di-acid-ended paired with di-amine-ended PCOD, DA/DB) have been covered in earlier chapters. Chapter 2 shows that the dynamics of the supramolecules formed by 50k DA/DB-PCOD at 0℃ is strikingly similar to that of linear covalent polymers. As the concentration increases from 1.2 wt% to 2 wt%, the fraction of the supramolecules that dominates the solution dynamics also increases. Chapter 3 reveals that temperature induces dramatic change in the end association, supramolecule formation, and eventually the dynamics of 50k DA/DB-PCOD solutions, in contrast to solutions of covalent polymers. Solutions of DA/DB-PCOD demonstrate markedly similar but still distinct dynamic features compared to solutions of linear covalent polymer.

This striking resemblance and discrepancy motivates us to explore the effect of another factor: polymer chain length, which is one of the most important parameter in the dynamics of linear covalent polymer. For better demonstration of the chain length effect on the dynamics of DA/DB-PCOD solutions, the introduction will illustrate the following aspects: 1) review the dynamics of linear covalent polymer solutions and the effect of chain length,

2) generalize the factors that influence ring-chain equilibrium, and 3) discuss the effects of backbone length on the association equilibrium of DA/DB ends.

4.1.1 Chain length effect on the dynamics of linear covalent polymer solutions

The dynamics of linear covalent polymer solutions has been reviewed in Chapter 1. Almost all important parameters for solution dynamics are strongly affected by the polymer chain length. The effect takes place in two ways: 1) chain length determines the critical concentrations (the overlap concentration C* and the entanglement concentration C_e) which define the three concentration regimes, and 2) the parameters for viscoelasticity (relaxation time, modulus, and viscosity) demonstrate distinct power-law dependence on the chain length within each concentration regime.

Depending on the polymer concentration, polymer solutions can be divided into three concentration regimes: dilute, semidilute unentangled, and semidilute entangled regimes (Figure 4.1A) [1]. The conformation of polymer coil in each regime differs greatly. In dilute solution, polymer chains are isolated from each other and exhibits self-avoiding walk conformation in good solvent, with its size $R \approx N^{0.588}b$ (Figure 4.1A, left). At the overlap concentration (C*), the total pervaded volume of polymer coils equals the solution volume,
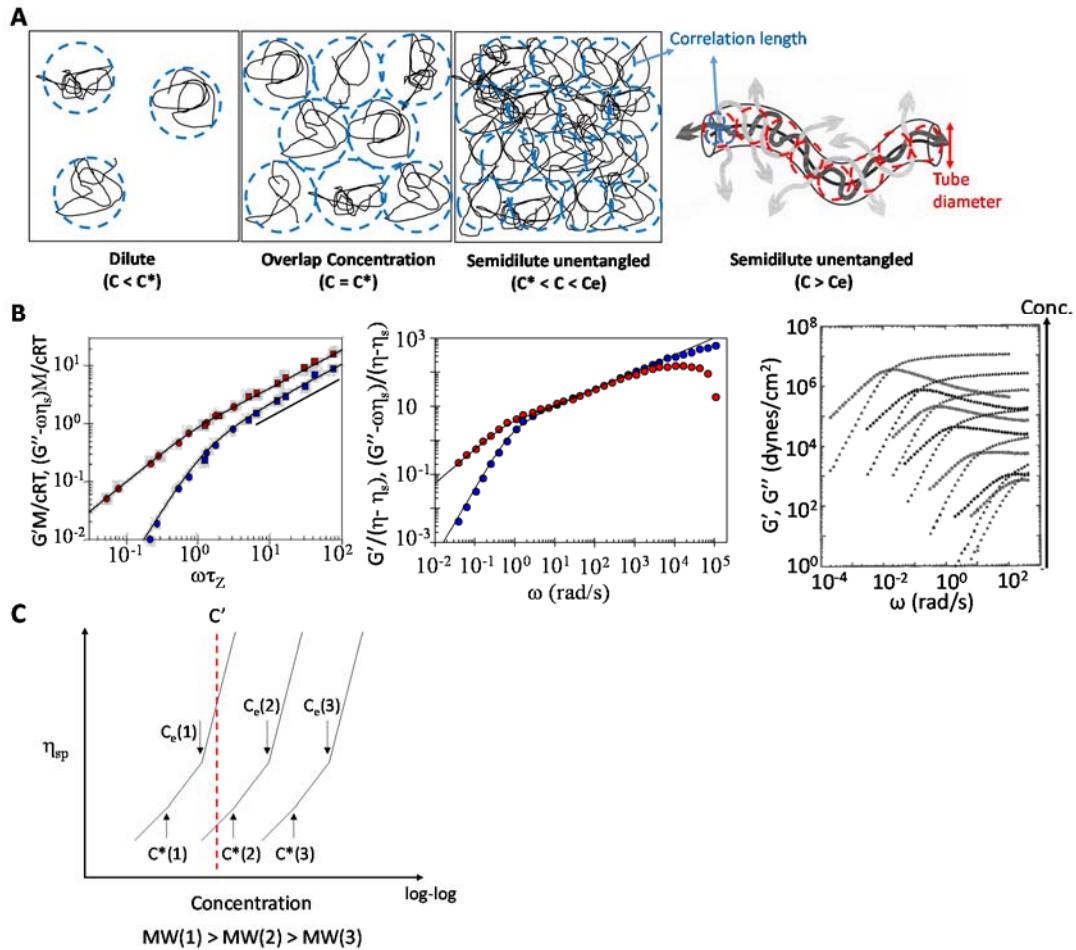
Figure 4.1 A. Schematic representation of the three concentration regimes: dilute, semidilute-unentangled and semidilute-entangled regimes. **B.** Literature on the dynamic moduli curves for dilute, semidilute-unentangled and semidilute-entangled solutions. **Left:** (Figure reproduced from reference [2]) Linear viscoelastic response expressed in terms of reduced moduli, for dilute polystyrene (MW = 860 kg/mol) solutions in two θ-solvents [3]. Red are reduced loss moduli, blue are reduced storage moduli, circles are in decalin at 16 °C, squares are in di-2-ethylhexylphthalate at 22 °C. Curves are predictions of the Zimm model with ν = ½. The black line reflects a slope of 2/3. **Middle:** (Figure reproduced from reference [4]) Reduced storage modulus (G', blue) and reduced loss modulus (G'', red) of a semidilute unentangled M_w = 400 kg/mol poly(α-methyl styrene) solution (c = 0.105 g/cm^3) in a high-viscosity solvent, Arochlor at 25 °C. Lines are predictions of the Rouse model. **Right:** (Figure reproduced from reference [5]) Oscillatory shear data on neutral polybutadiene M_w = 925 kg/mol entangled solutions. Polymer melt and six solutions in the good solvent phenyloctane at 25 °C with volume fraction of polymer from top to bottom φ =1, φ = 0.488, φ = 0.280, φ = 0.140, φ = 0.0621, φ = 0.0274, and φ = 0.0214. All solutions are entangled since φ_e = 0.01. **C.** Schematic diagram illustrating the concentration dependence of the specific viscosity (η_{sp}) of linear polymer solutions in the dilute, semidilute-unentangled and semidilute-entangled regimes for each of three successively higher molecular weight polymers.

and the volume fraction within its own pervaded volume equals the total volume fraction.

This gives the expression for overlap concentration: $C^* \approx \varphi^* \approx Nb^3/R^3 \approx Nb^3/(N^\nu b)^3 \approx N^{1-3\nu} \approx N^{-0.76}$ for $\nu = 0.588$ (Figure 4.1A, middle). It is clear that both R and C* is dependent on chain length N.

As polymer concentration is increased beyond C*, chains start to interpenetrate and the solution is called semidilute (Figure 4.1A, middle). A critical length scale comes up for semidilute solutions: the correlation length (ξ). Beyond the length scale of the correlation length, both the excluded volume effect and the hydrodynamic force are screened. Therefore, the polymer chain reserves self-avoiding walk conformation within ξ, but behaves as an ideal chain at length scale larger than ξ. When the concentration increases even further, another critical concentration emerges: the entanglement concentration (C_e); and each polymer chain becomes topologically entangled with other chains because they cannot cross each other (Figure 4.1A, right). The solutions with $C^* < C < C_e$ are considered to be semidilute unentangled solutions, and solutions with $C > C_e$ are considered to be semidilute entangled solutions. The derivation in Chapter 1 indicates that the entanglement concentration C_e can be estimated by the following equation: $C_e \approx [N_e(1)/N]^{0.76}$, in which $N_e(1)$ refers to the number of Kuhn segments in an entanglement strand in the melt. Thus, the entanglement concentration is proportional to the overlap concentration and depends on chain length N as well.

Besides different conformations, the solutions within each concentration regime display distinct dynamics as well. In dilute solution, a polymer chain diffuses with its whole pervaded volume like a solid object. The dynamics of polymer dilute solution is predicted by Zimm model, which is supported with experimental data, especially for data obtained in θ-solvent (Figure 4.1B, left) [3]. The prediction for good solvent is less satisfying

because the excluded volume effect diminishes hydrodynamic effect. In semidilute unentangled solution, the dynamics is dominated by the longest relaxation mode, which is the relaxation of polymer coils at length scales larger than the correlation length. Since polymers behave ideally within this length scale, the dynamics follows the Rouse model. The dynamic moduli curve exhibits a distinct power law region with a slope of ½ in the intermediate frequency range (Figure 4.1B, middle) [4]. For semidilute entangled solutions, the reptation process of the polymer chain controls the relaxation, resulting in a crossover relaxation time representing the reptation time, and a plateau modulus determined by the number density of entanglement strands (Figure 4.1B, right) [5].

Due to the different relaxation model for each concentration regime, the parameters for viscoelasticity (relaxation time, modulus, and viscosity) are related to the chain length with a different power law dependence respectively (Table 4.1). The derivation for the scaling

Table 4.1 Concentration Regimes and Rheological Properties of Linear Polymer Solutions

	Dilute	Semidilute unentangled	Semidilute entangled
Critical concentration	-	$C^* \sim N^{-0.76}$	$C_e \sim [N_e(1)/N]^{0.76}$
Concentration range	$C < C^*$	$C^* < C < C_e$	$C > C_e$
Longest relaxation time	$\tau_Z \sim N^{1.76}C^0$	$\tau_{chain} \sim N^2 C^{0.3}$	$\tau_{rep} \sim N^3 C^{1.6}$
Terminal modulus	$G(\tau_Z) \sim N^{-1}C^1$	$G(\tau_{chain}) \sim N^{-1}C^1$	$G_e \sim N^0 C^{2.3}$
Specific Viscosity	$\eta_{sp} \sim N^{0.76}C^1$	$\eta_{sp} \sim N^1 C^{1.3}$	$\eta_{sp} \sim N^3 C^{3.9}$

arguments are covered in details in Chapter 1. In general, the relaxation time and viscosity both increase with increasing chain length for all regimes.

There is an important feature that the solution viscosity shows stronger and stronger dependence on concentration as the solution enters a higher concentrated regime (Table 4.1, last row; Figure 4.1C, slope varies from 1 to 1.3 to 3.9), which is in fact related to the chain length effect. Since the overlap concentration and entanglement concentration are lower for a polymer with higher molecular weight, the solution of a high molecular weight polymer may be entangled while the solution of a low molecular weight polymer at the same concentration is dilute (Figure 4.1C, red dash at a specific concentration C'). The solution of the high molecular weight polymer thus displays a much higher viscosity, exaggerating the chain length effect solely due to the power law dependence of viscosity.

In summary, the chain length affects the viscoelasticity of polymer solutions through 1) determining the concentration regime which one specific solution is in, and 2) the chain length dependence of dynamic parameters within that regime. Both aspects make contributions to the solution dynamics in the same direction: longer chain length results in higher solution viscosity.

For ease of comparison between pairwise-associative polymers and linear covalent polymers, critical concentrations are estimated for the polymer backbone (polycyclooctadiene, same structure as perfect 1,4-polybutadiene, with no end association) with molecular weights used in this chapter (50 kg/mol, 100 kg/mol and 230 kg/mol, Table 4.2). The C* for 50 kg/mol polymer is measured by viscometry of a 50 kg/mol non-associative telechelic polymer. The concentration at which the specific viscosity of the polymer solution is 1 is chosen as the overlap concentration C*, since $\eta_{sp} = (\eta - \eta_s)/ \eta_s \approx$

Table 4.2 Overlap and entanglement concentrations for non-associative chains of each length examined

	C* (η_{sp} = 1, decalin)	$C_e \sim [N_e(1)/N]^{0.76}$ [c]
50k	0.8 wt% [a]	8.3 wt%
100k	0.47 wt% [b]	4.9 wt%
230k	0.25 wt% [b]	2.6 wt%

[a.] C* for 50k non-associative chains: measured using viscometry

[b.] C* for 100k and 230k nonassociative chains, calculated from C* of 50k nonassociative chains.

[c.] C_e: calculated using the equation $C_e \approx [N_e(1)/N]^{0.76} \approx [M_e/M]^{0.76}$. The entanglement molar mass (M_e) for 1,4-polybutadiene in the melt at 25°C is 1900 g/mol, and $N_e(1) = 18$ [1].

$\varphi*N^{3v-1} \approx N^{1-3v} N^{3v-1} \approx 1$ at $\varphi*$ according to Zimm model [1]. The C* for 100 kg/mol and 230 kg/mol are calculated from the C* for 50 kg/mol using the scaling relationship $C* \approx N^{1-3v} \approx N^{-0.76}$. The entanglement concentration for all three lengths are calculated using the equation shown in Figure 4.1B. Theoretically, the ratio between C_e and C* should be on the order of $[N_e(1)/N]^{0.76}/ N^{-0.76} \approx N_e(1)^{0.76} \approx 9$, since the $N_e(1)$ for 1,4-polybutadiene at 25°C is 18. The measured C* for 50 kg/mol is around 1/10 that of the calculated C_e (Table 4.2, 0.8 wt% *versus* 8.3 wt%), in consistence with the theoretical value fairly well.

It should be noted that the temperature dependence for solutions of linear covalent polymers is not significantly altered by molecular weight within the concentration range covered in this thesis. In the solutions of linear covalent polymers, the dominant factor for temperature dependence is that of the friction coefficient of the polymer backbone in the solvent, which is very weak when the volume fraction of the polymer is low. Thus linear covalent polymers display the same weak temperature dependence in their solutions, with very slight change with molecular weights.

4.1.2 Chain length effect on ring-chain equilibrium

The hypothesized supramolecules formed by DA/DB-PCOD are similar but different from linear covalent polymers. One difference is that the supramolecules consist of a distribution of linear and cylic species with various sizes. The distribution of supramolecules formed by pairwise-associative telechelic polymers is predicted by ring-chain equilibrium theory, first developed by Jacobson and Stockmayer in 1950 for polycondensation reaction [6]. After 2000s, the ring-chain equilibrium theory starts to be applied to physical assembly of bi-functional associative small molecules (such as ureidopyrimidone (UPy) functionalized ones) and pairwise-associative telechelic polymers [7,8]. Concentration and chain length are all important factors that affect the distribution of supramolecules.

One of the key predictions of the theory is that the partitioning of monomers into linear products increases as the total monomer concentration increases [6-9]. The distribution of supramolecule formation is determined by the balance between the enthalpy gain from end association and the conformational entropy lost for the polymer backbone. In dilute solutions, individual polymer coils are isolated from each other (Figure 4.2A, left top). Thus, the formation of small rings (e.g. dimer, Figure 4.2A, left bottom) is favored, because the entropy cost for restricting multiple chains in close proximity forming large supramolecules is expected to be enormous. In semidilute solutions, the telechelic polymers are well percolated (Figure 4.2A, right top), resulting in less entropy cost to link multiple chains together allowing long linear supramolecules to be formed (Figure 4.2A, right bottom).

Chain length also affects the distribution of cyclic and linear supramolecules. Since all possible cyclic supramolecules formed by individual telechelics are at least twice as long
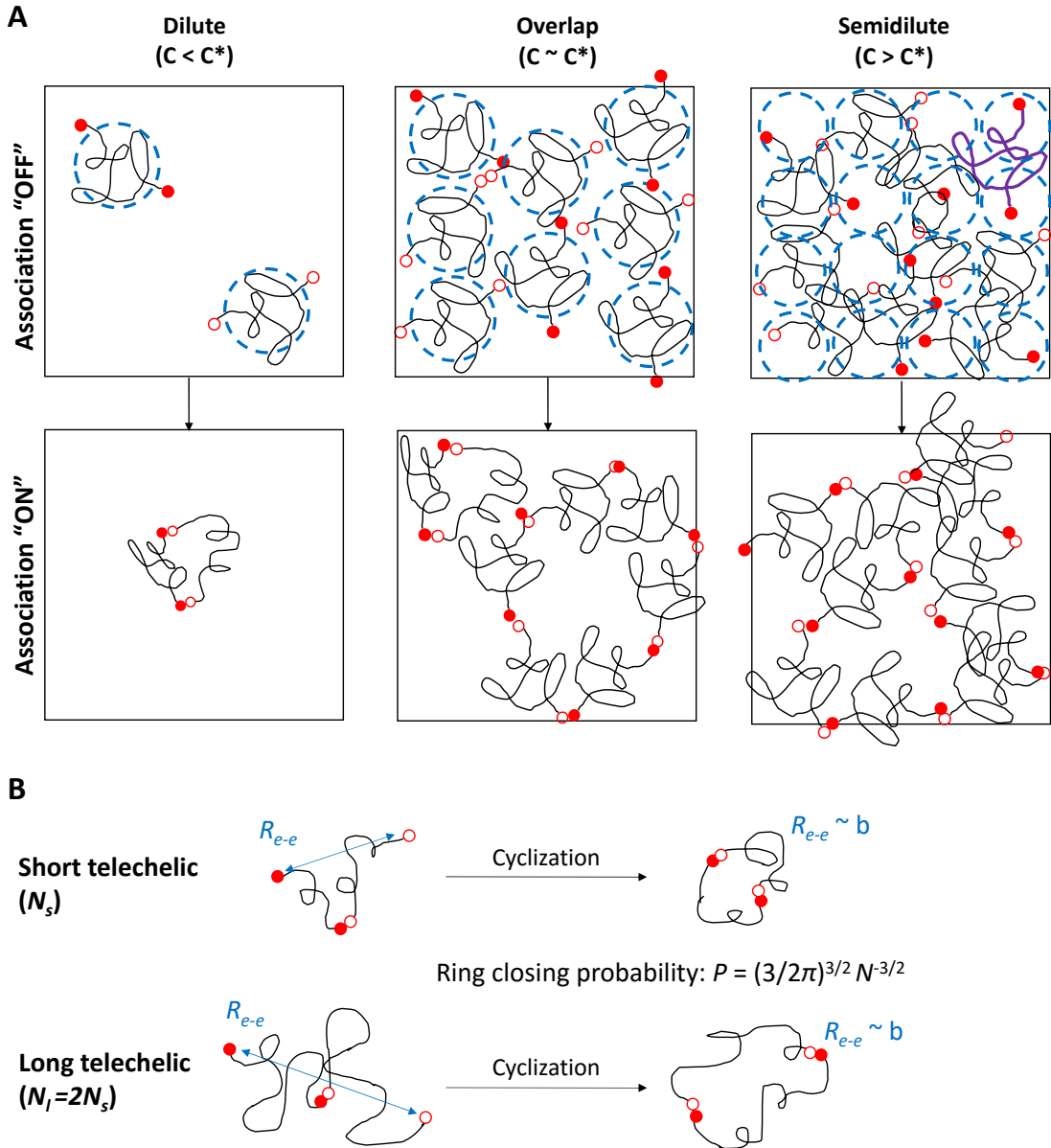
Figure 4.2 A. Schematic illustration on the concentration dependence of ring-chain equilibrium. The purple chain shows that polymer coils are well percolated, and each coil spans several correlation blobs. **B.** Schematic illustration on the chain length effect of the entropic cost to form dimer rings. Long telechelic polymers form linear dimer supramolecules with larger end-to-end distance, the cyclization of which leads to higher entropy cost in conformation energy.

as individual telechelic polymers, short-range steric hindrance is negligible. In this case,

the entropy cost of ring closure can be expressed as a well-defined function of ring size,

with the aid of well-known configuration theory [10] for polymer coil. For an ideal polymer

chain containing N Kuhn monomer (each with size b), its end-to-end distance $R_{e-e} = N^{1/2}b$ [10]. When the chain is closed to a ring, the first and last monomer will be confined together in a very small volume, v_s, which can be assumed to be $v_s = b^3$. The probability of finding those two monomers in v_s is then $P = (3/2\pi N)^{3/2}(v_s /b^3) = (3/2\pi)^{3/2} N^{-3/2}$, which decreases with increasing chain length [6]. For pairwise-associative telechelic polymers, increasing chain length results in longer average end-to-end distance of its formed supramolecules at the same aggregation number, diminishing the probability of the cyclization of the supramolecules. More quantitatively, increasing the chain length by 2-fold will lead to $(N_l/N_s)^{3/2} = 2^{3/2} = 2.8$ fold decrease in ring-closing probability (Figure 4.2B). Therefore, long chain length of pairwise-associative telechelic polymer disfavors ring formation and favors linear supramolecules.

4.1.3 Strength of association of pairwise-associative polymers (DA/DB)

The association between isophthalic acid (DA) and tertiary amine (DB) has been discussed in Chapter 1. They bind with each other through charge-assisted hydrogen bond (CAHB), because the pK_a for isophthalic acid (3.46) is very close the pK_a for the conjugate acid of trimethylamine (3) [12]. The free energy (ΔG) of the DA/DB association is estimated to be around 16 kT at room temperature (298K, Figure 4.3A) [11-13].

It has been well documented in literature that systems based on hydrogen bonds depend highly on temperature. The standard enthalpy ΔH and standard entropy ΔS in the H-bond formation can be calculated through the Van 't Hoff plot of hydrogen bonding systems, and are found to be a constant and independent of temperature in the temperature range encountered in this thesis [14-16]. And the H-bond strength (ΔG) decreases linearly with increasing absolute temperature since $\Delta G = \Delta H - T\Delta S$. The corresponding H-bond

dissociation constant (K_d) at various temperatures is directly related to ΔG: $K_d = \exp(\Delta G/kT)$ (Figure 4.3A). It is mentioned in Chapter 1 that the temperature dependence of ΔG and K_d can be estimated using two methods: 1) Van't Hoff equation: $\ln (K_{d1}/K_{d2}) = -\frac{\Delta H}{R}(\frac{1}{T2} - \frac{1}{T1})$, and 2) entropy-enthalpy compensation [17-19]: $\Delta G_1/\Delta G_2 = (\beta - T_1)/(\beta - T_2)$, in which $\beta = \Delta H/\Delta S$ and is named compensation temperature. Specifically, ΔH and β has been measured to be 12~16 kcal/mol (or 50 ~ 67 kJ/mol) and 453 ± 54 K respectively, for the interactions between benzoic/acetic acid (unsubstituted and substituted) and tertiary amine (triethyl-, tripropyl- and tributyl- amine) [11]. For the DA/DB-PCOD system, the H-bond free energy (ΔG) and dissociation constant (K_d) of the DA/DB association is then estimated for 60℃ (333K) and 0℃ (273K) from the value 16 kT at 25℃ (298K) (Figure 4.3A).

The change in the above estimated ΔG with temperature for DA/DB pair is in good agreement with literature: around 20% change in ΔG is induced by varying 30K [14-16] (Figure 4.3A). The corresponding H-bond dissociation constant (K_d) at various temperatures is directly related to ΔG: $K_d = \exp(\Delta G/kT)$. As expected, the dissociation constant decreases with decreasing temperature (Figure 4.3A).

Chain length does not affect the binding affinity between end groups directly. However, it changes the end group concentrations, and in turn influences the fraction of the unbound ends in the solution. The total end group concentration for DA/DB-PCOD solution is the same as the molar concentration of polymer coils multiplied by 2, which is inversely proportional to the chain length ($C_{end} \sim N^{-1}$). Since DA/DB-PCOD solution contains equiv. molar of DA and DB ends, the concentration for each type of end equals the molar concentration of polymer coils ($C_A = C_B = C_{pol} \sim N^{-1}$) (Figure 4.3B). Knowing the total concentration for A and B end, the fraction of unbound ends can be estimated using the

A

$$K_d = \exp(\Delta G/RT)$$

60℃ (333 K)	25℃ (298 K)	0℃ (273 K)
ΔG(333K) = 30±3 kJ/mol	ΔG(298K)=16 kT = 40 kJ/mol	ΔG(273K) = 46±3 kJ/mol
K_d = 8 ~ 33 μM	K_d = 0.11 μM	K_d = 0.0008 ~ 0.003 μM

B

	50k	100k	230k
0.3%	0.05 mM	0.025 mM	0.012 mM
0.6%	0.1 mM	0.05 mM	0.024 mM
0.9%	0.16 mM	0.08 mM	0.036 mM
1.2%	0.21 mM	0.1 mM	0.048 mM
1.5%	0.26 mM	0.13 mM	0.06 mM
2%	0.36 mM	0.18 mM	0.08 mM
2.5%	0.44 mM	0.22 mM	0.1 mM
4%	0.72 mM	0.36 mM	0.16 mM

C

		50k	100k	230k
0.3%	60℃ (K_d = 8~33 μM)	22±5 μM (44±10 %)	13±2 μM (54±10%)	7.8±1.2 μM (65±10%)
	25℃ (K_d = 0.11 μM)	2.2 μM (4%)	1.7 μM (6%)	1.1 μM (9%)
	0℃ (K_d = 0.0008~0.003 μM)	0.3±0.1 μM (0.6±0.2%)	0.21±0.06 μM (0.85±0.25 %)	0.15±0.05 μM (1.2±0.4%)
2.5%	60℃ (K_d = 8~33 μM)	83±20 μM (20±5%)	55±15 μM (25±7%)	35±10 μM (35±10%)
	25℃ (K_d = 0.11 μM)	7 μM (2%)	5 μM (2%)	3.3 μM (3%)
	0℃ (K_d = 0.0008~0.003 μM)	0.9±0.3 μM (0.2±0.06%)	0.6±0.2 μM (0.3±0.1%)	0.4±0.1 μM (0.4±0.1%)

Figure 4.3 A. The estimated binding energy (ΔG) and dissociation constant (K_d) at 60, 25 and 0℃, using Van't Hoff equation, ln (K_1/K_2) = - $\frac{\Delta H}{R}$ $(\frac{1}{T2}$ - $\frac{1}{T1})$, with 25℃ as the reference temperature. **B.** The end group concentrations for each backbone length at each concentration examined in this chapter. **C.** The estimated concentration and fraction (in brackets) of unbound end groups for each backbone length at 60, 25, and 0℃ at two concentrations (0.3% and 2.5%).

relationship K_d= [A][B]/[AB], in which [A] and [B] refer to the unbound end concentration, [AB] reflects the bound end concentration, and [A] = [B] = C_A - [AB] (Figure 4.3C). The fraction of dangling ends increases with longer chain length (100k and 230k) in all cases. The temperature has more dramatic effect on the equilibrium: the fraction of dangling ends is huge for telechelics of all molecular weights at high temperature (~ 50% at 60℃), and becomes negligible at low temperature (≤ 1% at 0℃) (Figure 4.3C). Considering the DA/DB association equilibrium, longer chain length leads to lower end group concentration and higher fraction of unbound ends, having opposite effect in supramolecule formation compared to its effect in ring-chain equilibrium.

4.1.4 Scope of this chapter

In earlier chapters, the distinct morphology and dynamics of pairwise associative polymers (di-acid-ended paired with di-amine-ended PCOD, DA/DB-PCOD) have been covered, as well as their concentration (Chapter 2) and temperature dependence (Chapter 3). The range for each parameter discussed in each chapter is illustrated in Figure 4.4.

In Chapter 2, the dynamic pattern of DA/DB-PCOD is compared with that of DA-PCOD and of linear covalent polymers, using telechelic polymers with one molecular weight (50 kg/mol) at one temperature (0 ℃) (Figure 4.4, blue). DA-PCOD is demonstrated to form flower-like micelles as expected, which start to bridge with each other as the concentration increases and form interconnected network. When only half of the end groups (< 0.5% of total weight) are replaced with tertiary amine (DB), the solutions of DA/DB-PCOD exhibit dramatically different features: the dominant relaxation process is the conformation relaxation of the supramolecules, and the dissociation of DA/DB does not appear to occur in the measured dynamics.
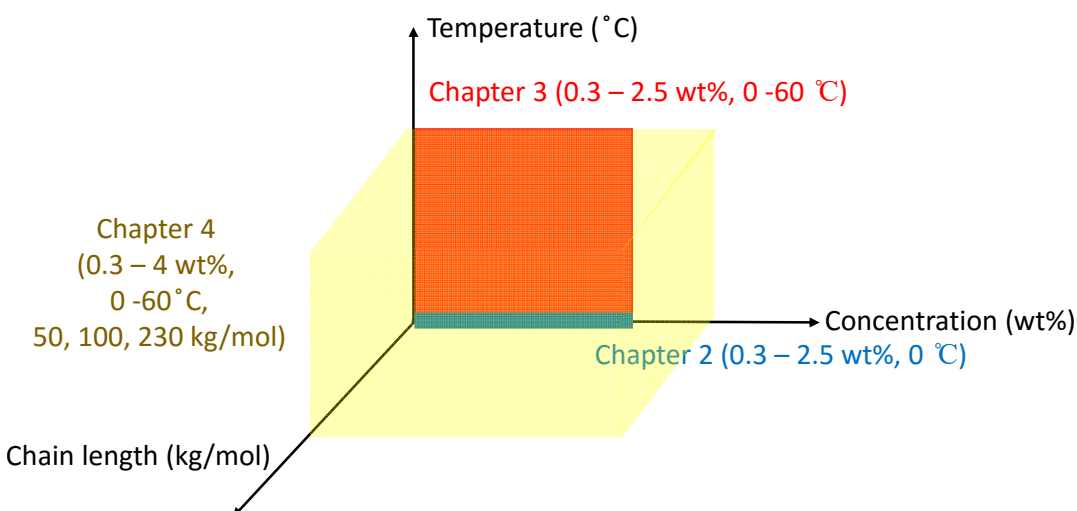

Figure 4.4 Summary of the type and range of parameters discussed in each chapter

This phenomenon is due to the difference in binding strength of DA/DB and DA. The binding free energy for DA ends (ΔG_{DA}) is estimated to be 13 kT, while $\Delta G_{DA/DB}$ for DA/DB pair is around 16 kT. The end-exchange time (τ_{ex}), which is inverse dissociation rate constant ($1/k_d$), is related to an activation energy (E_a) through Arrhenius equation, $\tau_{ex} \sim A$ exp (E_a /RT). Although the kinetic activation energy (E_a) cannot be replaced by the thermodynamic energy (ΔG) in calculating the end-exchange time (τ_{ex}), literature has observed correlation between thermodynamic energy and end-exchange time: high hydrogen bonding strength slows down its dissociation [20-21]. Hence the lifetime of DA/DB binding should be longer than that of DA.

The end-exchange time (τ_{ex}) of DA is measured directly as the relaxation time of DA-PCOD solutions (Table 4.3C). The dissociation of DA/DB, if ever occurs within the measured time scale, should occur at much longer time than the exchange time for DA-PCOD solutions. Obviously, the crossover relaxation time for DA-PCOD is already in the terminal region in the dynamic curves for DA/DB-PCOD solutions at the same concentration. It demonstrates that the solution dynamics is dominated by the conformation relaxation of the supramolecules formed by DA/DB-PCOD, in contrast to DA solutions.

It is also interesting to find that, the solution of 50k DA/DB-PCOD exhibits transition from semidilute unentangled regime to semidilute entangled regime as the concentration increases from 1.2 wt% to 2.5 wt%, just like linear covalent polymers do. The clear

Table 4.3 Comparison between the crossover relaxation time for 50 kg/mol DA-PCOD and DA/DB-PCOD solutions at 0 ℃.

	1.2%	1.5%	2.0%	2.5%
τ_{DA} (s)	0.70	1.93	3.16	3.16
τ_x for DA/DB (s)	-	-	0.1	0.13

distinction is that the fraction of the rheologically effective species increases significantly with concentration.

In Chapter 3, it is illustrated that temperature exerts a more remarkable effect on the distribution of supramolecules and furthermore, on the dynamics of the solutions (Figure 4.4, red). Decreasing temperature causes the supramolecular distribution to shift intensely to species with higher molecular weight, making significant additional contribution to the solution viscosity. Therefore the Arrhenius plots for solutions of 50k DA/DB PCOD take the form of a curved line, instead of a linear line for solutions with constant composition. In addition, SANS provides direct proof that the size of supramolecules formed by DA/DB-PCOD decreases monotonically with increasing temperature, confirming the hypothesis based on rheology data.

An additional parameter, chain length, is taken into account in the current chapter (Figure 4.4, yellow). As mentioned above, chain length can influence the solution dynamics and supramolecular formation through ring chain equilibrium and through the equilibrium of DA/DB association. However, the effects from the two aspects are opposite to each other, indicating that one of them may preside over the other under certain circumstance. Furthermore, the ring-chain equilibrium and DA/DB end association are influenced by temperature and polymer concentration, which make the chain length effect dependent on temperature and concentration as well. It is thus intriguing to check how the net effect of chain length turns out on the solution dynamics of DA/DB-PCOD at specific temperature and concentration.

Although numerous telechelic polymers capable of non-covalent pairwise-association have been synthesized over the past 30 years, little systematic study has been performed on the

dynamics of the supramolecules formed by pairwise-associative telechelics and how the dynamics can be affected by concentration, temperature and polymer chain length, etc [9, 22-24]. These studies can identify the structure-function relationship for supramolecular formation, and serve as a guidance for rational design of supramolecules and the related functional materials.

In this chapter, I explore the chain length effect on the dynamics of pairwise-associative polymers, and check whether the concentration and temperature dependence observed with 50k DA/DB-PCOD are shown with longer telechelic polymers as well. I also investigate the interplay between concentration, temperature, and chain length. Indeed, the rheology results reveal a surprising non-monotonic effect of backbone length, which is guided by the specific temperature and concentration.

4.2 Experimental

4.2.1 Materials

The decahydronaphthalene (decalin, mixture of cis/trans) used for rheology experiments and 2,6-Di-tert-butyl-4-methylphenol (BHT) used as an anti-oxidant in the polymer solutions were purchased from Sigma Aldrich. The non-associative polycyclooctadiene control (1.1M PCOD, M_w = 1.08 Mg/mol) was synthesized by Dr. Xuelian He *via* ring opening metathesis polymerization (ROMP) with alkane-ended chain transfer agent (CTA). The 50 kg/mol isophthalic acid-ended polycyclooctadiene (50k DA-PCOD) was synthesized *via* ring opening metathesis polymerization (ROMP) with custom-made isophthalic acid-ended chain transfer agent (CTA). The 100 kg/mol and 230 kg/mol DA-PCOD were synthesized *via* chain extension from the 50 kg/mol DA-PCOD using ROMP.

The di-tertiary amine ended polycyclooctadiene (DB-PCOD, 50, 100 and 250 kg/mol) was synthesized via ring opening metathesis polymerization (ROMP) with custom-made chloride-ended chain transfer agent (DCl-CTA), followed by two steps of post-polymerization modification. The synthetic schemes of CTAs, ROMP procedure, post-polymerization modification, and the characterization (GPC and NMR) of the CTAs and telechelic polymers were described in Appendix A. The molecular weights of the polymers used in this Chapter are listed in Table 4.4.

4.2.2 Solution preparation

Solutions of polymers (three chain lengths, DA/DB: equiv. molar ratio of isophthalic acid-ended polycyclooctadiene and di-tertiary amine-ended polycyclooctadiene) were prepared by weighing out polymer on a Mettler precision balance (±0.01mg) into new glass scintillation vials with PTFE lined caps and subsequently adding the appropriate amount of decalin using a precision syringe (±1%). The decalin was pretreated with 0.1 wt% of BHT. The solutions of telechelic polymers were placed on a wrist-action shaker at room temperature overnight.

Table 4.4 Molecular weights for the telechelic polymers used in this chapter.

Polymer	M_w[a] (kg/mol)	M_n[a] (kg/mol)	PDI[a]
50kDA	50	34	1.47
50kDB	50	35	1.44
100kDA	103	67.5	1.52
100kDB	94	62	1.52
230kDA	229	150	1.52
230kDB	255	155	1.65

[a]: determined by GPC-MALLS in THF

4.2.3 Rheological measurement

Steady shear viscosity and oscillatory shear dynamic moduli were measured from 0℃ to 60℃ with a strain-controlled rheometer TA ARES-RFS, equipped with a cone-plate geometry (angle 2°, diameter 50mm) and a solvent vapor trap. The steady shear rate range typically was chosen from 100 s^{-1} to 1 s^{-1} (or 10 s^{-1} to 0.1 s^{-1}) based on the temperature and polymer composition for each run to avoid overloading the force transducer. The viscosities are averages of values obtained at low shear rates that give viscosity independent of shear rate.

An oscillatory shear strain sweep was performed from 0.5% to 50% at 10 rad/s frequency at 0℃ and 25℃ for each polymer solution to measure the strain range for linear viscoelasticity. A strain within the linear range was chosen for the subsequent frequency sweep, which was usually 1%, 5%, 10%, or 20% strain, depending on the concentration and temperature. Dynamic moduli were measured for each polymer solution from 0℃ to 60℃ with frequency ranging from 100 rad/s to a lower frequency of 1 rad/s, or 0.1 rad/s, or 0.01 rad/s, depending on the relaxation time for the specific composition and temperature.

4.3 Results

To study the effect of polymer backbone length, solutions of isophthalic acid-ended polymers paired with di-tertiary amine-ended polymers having three molecular weights (DA/DB-PCOD, M_w = 50 kg/mol, 100 kg/mol and 230 kg/mol) are chosen, with which oscillatory and shear rheology experiments were performed in decalin at temperatures
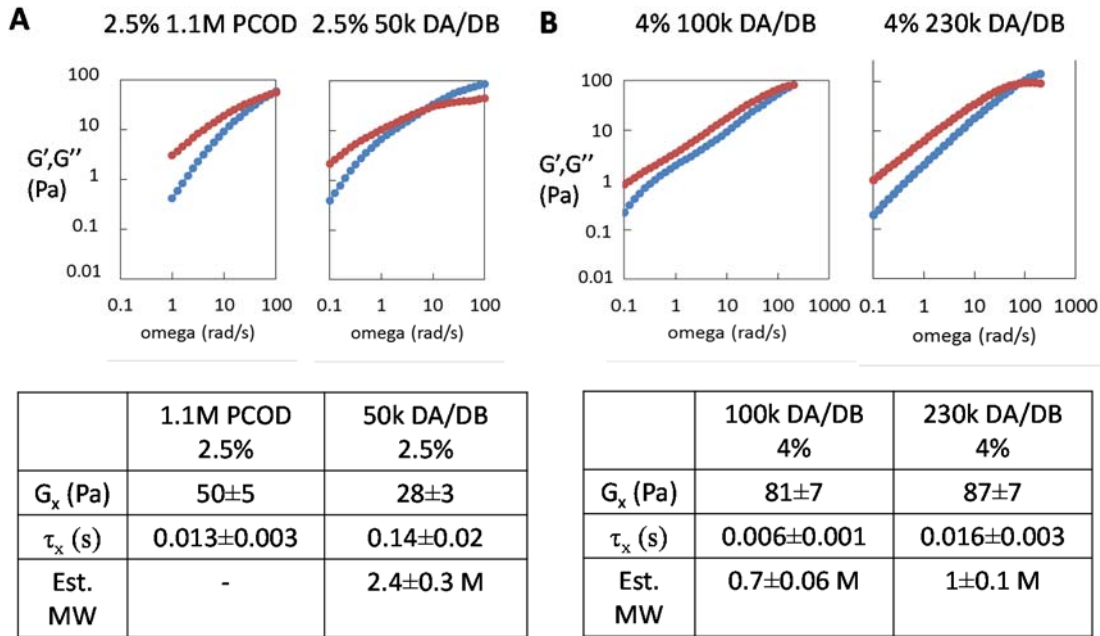
Figure 4.5 A. Storage (G', blue circles) and loss modulus (G", red circles) for DA/DB-PCOD (M_w = 50 kg/mol) compared to 1.1M PCOD (M_w = 1,100 kg/mol) at 0 ℃ at 2.5 wt%, with their crossover modulus (G_x) and relaxation time (τ_x) compared. **B.** Storage (G', blue circles) and loss modulus (G", red circles) for DA/DB-PCODs (M_w = 100 and 230 kg/mol) at 0 ℃ at 4 wt%, with their crossover modulus (G_x) and relaxation time (τ_x) compared.

ranging from 0 ℃ to 60 ℃ with a wide range of concentrations. Their dynamics and temperature dependence are compared below.

4.3.1 Demonstration of entanglement at 0 ℃

In Chapter 2, it is demonstrated that significant entanglement occurs for 50k DA/DB-PCOD at 2 wt% and 2.5 wt%. And the fractions of long linear supramolecular species that contribute to the entanglement at both concentrations are high (> 90%). By comparing to the relaxation time of a 2.5 wt% solution of a linear PCOD polymer (1.1M PCOD, M_w = 1100 kg/mol), it is calculated that the supramolecules in 2.5 wt% 50k DA/DB-PCOD solutions relax like a linear PCOD chain with 2400 kg/mol molecular weight using the scaling equation $\tau_{rep} \sim N^3 * C^{1.6}$ (Figure 4.5A).
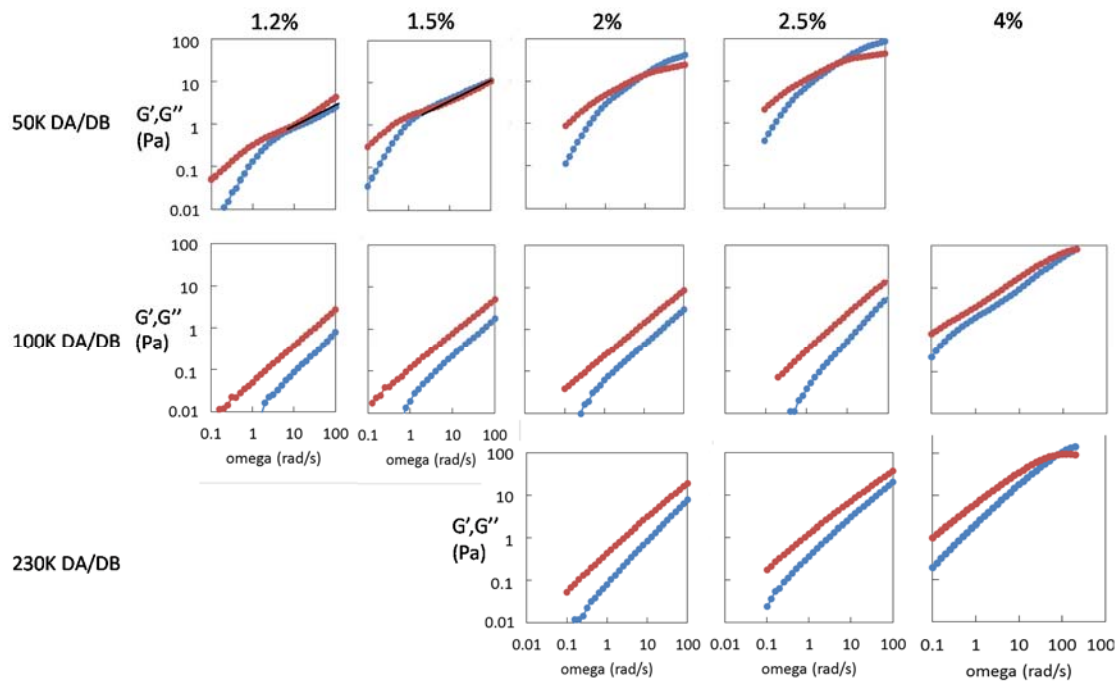
Figure 4.6 Storage (G', blue circles) and loss modulus (G", red circles) for DA/DB-PCOD (M_w = 50, 100, 230 kg/mol) at 0℃ at concentrations from 1.2 wt% to 4 wt%.

To make contact to Chapter 2, the oscillatory frequency sweep results for DA/DB-PCOD

of three chain lengths (M_w = 50 kg/mol, 100 kg/mol and 230 kg/mol, referred as 50k, 100k,

and 230k respectively) at 0℃ are plotted together in Figure 4.6. Increasing the molecular

weight of telechelic polymers clearly reduces the relaxation time and modulus at 0℃

(Figure 4.6). For 100k and 230k DA/DB-PCOD, the crossover point of G' and G'' is only

measurable within the frequency range of our instrument (< 200 rad/s) at concentration up

to 4 wt%.

Despite the lower modulus and shorter relaxation time, it is intriguing to examine whether

linear supramolecules are still formed 100k and 230k, and whether the crossover point for

4 wt% solutions is still due to entanglement. Thus the crossover relaxation time (τ_x) and

crossover modulus (G_x) of the 4 wt% solutions of 100k and 230k are compared with those

of the 2.5 wt% 50k solution with 2.5 wt% 1.1M PCOD solution as a control (Figure 4.5A

and B). In semidilute entangled solutions of linear covalent polymers, the plateau modulus is predicted to be independent on the chain length ($G_e \sim N^0 * C^{2.3}$); and the crossover modulus (G_x) should follow the same scaling law and stay constant with varying N. The G_x of the 4 wt% solutions of 100k and 230k DA/DB-PCOD are nearly identical (Figure 4.5B, 81 Pa and 87 Pa), indicating that the G_x is indeed independent of the chain length of the individual telechelic polymer or of the formed supramolecule. In addition, if the reptation of long linear supramolecular species is truly the dominant relaxation mode for 100k and 230k DA/DB solutions at 4 wt%, a theoretical G_x for these 4 wt% entangled solutions can be calculated from the G_x for 2.5 wt% 50k DA/DB-PCOD solution using the scaling relationship $G_x \sim N^0 * C^{2.3}$. The theoretical G_x turns out to be 83 Pa, which agrees well with the experimental data for 4 wt% solutions of 100k and 230k DA/DB-PCOD (Figure 4.5B). The data confirms the postulation that linear supramolecules still form and entangle for 100k and 230k DA/DB-PCOD solutions at 4 wt%.

Since the crossover is due to entanglement, an average length of the linear supramolecules can be estimated based on the relaxation time, which is a function of chain length and concentration: $\tau_{rep} \sim N^3 * C^{1.6}$. Using the relaxation time for 2.5 wt% 1.1M PCOD solution as a reference, the average length of linear supramolecules is estimated to be 700 kg/mol and 1000 kg/mol for 4 wt% solutions of 100k and 230k DA/DB-PCOD respectively (Figure 4.5B). Interestingly, although 100k and 230k DA/DB-PCOD do assemble into linear supramolecules which are longer than their own length, their linear supramolecules formed at even higher concentration are apparently shorter compared to 50k DA/DB-PCOD (Figure 4.5A compared with B), which contradicts the predication for solutions of linear covalent polymer. The unexpected result indicates that the solutions of DA/DB-PCOD

cannot be treated ideally like only linear supramolecules are formed even though the reptation of linear supramolecules truly dominate the solution dynamics. A more detailed hypothesis will be proposed in the Discussion.

4.3.2 Chain length effect on the temperature dependence

The temperature dependence of the dynamics of 100k and 230k DA/DB-PCOD solutions is also compared with the dependence observed with 50k DA/DB-PCOD. The Cole-Cole plots for 2.5 wt% solutions of 50k, 100k, and 230k DA/DB-PCOD are shown in the temperature range of 0℃ to 20℃ in Figure 4.7 as an example. The time temperature
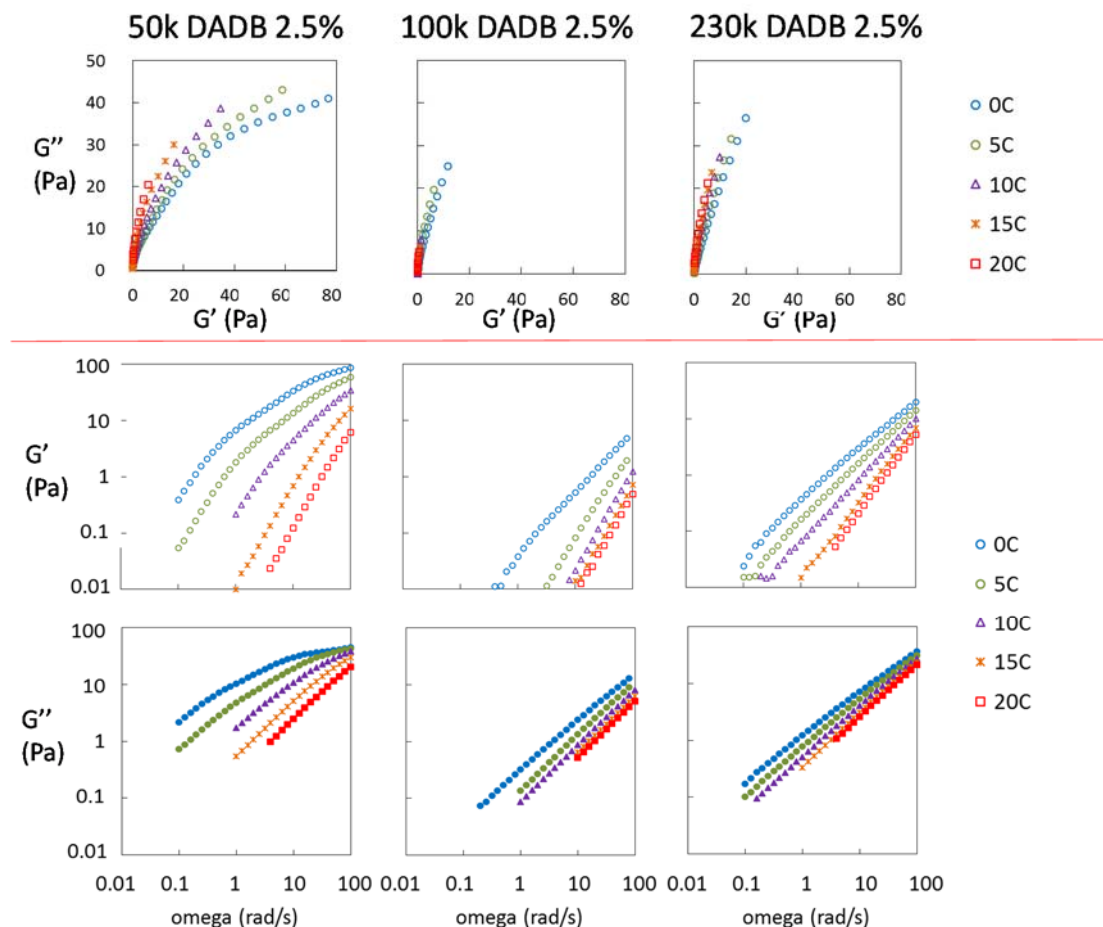

Figure 4.7 Oscillatory shear data of 2.5 wt% decalin solutions of 50k, 100k and 230k DA/DB-PCOD at temperatures 0-20℃, in the forms of Cole-Cole plot (top), and with G' and G'' plotted against frequency individually (bottom).

superposition (TTS) clearly fails for all three molecular weights, indicating that the

supramolecular composition changes with temperature for DA/DB-PCOD with 100k and

230k as well, just like 50k. On the other hand, an interesting trend is observed for the shift

factor (Figure 4.7, middle and bottom line). The dynamic moduli curves shift less for

solutions of DA/DB-PCOD with longer length (e.g. 230k compared to 50k). Smaller shift
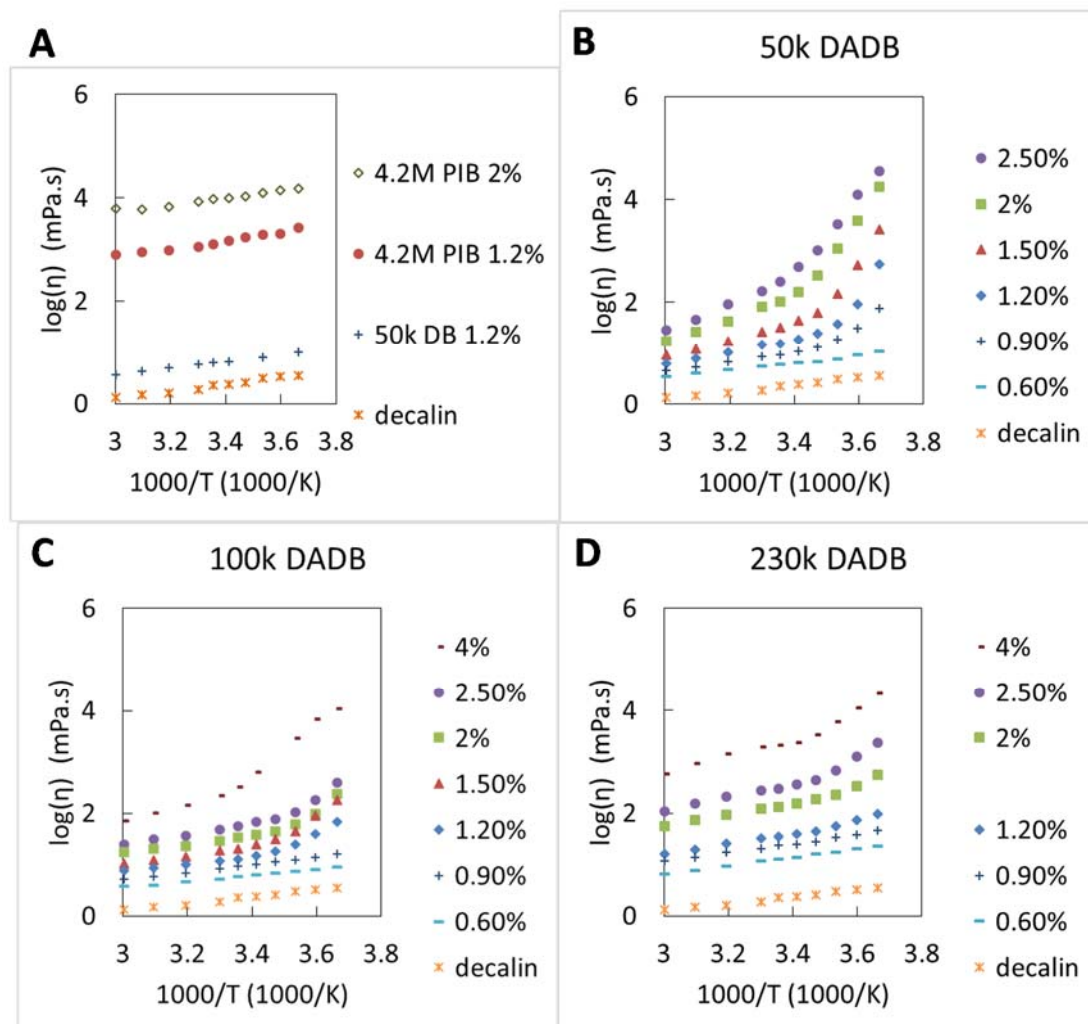
Figure 4.8 Arrhenius plots of solution viscosity against inverse temperature for **A.** non-associative polymer controls (4.2M PIB at 1.2 and 2 wt% and 50 kg/mol DB-PCOD at 1.2 wt%), **B.** 50 kg/mol DA/DB-PCOD at concentrations from 0.6 to 2.5 wt%, C. 100 kg/mol DA/DB-PCOD at concentrations from 0.6 to 4 wt%, **D.** 230 kg/mol DA/DB-PCOD at concentrations from 0.6 to 4 wt%.

factor infers slighter compositional change in the solutions. Chain length is thus shown to influence the temperature dependence of the distribution of supramolecules.

The analogy and discrepancy in temperature dependence for various chain lengths is also reflected by the Arrhenius plot. The plots for DA/DB-PCOD solutions with three lengths at a series of concentrations are compared, with non-associative covalent polymers as control (Figure 4.8). As mentioned in the introduction, the dynamics of covalent polymer solutions display similar weak temperature dependence, with negligible change with molecular weight. Our experimental data confirms this argument (Figure 4.8A). Despite the over 10-fold difference in chain length, and the over two orders of magnitude difference in solution viscosity, the 1.2 wt% solutions of 50 kg/mol DB-PCOD and 4200 kg/mol PIB share comparable temperature dependence (Figure 4.8A). Increasing concentration from 1.2% to 2% has minimal effect on the slope as well. The Arrhenius plots for 50k DA/DB-PCOD solutions exhibit distinct features compared to covalent polymers because of end association, especially at high concentration (Figure 4.8B). As indicated in Chapter 3, the ring-chain equilibrium of supramolecules shifts to longer linear supramolecules as the temperature decreases, and the longer species provide additional contribution to the solution viscosity. Therefore the increase in viscosity becomes steeper and steeper at lower temperature, resulting in the curvature in the Arrhenius plot.

The Arrhenius plots for 100k and 230k reveal same shape as those for 50k DA/DB-PCOD (Figure 4.8C-D), confirming that the supramolecular composition changes with temperature for DA/DB-PCOD with all chain lengths. In consistency with the smaller shift factor seen with longer telechelics, the plots are less curved for solutions of longer telechelics (Figure 4.8B-D). This observation supports the previous statement that the
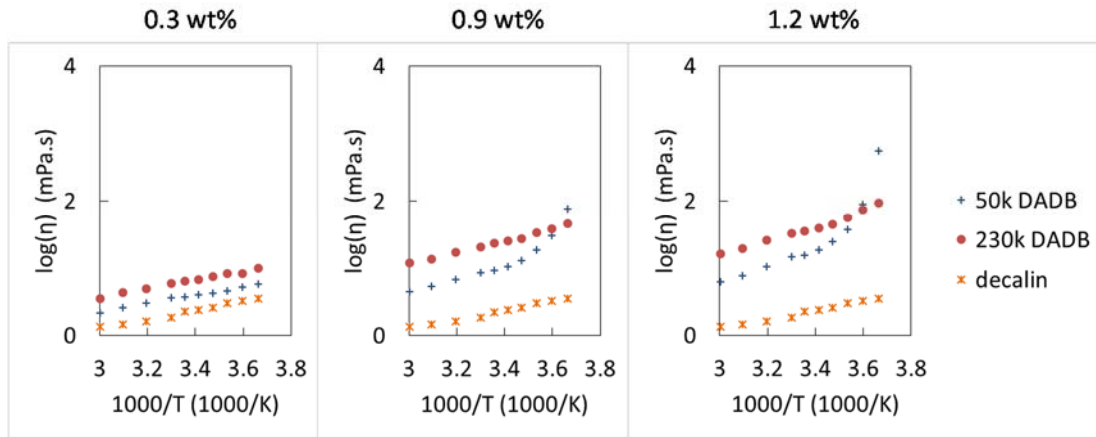
Figure 4.9 Arrhenius plots of solution viscosity against inverse temperature for 50 and 230 kg/mol DA/DB-PCOD at 0.3, 0.9, and 1.2 wt%.

compositional change of supramolecular species is smaller when individual telechelic is longer. A molecular explanation is postulated in Discussion.

4.3.3 Non-monotonic chain length effect at various concentrations and temperatures

Interestingly, the trend of the chain length effect is not consistent for all concentrations and temperatures. For example, 230k DA/DB-PCOD solution exhibits higher viscosity compared to 50k throughout the temperature range in dilute solution (Figure 4.9, 0.3%). However, 50k DA/DB-PCOD solution shows steeper upturn in Arrhenius plot as the concentration increases into semidilute regime (Table 4.3), resulting in especially high viscosity at low temperature, exceeding the viscosity for 230k (Figure 4.9, 0.9%). This is consistent with the observation that the semidilute solutions of 230k display lower modulus and shorter relaxation time in the oscillatory data at 0℃ compared to 50k (Figure 4.6). In addition, higher concentration induces higher critical temperature at which the viscosity of 50k surpasses that of 230k (Figure 4.9, 0.9% compared to 0.3%). The phenomenon indicates that the net outcome of varying chain length is due to a combination effect of all three factors. More detailed analysis is covered in Discussion.

4.4 Discussion

The above rheology data indicates that DA/DB-PCOD at all lengths (50, 100, and 230 kg/mol) show dynamic features resembling those of linear covalent polymers, especially the entanglement features at high concentration (Figure 4.5 and 4.6; > 2% for 50k, 4% for 100 and 230k). And the temperature dependence also holds true for all lengths: the distribution of the formed supramolecular species shifts to longer linear supramolecules at lower temperature (Figure 4.7 and 4.8).

In contrast to the monotonic effect induced by temperature and concentration on the dynamics of DA/DB-PCOD, the net effect of chain length varies with the specific temperature and concentration. Especially in the semidilute regime, short backbone diminishes solution viscosity at high temperature, and nevertheless exhibits particularly high viscosity at low temperature (Figure 4.9). This behavior also leads to the apparent stronger temperature dependence for short DA/DB-PCOD. These features differ strikingly from those observed with solutions of linear covalent polymers, as reviewed in Section 4.1.1. To explain the unexpected non-monotonic chain length effect, more detailed analysis is stressed and a molecular picture is proposed below.

4.4.1 Molecular picture of the DA/DB association guided by temperature, concentration and backbone length

Chain length influences the solution dynamics through multiple aspects: 1) through the power-law dependence of dynamic parameters like covalent polymers, 2) through the ring-chain equilibrium, and 3) through the equilibrium of end association. Since the latter two

aspects are also governed by temperature and concentration, it is straightforward that the net effect of chain length depends on specific temperature and concentration.

At high temperature, the fraction of unbound ends is huge (Figure 4.3C, 60℃) and the formation of linear supramolecules with large aggregation number is disfavored for all backbone lengths and concentrations (Figure 4.10, left). At an extreme temperature at which the fraction of dangling ends is approaching 100%, no end association would exist and DA/DB-PCOD would be simplified to linear covalent polymer. Since longer backbone length leads to higher viscosity, as illustrated in Section 4.1.1, the solutions of 230k
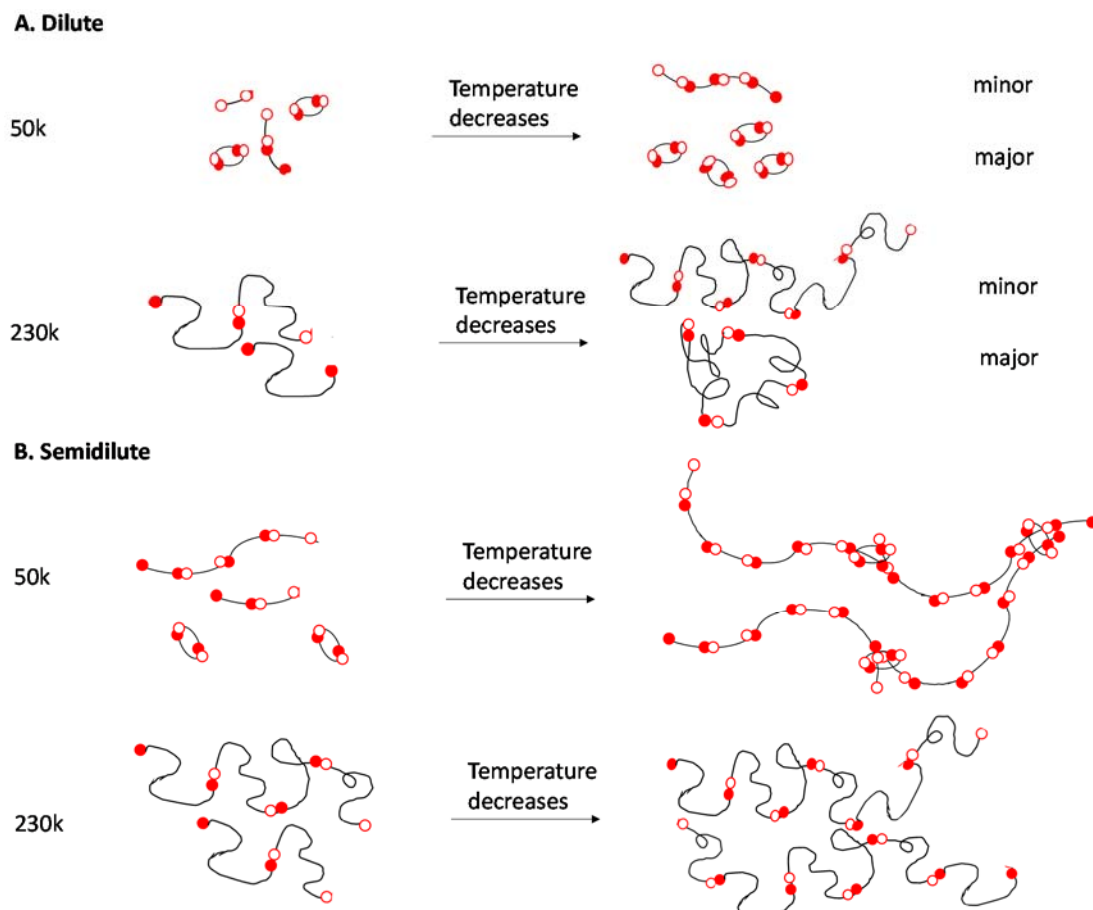

Figure 4.10 Postulated temperature dependence of molecular compositions including cyclic and linear supramolecules formed by DA/DB-PCOD with 50 and 230 kg/mol in **A.** dilute and **B.** semidilute solutions.

DA/DB-PCOD at all concentrations has higher viscosity compared to 50k (Figure 4.9, left end of Arrhenius plots).

When the temperature is low, especially approaching 0℃, the fraction of free ends can be neglected (≤ 1%, Figure 4.3C, 0℃). The ring-chain equilibrium in dilute and semidilute solutions differs. In dilute solutions, individual telechelic polymer is far away from each other, causing high entropy cost in forming large linear or cyclic aggregates (Figure 4.2A, dilute). Thus the majority of telechelic polymers distribute into small cyclic species (e.g. dimers) and a few distribute into linear species with multiple chains linked together (Figure 4.10A, right). Since the supramolecules formed by longer telechelics are expected to be larger, and longer backbone disfavors ring formation compared to shorter one (Figure 4.2B), the polymer contribution to the solution viscosity is greater for longer telechelics (Figure 4.9A).

At low temperature in semidilute solutions, polymer chains are well-percolated and almost all ends are bound. Linear supramolecules with large aggregation number are favored (Figure 4.10B, right; Figure 4.2A, semidilute). On the other hand, short backbone induces the formation of small rings due to the low entropy lost (Figure 4.2B), according to ring-chain equilibrium. It is reasonable to postulate that a larger portion of 50k DA/DB-PCOD partition into dimer rings compared to 230k. It seems that the solution of 230k DA/DB-PCOD should display higher viscosity than 50k, which is opposite to the experimental observation (Figure 4.9B-C). A molecular picture is thus postulated for short DA/DB-PCOD (50k) to explain the unexpectedly high viscosity at low temperature (Figure 4.10B, 50k right).

50k DA/DB-PCOD truly distributes into both linear and cyclic supramolecules. However, in contrast to the case in dilute solutions where the dimer rings provide little contribution to viscosity, the rings in semidilute solutions can interpenetrate long linear supramolecules, slowing down their relaxation (or reptation for entangled solutions) (Figure 4.10B, 50k right). Therefore, although 50k DA/DB-PCOD forms more cyclic supramolecules and maybe shorter linear supramolecules than 230k, the supramolecular mixture of 50k relaxes much slower than 230k solution, and even like a linear covalent polymer with very high molecular weight (e.g. apparent $M_w \sim 2400$ kg/mol for 2.5 wt% 50k solution in Figure 4.5A).

The interpenetration of rings and chains and its effect in significantly increasing the viscosity is not postulated here for the first time. The relaxation of rings and ring/chain blend is actually a 30-year problem [25]. Recently, Kapnistos *et al* discovered that a linear polymer contaminant significantly modifies the rheological response of the melt of rings with the same molecular weight at concentration as low as 1/50 of its overlap concentration [25]. It is proposed that the linear polymers are "bridged" by rings and form a long-lived percolating species which substantially slows the relaxation. This observation is later confirmed qualitatively by a simulation study [26], supporting the molecular postulation. The simulation also predicts a maximum viscosity of melts of ring-chain blend (with same molecular weight) at a 1:1 ratio of ring and chain, instead of pure linear component [26]. Although literature mostly focuses on the melts instead of solutions, it is indicated that the interaction between cyclic and linear species can dramatically alter the relaxation process of the system.

In summary, a molecular picture is proposed above considering the combined effect of temperature, concentration, chain length, and topological properties, which can accommodate the measured data at each specific condition. In dilute solutions, short telechelics have small coil size which favors the formation of small cyclic supramolecule, and leads to lower viscosity compared to long telechelics in the whole temperature range (Figure 4.10A, Figure 4.9A). In semidilute solutions at high temperature, short telechelics cannot form long linear supramolecules due to high fraction of dangling ends, and hence still display low viscosity (Figure 4.10B, left). However, at low temperature, the small rings formed by short telechelics start to "bridge" the linear supramolecules, dramatically slowing down their relaxation, leading to especially enhanced viscosity, which is even higher than that of long telechelics (Figure 4.10B, right; Figure 4.9B-C; Figure 4.6).

4.4.2 The interplay of temperature, concentration and chain length on solution viscosity of DA/DB-PCOD

The dynamics of DA/DB-PCOD solutions is demonstrated to be guided by temperature, concentration, and chain length. In contrast to the monotonic effect of temperature and concentration on the dynamics of DA/DB-PCOD, the net effect of chain length is non-monotonic and depends on specific temperature and concentration. It is because that backbone length influences the solution dynamics through the ring-chain equilibrium and the equilibrium of end association, both of which are also governed by temperature and concentration. The postulation stated above provide means to explain all the experimental data obtained so far. It would be beneficial to generalize the interplay of all three factors and their net effect on the dynamics of the solutions at each specific condition.

The concentration dependence of solution viscosity of DA/DB-PCOD resembles that for linear polymer for all tested molecular weights and temperatures: an increase in slope with increased concentration is clearly observed in all curves (Figure 4.11A). For solutions of linear covalent polymers, the slope increases when the solution transits into a higher concentrated regime: from dilute to semidilute unentangled, and to semidilute entangled. For DA/DB-PCOD solutions (three lengths, three concentrations), the actual critical concentrations where the slope shifts are smaller than the calculated overlap concentration (C*) and entanglement concentration (C_e) for non-associative controls (Figure 4.11A), because supramolecules much longer than individual telechelics are formed, shifting the critical concentration to lower values. In fact, the critical concentration is different for each temperature and chain length, because the supramolecular species distribute differently for each condition. For example, at 60℃, short supramolecules are the dominant species, and the critical concentration is bigger and closer to the estimated values for non-associative control (Figure 4.11A, red).

Due to the high binding strength of the charge-assisted hydrogen bond of DA/DB, the end association is highly temperature-dependent. The fraction of unbound ends decreases from > 20% at 60℃ to < 1% at 0℃ (Figure 4.3C), and the distribution of supramolecular species changes with it. At high temperature, the role of end association diminishes, and telechelic polymer with higher molecular weight exhibits higher viscosity because of the power-law dependence of viscosity on chain length (Figure 4.11B, 60℃).

At low temperatures, significant formation of supramolecules occurs (Figure 4.11B, 25 and 0℃). At low concentrations, short telechelics tend to form small cyclic supramolecules which do not contribute much to the solution viscosity, and hence have lower viscosity
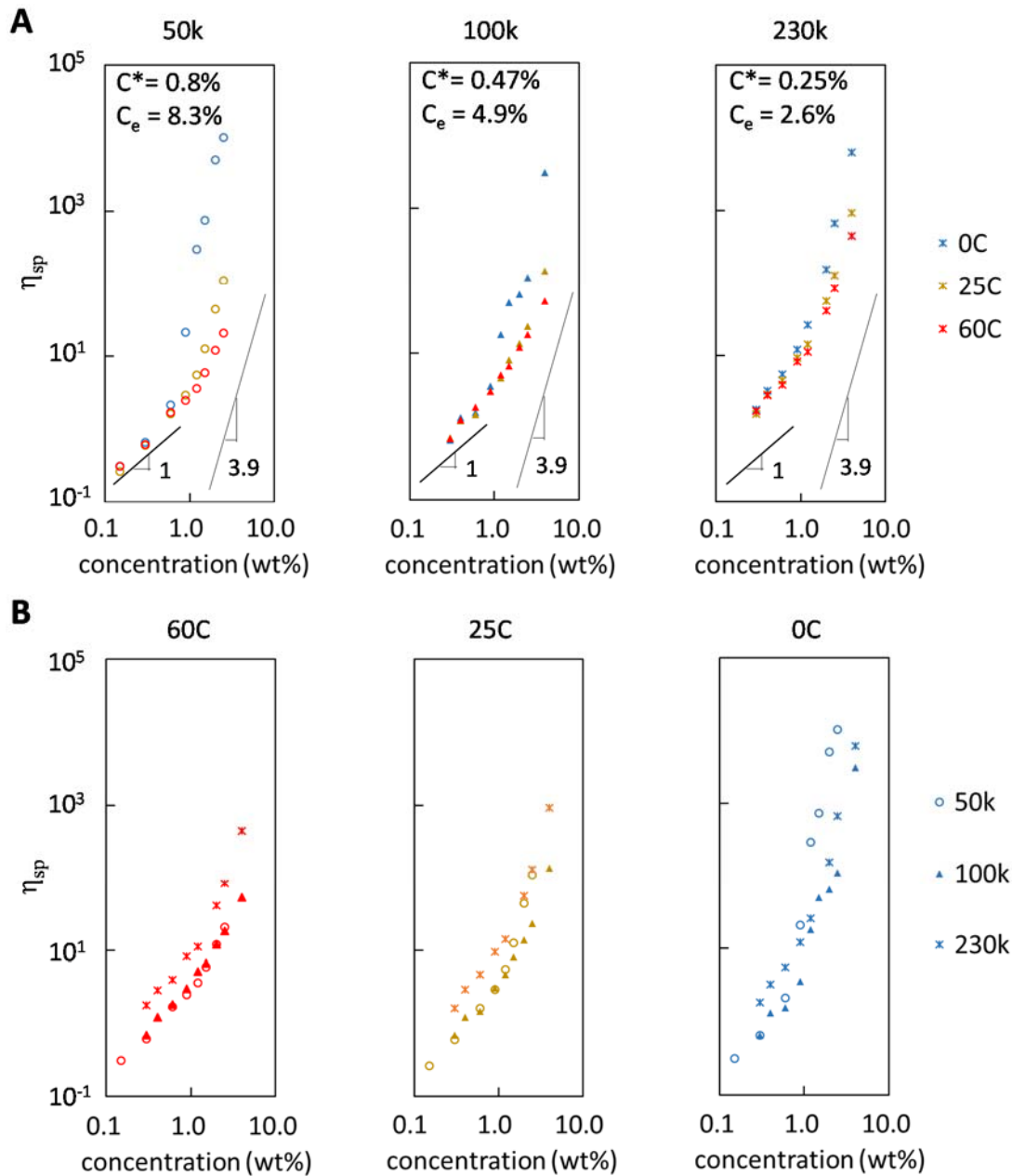
Figure 4.11 Specific viscosity plotted against concentration for **A.** each chain length (50, 100, 230 kg/mol) at three temperatures (0, 30, 60℃), and **B.** each temperature (0, 30, 60℃) with three chain lengths (50, 100, 230 kg/mol).

than 230k. As the concentration goes higher, chains start to overlap and more linear long supramolecules are able to form. The existing rings of 50k DA/DB-PCOD begin to play a role in viscosity as well by interacting with the long linear species as described earlier, resulting in an even higher viscosity than 230k.

Literature and earlier discussion in Chapter 3 (Figure 3.18) and Section 4.1.3 (Figure 4.3C) indicates that lower temperature increases the fraction of both long linear supramolecules and small rings due to the lower fraction of dangling ends. It can then be predicted that the onset concentration of the ring-chain interaction should be easier to achieve (smaller) for lower temperature. And indeed, it is what is observed in the data (Figure 4.11B, 25 ℃ compared with 0 ℃). This phenomenon also supports the hypothesis on ring-chain interpenetration described above.

4.5 Conclusions

DA/DB-PCOD at all measured lengths (50, 100, and 230 kg/mol) show dynamic features resembling those of linear covalent polymers, especially the entanglement features at high concentration (≥ 2% for 50k, 4% for 100 and 230k). And the distribution of the supramolecular species formed by DA/DB-PCOD of three lengths all shifts to longer linear supramolecules at lower temperature. However, the net effect of chain length on the dynamics of DA/DB-PCOD varies with the specific temperature and concentration.

Especially in the semidilute regime, short backbone diminishes solution viscosity at high temperature, nevertheless, exhibits particularly high viscosity at low temperature. This behavior also leads to the apparent stronger temperature dependence for short DA/DB-PCOD. These features differ strikingly from those observed with solutions of linear covalent polymers, as reviewed in Section 4.1.1. A molecular picture is proposed to explain the unexpected non-monotonic chain length effect. The interpenetration of the small cyclic supramolecules and linear supramolecules formed by 50k DA/DB-PCOD may be responsible for the particularly high viscosity at low temperatures (approaching 0 ℃) in its semidilute solutions.

References

[1] M. Rubinstein, R. H. Colby, *Polymer Physics*, Oxford Univ. press, Oxford, 2003. Reprinted 2012.

[2] R. H. Colby, *Rheol. Acta*, **2010**, *49*, 425-442.

[3] R. M. Johnson, J. L. Schrag, J. D. Ferry, *Polym. J.* **1970**, *1*, 742-749.

[4] Lodge, T. P., Miller, J. W. and Schrag, J. L. *J. Polym. Sci. Polym. Phys. Ed.*, **1982**, *20*, 1409–1425.

[5] R. H. Colby, L. J. Fetters, W. G. Funk, W. W. Graessley, *Macromolecules*, **1991**, *24*, 3873 – 3882.

[6] H. Jacobson, W. H. Stockmayer, *J. Chem. Phys.* **1950**, *18*, 1600-1606.

[7] A. T. ten Cate, et al, *J. Am. Chem. Soc.* **2004**, *126*, 3801–3808.

[8] S. K. Yang, A. V. Ambade, and M. Weck *Chem. Eur. J.* **2009**, *15*, 6605–6611.

[9] R. P. Sijbesma et al, *Science,* **1997***, 278*, 1601-1604.

[10] W. J. Taylor, *J. Chem. Phys.*, **1948**, *16*, 257-267.

[11] E. N. Gur'yanova, I. P. GoI'dshtein, T. I. Perepelkova, *Russian Chemical Reviews*, **1976**, *45*, 792–806.

[12] M. M. Davis, M. Paabo, *J. Am. Chem. Soc.*, **1960**, *82*, 5081–5084.

[13] H. Nakanishi, H. Morita, S. Nagakura, *J. Mol. Spectrosc.*, **1977**, *65*, 295-305.

[14] L.Sun, C. D. Wick, J. I. Siepmann, M. R. Schure, *J. Phys. Chem. B,* **2005,** *109,* 15118-15125.

[15] A. D. H. Clague, H. J. Bernstein, *Spectrochim. Acta*, **1969**, *25*, 593-596.

[16] G. Allen, J. G. Watkinson, K. H. Webb, *Spectrochim. Acta*, **1966**, *22*, 807-814.

[17] G.Gilli, P.Gilli, *The Nature of the Hydrogen Bond: outline of a comprehensive hydrogen bond theory.* Oxford Univ. press, 2009.

[18] G. C. Pimentel, A. L. McClellan, *Annu. Rev. Phys. Chem.*, **1971**, *22*, 347-385.

[19] M.D. Joesten, L. J. Schaad, *Hydrogen bonding*, Marcel Dekker, New York, 1974.

[20] L. E. Cramer, K. G. Spears, *J. Am. Chem. Soc.*, **1978**, *100*, 221–227.

[21] J. Zheng, M. D. Fayer, *J. Phys. Chem. B* **2008,** *112,* 10221–10227.

[22] S. K. Yang, A. V. Ambadec, M. Weck, *Chem. Soc. Rev.*, **2011**, *40*, 129–137.

[23] T. F. A. de Greef, E. W. Meijer, *Nature*, **2008**, *453*, 171-173.

[24] S.-L. Li, T. Xiao, C. Lin, L. Wang, *Chem. Soc. Rev.*, **2012**, *41*, 5950–5968

[25] M. Kapnistos et al, *Nature Mater.* **2008**, *7*, 997-1002.

[26] J. D. Halverson, G. S. Grest, A. Y. Grosberg, K. Kremer, *Phys. Rev. Lett.*, **2012**, *108*, 038301.

Chapter V

Effect of Chain Length on Self-Associative Telechelic Polymers

5.1 Introduction

In earlier chapters, the distinct morphology and dynamics of self-associative polymers (di-acid-ended PCOD, DA) and pairwise associative polymers (di-acid-ended paired with di-amine-ended PCOD, DA/DB) have been covered, as well as their concentration and temperature dependence. Self-associative and pairwise-associative polymers are proved to exhibit dramatically different features, even though the polymer backbone are exactly the same, and only half of the end groups (< 0.5% of total weight) are different.

DA-PCODs make contact with prior literature on self-associative polymers. It is demonstrated that they form flower-like micelles, which start to bridge with each other as the concentration increases and form interconnected network. Two temperature regimes are discovered in which the temperature dependence of supramolecular topology differs: 0℃ to 30℃, and above 30℃. Both SANS and rheology data suggest that the micelle structure of the solutions stays unchanged at temperatures below 30℃, but the aggregates become smaller as the temperature is raised above 30℃.

When chain length is taken into consideration, more complexities are introduced into the system. Increasing chain length leads to two results that affects the association and dynamics of self-associative telechelic polymers in contradictory ways: 1) each telechelic polymer has larger radius of gyration, and 2) the concentration of end groups is reduced. Larger radius of gyration of telechelic polymers results in lower overlap concentration (C*). The telechelic polymer with higher molecular weight can thus associate with each other at

lower concentration. In addition, increasing chain length results in longer average end-to-end distance ($R_{e\text{-}e}$) of a polymer chain, diminishing the probability of loop formation, and hence should theoretically facilitate the bridge formation.

On the other hand, low concentration of end groups directly decreases the maximum number of bridges that could be achieved at very high concentration. Therefore, low concentration of end groups should hinder the formation of supramolecules and work against the effect induced by the simultaneously increased radius of gyration of each telechelic polymer.

These two opposing mechanisms have been discussed extensively in literature for self-associative telechelic systems, including ionomer telechelics and HEURs. Generally, the size of telechelic polymers is the dominant factor at dilution conditions, while the end-group concentration is more important when the concentration is high.

Ionomer telechelic polymer refers to a telechelic polymer with ionized ends. Their capacity in dramatically modifying the rheological behavior of non-polar solutions has attracted great attention since the 1980s, and numerous studies on their structure-rheology relationship have been reported [1-4]. Broze *et al* observed that the solution viscosity increases abruptly at low concentration for many types of telechelic ionomers (Figure 5.1A), including magnesium α,ω-carboxylato-polyisoprene(PIP), -polybutadiene (PBD), -polystyrene (PS), -poly(tert-butylstyrene) (PTBS), and -poly(α-methylstyrene) (PMS). And this critical concentration (called C_{gel} in the paper) decreases with increasing molecular weight of telechelic, with an apparent general relationship: $C_{gel} \sim M_n^{-0.5}$ [1,2]. This result indicates that the size of telechelic polymers plays a more important role for dilute solutions.
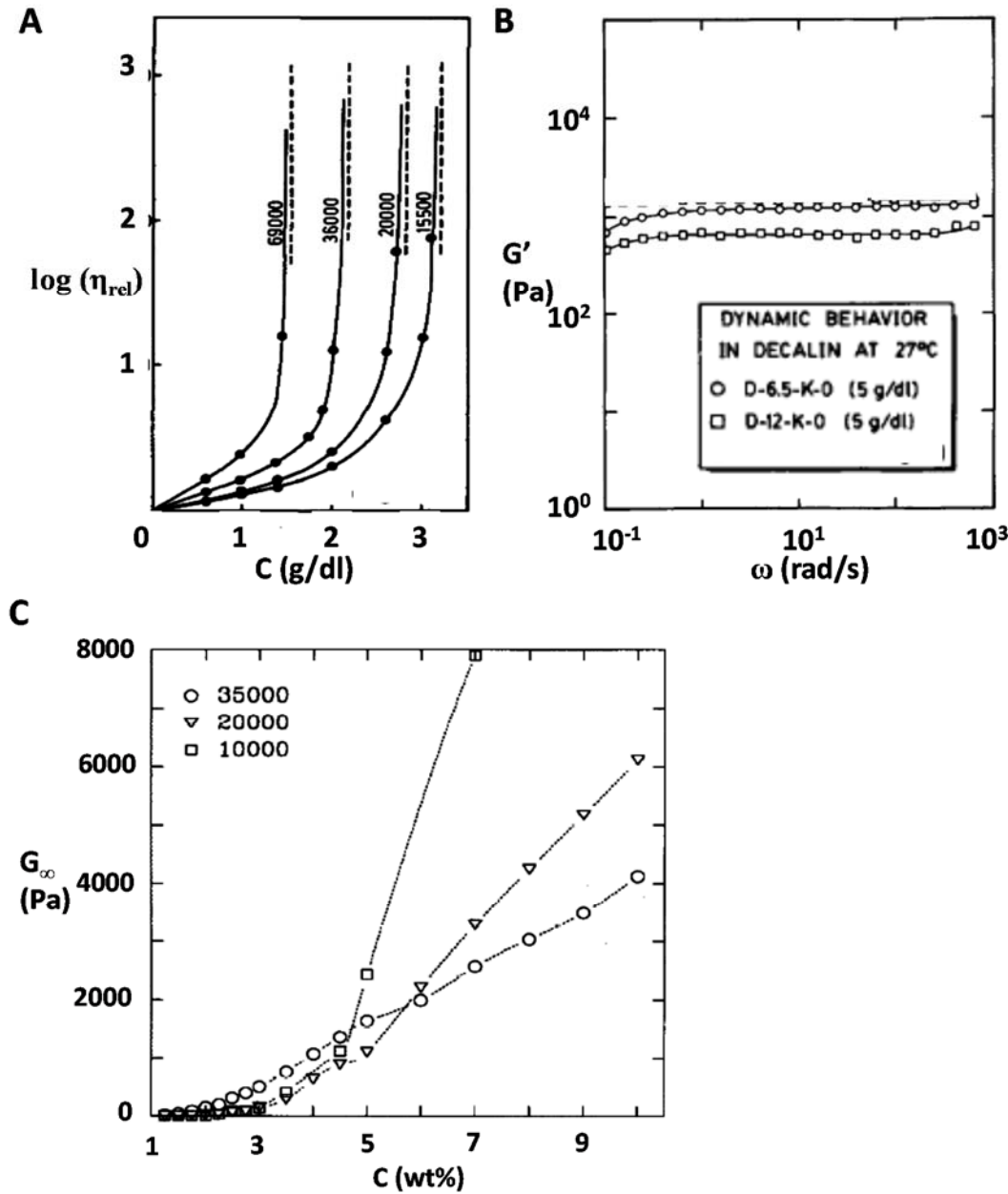
Figure 5.1 A. (Figure reproduced from reference [2]) The relative viscosities are plotted against the polymer concentrations for solutions of Mg α,ω-carboxylate-polyisoprenes with 4 different molecular weights (15500, 20000, 36000, 69000 kg/mol) at 25 ℃ in toluene. **B.** (Figure reproduced from reference [3]) The storage modulus (G') for solutions of α,ω-sulfonated polyisobutylene (PIB) with two chain lengths (M_n = 12 kg/mol and M_n = 6.5 kg/mol, PDI ~ 1.7, named D-12-K-0 and D-6.5-K-0, respectively) neutralized stoichiometrically with KOH at a concentration of 50 mg/mL in decalin **C.** (Figure reproduced from reference [5]) The high frequency modulus (G_∞) at various concentrations for HEURs with C16 as the hydrophobe at three molecular weights (10, 20, and 35 kg/mol) at 25 ℃.

In the semidilute regime, Tant *et al* compared the plateau modulus for solutions of α,ω-

sulfonated polyisobutylene (PIB) with two chain lengths (M_n = 12 kg/mol and M_n = 6.5 kg/mol, PDI ~ 1.7, named D-12-K-0 and D-6.5-K-0, respectively) neutralized stoichiometrically with KOH at a concentration of 50 mg/mL in decalin [3]. The modulus for D-6.5-K-0 is substantially higher than that of D-12-K-0 (Figure 5.1B), indicating that D-6.5-K-0 forms a network with a higher ionic crosslink density than D-12-K-0 due to higher end group concentration.

The same trend has been observed with HEUR self-associative system as well. Annable *et al* analyzed the concentration effect on the high-frequency modulus of HEUR solutions at three chain lengths (M_w = 10, 20, and 35 kg/mol) [5]. It is found that the viscosity of 35 kg/mol HEUR solution starts to rise at lower concentration compared to 10 and 20 kg/mol telechelics, due to the lower overlap concentration for 35 kg/mol polymer. As the concentration increases, the modulus rises linearly with concentration for all three polymers. The slope of this linear region increases as the molecular weight of the polymer falls as a consequence of the increasing molar density of chain ends (and therefore associations) (Figure 5.1C). Barmar *et al* confirmed that the HEUR with smaller molecular weight (M_n = 6 kg/mol) exhibits higher high-frequency modulus compared to HEUR with bigger molecular weight (M_n = 8 kg/mol) [6]. Therefore, it is clear that two opposite trends are observed at dilute and semidilute concentration regimes, with the effect of chain size dominating the dilute condition and the effect of end-group concentration dominating the semidilute condition.

Although the effect of molecular weight on the association of self-associative polymers has been discussed in literature, DA-PCOD associates with itself through directional hydrogen bonding, not micro phase separation due to low solubility, in contrast to traditional self-

associative polymers. Despite their similarity in dynamics, DA-PCOD may be affected by chain length in a different way. In addition, chain length is postulated to influence the morphology and dynamics of DA-PCOD through two aspects that work against each other. It is unknown which one of them may dominate over the other. It is thus intriguing to investigate the net effect of chain length on the solution dynamics of DA-PCOD.

Here, I will examine the chain length effect on the dynamics of self-associative polymers (DA-PCOD), and investigate the molecular picture lying behind the chain length effect. It is demonstrated that increasing chain length and decreasing polymer concentration has comparable effect on solution dynamics. An interesting "apparent pairwise-association" pattern is observed with DA-PCOD when the end group concentration is low (due to low polymer concentration or long polymer length).

5.2 Experimental

5.2.1 Materials

The decahydronaphthalene (decalin, mixture of cis/trans) used for rheology experiments and 2,6-Di-tert-butyl-4-methylphenol (BHT) used as an anti-oxidant in the polymer solution were purchased from Sigma Aldrich. The 50 kg/mol isophthalic acid-ended polycyclooctadiene (50k DA-PCOD) was synthesized *via* ring opening metathesis polymerization (ROMP) with custom-made isophthalic acid-ended chain transfer agent (CTA). The 100 kg/mol and 230 kg/mol DA-PCOD were synthesized *via* chain extension from the 50 kg/mol DA-PCOD using ROMP. The di-tertiary amine ended polycyclooctadiene (DB-PCOD, 50, 100, and 250 kg/mol) was synthesized via ring opening metathesis polymerization (ROMP) with custom-made chloride-ended chain

transfer agent (DCl-CTA), followed by two steps of post-polymerization modification. The synthetic schemes of CTAs, ROMP procedure, post-polymerization modification, and the characterization (GPC and NMR) of the CTAs and telechelic polymers were described in Appendix A.

5.2.2 Solution preparation

Solutions of polymers (three chain lengths, DA: isophthalic acid-ended polycyclooctadiene, and DA/DB: equiv. molar ratio of isophthalic acid-ended polycyclooctadiene and di-tertiary amine-ended polycyclooctadiene) were prepared by weighing out polymer on a Mettler precision balance (±0.01mg) into new glass scintillation vials with PTFE lined caps and subsequently adding the appropriate amount of decalin using a precision syringe (±1%). The decalin was pretreated with 0.1 wt% of BHT. The solutions of telechelic polymers were placed on a wrist-action shaker at room temperature overnight.

5.2.3 Rheological measurement

Steady shear viscosity and oscillatory shear dynamic moduli were measured from 0℃ to 60℃ with a strain-controlled rheometer TA ARES-RFS, equipped with a cone-plate geometry (angle 2°, diameter 50mm) and a solvent vapor trap. The steady shear rate range typically was chosen from 100 s^{-1} to 1 s^{-1} (or 10 s^{-1} to 0.1 s^{-1}) based on the temperature and polymer composition for each run to avoid overloading the force transducer. The viscosities are averages of values obtained at low shear rates that give viscosity independent of shear rate.

An oscillatory shear strain sweep was performed from 0.5% to 50% at 10 rad/s frequency at 0℃ and 25℃ for each polymer solution to measure the strain range for linear

Figure 5.2 Storage (G', blue circles) and loss modulus (G", red circles) for DA-PCOD (M_w = 50 kg/mol) at 0℃ at concentrations from 0.9 wt% to 2.5 wt%.

viscoelasticity. A strain within the linear range was chosen for the subsequent frequency sweep, which was usually 1%, 5%, 10%, or 20% strain, depending on the concentration and temperature. Dynamic moduli were measured for each polymer solution from 0℃ to 60℃ with frequency ranging from 100 rad/s to a lower frequency of 1 rad/s, or 0.1 rad/s, or 0.01 rad/s, depending on the relaxation time for the specific composition and temperature.

5.3 Results

For solutions of isophthalic acid-ended polymers with three molecular weights (DA-PCOD, M_w = 50 kg/mol, 100 kg/mol, and 230 kg/mol), oscillatory rheology and shear rheology experiments were performed in decalin at temperatures ranging from 0℃ to 60℃ with concentrations of a wide range. The solution dynamics and temperature effect of DA-PCOD at each chain length (50, 100, 230 kg/mol) will be first discussed separately, and then generalized together to illustrate the chain length effect. Three parameters are affected by the polymer concentration and molecular weight: crossover relaxation time, high-frequency modulus, and even the basic shape of the dynamic moduli curve.

5.3.1 Apparent pairwise association for 50 kg/mol DA-PCOD at low concentration

The dynamics of 50 kg/mol DA-PCOD at 0 ℃ at various concentrations has been discussed in Chapter 2 (Figure 5.2). From 1.2 wt% to 2.5 wt%, the high-frequency modulus increases dramatically, consistent with the features observed with HEURs. The relaxation time also increases slightly with concentration. Both features were explained by Annable *et al*, introducing the concentration effect on the topological of the network [5]. However, the network of micelles is formed throughout the concentration range discussed above, and the low concentration regime where the clusters of micelles are less connected is not covered.

It is surprising to observe that the DA-PCOD solution starts to show dynamic features of pairwise-associative polymers (like the dynamics for 50k DA/DB-PCOD) as the concentration decreases to a point that micelle clusters are too far away from each other and bridging becomes difficult. For 50 kg/mol DA-PCOD, the critical concentration is around 0.9 wt% (Figure 5.2), which is close to the overlap concentration of the 50 kg/mol PCOD backbone with no end association (0.8 wt%). For the 0.9 wt% 50k DA-PCOD solution, the storage and loss modulus lie parallel with each other at high frequencies (> 10 rad/s) with a slope between ½ and 1. The perfect Rouse-like dynamics for a semidilute unentangled solution of a linear covalent polymer should have storage modulus the same as loss modulus, and the slope should be ½. The discrepancy of the 0.9 wt% 50k DA-PCOD solution from Rouse model may be attributed to the presence of a distribution of supramolecules with various sizes. Nevertheless, the shape of the dynamic moduli curve obviously exhibits pairwise-association characteristics.

The temperature dependence of the dynamics of 0.9 wt% 50k DA-PCOD solution also differs from that of DA-PCOD solution at higher concentrations when the network is well connected. The oscillatory shear data of 0.9 wt% decalin solutions of 50k DA-PCOD, 50k DA/DB-PCOD and 2 wt% 50k DA-PCOD are compared (Figure 5.3). While time temperature superposition (TTS) succeeds with 2 wt% DA-PCOD solution as expected (Figure 5.3, middle), it is clear that it fails for the 0.9 wt% DA-PCOD solution (Figure 5.3,
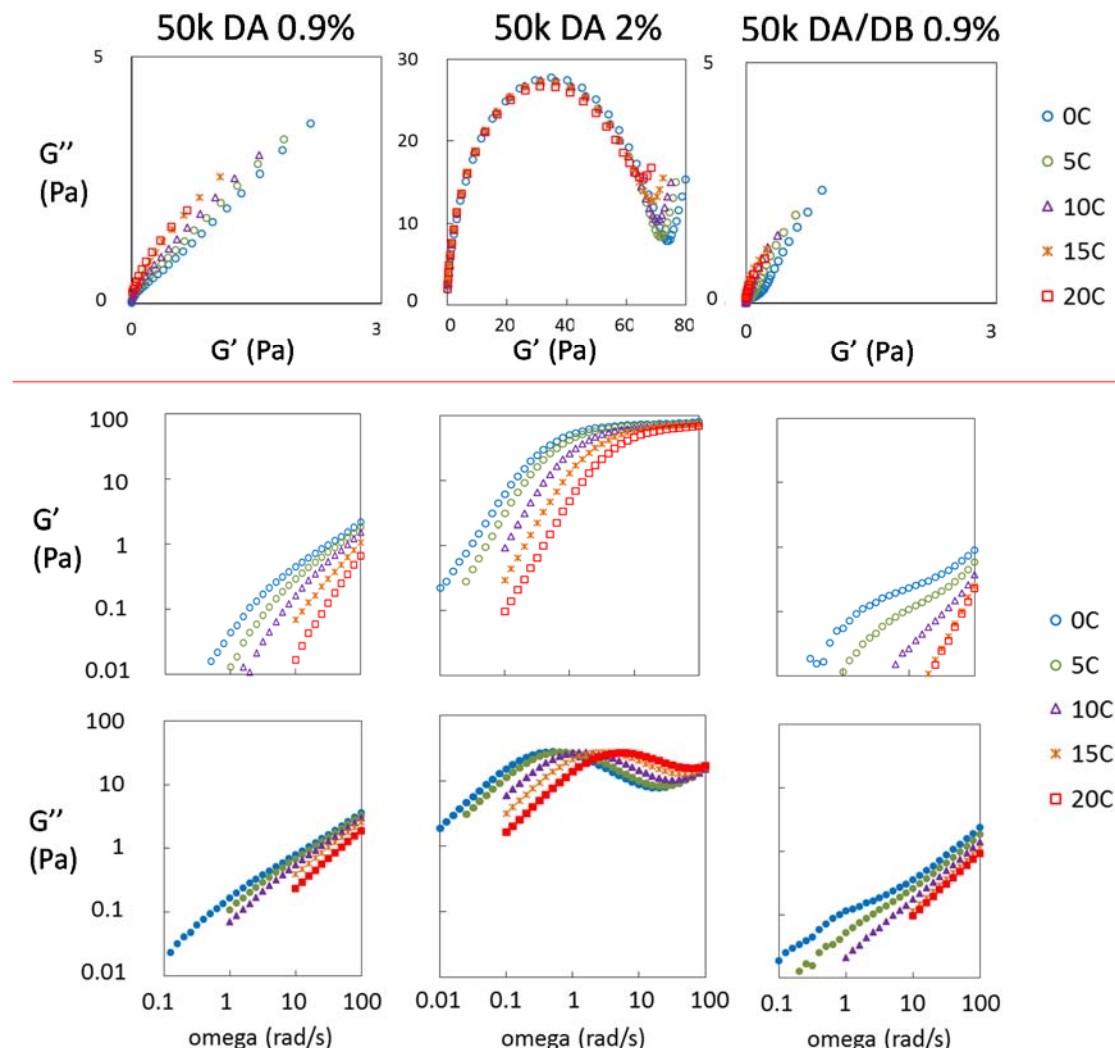

Figure 5.3 Oscillatory shear data of decalin solutions of 0.9 wt% 50k DA-PCOD and DA/DB-PCOD, and 2 wt% 50k DA-PCOD at temperatures 0-20℃, in the forms of Cole-Cole plot (top), and with G' and G'' plotted against frequency individually (bottom).

left). In fact, the feature for the 0.9 wt% DA-PCOD solution resembles that for the 0.9 wt% DA/DB-PCOD solution (Figure 5.3, right). Both the dynamic moduli curve shape and the temperature dependence suggest that 50k DA-PCOD at low concentration (< 0.9 wt%) relaxes more like pairwise-associative polymers.

The above concentration effect can be further supported by the Arrhenius plot. (Figure 5.4). When the concentration is low (0.9 wt% and 0.6 wt%), the slope of the Arrhenius plot is lower, which has not been reported in literature. It might be attributed to the fact that the viscosity is less dominated by the dissociation/exchange of end group when the network is not fully formed, but instead probably by the relaxation of the aggregates. The critical concentration around which the Arrhenius slope changes (0.9 wt%, in Figure 5.4) coincides with the critical concentration shown in the dynamic moduli curves (Figure 5.2). It indicates that the mechanism that governs the dynamic features which resembles pairwise association, determines its temperature dependence as well. And the mechanism should stem from the micelle structure in the solutions, which will be covered in Discussion.
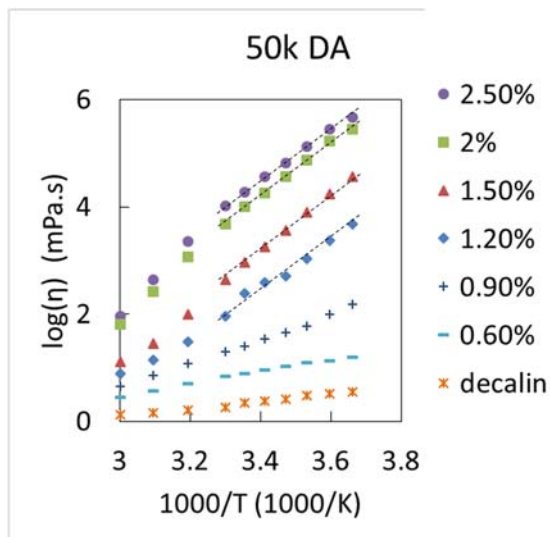

Figure 5.4 Arrhenius plot of solutions of 50 kg/mol DA-PCOD at concentrations from 0.6 wt% to 2.5 wt% in the temperature range of 0-60 ℃.

5.3.2 Data for 100 kg/mol and 230 kg/mol DA-PCOD

When chain length is taken into account, more complexities are introduced to the system. The oscillatory frequency sweep results for DA-PCOD of three chain lengths (M_w = 50 kg/mol, 100 kg/mol, and 230 kg/mol) at various concentrations at 0 ℃ are plotted together in Figure 5.5. For 100 kg/mol DA-PCOD, the same concentration dependence in high-frequency modulus, relaxation time and curve shape is observed like the trend illustrated above for 50 kg/mol DA-PCOD solutions (Figure 5.5, "100K DA"). However, the critical concentration for the formation of interconnected network, or say for the dynamics to be Maxwellian, is increased to 1.2 wt% for 100 kg/mol DA-PCOD, compared to 0.9 wt% for 50 kg/mol chain.
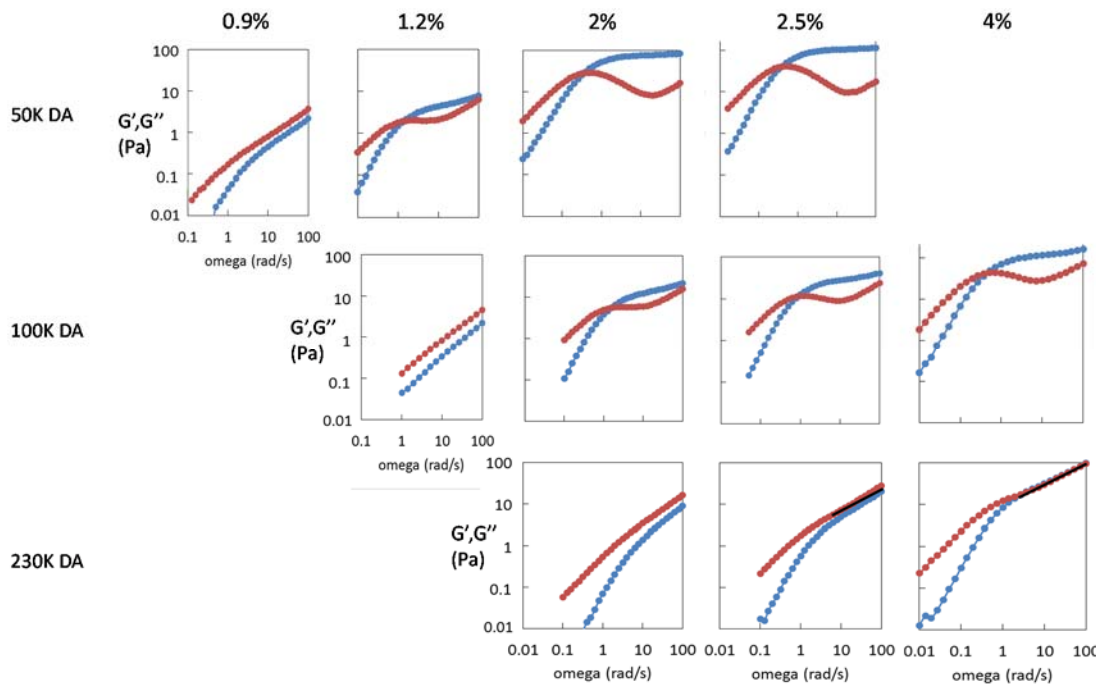
Figure 5.5 Storage (G', blue circles) and loss modulus (G", red circles) for DA-PCOD (M_w = 50, 100, and 230 kg/mol) at 0 ℃ at concentrations from 0.9 wt% to 2.5 wt%. The black line in the figures represents the slope of ½.

Interesting properties are observed for 230 kg/mol DA-PCOD. The solutions with concentration up to 4 wt% all exhibit dynamic features like pairwise-associative polymer (Figure 5.5,"230k DA"). The temperature dependence of the dynamics of 230 kg/mol DA-PCOD solutions also resembles that of pairwise-associative polymers (Figure 5.6). From the Cole-Cole plots of three solutions, it is obvious that the 2.5 wt% solution of 230k DA-PCOD does not follow time-temperature superposition principle, while the solutions of 50k and 100k DA-PCOD do. Both the curve shape and the temperature dependence indicate
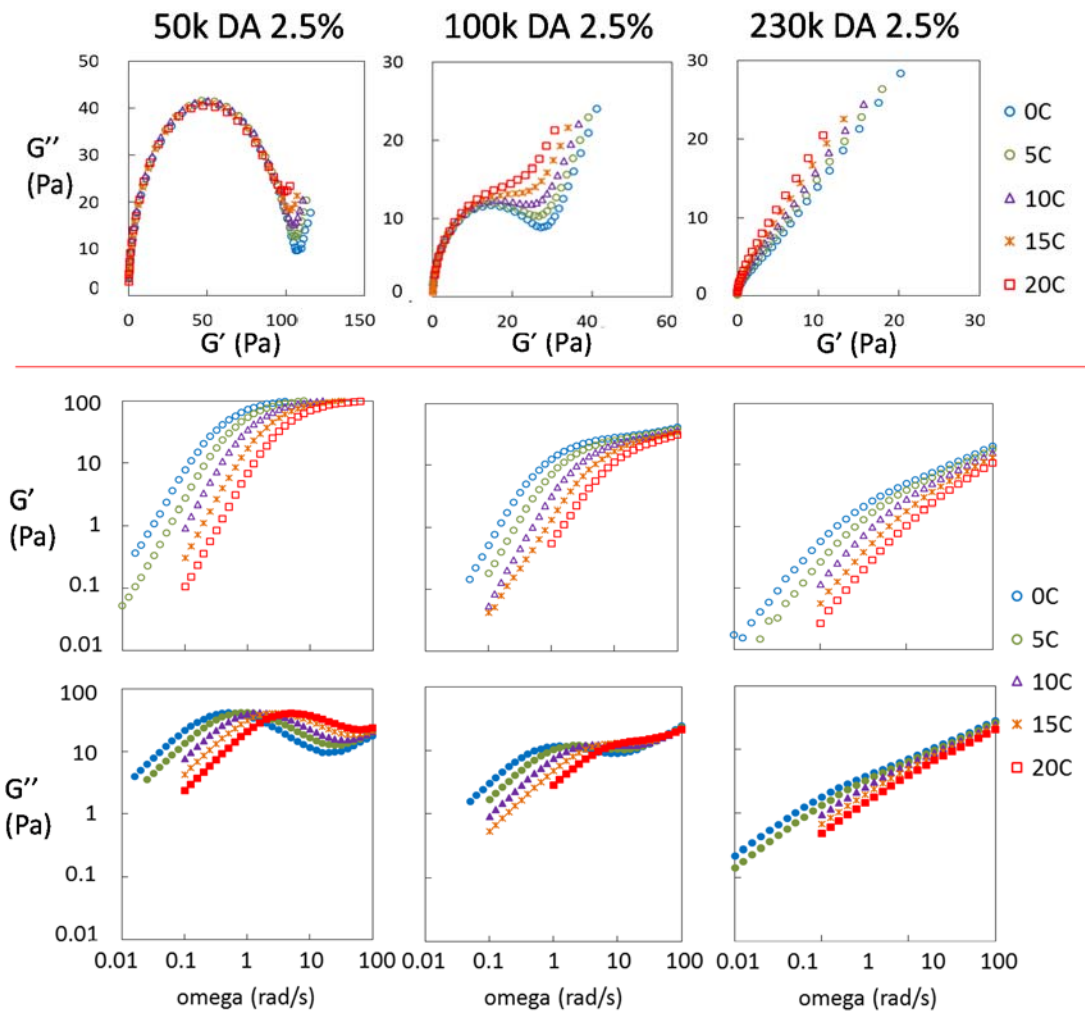
Figure 5.6 Oscillatory shear data of 2.5 wt% decalin solutions of 50k, 100k and 230k DA-PCOD at temperatures 0-20℃, in the forms of Cole-Cole plot (top), and with G' and G'' plotted against frequency individually (bottom).

Table 5.1 Activation energy calculated from the slope in the Arrhenius plots of solution viscosity for 50 and 100 kg/mol DA-PCOD solutions at concentrations of 1.2-2.5 wt% and 2-4 wt% respectively.

	50 k DA-PCOD	100 k DA-PCOD
Ea (kJ/mol)	93 ± 7	87 ± 6

that 230k DA-PCOD in solutions with concentrations up to 4 wt% relaxes like pairwise-associative polymers.

This same concentration dependence seen in the Arrhenius plot for 50k DA-PCOD solutions is observed with 100k and 230k DA-PCOD solutions as well (Figure 5.7). For 100k DA-PCOD at high concentrations (> 2 wt%), the slope reaches its maximum, depicting the activation energy for the dissociation/exchange of the end group (Figure 5.7A). The calculated activation energy for 50k DA-PCOD and 100k DA-PCOD are listed in Table 5.1. The *Ea* for 100k DA-PCOD is very close to that for 50k DA-PCOD, indicating that the micelle structures, once they are connected, are similar for 50k and 100k DA-PCOD solutions. The Arrhenius slope also decreases at low concentration (1.2 wt%, Figure 5.7A), the concentration at which the dynamic moduli curve show signs of pairwise
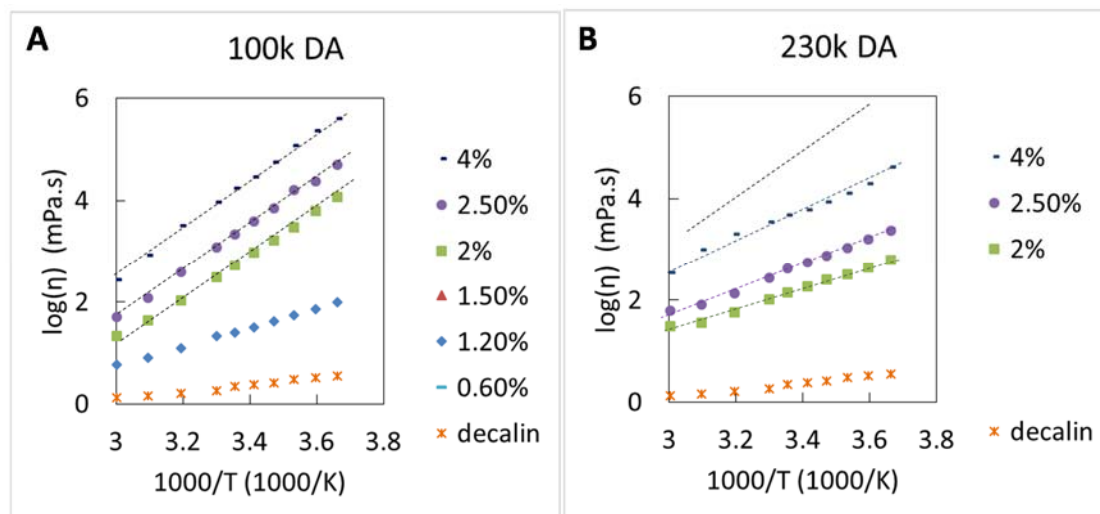

Figure 5.7 Arrhenius plot of solutions of 100 and 230 kg/mol DA-PCOD at various concentrations in the temperature range of 0-60 ℃.

association. For 230k DA-PCOD solutions, the slope turns steeper as the concentration increases up to 4%, but is still smaller than the maximum value seen for 50k and 100k DA-PCOD solutions, which is shown in Figure 5.7B as a dash black line. This observation is again consistent with the fact that 230k DA-PCOD relaxes like pairwise-associative polymers at concentrations up to 4%, as indicated in their dynamic moduli curves. It is possible that network will form with 230k DA-PCOD at even higher concentrations.

5.3.3 The chain length effect on the relaxation pattern of DA-PCODs

It is clearly demonstrated above that the systematically varied chain length at a fixed concentration exerts dramatic effect on the dynamics of self-associative telechelic polymer solutions, including high-frequency modulus, relaxation time and the whole dynamic moduli curve shape (Figure 5.5). Take the solutions at 2.5 wt% for an example (Figure 5.5, 2.5 %). The crossover moduli for solutions of 50k DA-PCOD and 100k DA-PCOD are 40 Pa and 11 Pa, respectively. Increasing the chain length by one fold (50k to 100k) reduces the crossover moduli to one fourth of the original value (40 Pa to 11 Pa). The relaxation time is also shortened slightly as the molecular weight goes up: from 3.1 s for 50k to 1 s for 100k. When the molecular weight increases to 230 kg/mol, the shape of the curve totally changes and shows features of pairwise association. In summary, the effect on the dynamics of the solutions is the same for the following two processes: 1) increase chain length (from 50 kg/mol to 100 kg.mol to 230 kg/mol) at a fixed concentration, and 2) decrease polymer concentration at fixed chain length (e.g. from 2.5 wt% to 0.9 wt% for 50 kg/mol).

The above similarity between the concentration effect and the chain length effect on the dynamics of DA-PCOD solutions can be further supported by the Arrhenius plot (Figure 5.4 and 5.7). It has been demonstrated that decreasing concentration at a fixed chain length to a critical point leads to smaller Arrhenius slope, corresponding to incomplete network formation. When the concentration is kept constant, increasing chain length can also reduce the slope, as in the case of 1.2 wt% 50k compared with 1.2 wt% 100k, and 2 wt% 100k compared with 2 wt% 230k (Figure 5.4 and 5.7). Therefore, DA-PCOD with higher
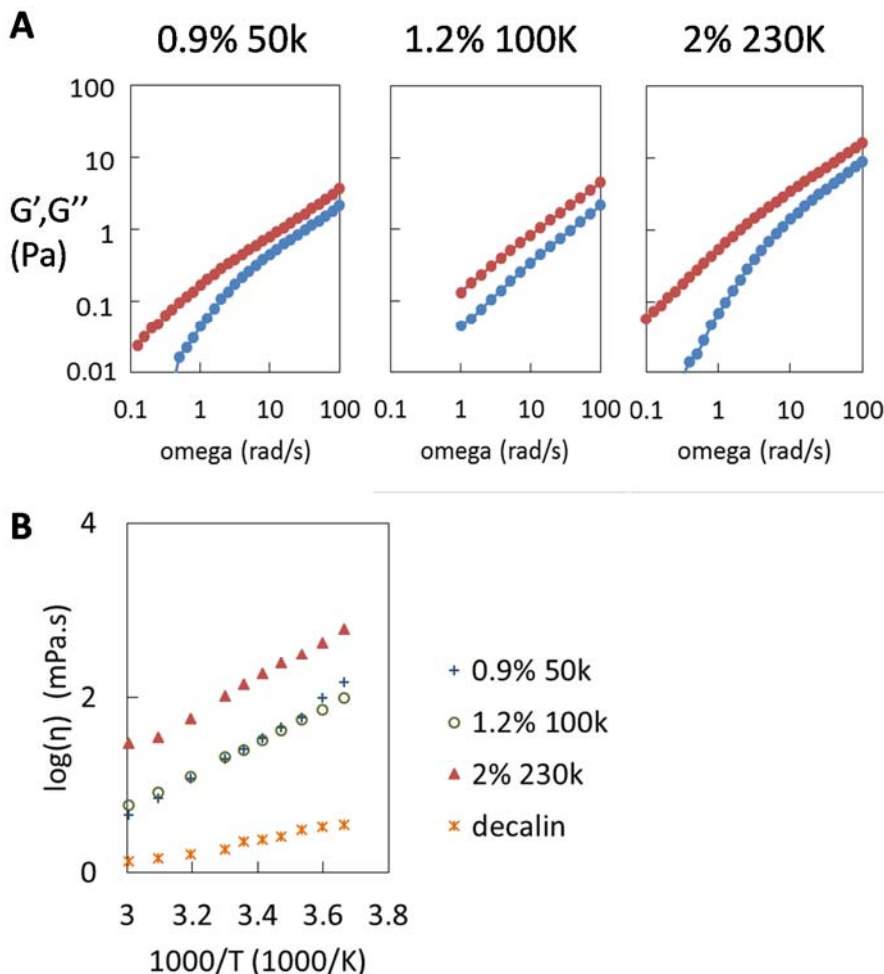
Figure 5.8 A. Storage (G', blue circles) and loss modulus (G", red circles) for solutions of 0.9 wt% 50k, 1.2 wt% 100k and 2 wt% 230k DA-PCOD at 0 ℃. **B.** The Arrhenius plot of the viscosity for the above three solutions.

molecular weight is expected to reach same Arrhenius slope at higher concentration compared to DA-PCOD with lower molecular weight. And it is indeed what has been observed. Similar shapes in the dynamic moduli curves are discerned for solutions of 50k DA-PCOD at 0.9 wt%, 100k DA-PCOD at 1.2 wt%, and 230k DA-PCOD at 2 wt% (Figure 5.8A), all indicating relaxation pattern resembling pairwise-association. Accordingly, the Arrhenius slopes for all three solutions are almost the same as well (Figure 5.8B). These results further support the argument that increasing chain length and decreasing polymer concentration has comparable effect on solution dynamics. And the mechanism that governs the dynamic features that resemble pairwise association determines its temperature dependence as well. And the mechanism is related to the micelle structure in the solutions, which will be covered below.

5.4 Discussion

5.4.1 Two opposing factors in chain length effect

As mentioned above, increasing chain length leads to two results that affects the association and dynamics of self-associative telechelic polymers in contradictory directions: 1) each telechelic polymer has larger radius of gyration, and 2) the concentration of end groups is reduced. Larger radius of gyration of telechelic polymers results in lower overlap concentration (C*), enabling the telechelic polymer with higher molecular weight to associate with each other at lower concentration. In addition, increasing chain length reduces the probability of loop formation, favors bridge conformation in micelle solutions, and hence should theoretically facilitate the network formation. On the other hand, low concentration of end groups directly decreases the maximum number of bridges that could

be achieved at very high concentration. Thus, it may diminish the high plateau modulus and hinder micelle network formation.

The experimental data described in this chapter indicates that increasing chain length has similar effect on solution dynamics as decreasing polymer concentration. Since both of the two processes result in reduced concentration of end groups, the end-group concentration clearly determines the dynamic feature of the solutions in the semidilute regime, which agrees with the prior literature. Note that the dropping of end-group concentration is inversely proportional to the chain length ($C_{end} \sim N^{-1}$), while the size of polymer coil only
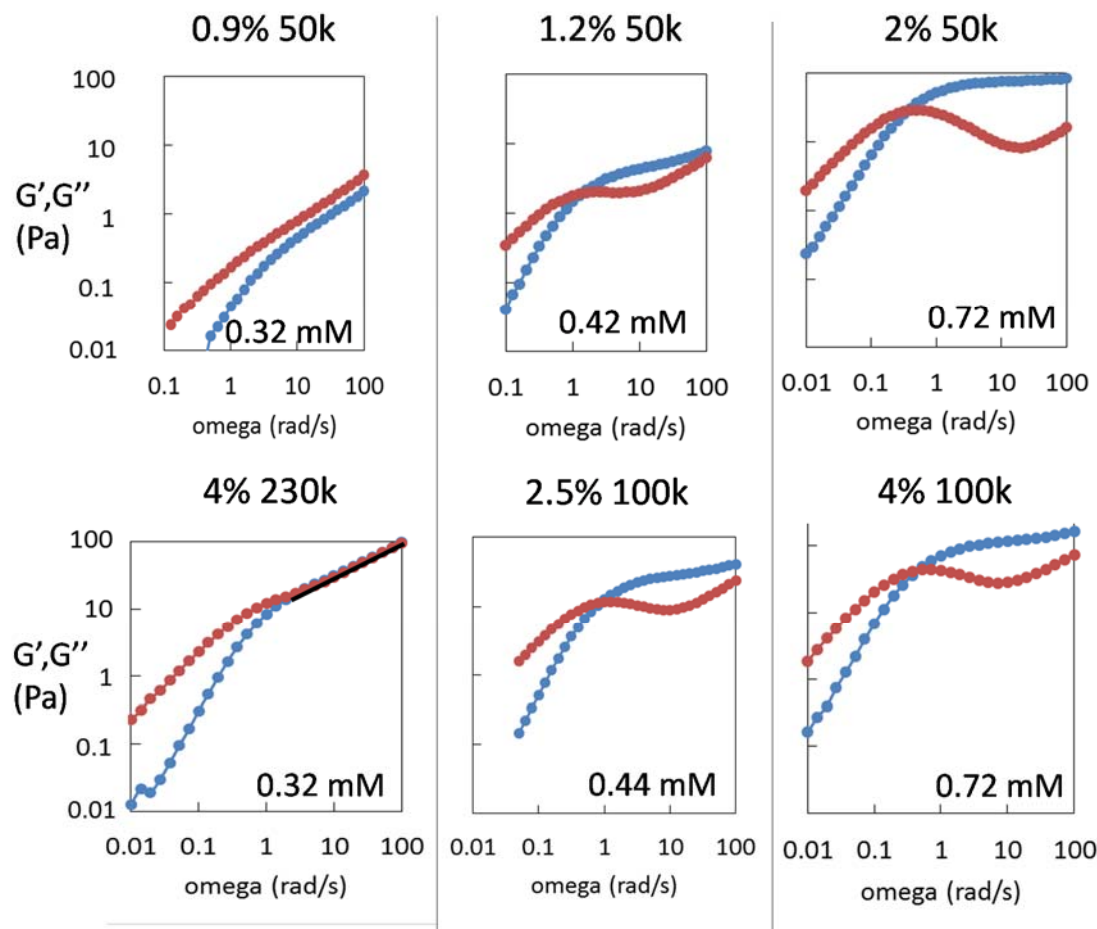
Figure 5.9 Storage (G', blue circles) and loss modulus (G", red circles) for solutions of 50k, 100k and 230k DA-PCOD at various concentrations with matching end group concentrations at 0 °C.

increases with chain length with a power law less than 1 ($R_{chain} \sim N^{0.5}$ for semidilute solutions). It is reasonable that the importance of the effect of end-group concentration becomes dominant as the polymer length turns longer.

Therefore, the end-group concentration in the unit of mM (mmol/L) is calculated for each solution composition with specific polymer concentration and molecular weight (as in Figure 5.5). And the solution compositions with nearly identical end group concentrations are listed and compared in Figure 5.9. From left to right, the concentration dependence described earlier is recovered as the end-group concentration increases. At each specific end-group concentration, longer DA-PCOD always provides higher modulus (Figure 5.9, bottom compared to top), which is strong evidence that larger chain length favors bridge conformation over loops in micelle solutions.

The result is in consistence with theoretical evaluation. Take the comparison between 1.2 wt% 50k and 2.5 wt% 100k DA-PCOD solutions as an example. Assuming an aggregation number (p) of 6 for DA-PCOD, the average distance between clusters of ends (D_{e-e}) can be estimated using the end group concentration if the ends distribute homogeneously (Figure 5.10A). Since the solutions are semidilute, the radius of gyration of individual telechelic coil follows the equation: $R_g \approx (1/6)bN^{1/2}C^{-0.23}$ (Figure 5.10A). Their similar end group concentration determines that their D_{e-e} should be close, and 100k DA-PCOD obviously has a larger radius of gyration (11.5 nm *versus* 9.5 nm) than 50k (Figure 5.10A). Therefore, less stretching is needed for 100k telechelic coil to form a bridge than for a 50k coil (Figure 5.10B), consistent with the observation that 100k DA-PCOD at 2.5 wt% has higher high-frequency modulus than 50k DA-PCOD at 1.2 wt%.

A $R_g \approx 1/6\ \xi\ (N/g)^{1/2} \approx 1/6\ b\ N^{1/2}\ C^{-0.23}$
M_0 = 113 g/mol, b = 0.99 nm for 1,4-polybutyldiene [7]

	1.2% 50k	2.5% 100k
C_{end}	0.42mM	0.44mM
D_{e-e} (p=6)	28.7 nm	28.3 nm
N	442	885
R_g	9.5 nm	11.5 nm

B

| 28 nm | 28 nm |
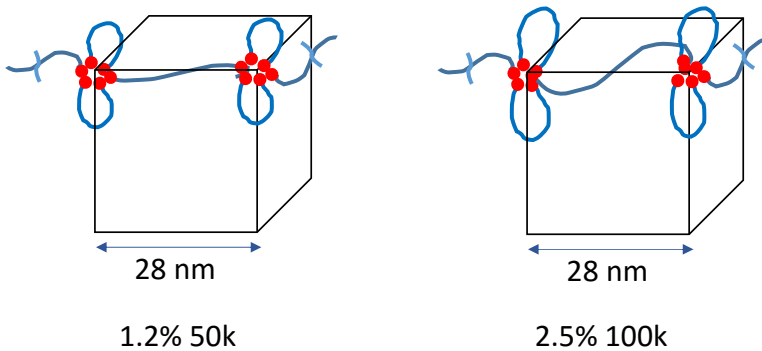
1.2% 50k   2.5% 100k

Figure 5.10 A. Estimated average distance between clusters of ends (D_{e-e}) and radius of gyration (R_g) of an individual coil for decalin solutions of 1.2% 50kg/mol and 2.5% 100kg/mol DA-PCOD. B. Schematics to show that less stretching is needed for a 100k coil for bridge formation tan for a 50k coil.

In summary, even though the effect of end-group density dominates the dynamic pattern in the semidilute regime, the size of telechelic polymers still plays a role in the topology of micelle structures.

5.4.2 Possible molecular picture for the apparent pairwise-associative dynamics for DA-PCOD at low end-group concentration

It is interesting that DA-PCOD exhibits the dynamic features of pairwise-associative polymers at low end-group concentration, while the ends usually associate with multiple counterparts. There are two possible molecular scenarios that may lead to the apparent pairwise-associative dynamics. The first scenario is that the functionality of each micelle decreases as the concentration drops, until the functionality of all micelles equals two
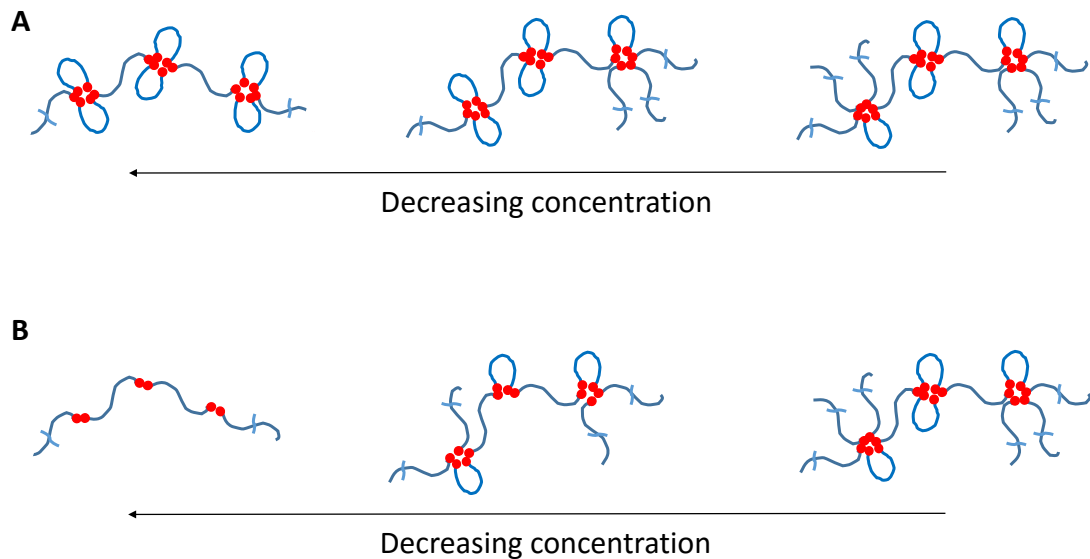
Figure 5.11 Two postulations on the mechanism the apparent pairwise-associative dynamics for DA-PCOD at low end-group concentration. **A.** Functionality of micelle decreases with concentration, with a constant aggregation number. **B.** Aggregation number decreases with concentrations.

(Figure 5.11A). Since each individual loop follows Rouse relaxation and relaxes too fast to contribute to the dynamics of the whole system, the superbridge resembles a linear supramolecule formed by pairwise association, although the aggregation number in each micelle core is bigger than two and does not change with concentration. The second molecular picture is that the aggregation number truly decreases with decreasing concentration until it finally reaches a value of 2, which corresponds to pairwise association (Figure 5.11B).

Scenarios analogous to the above two pictures have been postulated in earlier literature. Annable *et al* established the topological change of the micelle structure as a function of polymer concentration and the existence of superbridge to account for the quadratic increase of high-frequency modulus at low concentration [5]. Loops are favored at low concentration and a large fraction of telechelic polymers are distributed into local

topologies like superbridges, with many micelles having functionality equaling to or less than 2. Since the dissociation of one of the bridging chain in the middle relaxes the whole superbridge structure, the relaxation time is shortened and the modulus is low. Increasing concentration turns more loops into bridges, leading to higher modulus and longer relaxation time. Throughout the process, the aggregation number keeps constant while the network topology changes, depicting the proposed Scenario A above (Figure 5.11A).

Meng *et al* deduced the most probable size and aggregation number of individual micelle by minimizing the free energy of micellization, balancing the interfacial energy against the energy of stretching the end blocks to form the core, the configurational entropy, and excluded-volume interactions of the soluble chains that form the corona. Their theory predicted a slightly decreasing aggregation number with increasing molecular weight of the backbone, which agrees fairly well with experimental data in earlier reports [8]. The model by Meng *et al* supports the hypothesis in Figure 5.11B.

In fact, literature has stated that Annable *et al* assumes a small constant aggregation number, which contradicts the experimental data with HEUR system, despite its success in introducing the concentration-dependent topology of micelle structures [9,10]. However, it does not necessarily mean that scenario A is not applicable for our DA-PCOD systems. Since the hydrogen bonding origin of self-association for DA-PCODs, in contrast to the hydrophobic interaction for HEURs, already leads to unique temperature dependence on the morphology and dynamics, it is straightforward to suggest that the mechanism for the apparent pairwise association of DA-PCODs is related to their specific chemical structure. Therefore, a more scrutinized inspection into the structure of isophthalic acid is needed to check which scenario is closer to the real situation with DA-PCODs.

Isophthalic acid forms multiple association due to its characteristic chemical structure: the 120° angel between the two carboxylic acid groups in the isophthalic acid, which leads to a 120° angel between the two hydrogen bonding generated from the acid groups (Figure 5.12), since the bond angle for hydrogen bonds is 180°. Therefore multiple isophthalic acid ends are able to associate with each other through hydrogen bonding between their carboxylic acid groups. The six-membered ring structure shown (Figure 5.12, P =6) is the most stable state for the self-assembly of isophthalic acid on a surface (2D) as a small molecule, with all hydrogen bonds remaining in their energy favorable state, having a bond angle of 180°. If the aggregation number (p) is forced to decrease, hydrogen bonds will be forced to bend, and the modified angle for H-bond can be simply calculated by treating the aggregated cluster as a polygon with 2p sides (Figure 5.12). Or if the hydrogen bond angle remains to be 180°, some carboxylic acid group will be left unbound to achieve smaller aggregation number (Figure 5.12). Therefore, the H-bond angle has to be bowed from 180° to 60°, or 50% of the acid ends has to be dangling for p = 2.

Next step is to check whether low aggregation number (p=2) is energetically feasible, especially for temperatures < 30℃ (All the "apparent pairwise association" are observed at temperatures including < 30℃). If 50% of the acid ends are dangling, the binding energy is straightly reduced to 50%, which is unlikely at temperatures < 30℃. It actually contradicts the calculation done in Chapter 3, which predicts that > 50% unbound end fraction can only be achieved at around 60℃.

Then the question becomes whether the H-bond angle can be bent to 60°. A simulation study using Monte Carlo and Molecular Dynamics has demonstrated that a single H-bond out of the dimer formed by one carboxylic acid has its enthalpy reduced 11% when it forms part
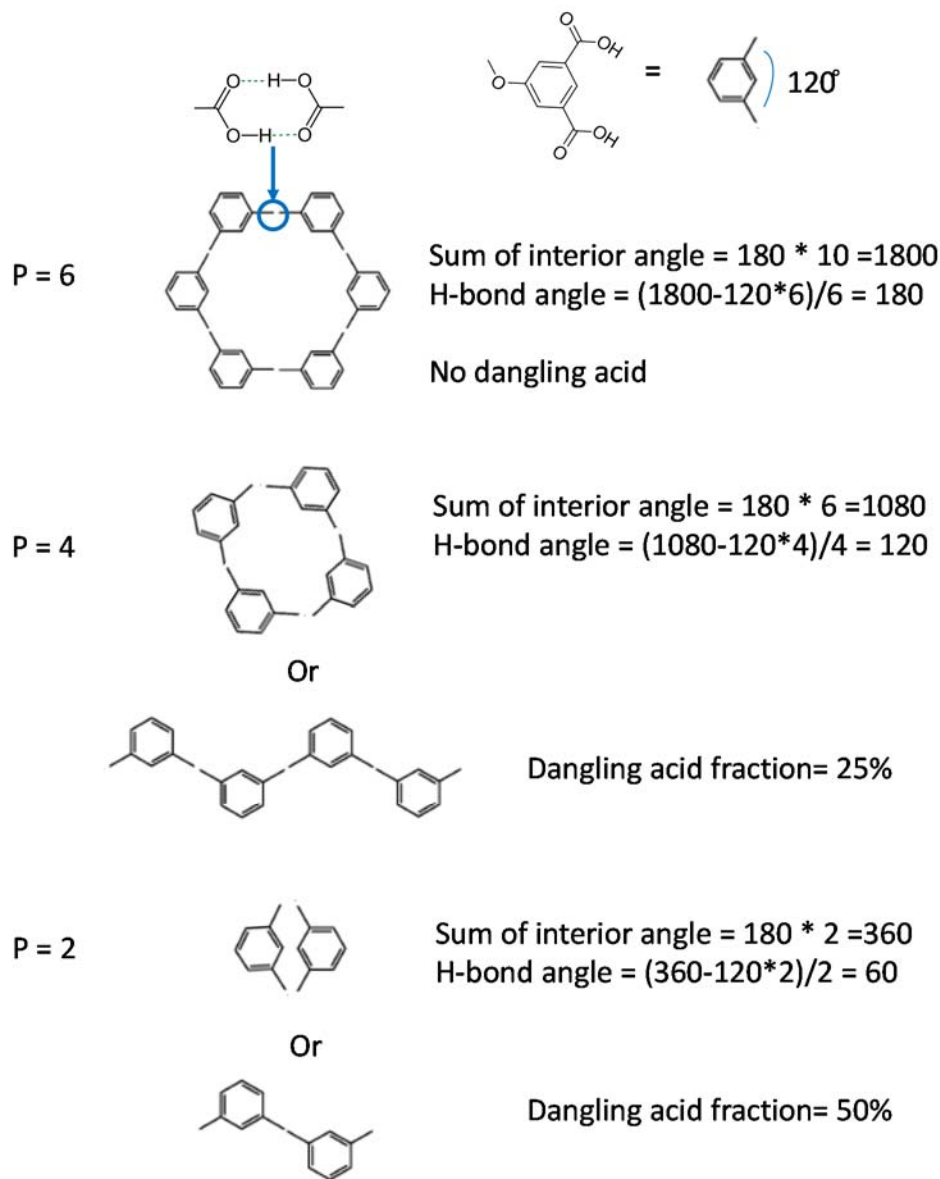
Figure 5.12 (Figure inspired by reference [13]) Estimated H-bond angle or dangling acid fraction for aggregation number less than 6.

of a trimer, with its bond angle decreases from 180° to around 120° (8 kcal/mol for 180° compared to 7.1 kcal/mol for the latter) [11]. And an H-bond angle smaller than 120° has never been observed in the simulation or experiments [11,12], indicating that it is energetically disfavored.
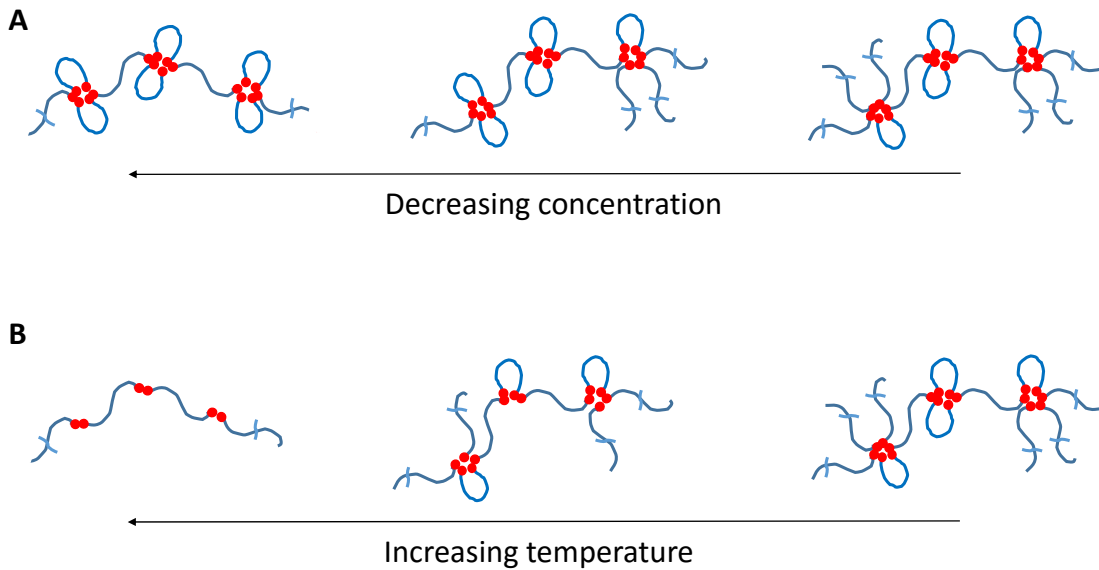
Figure 5.13 Molecular pictures on how the aggregation number of DA-PCOD micelles reacts with **A.** decreasing concentration, and **B.** increasing temperature.

It can be then postulated that, a true aggregation number of 2 in Scenario B (Figure 5.11) is difficult to achieve thermodynamically for temperatures < 30 ℃. Thus it is more likely that the aggregation number does not change much with polymer concentration or chain length, and it is the dominant superbridge topology that governs the pairwise-like dynamics.

Recall the discussion on the temperature dependence in Chapter 3, it is interesting to summarize that temperature and chain length (end group concentration) may have different effect on the aggregation number of micelles. Increasing temperature weakens the hydrogen bonding strength between DA ends, leading to higher dissociation constant and larger fraction of dangling ends. Thus it is very likely that aggregation number decreases with increasing temperature (Figure 5.13B). On the other hand, almost all ends are bound at temperatures < 30 ℃, making low aggregation number at low temperatures energetically disfavored. Therefore the "apparent pairwise association" observed with DA-PCOD at low end group concentration (long chain length) at low temperatures can only be attributed to

the "superbridge" topology, while the aggregation number does not change with concentration (Figure 5.13A).

5.5 Conclusions

Increasing chain length leads to two results that affects the association and dynamics of self-associative telechelic polymers (DA-PCOD) in contradictory directions: 1) each telechelic polymer has larger radius of gyration, and 2) the concentration of end groups is reduced. Larger radius of gyration of telechelic polymers reduces the probability of loop formation, favors bridge conformation in micelle solutions, and hence should theoretically facilitate the network formation. On the other hand, low concentration of end groups directly decreases the maximum number of bridges that could be achieved at very high concentration. Thus, it may diminish the high plateau modulus and hinder micelle network formation.

Rheology data demonstrates that increasing chain length has similar effect on solution dynamics as decreasing polymer concentration. Since both of the two processes result in reduced concentration of end groups, the end-group concentration clearly determines the dynamic feature of the solutions in the semidilute regime. However, despite the effect of end-group density being the dominant factor, the size of telechelic polymers still plays a role in the topology of micelle structures: DA-PCOD with higher molecular weight exhibits higher modulus compared to that of lower molecular weight, when the end group concentration is kept constant.

An interesting "apparent pairwise-association" dynamic pattern is observed with DA-PCOD at low end-group concentration (low polymer concentration or long chain length),

while the ends of DA-PCOD usually associate with multiple counterparts. A molecular picture is postulated for this phenomenon: the functionality of each micelle decreases as the concentration drops, until the functionality of all micelles equals two, during which process the actual aggregation number in each micelle core does not change with concentration.

References

[1] G. Broze, R. Jérôme, P. Teyssié, *Macromolecules*, **1982**, *15*, 1300-1305

[2] G. Broze, R. Jérôme, P. Teyssié, *Macromolecules,* **1982**, *15*, 920-927

[3] M. R. Tant, G. Wilkes, J. P. Kennedy, *J. Appl. Polym. Sci.*, **1991**, *42*, 523-532

[4] M.R. Tant, K.A. Mauritz, G.L. Wilkes, Ionomers: Synthesis, Structure, Properties and Applications, Springer, Netherlands, 1997.

[5] T. Annable, R. Buscall, R. Ettelaie, & D. Whittlestone, *Journal of Rheology* **37**, 695-726 (1993).

[6] M. Barmar, M. Barikani, B. Kaffashi, Iranian Polymer Journal 13 (3), 2004, 241-246

[7] M. Rubinstein, R. H. Colby, Polymer Physics, Oxford University Press, Oxford, 2003.

[8] X.-X. Meng, W. B. Russel, *Macromolecules* **2005,** *38,* 593-600

[9] Q. T. Pham, W. B. Russel, J. C. Thibeault & W. Lau, *Macromolecules,* **1999**, *32*, 2996-3005.

[10] Q. T. Pham, W. B. Russel, J. C. Thibeault & W. Lau, *Macromolecules,* **1999**, *32,* 5139-5146.

[11] N. Martsinovich, A. Troisi, *J. Phys. Chem. C,* **2010,** *114,* 4376–4388.

[12] M. Lackinger, W. M. Heckl, *Langmuir* **2009**, *25*, 11307–11321.

[13] S. De Feyte *et al*, *Nano Letters*, **2003**, 3, 1485–1488.

Chapter VI

Future Work on the Topology-Dynamic Relationship of Supramolecules by Telechelic Associative Polymers

6.1 Topology regulated by the chemical structure of end groups

Chemical entity of the end, which takes only < 1% of the total weight of the polymer, guides the mechanism of end association. Isophthalic acid (DA) is capable of multimeric association through pairwise hydrogen bonding, due to its specific chemical structure. When half of the isophthalic acid end is replaced with di-tertiary amine end group (DB) (<0.5% total weight), acid predominantly associates with amine pairwisely (DA/DB), because of the higher binding strength of the charge-assisted hydrogen bond between acid and amine. The multimeric *versus* pairwise association thus determines the topology of the supramolecules formed in two systems (self- and pairwise- association), network *versus* rings/chains, and furthermore, leads to distinct dynamic features observed in this thesis.

The fascinating effect of DA and DB end groups motivates us to explore more chemical structures. The dendron architecture introduced to the telechelic polymer system by Dr. Jeremy Wei can be utilized for a systematic study on the structure-topology relationship of the formation of supramolecules (Figure 6.1). Using the knowledge obtained with DA and DB system, the topology of supramolecular assembly is postulated below for some other specific combinations of ends.

6.1.1 Self-association of carboxylic acid ends
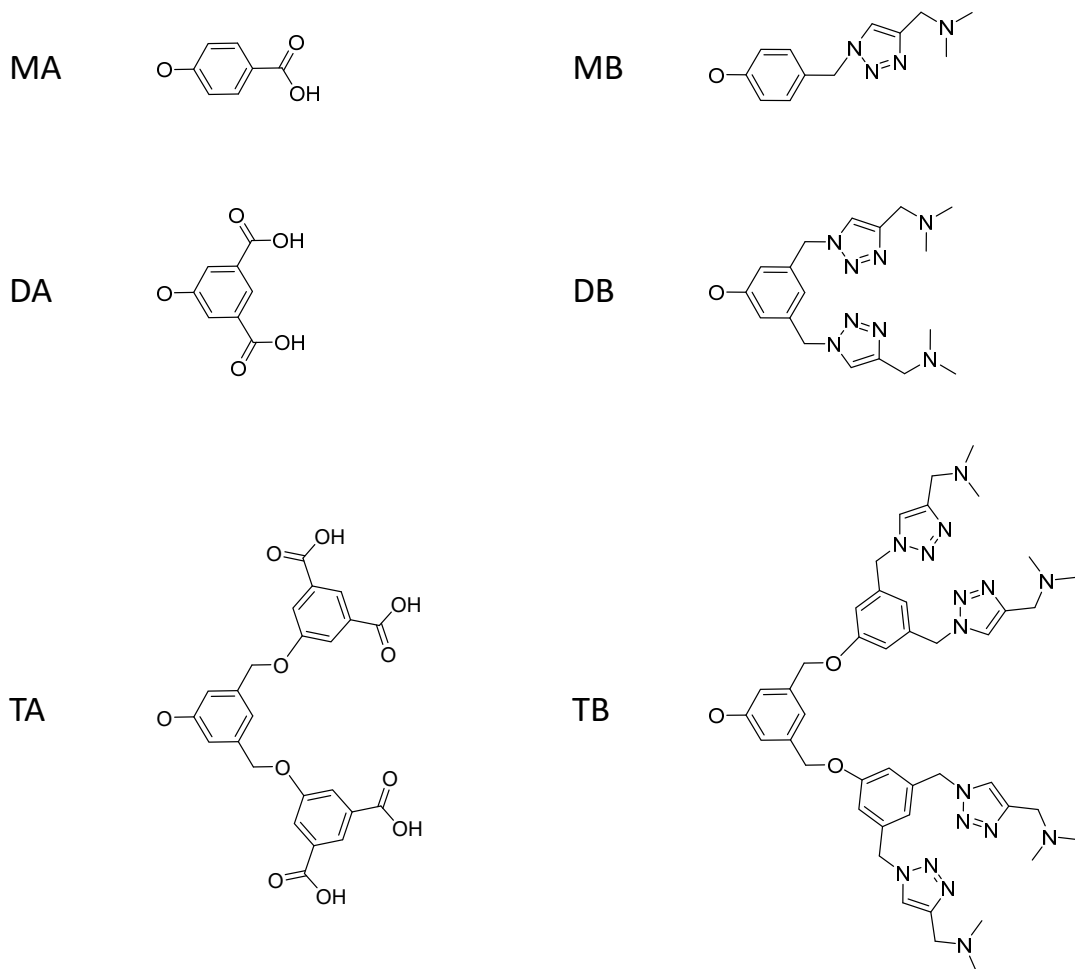
Figure 6.1 The dendron architectures bearing systematically varying number of acid/base ends

Carboxylic acid binds with itself through resonance assisted hydrogen bond (RAHB) between the carbonyl and hydroxyl group. It is mentioned earlier that although the RAHB between the carboxylic acid dimer is pairwise and has an 180° bond angle, multimeric association is managed for DA because of the 120° angle between the two acid groups on isophthalic acid (Figure 6.2, DA). Only one acid is presence in benzoic acid, leading to pairwise association between MA (mono-acid) end groups (Figure 6.2, MA). And MA-PCOD may behavior similarly to DA/DB-PCOD, although with much weaker end association ($\Delta G = 6.5\ kT$ and $16\ kT$ for MA and DA/DB respectively [1-5]).

The situation with TA (tetra-acid) end group is a bit complicated. Two isophthalic acid moieties are connected to one benzene ring through a flexible -CH$_2$O- (oxymethylene) linker in TA. Therefore TA is represented as two isophthalic acids tied with a blue curve (Figure 6.2, TA), with the two moieties not necessarily on the same plane. In fact, to keep each one of the moiety in the six-membered ring structure as observed with individual isophthalic acid, the steric hindrance may be very large, and the final aggregated structure can be distorted to certain extent. Nevertheless, TA-PCOD should tend to exhibit larger aggregation number, and forms micellar network more readily than DA-PCOD. The dynamics of TA-PCOD is expected to follow Maxwell model as well, with a single relaxation time guided by the dissociation/exchange of ends between micelle cores.
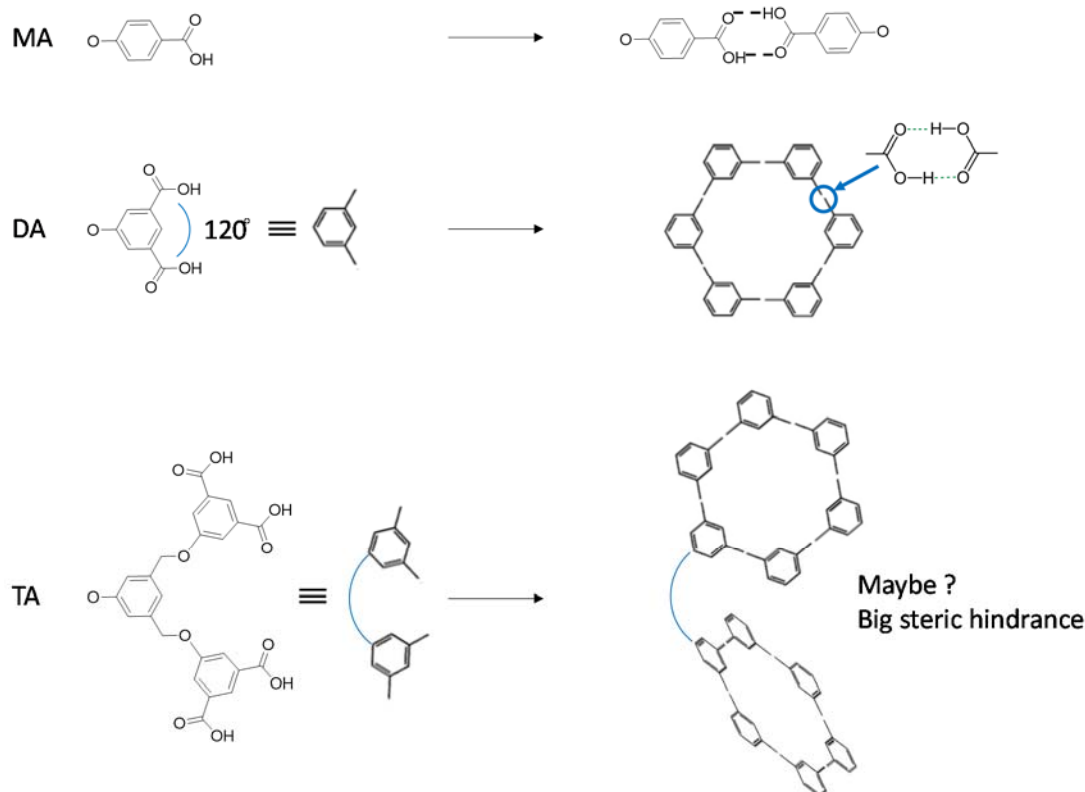
Figure 6.2 (Figure inspired by reference [9]) Hypothesized topology due to self-association of carboxylic acid ends

Like with DA-PCOD, an activation energy (E_a) can be calculated through the Arrhenius plot of solutions viscosity or relaxation time against inverse absolute temperature. The activation energy (E_a), although not replaceable by the binding strength (ΔG), is correlated with ΔG. In an ideal case, ignoring the effect of steric hindrance and of polymer backbone on the end association, the E_a for TA-PCOD should be twice of that for DA-PCOD. If TA-PCOD turns out to exhibit even higher value, it could be due to the synergetic effect of multiple acid groups tied together. If the value for TA-PCOD is much lower than expected, it may suggest that the distortion of RAHB between TA ends is significant.

6.1.2 Association between carboxylic acid and tertiary amine

The combinations of acid/base pairs with each having various numbers of ends are evaluated here. MA/MB and DA/DB pairs are most straightforward: both are pairwise associative, and linear/cyclic supramolecules are supposed to form (Figure 6.3, top line). TA and TB dendrons both present branch-like structure, radiating out spherically.
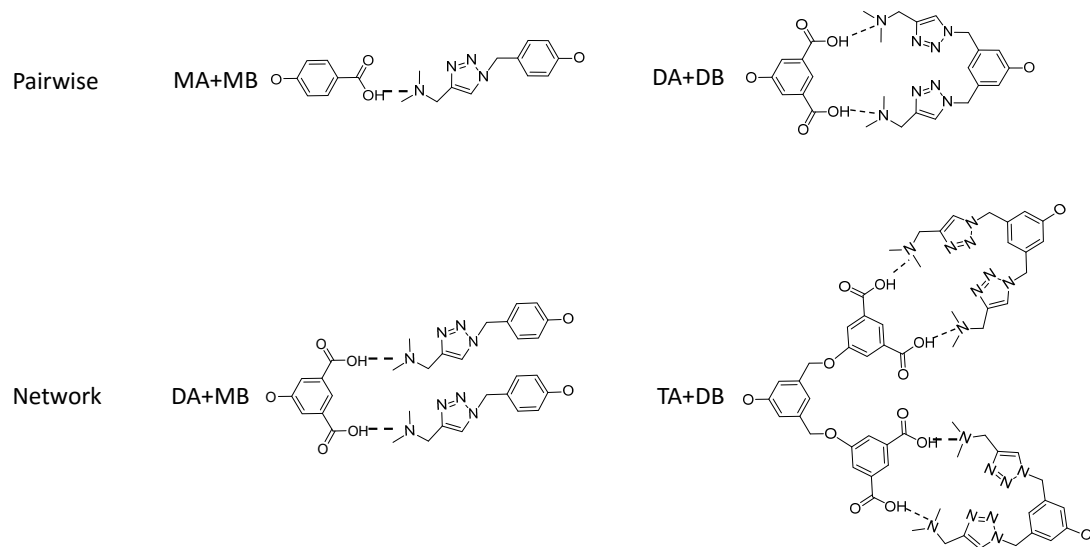
Figure 6.3 Hypothesized topology due to association between carboxylic acid and tertiary amine

Geometrically, the four acids groups from one TA molecule cannot all bind with the amine groups from one individual TB molecule. Therefore, it is mostly likely that one TA end will bind with two or more TB ends, resulting in network formation in TA/TB-PCOD solutions.

It is interesting to consider paring acid/base ends with different numbers of associative groups. When DA is coupled with MB, one isophthalic acid can bind with two MB-ended PCOD, and *vice versa*. The same rule goes with matching TA and DB. In all cases, the network is expected to be constructed (Figure 6.3, bottom line). And the molar ratio of acid and amine-ended polymers to achieve full association should no longer be 1:1; for example, the best ratio for polymers ending with DA/MB is 1:2, at which the numbers of acid/amine ends are matched.

6.2 Topology regulated by the association strength of end groups: solvent effect

The discussion about the end association strength is connected with the temperature effect in earlier chapters. Although the binding enthalpy and entropy is considered independent of temperature for hydrogen bonding systems, the binding free energy decreases linearly with increasing temperature: $\Delta G = \Delta H - T\Delta S$. Temperature thus plays a significant role in the binding strength, the equilibrium of end association, and eventually the topology of the supramolecules. For example, the aggregation number of DA is postulated to decrease with increasing temperature at temperatures above 30℃ (Figure 6.4). It is attributed to the fact that a large fraction of unbound acid groups is allowed to exist as a result of high dissociation constant at high temperature (Chapter 3, Section 3.1.3).

Solvent also affects the binding strength of hydrogen bonds, and thus may have similar effect on the topology of the supramolecules as changing temperature. In fact, different solvent is demonstrated to induce different binding enthalpy (ΔH) [6-7], in contrast to the case with temperature where ΔH is constant and only ΔG is changing. Therefore, solvent is supposed to lead to a more fundamental influence on end association and furthermore supramolecular topology.

DA's self-association is reported in literature to be affected much more dramatically by solvents than DA/DB binding. Allen *et al* demonstrated that the magnitude of the binding enthalpy (ΔH) of the hydrogen bond between benzoic acid dimer varies with the medium from 6.1 to 3.8 kcal/mol (26 to 16 kJ/mol), in the order of cyclohexane >carbon tetrachloride >benzene [7]. Chocholoušová *et al* reported in a simulation study that the
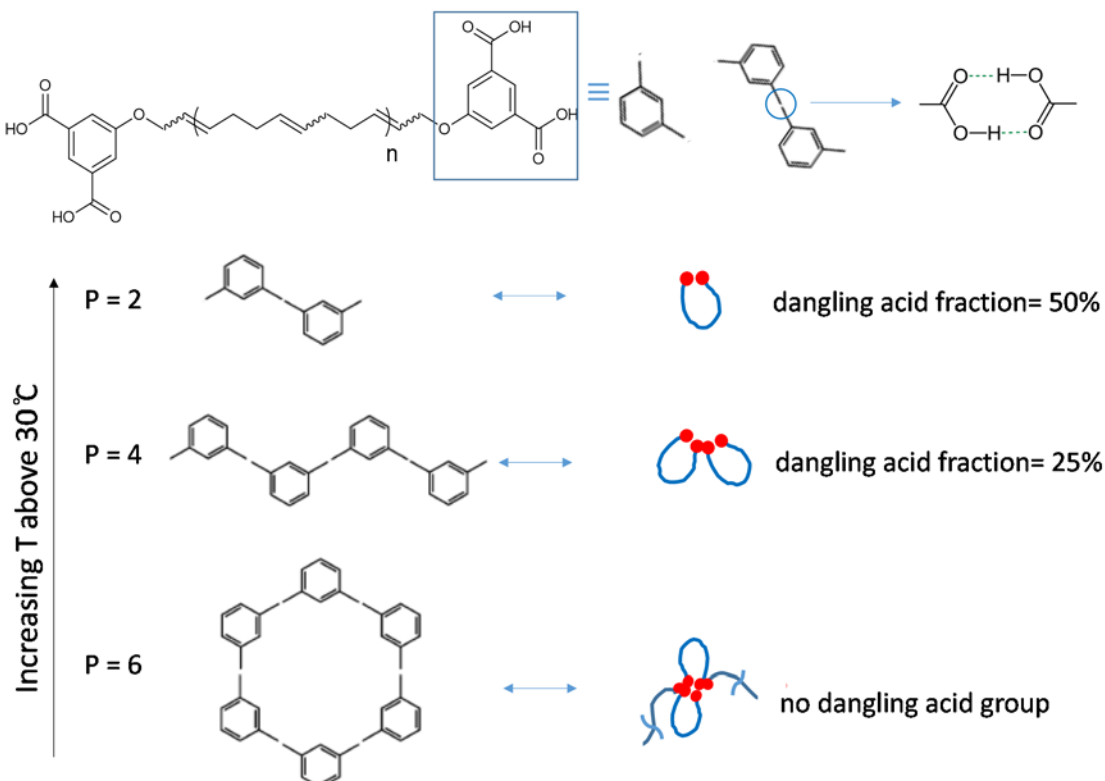
Figure 6.4 (Figure inspired by reference [9]) Hypothesis for the temperature dependence of aggregation number (p) for DA-PCOD

Table 6.1 Dielectric constant for representative solvents

	cyclohexane	decalin	Benzene	Choloroform	tetralin
Dielectric constant (ε)	2.02	2.23	2.28	4.81	2.77

binding free energy (ΔG) of the hydrogen bond between acetic acid dimer decreases from 3.35 to 0.85 kcal/mol (14 to 3.6 kJ/mol) when the media shifts from vapor to chloroform [6]. On the other hand, the binding free energy (ΔG) of the hydrogen bond between some acids and tertiary amine is measured to be around 4.7 ± 0.2 kcal/mol (19.7 ± 0.8 kJ/mol) in multiple solvents including cyclohexane, n-heptane and benzene [3-5]. In summary, literature shows that the binding strength of DA is strongly related to solvent property, probably especially to the polarity of the solvent, which can be evaluated via its dielectric constant (Table 6.1); while the strength of DA/DB depends less on solvents.

Our prior viscometry indeed indicates the solvent effect on the dynamics of our associative telechelic polymers (Figure 6.5) [8]. Cyclohexane (CH) and tetralin are both good solvents for the polycyclooctadiene (PCOD) backbone, leading to matching specific viscosity for
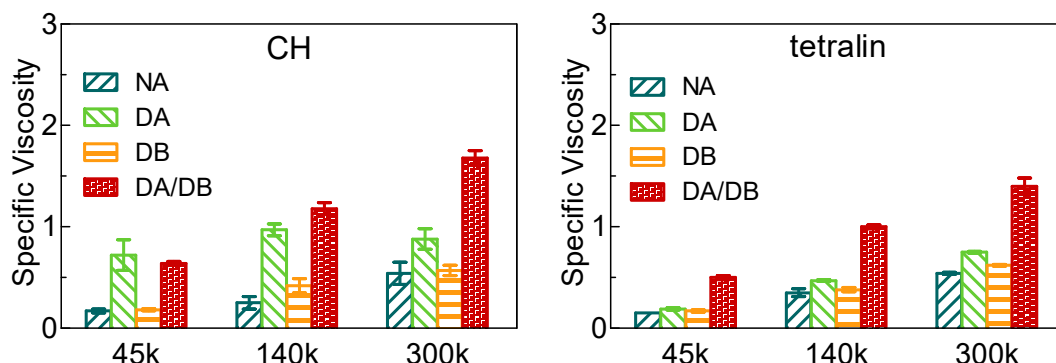
Figure 6.5 Specific viscosity of telechelic polymers with molecular weights of 45 kg/mol (45k), 140 kg/mol (140k) and 300 kg/mol (300k) in cyclohexane (CH) and tetralin at 25 ℃ at 2.3 mg/ml (~ 0.3 wt%). The four polymer compositions are non-associative (NA), isophthalic acid ended- (DA), di-tertiary amine ended- (DB) and 1:1 molar ratio of acid and amine ended- (DA/DB) polycyclooctadiene (PCOD).

NA-PCOD control at the same concentration in both solvents (Figure 6.5, NA). The pairwise-associative telechelics (DA/DB-PCOD) show slightly higher viscosity enhancement in cyclohexane than in tetralin ((Figure 6.5, DA/DB). The self-associative telechelics (DA-PCOD) exhibit much more prominent solvent effect: high viscosity, which is even higher than that of DA/DB-PCOD (especially for 45k and 140k) is obtained in cyclohexane, while only barely enhanced viscosity compared to NA-PCOD control is measured in tetralin. At higher concentration (> 0.6 wt%), DA-PCOD actually forms very viscous, gel-like solutions in cyclohexane (data not shown), indicating the existence of connected network, which is in consistent of our later observation with decalin solutions. The data confirms that the polarity of the solvent controls the efficiency of DA-PCOD in modifying rheology (Table 6.1), while DA/DB-PCOD is a promising rheological modifier in multiple solvents.

The preliminary viscometry data indicates the solvent effect on the dynamics of DA-PCOD and DA/DB-PCOD, which motivates us to uncover its underlying molecular mechanism. Using our knowledge about the temperature effect on the topology of DA-PCOD, it is straightforward to postulate that the aggregation number of DA-PCOD is smaller in a solvent with higher dielectric constant at the same polymer concentration, due to the weaker hydrogen bond. For example, the aggregation number could be 2 for DA-PCOD in tetralin, which can explain the weak enhancement in solution viscosity observed above. And solvents with similar dielectric constant should provide DA-PCOD solutions with comparable dynamic properties. On the other hand, the basic dynamic pattern of DA/DB-PCOD should not change much with different solvents. More dynamic experiments of DA-

PCOD and DA/DB-PCOD in solvents with various dielectric constants can be performed to examine the above postulations.

References

[1] A. D. H. Clague, H. J. Bernstein, *Spectrochim. Acta*, **1969**, *25*, 593-596.

[2] J. Chocholoušová, J. Vacek, P. Hobza, *J. Phys. Chem. A,* **2003,** *107,* 3086-3092.

[3] E. N. Gur'yanova, I. P. GoI'dshtein, T. I. Perepelkova, *Russian Chemical Reviews*, **1976**, *45*, 792–806.

[4] M. M. Davis, M. Paabo, *J. Am. Chem. Soc.*, **1960**, *82*, 5081–5084.

[5] H. Nakanishi, H. Morita, S. Nagakura, *J. Mol. Spectrosc.*, **1977**, *65*, 295-305.

[6] J. Chocholoušová, J. Vacek, P. Hobza, *J. Phys. Chem. A,* **2003,** *107,* 3086-3092.

[7] G. Allen, J. G. Watkinson, K. H. Webb, *Spectrochim. Acta*, **1966**, *22*, 807-814.

[8] M.-H. Wei*, B. Li*, R. L. A. David, S. C. Jones, V. Sarohia, J. A. Schmitigal & J. A. Kornfield (*: authors contributed equally), *Science*, **2015**, *350*, 72-75.

[9] S. De Feyte *et al*, *Nano Letters*, **2003**, 3, 1485–1488.

Appendix A

Synthesis and Characterization of the Small Molecule Chain Transfer Agents and Telechelic Polymers

1. Synthesis of Di-acid ended chain transfer agent (DA-CTA)
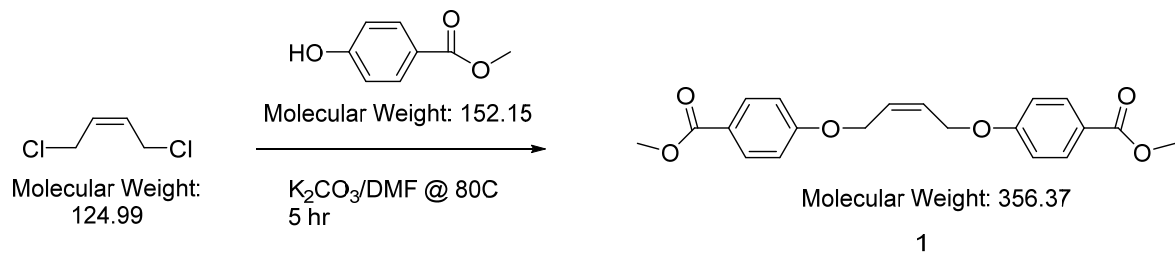
Scheme A.1 Synthesis of compound 1

Cis-1,4-dichloro-2-butene (5 g, 4.2 ml, 0.04 mol) is transferred to a 250 ml round-bottom flask charged with a magnetic stir bar, and dissolved with 100ml of dimethylformamide (DMF). Methyl 4-hydroxybenzoate (2.2 equiv., 0.087 mol, 13.4 g) and K_2CO_3 (3 equiv., 0.12 mol, 16.4 g) are weighed into the reaction vessel. The reaction is stirred under Argon in oil bath at 80℃ for 5 hours. After the reaction is completed, the suspension is filtered with Buchner funnel under vacuum while it is still hot to remove K_2CO_3. DMF in the filtrate is evaporated by rotavap under high vaccum (oil pump), and the resulting solid is recrystallized with MeOH at -20℃ overnight. The crystals (product 1) are then filtered, collected, and vacuum dried overnight in a vacuum oven. ^{1}H NMR (CDCl$_3$): δ 8.01 (d, 4H, Ph-*H*, ortho to carboxylate), 6.95 (d, 4H, Ph-*H*, ortho to phenol), 5.98(t, 2H, -*H*C=C*H*-), 4.75 (d, 4H, -OC*H*$_2$-), 3.90 (s, 6H, -C*H*$_3$) ppm.
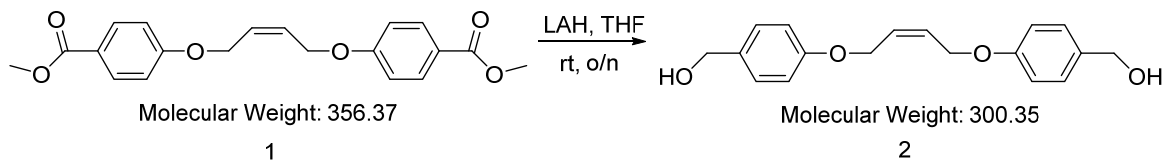
Scheme A.2 Synthesis of compound 2

Compound 1 (10 g, 0.028 mol) is dissolved in 40 ml of THF. Lithium aluminum hydride

(LAH, 3 equiv., 0.084 mol, 3.2 g) is suspended in 40 ml of THF and pipetted slowly into

the reaction mixture in a water bath. Another 20 ml of THF is used to rinse the LAH bottle

and the reaction flask. The reaction is stirred at room temperature overnight. After the

reaction is finished, 3.2 ml of H_2O (n ml for n g of LAH), 3.2 ml of 15% NaOH aqueous

solution (n ml for n g of LAH) and 12.6 ml of H_2O (3n ml for n g of LAH) are added drop-

wisely into the reaction mixture in a water bath to consume the LAH and form granular

inorganic precipitate, the procedure of which is referred as Fieser work-up. The mixture is

filtered and product 2 is obtained as white powder by evaporating the THF with rotavap

and then vacuum oven. ^1H NMR (DMSO-d^6): δ 7.22 (d, 4H, Ph-*H*, ortho to methylene),

6.91 (d, 4H, Ph-*H*, ortho to phenol), 5.85(t, 2H, -*H*C=C*H*-), 5.06(br, 2H, -O*H*), 4.70 (d, 4H,

-OC*H₂*CH=), 4.41 (d, 4H, HOC*H₂*-) ppm.
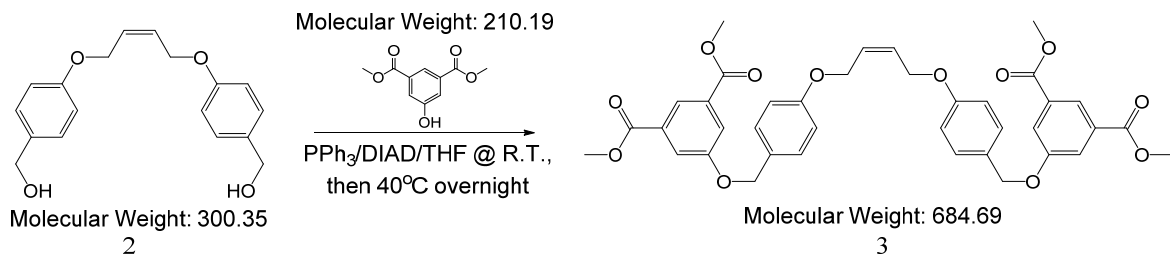
Scheme A.3 Synthesis of compound 3

Compound 2 (3 g, 9.8 mmol), Dimethyl 5-hydroxyisophthalate (3 equiv., 0.029 mol, 6.2 g)

and triphenyl phosphate (PPh₃, 3equiv., 0.029 mol, 7.8 g) are weighed into a 250 ml round

bottom flask, and dissolved with 100 ml THF. Diisopropyl azodicarboxylate (DIAD, 3 equiv., 0.029 mol, 6.1 ml) is added via a syringe at room temperature. The reaction is then transferred to a 40 ℃ water bath and stirred overnight. The reaction mixture is concentrated using rotavap, and subjected to column chromatography with silica gel as mobile phase and hexane/ethyl-acetate (1 to 1 ratio) as eluent. The elution fraction is monitored by thin layer chromatography (TLC), and the fractions with product 3 are collected and evaporated of solvent, providing 3 as white powder. ^{1}H NMR (CDCl$_3$): δ 8.29 (t, 2H, Ph-*H*, ortho to two carboxylates), 7.84 (d, 4H, Ph-*H*, ortho to phenol and two carboxylates), 7.39 (d, 4H, Ph-*H*, ortho to methylene), 6.95 (d, 4H, Ph-*H*, ortho to phenol), 5.96(t, 2H, -*H*C=C*H*-), 5.08 (s, 4H, -OC*H*$_2$Ph), 4.70 (d, 4H, -OC*H*$_2$CH=), 3.95 (s, 12H, -C*H*$_3$) ppm.

Molecular Weight: 684.69

3

Molecular Weight: 628.59
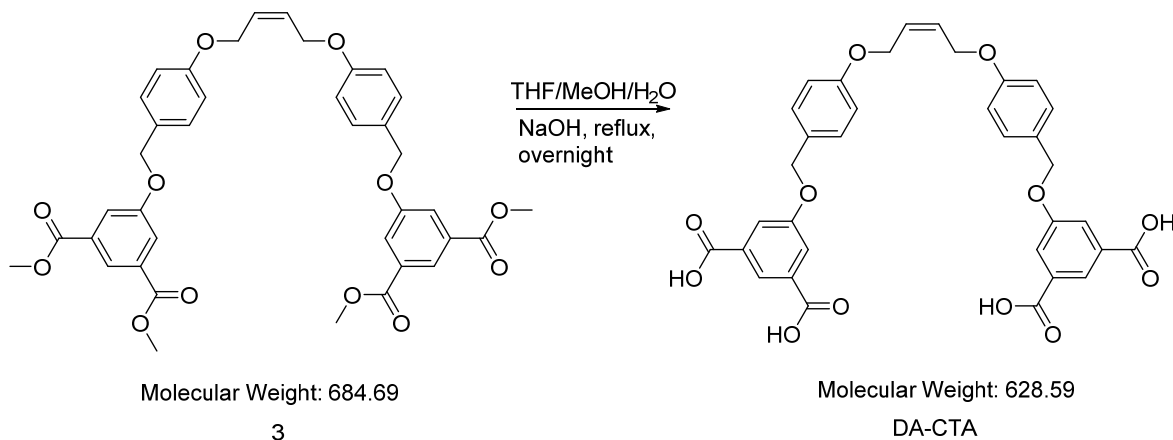
DA-CTA

Scheme A.4 Synthesis of DA-CTA

To a solution of compound 3 (1 g, 1.5 mmol) in 20 ml THF, 10 ml MeOH, NaOH (8 equiv., 0.011 mol, 0.46 g) dissolved in 2 ml H$_2$O is added. The reaction is refluxed overnight. The mixture is then adjusted to pH = 3 with 1M HCl, and concentrated to around 5 ml using rotavap. The mixture is extracted with 30 ml of ethyl acetate (EA) and washed with 20 ml of DI H$_2$O three times. The EA phase is dried with MgSO$_4$, filtered, and the solvent is

removed under reduced pressure to provide DA-CTA. ^{1}H NMR (DMSO-d[6]): δ 8.07 (t, 2H, Ph-H, ortho to two carboxylates), 7.71 (d, 4H, Ph-H, ortho to phenol and two carboxylates), 7.40 (d, 4H, Ph-H, ortho to methylene), 6.99 (d, 4H, Ph-H, ortho to phenol), 5.87(t, 2H, -HC=CH-), 5.15 (s, 4H, -OCH_2Ph), 4.75 (d, 4H, -OCH_2CH=) ppm.

2. Synthesis of Di-chloride ended chain transfer agent (DCl-CTA)
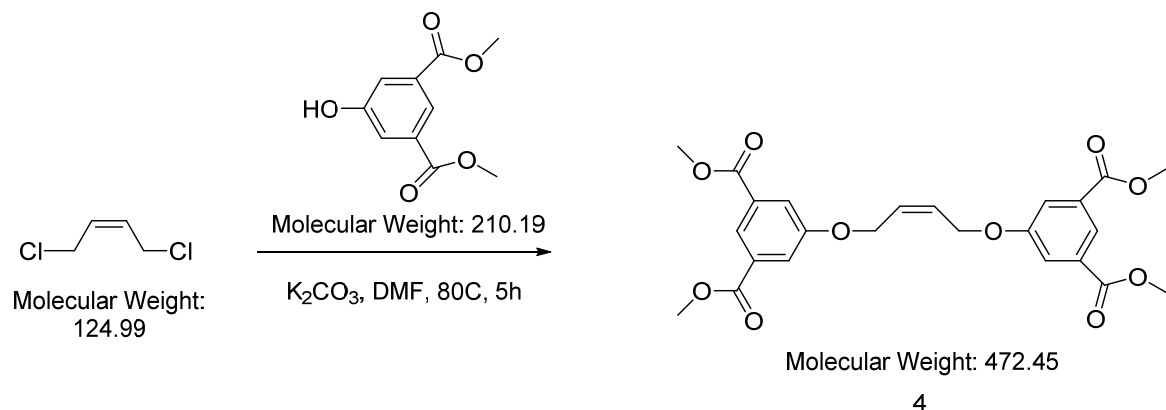

Scheme A.5 Synthesis of compound 4

Cis-1,4-dichloro-2-butene (3 g, 2.5 ml, 0.024 mol) is transferred to a 250 ml round-bottom flask charged with a magnetic stir bar, and dissolved by 70ml of dimethylformamide (DMF). Methyl 4-hydroxyisophthalate (2.2 equiv., 0.052 mol, 11.1 g) and K_2CO_3 (3 equiv., 0.071 mol, 9.8 g) are weighed into the reaction vessel. The reaction is stirred under Argon in oil bath at 80℃ for 5 hours. After the reaction is completed, the suspension is filtered with Buchner funnel under vacuum while it is still hot to remove K_2CO_3. Product crystalizes quickly from DMF when it gets cold. Therefore the pellet resulting from the filtration is extracted with 30 ml tetrahydrofuran (THF) and filtered again. The THF and DMF are combined and then evaporated by rotavap under high vaccum (oil pump), and the resulting solid is recrystallized with

MeOH at -20 ℃ overnight. The crystals (compound 4) are then filtered, collected, and vacuum dried overnight in a vacuum oven. ^{1}H NMR (CDCl$_3$): δ 8.31 (t, 2H, Ph-H, ortho to two carboxylates), 7.78 (d, 4H, Ph-H, ortho to phenol and two carboxylates), 6.00 (t, 2H, -HC=CH-), 4.80 (d, 4H, -OCH_2CH=), 3.95 (s, 12H, -CH_3) ppm.
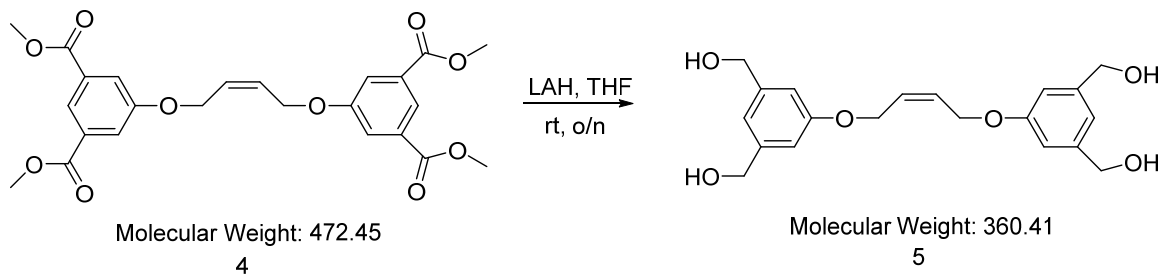
Scheme A.6 Synthesis of compound 5

Compound 4 (11 g, 0.031 mol) is dissolved in 60 ml of THF. Lithium aluminum hydride (LAH, 6 equiv., 0.18 mol, 7 g) is suspended in 40 ml of THF and pipetted slowly into the reaction mixture in a water bath. Another 20 ml of THF is used to rinse the LAH bottle and the reaction flask. The reaction is stirred at room temperature overnight. After the reaction is finished, 7 ml of H$_2$O (n ml for n g of LAH), 7 ml of 15% NaOH aqueous solution (n ml for n g of LAH) and 21 ml of H$_2$O (3n ml for n g of LAH) are added drop-wisely into the reaction mixture in a water bath to consume the LAH and form granular inorganic precipitate, the procedure of which is referred as Fieser work-up. The mixture is filtered and compound 5 is obtained as a white powder by evaporating the THF with rotavap and then vacuum oven. The pellet resulting from filtration is extracted with 50 ml of 2-butanone two times for compound 5 due to the low solubility of 5 in THF. ^{1}H NMR (DMSO-d^6): δ 6.86 (t, 2H, Ph-H, ortho to two methylene), 6.77 (d, 4H, Ph-H, ortho to phenol and two methylene), 5.85 (t, 2H, -HC=CH-), 5.16(t, 4H, -OH), 4.70 (d, 4H, -OCH_2CH=), 4.44 (d, 8H, HOCH_2-) ppm.
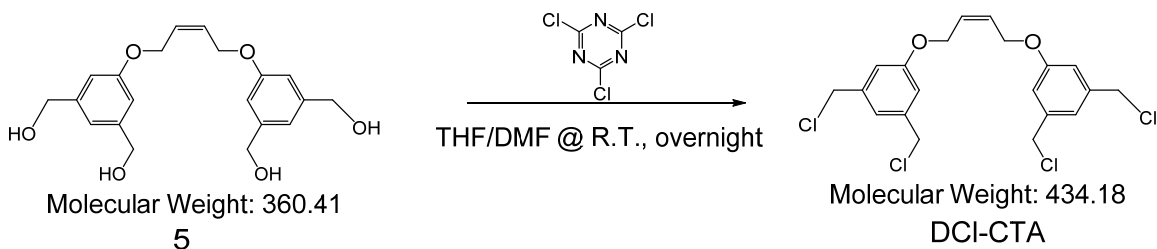
Scheme A.7 Synthesis of compound DCl-PCOD

Compound 5 (2 g, 5.5 mmol) and cyanuric chloride (12 equiv., 0.066 mol, 12.4 g) are suspended in 100 ml of THF. DMF (20 equiv., 0.11 mol, 8.7 ml) is added slowly into the mixture in a water bath. The reaction mixture turns clear upon addition of DMF, and then white powder starts to precipitate out due to the formation of byproducts. The reaction is allowed to stir at room temperature overnight. The mixture is filtered and the solvent is removed by rotavap. The resulting solid is dissolved with 30 ml of ethyl acetate and washed three times with 30 ml of saturated $NaHCO_3$ solutions to remove the derivatives of cyanuric chloride (e.g. cyanuric acid). The EA phase is then dried with $MgSO_4$, filtered, and concentrated. The resulting product is then recrystallized with MeOH at -20 °C overnight. The crystals (DCl-CTA) are then filtered, collected, and vacuum dried overnight in a vacuum oven. ^{1}H NMR (CDCl$_3$): δ 7.03 (t, 2H, Ph-*H*, ortho to two methylene), 6.92 (d, 4H, Ph-*H*, ortho to phenol and two methylene), 5.96 (t, 2H, -*H*C=C*H*-), 4.72 (d, 4H, -OC*H₂*CH=), 4.56 (d, 8H, ClC*H₂*-) ppm.

3. Purification of cyclooctadiene (COD) monomer.

Redistilled-grade COD (72.3 g, 0.67 mol) is syringe-transferred to a 250 ml Schlenk flask in an ice bath under argon. 1 M BH$_3$·THF complex in THF (108 ml, 0.11 mol) is slowly added into the flask over 10 min. The flask is taken out of the ice bath, and left to stir under argon at room temperature for 2 h. THF is evaporated under reduced pressure at room

temperature to an extent that the concentration of residual THF in the mixture is below 1000 ppm (verified by ^{1}H NMR analysis). The monomer is vacuum distilled from the mixture into a 100 ml Schlenk flask (loaded with 10 g of calcium hydride (CaH_2) and a stir bar) in a dry-ice tub. After stirring at room temperature for 3 h under argon flow, the monomer is vacuum distilled from the mixture into a 100 ml Schlenk flask in a dry-ice tub. After being warmed to ambient temperature, the flask is sealed with a Suba-Seal rubber septum while argon is flowing through the flask, and placed in a freezer at -30°C for storage of the purified COD (40.0 g, 55.3% yield). The rigorously purified monomer is vacuum distilled again prior to use.

4. Representative procedure for synthesis of telechelic polycyclooctadienes of $M_w \sim$ 50 kg/mol by ROMP

Isophthalate-terminated CTA (DA-CTA, 40 mg, 63.2 µmol) is placed in a 50 ml Schlenk flask, and degassed by 5 cycles of pulling vacuum/filling argon. Degassed, anhydrous THF (4 ml) is syringe-transferred into the flask to dissolve the CTA. 0.67 ml of 1 mg/ml anhydrous THF solution of Grubbs II (0.67 mg, 0.79 µmol, CTA:cat. = 80:1) is syringe-transferred into the mixture to equilibrate with the CTA, followed immediately by the addition of degassed, freshly vacuum-distilled purified COD (2 g, 17.6 mmol, COD:CTA = 278:1) to the mixture to start the polymerization reaction. The mixture is stirred at 40°C overnight. The reaction is stopped by exposure to air, and additional THF (15 ml) + 0.1 g of BHT are added. The diluted mixture is precipitated into 400 ml of methanol at room temperature. The precipitated polymer is collected and dried under reduced pressure at room temperature overnight. Polymer with designed molar mass and PDI around 1.5 is

obtained. For DCl-ended polymers, the procedure is the same as described above, except for using DCl-CTA and using DCM as the reaction solvent.

5. Representative procedure for synthesis of telechelic polycyclooctadienes of $M_w \sim$ 230 kg/mol by ROMP chain extension

Macro CTA (DA- or DCl- ended 50 kg/mol telechelics, 0.4 g, 8 µmol) is placed in a 50 ml Schlenk flask, and degassed by 5 cycles of pulling vacuum/filling argon. Degassed, anhydrous DCM (4 ml) is syringe-transferred into the flask to dissolve the MCTA. 0.16 ml of 0.5 mg/ml anhydrous DCM solution of Grubbs II (0.08 mg, 0.1 µmol, MCTA:cat. = 80:1) is syringe-transferred into the mixture to equilibrate with the MCTA, followed immediately by the addition of degassed, freshly vacuum-distilled purified COD (1.6 g, 14 mmol, COD:MCTA = 4:1) to the mixture to start the polymerization reaction. The mixture is stirred at 40°C overnight. The reaction is stopped by exposure to air, and additional DCM (15 ml) + 0.1 g of BHT are added. The diluted mixture is precipitated into 400 ml of methanol at room temperature. The precipitated polymer is collected and dried under reduced pressure at room temperature overnight. Polymer with designed molar mass and PDI around 1.5 is obtained.

6. Post-polymerization of DCl-PCOD to obtain DB-PCOD
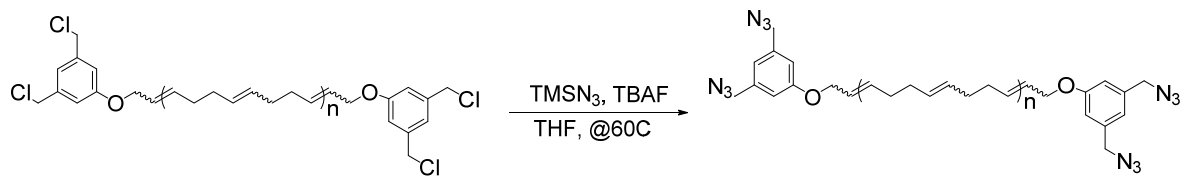
Scheme A.8 Conversion from DCl-PCOD to DN$_3$-PCOD

DCl-PCOD (50 kg/mol, 1 g, 20 µmol) is weighed into a 50 ml Schlenk flask charged with a star bar and dissolved in 15 ml of THF. Trimethylsilyl azide (TMSN$_3$, 40 equiv., 0.8 mmol) and Tetra-n-butylammonium fluoride (TBAF, 40 equiv., 0.8 mmol) are added into the mixture, which is then degassed by 3 cycles of pulling vacuum/filling argon. The reaction is allowed to stir at 60°C overnight. The reaction is stopped, and the mixture is precipitated into 400 ml of methanol at room temperature. The precipitated polymer is collected and dried under reduced pressure at room temperature overnight.
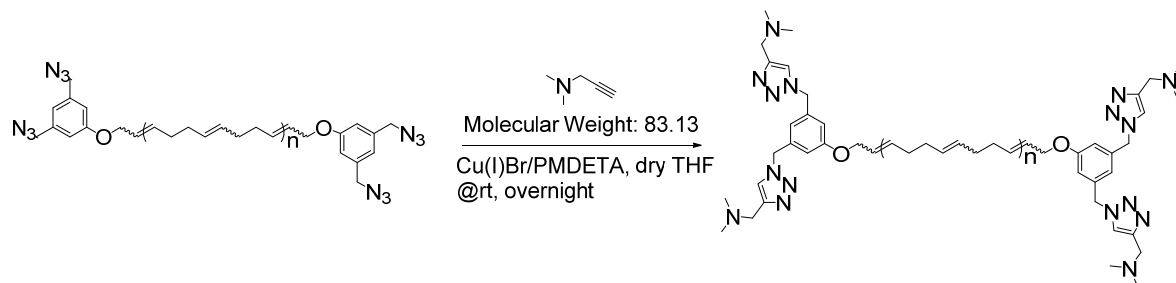
Scheme A.9 Conversion from DN$_3$-PCOD to DB-PCOD

DN$_3$-PCOD (50 kg/mol, 1 g, 20 µmol) is weighed into a 50 ml Schlenk flask charged with a star bar and dissolved in 10 ml of THF. 3-Dimethylamino-1-propyne (40 equiv., 0.8 mmol) and N,N,N',N',N''-pentamethyldiethylenetriamine (PMDETA, 1 equiv., 20 µmol) are added into the mixture, which is then degassed by 3 cycles of pulling vacuum/filling argon. Cu(I)Br (1 equiv., 20 µmol) is added under Ar flow while the mixture is frozen. The flask is sealed and degassed by 2 more cycles of pulling vacuum/filling argon. The reaction is allowed to stir at room temperature overnight. The reaction is stopped and passed through a short neutral Al$_2$O$_3$ column to remove the Cu. The mixture is then precipitated into 400 ml of methanol at room temperature. The precipitated polymer is collected and dried under reduced pressure at room temperature overnight.

7. ¹H-NMR spectrum for small molecules


Figure A.1 ¹H-NMR spectrum for compound 1.

**Figure A.2** ¹H-NMR spectrum for compound 2.
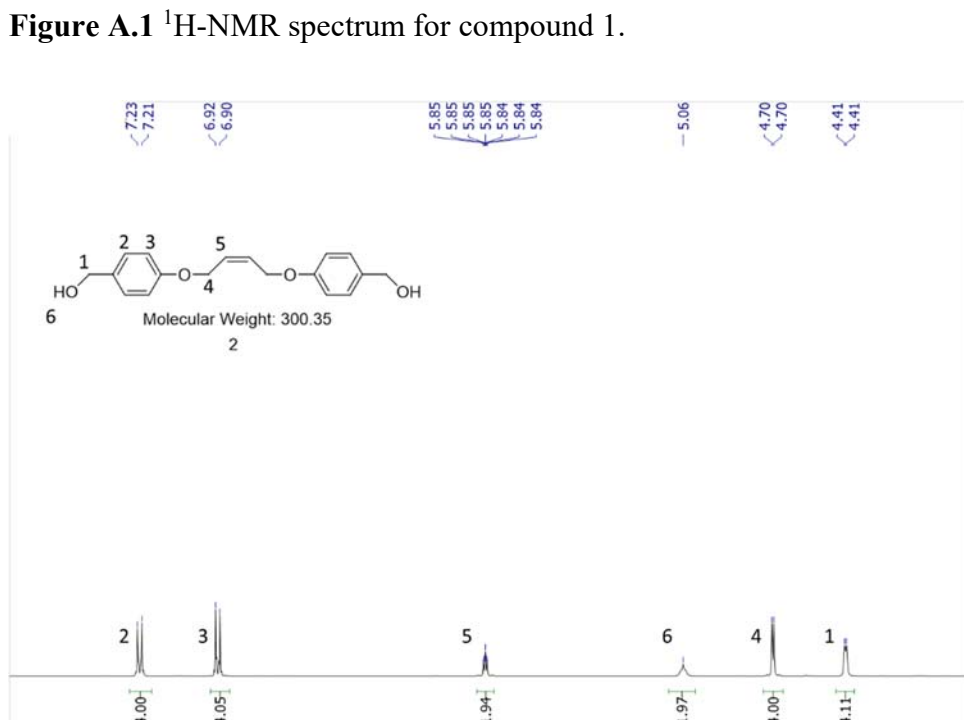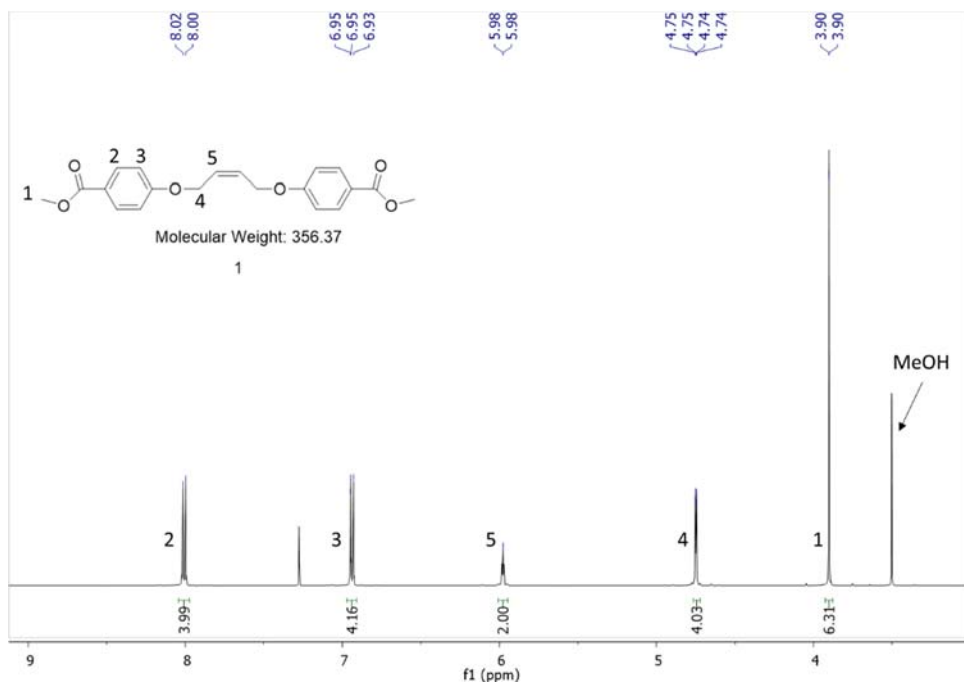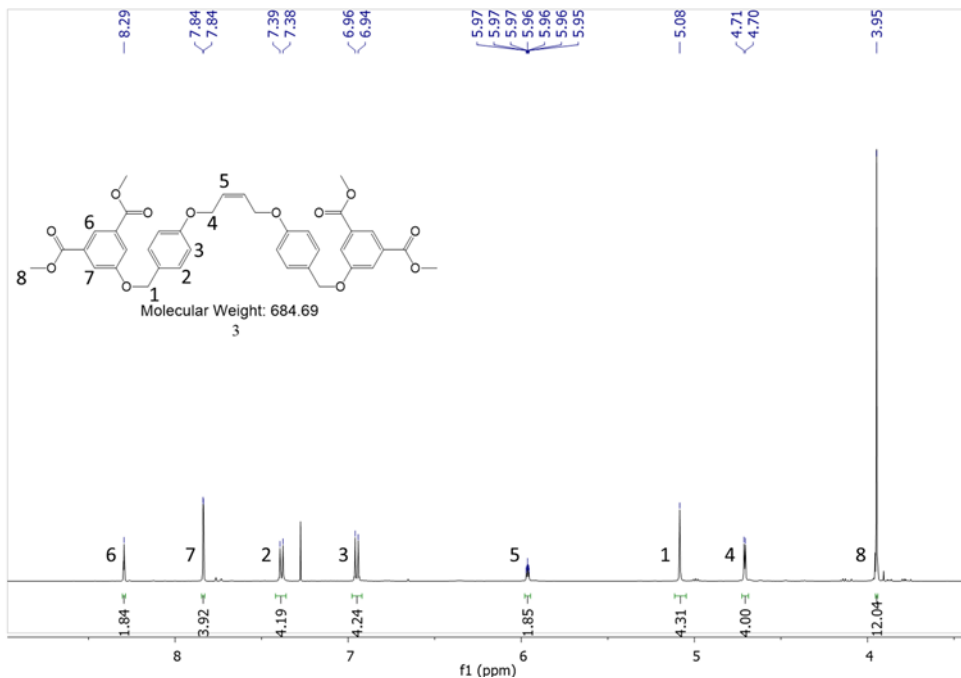
Figure A.3 ¹H-NMR spectrum for compound 3.
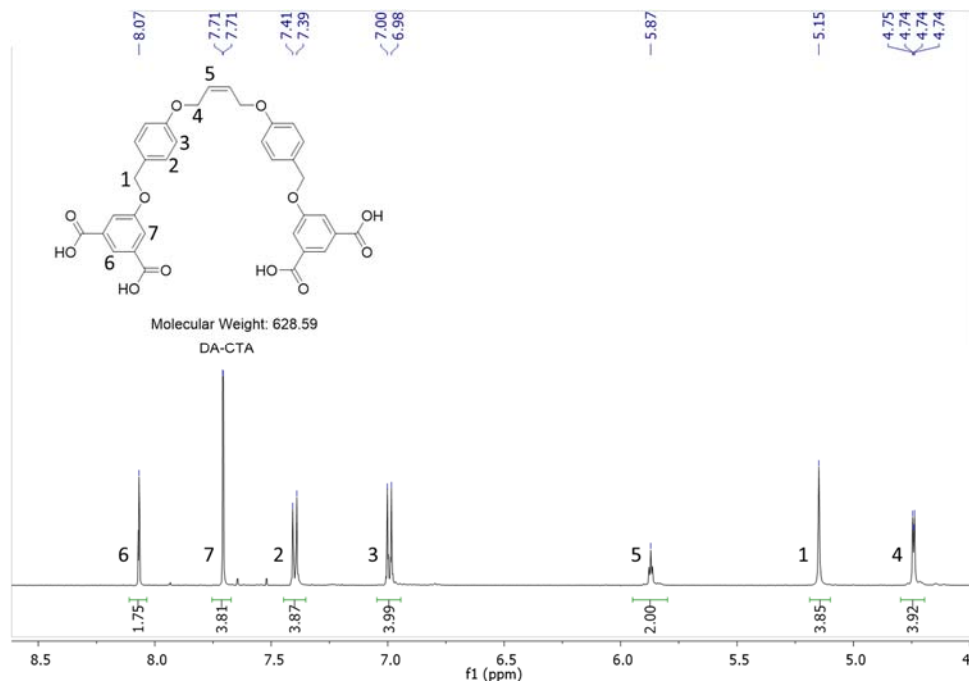
Figure A.4 ¹H-NMR spectrum for DA-CTA.
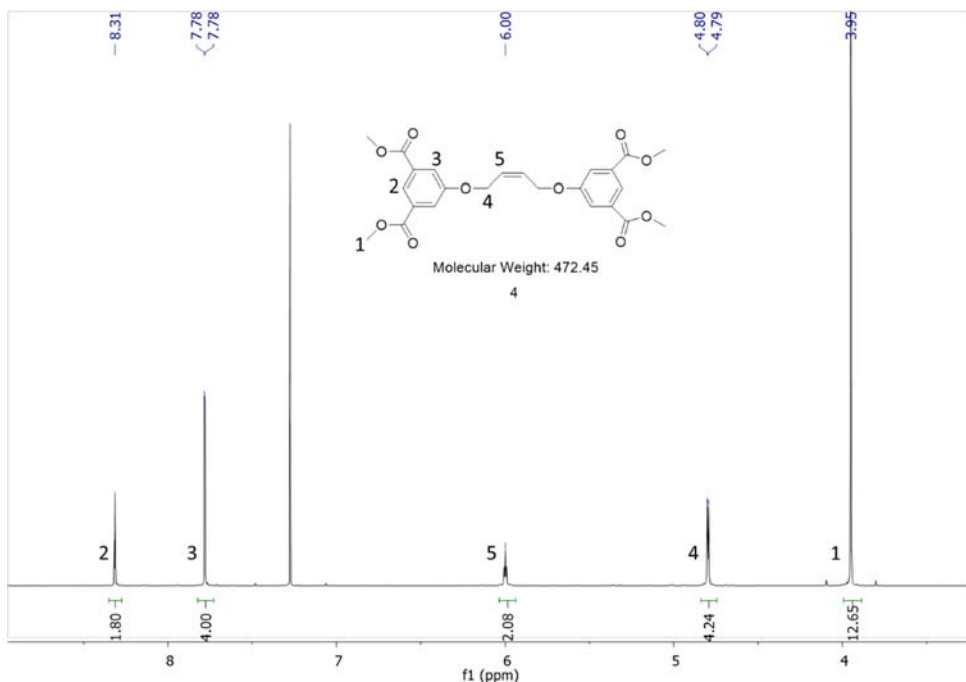
Figure A.5 ¹H-NMR spectrum for compound 4.
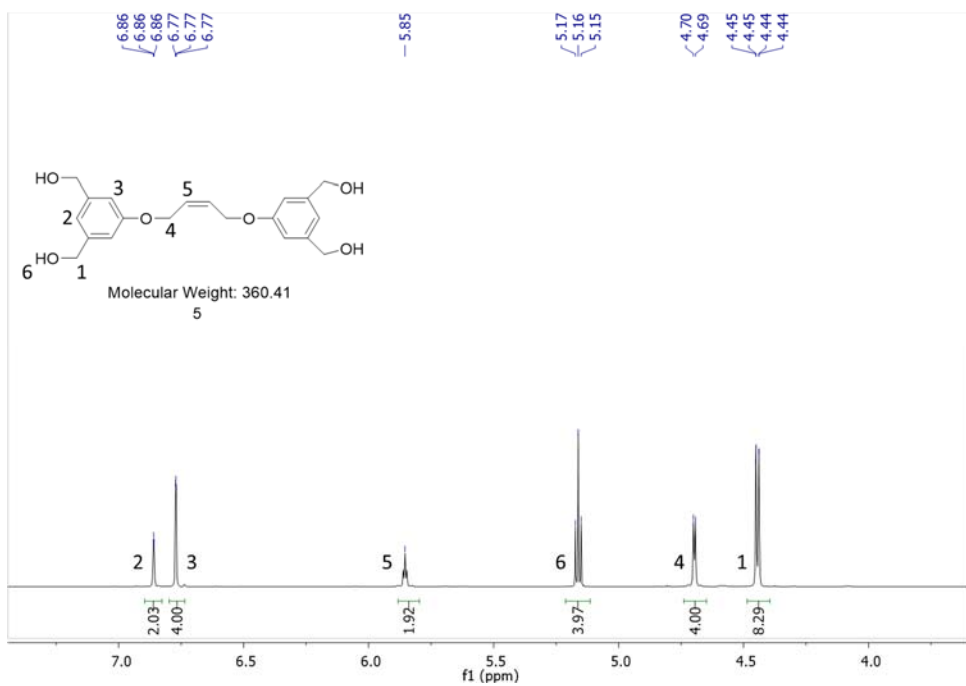
Figure A.6 ¹H-NMR spectrum for compound 5.
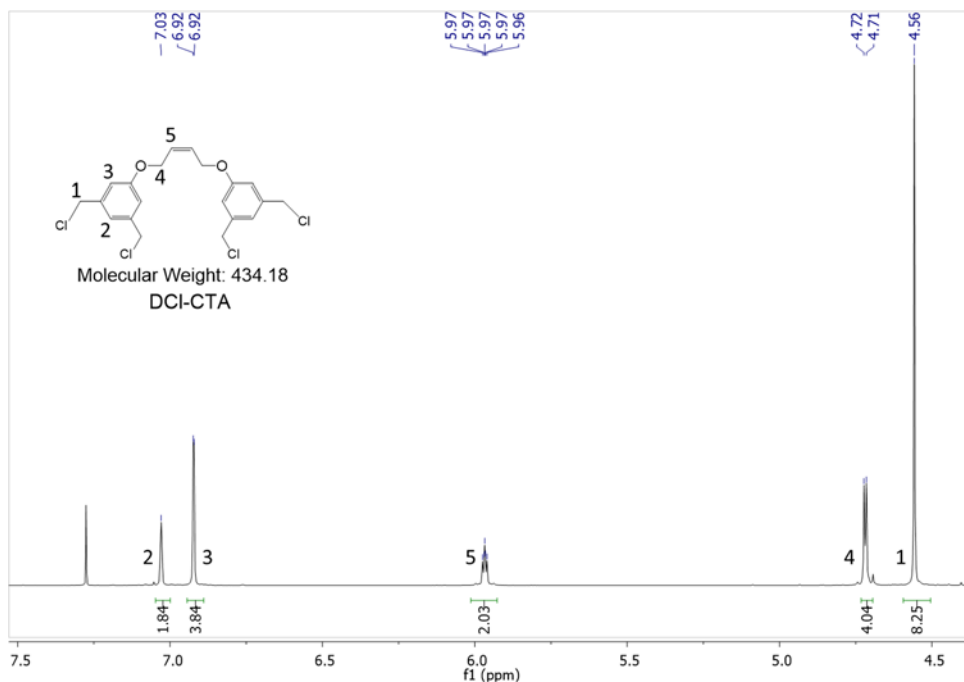
Figure A.7 ¹H-NMR spectrum for DCl-CTA.

8. List of all telechelic polymers used in the thesis

Polymer	M_w[a] (kg/mol)	M_n[a] (kg/mol)	PDI[a]
50kDCl (NA)	50	35	1.44
50kDA	50	34	1.47
50kDB	50	35	1.44
100kDCl	94	62	1.52
100kDA	103	67.5	1.52
100kDB	94	62	1.52
230kDCl	255	155	1.65
230kDA	229	150	1.52
230kDB	255	155	1.65

[a]: determined by GPC-MALLS in THF

9. Gel Permeation Chromatography (GPC) traces for telechelic polymers and CTAs

The y-axis depicts Rayleigh ratio measured by Multi-Angle Laser Light Scattering (MALLS) in all spectra.
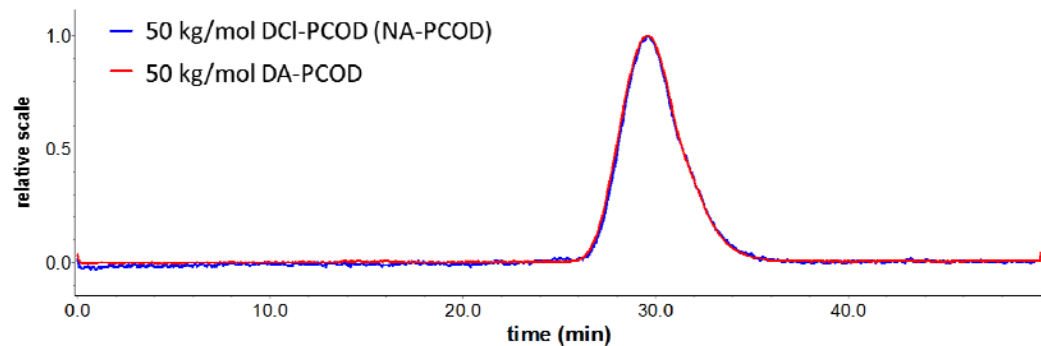
Figure A.8 GPC traces for 50 kg/mol DCl-PCOD and DA-PCOD.
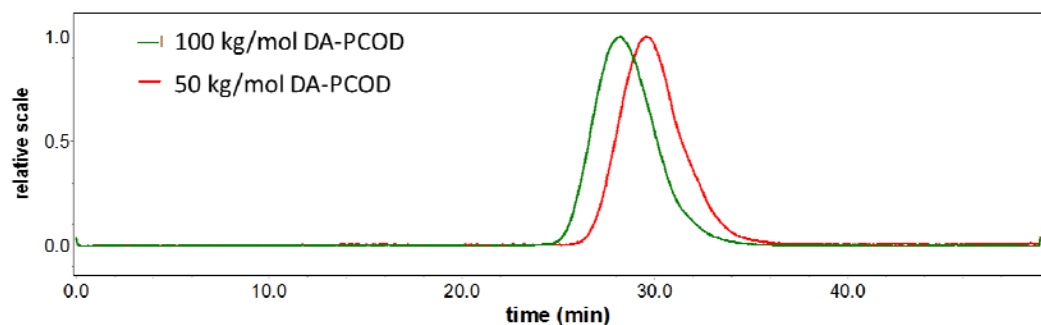
Figure A.9 GPC traces for 50 kg/mol and 100 kg/mol DA-PCOD, to show completeness of chain extension.
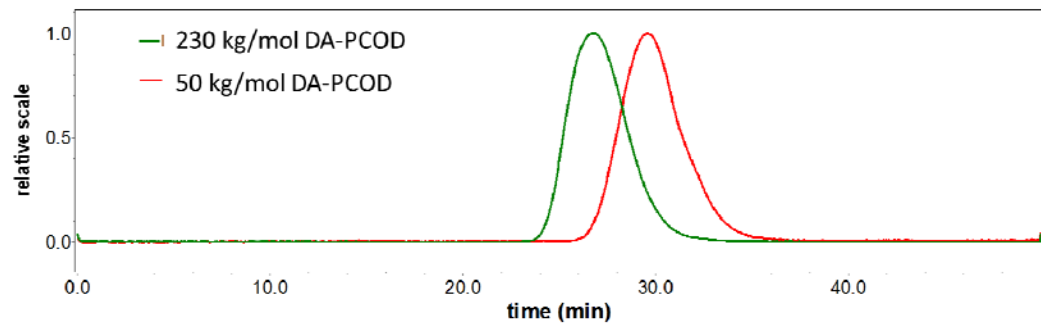

Figure A.10 GPC traces for 50 kg/mol and 230 kg/mol DA-PCOD, to show completeness of chain extension.

Figure A.11 GPC traces for 50 kg/mol and 100 kg/mol DCl-PCOD, to show completeness of chain extension.

Figure A.12 GPC traces for 50 kg/mol and 230 kg/mol DCl-PCOD, to show completeness of chain extension.
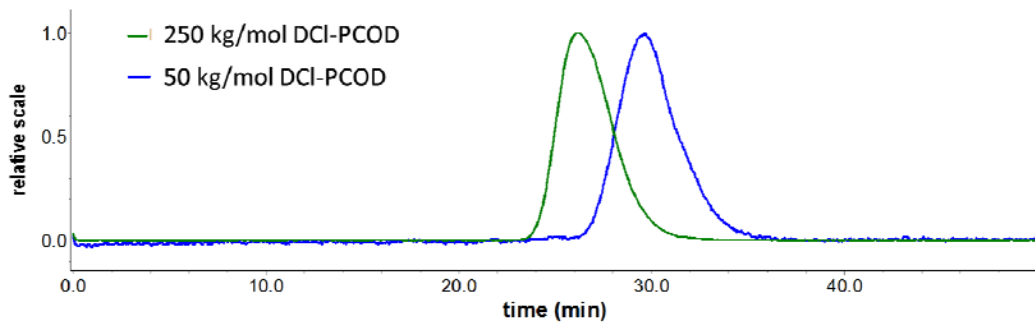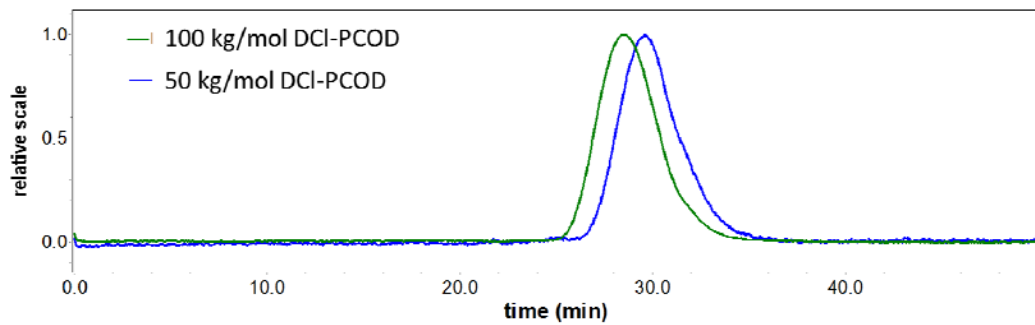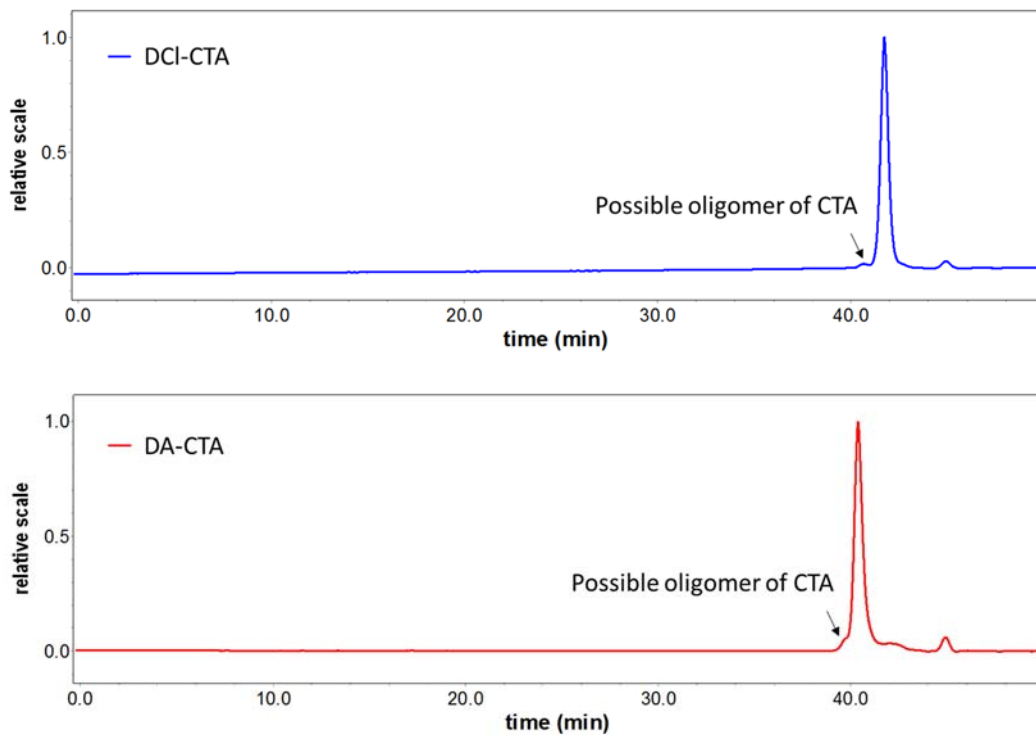
Figure A.13 GPC traces for DCl-CTA and DA-CTA, to show the content of possible oligomer of CTA, which may introduce branched telechelic polymer contributing to the non-idealities in the molecular structure. The traces here are refractive index data, showing the concentration of objects in the solution. By integrating the intensity of the shoulder on the left of the CTA peak (indicated by the arrow), the content of the possible oligomer of CTA is 1% and 3.5% for DCl-CTA and DA-CTA respectively.

10. ^{1}H-NMR spectrum for telechelic polymers
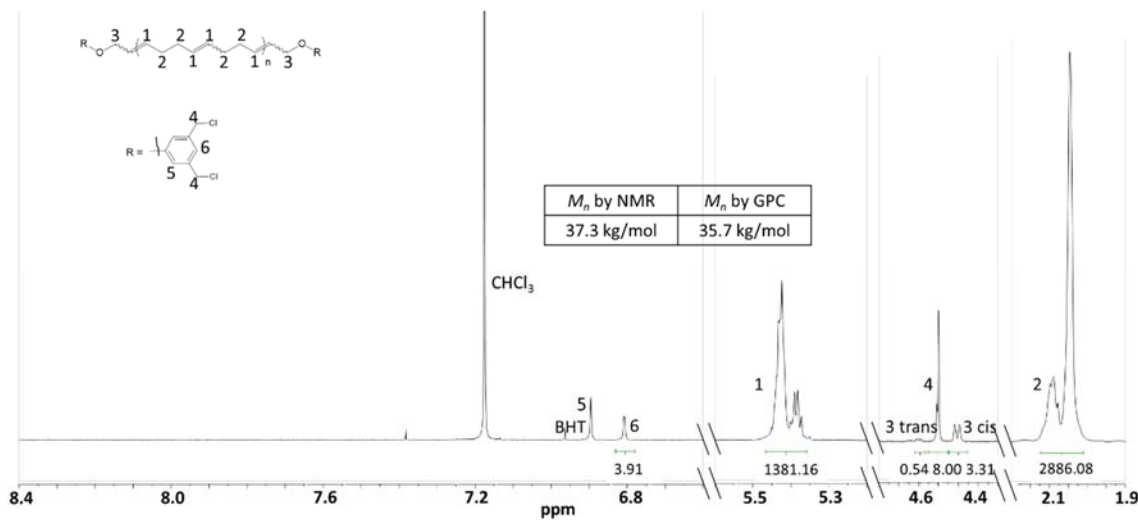
Figure A.14 H^1-NMR of 50k DCl-PCOD ($M_w = 50$ kg/mol). The intensities of end groups peaks were increased for ease of view. The M_n calculated by NMR is in good agreement with the that measured by GPC, considering the inherent uncertainty in NMR integration and the inherent uncertainty in GPC measurement (5-10%), confirming that the polymers are mainly α,ω-telechelic polymers.
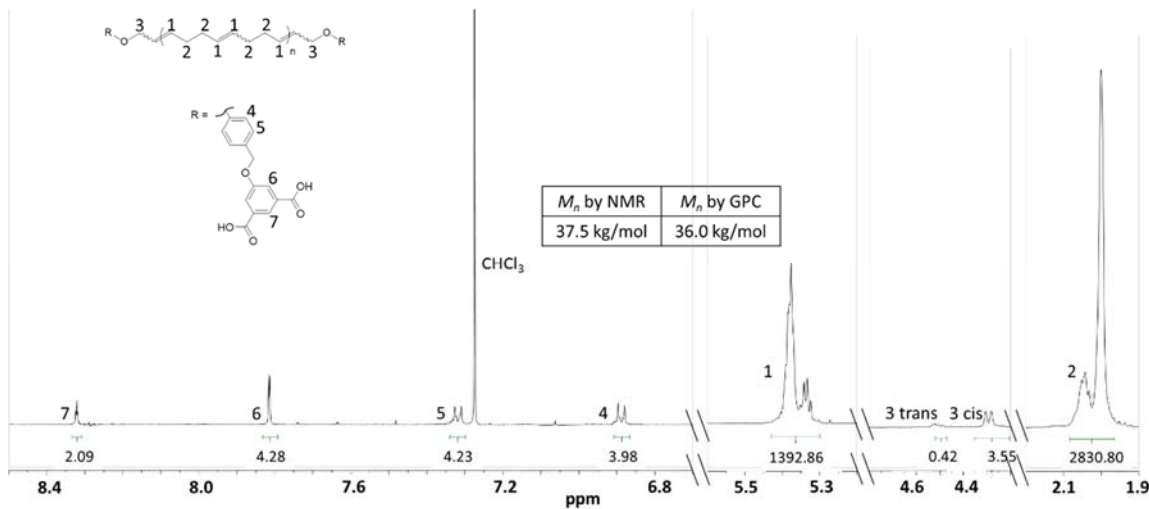

Figure A.15 H^1-NMR of 50k DA-PCOD ($M_w = 50$ kg/mol). The intensities of end groups peaks were increased for ease of view. The M_n calculated by NMR is in good agreement with the that measured by GPC, considering the inherent uncertainty in NMR integration

and the inherent uncertainty in GPC measurement (5-10%), confirming that the polymers are mainly α,ω-telechelic polymers.
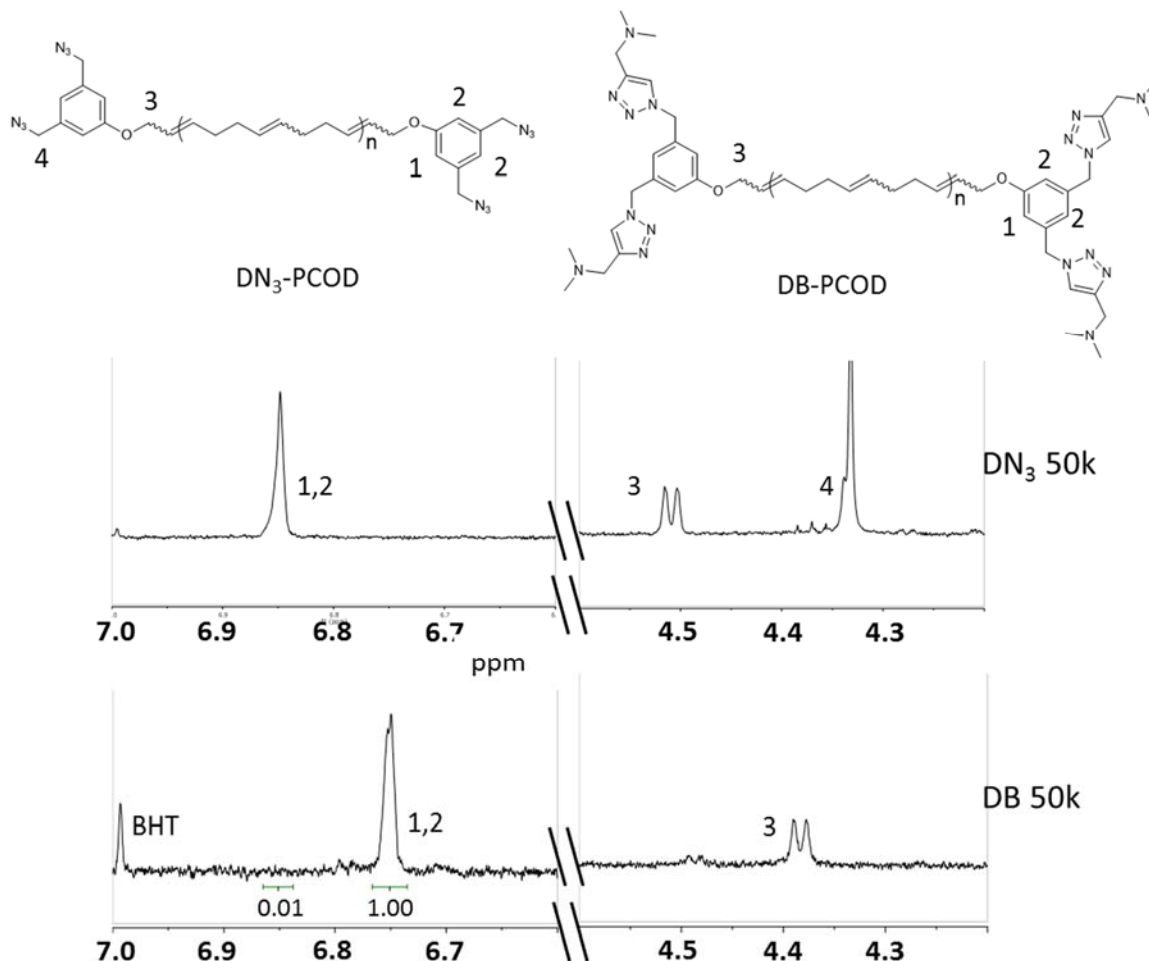

Figure A.16 ^{1}H NMR spectra of azide ended (DN$_3$) and tertiary amine ended (DB) polycyclooctadiene (M_w = 50 kg/mol) to show high degree of conversion of the end-groups. The peak for protons on the phenyl ring (at positions 1 and 2) shifts from 6.85ppm before (top) to 6.75ppm after the cycloaddition reaction (bottom): integration of the peak for protons at 1 and 2 (~6.75 ppm, relative integral integral = 1) in the spectrum of DB (bottom) and of the baseline at ~ 6.85 ppm (no detectable 1,2 of DN$_3$, relative integral = 0.01) places an upper bound of < 1% unconverted end-groups.